CSIC
CONSEJO SUPERIOR DE INVESTIGACIONES CIENTÍFICAS

Universidad de Oviedo

Programa de Doctorado en Ingeniería Energética

Desarrollo de nuevos procesos de combustión con captura de CO_2 empleando óxidos metálicos

Tesis doctoral

JUANA MARÍA ALARCÓN RODRÍGUEZ

2017

AGRADECIMIENTOS

En primer lugar me gustaría agradecer a los Doctores José Ramón Fernández y Juan Carlos Abanades, bajo cuya dirección se ha desarrollado esta tesis doctoral, por su dedicación, asesoramiento y apoyo. Gracias también por todo lo aprendido en esta etapa.

Al Ministerio de Economía y Competitividad por la concesión de una beca predoctoral FPI (BES-2013-063298) en el marco del proyecto "*Producción de hidrógeno con captura de CO_2 mediante nuevos ciclos de reformado Ca-Cu*" ENE2012-(37936-CO2-02) que me ha permitido el desarrollo de este trabajo.

Al Consejo Superior de Investigaciones Científicas, y en especial al Instituto Nacional del Carbón (INCAR), por facilitar el desarrollo de esta tesis doctoral en sus instalaciones.

Gracias también a la Doctora María Belén Folgueras de la Escuela de Ingeniería de Minas de la universidad de Oviedo por aceptar ser tutora de esta tesis.

A todas las personas que forman y han formado parte del grupo de captura de CO_2: Borja, Mónica, Montse, Sandra, Yolanda, Fernando, Alberto, David, Marlén y Chema.

A los Doctores Martin Van Sint Annaland y Fausto Gallucci de la universidad técnica de Eindhoven (TUe), por acogerme en su grupo de investigación y colaborar en las tareas en común con el grupo de captura de CO_2 dentro del proyecto europeo ASCENT (7º programa marco de la Comisión Europea). Gracias también a todos los compañeros de la TUe: Vincenzo, Kai, Giulia, Alba, Aitor, Jose, Nick y en especial a Michela con quién he trabajado mano a mano durante mi estancia en Eindhoven.

A Marlén, Cris, Julián, Sara, Sandra, Jose, Miguel, Ángela, Rubén y todos los que forman o han formado parte del grupo del café que tan buenos momentos me han hecho pasar durante este tiempo.

A mis amigos asturianos, porque sin vosotros no habría sido igual esta etapa y por todo el apoyo que me habéis brindado. Gracias también al grupo de montaña de la Universidad de Oviedo por esas magníficas rutas y post-rutas y a toda su gente.

A los “Renorgivables”, por vuestras charlas motivadoras que siempre me han sacado una sonrisa. Gracias también a mis amigos de Almería y en especial a María quienes me han ayudado a fijar la atención en lo que realmente importa.

Finalmente, en especial a mis padres, por estar siempre ahí, por haberme permitido llegar hasta aquí, por vuestro apoyo y por todos los consejos que me habéis dado. A mi hermano por darme un punto de vista distinto de las cosas y saber que puedo contar con él siempre. A mis abuelos, por todo su cariño y por tan buenos momentos en familia que hemos compartido y aún nos quedan.

ÍNDICE

RESUMEN

El uso de combustibles fósiles como principal fuente de energía para satisfacer la demanda energética mundial, ha supuesto un gran incremento de las emisiones de CO_2 en los últimos dos siglos, contribuyendo decisivamente al cambio climático observado en las últimas décadas. Por tanto, se necesita disponer de opciones que permitan adaptarnos a un sistema energético con bajas emisiones de gases de efecto invernadero, con el objetivo de cambiar las tendencias climáticas actuales. En el compromiso de reducción de las mismas, la captura, el transporte y el almacenamiento de CO_2 se presenta en muchos escenarios como una alternativa efectiva a corto medio plazo para desacoplar las emisiones de CO_2 con el uso de combustibles fósiles.

El presente trabajo se enmarca dentro de la captura de CO_2 en procesos de combustión empleando transportadores sólidos de oxígeno, y la captura de CO_2 en la producción de H_2, mediante la combinación de ciclos de cobre y calcio. Para ello se han llevado a cabo estudios tanto a nivel de desarrollo conceptual como de modelado de reactores, con su validación experimental a escala de laboratorio. En esta tesis se investigan dos procesos distintos relacionados entre sí por el uso del mismo tipo de reactores y los mismos principios de reacción entre gases y sólidos a muy altas temperaturas.

En el primer proceso, desarrollado solo a nivel de diseño conceptual de procesos y reactores, se lleva a cabo la combustión de metano con captura de CO_2 en reactores de lecho fijo a alta presión mediante el uso de ilmenita, que es un transportador sólido de bajo coste ampliamente estudiado en la literatura. Se ha demostrado que este proceso permite usar ciclos de potencia muy eficientes al trabajar a presión elevada. Operar en reactores de lecho fijo requiere estrategias complejas para gestionar el calor generado y/o requerido, y así evitar excesivos incrementos de temperatura en los frentes de reacción. En este trabajo se evalúa el uso de recirculaciones de gas para controlar el progreso de los frentes de reacción y de intercambio de calor para este fin. Para operar en continuo, se requieren cuatro etapas correspondientes a la reducción del transportador de oxígeno, reformado con vapor, oxidación del transportador de oxígeno y extracción del calor para la generación de energía. Cinco reactores en paralelo son necesarios para asegurar la producción continua de electricidad y la obtención de una corriente de CO_2 fácilmente purificable para su posterior captura y almacenamiento.

El segundo proceso corresponde con la producción de H_2 con captura "insitu" de CO_2 a partir de metano combinando ciclos de $CaO/CaCO_3$ y Cu/CuO en reactores de lecho fijo. El proceso, patentado por el CSIC, consta de tres etapas principales: reformado mejorado de metano con vapor, oxidación de Cu con aire y reducción de CuO con calcinación de $CaCO_3$ simultáneas. Este trabajo se centra en el modelado de reactor durante la etapa de reducción de CuO y calcinación de $CaCO_3$ simultáneas. La calcinación del $CaCO_3$ formado en la etapa de reformado de metano es una reacción altamente endotérmica, mientras que la reducción exotérmica de CuO con un combustible gaseoso (CH_4, CO y/o H_2) suministra el calor necesario para llevarla a cabo, evitando el aporte de energía externa. Se ha realizado un análisis de sensibilidad para estudiar la influencia de variables clave en esta etapa del proceso tales como el ratio $CuO/CaCO_3$, la temperatura inicial de los sólidos y la composición del gas reductor. Se ha demostrado que un ratio adecuado $CuO/CaCO_3$ asegura que los frentes de reducción y calcinación avancen a la misma velocidad dejando atrás sólidos totalmente convertidos y limitando la temperatura máxima en el lecho a 900ºC. El uso de CO como gas combustible minimiza dicho ratio a 1.3, disminuyendo la demanda energética del proceso. Por último, se han llevado a cabo ensayos experimentales de las etapas de reducción de CuO/calcinación de $CaCO_3$ y de oxidación de Cu bajo diferentes condiciones de operación. Se ha confirmado que para distintas composiciones del gas combustible (empleando H_2 y mezclas de CO y H_2), temperaturas iniciales en el lecho de 650ºC y un ratio ajustado $CuO/CaCO_3$ permite la calcinación total del $CaCO_3$. Asimismo, un incremento de CO en la composición del gas reductor reduce el ratio $CuO/CaCO_3$. Durante la etapa de oxidación del Cu, reacción altamente exotérmica, el efecto de la dilución de O_2 mediante recirculaciones de gas producto (N_2) como método para controlar la temperatura en el frente de oxidación ha sido demostrada. Se ha encontrado que el comportamiento que presentan los datos experimentales concuerda con los resultados predichos por el modelo.

ABSTRACT

Over the last two centuries, the extensive use of fossil fuels to satisfy the world energy demand has been responsible for almost all of the increase in greenhouse gases in the atmosphere, and therefore for the global warming observed over the last few decades. It is for this reason that alternative low-emission energy systems are necessary to counteract these current climate trends. The capture, transport and storage of CO_2 is recognized in many climate scenarios as a powerful solution for decoupling CO_2 emissions with the use of fossil fuels.

This work deals with the capture of CO_2 in combustion processes using solid oxygen carriers and the production of H_2 with insitu capture of CO_2 by combining calcium and copper looping cycles. Studies performed at conceptual and reactor modelling level, with their experimental validation at laboratory scale were carried out.

A first process is developed at conceptual level using known principles and design rules in the field of high temperature solid looping cycles using packed bed reactors. It consists in the combustion of methane and CO_2 capture in fixed bed reactors using ilmenite as solid oxygen carrier, a low-cost material extensively studied in the literature. The operation at high pressure allows the use of highly efficient power cycles. The use of fixed bed reactors requires specific heat management strategies to control the heat generated and/or consumed in the reaction fronts in order to avoid hot spots. In this work, the use of gas recycles is evaluated to control the progress of the reaction and heat exchange fronts. In order to ensure a continuous cyclic operation, a sequence of four stages is required: reduction, steam reforming, oxidation and heat removal for power generation. A minimum of five reactors working in parallel is necessary to ensure continuous power production and the generation of a high concentrated CO_2 stream suitable for transport and storage.

The second process corresponds to the production of H_2 with in situ CO_2 capture using methane as a fuel and combining $CaO/CaCO_3$ and Cu/CuO chemical loops in fixed bed reactors. This process, which has been patented by CSIC, consists of a sequence of three main stages: the sorption enhanced reforming of methane, the oxidation of copper with air and the exothermic reduction of CuO to promote the simultaneous calcination of $CaCO_3$. The reduction of CuO with a fuel gas (CH_4, CO and/or H_2) supplies the energy needs for the calcination of $CaCO_3$ (produced in the steam reforming step) which is highly endothermic. A sensitivity analysis was carried out to evaluate the

influence of key design variables, such as the $CuO/CaCO_3$ molar ratio, the initial solids temperature and the fuel gas composition. A balanced $CuO/CaCO_3$ ratio ensures a suitable bed performance, allowing the reduction and calcination fronts to advance together, reach moderate maximum temperatures of around 900 ºC and leave behind totally converted solids. The use of CO as fuel gas minimizes the $CuO/CaCO_3$ ratio to 1.3, thereby reducing the energy demand of the process. Experiments to evaluate the reduction of CuO/calcination of $CaCO_3$ and the oxidation of Cu were carried out under different operating conditions. It was confirmed in these experiments that with different fuel gas compositions (using H_2 or H_2 and CO mixtures) and initial temperatures in the solids bed of more than 650ºC it is possible to achieve the complete calcination of $CaCO_3$. Moreover, an increase in the concentration of CO in the fuel gas reduces the $CuO/CaCO_3$ molar ratio. During the oxidation of Cu, which is a highly exothermic reaction, the effect of diluting the O_2 in the inlet gas was evaluated. The recirculation of a large part of the product gas (N_2) in order to control the temperature in the reaction front was demonstrated. A good agreement between the experimental data and the results predicted by the model was obtained.

LISTA DE PUBLICACIONES

La Tesis doctoral presentada en esta memoria está basada en el trabajo contenido en los artículos que se indican a continuación, y que serán referidos en el texto por números romanos.

I. Fernández, J.R., Alarcón, J.M., (2015). Chemical looping combustion in fixed-bed reactors using ilmenite as oxygen carrier: conceptual design and operation strategy. Chemical Engineering Journal, 264, 797-806.

II. Alarcón, J.M, Fernández, J.R., (2015). $CaCO_3$ calcination by the simultaneous reduction of CuO in a Ca/Cu chemical looping process. Chemical Engineering Science, 137, 254-267.

III. Fernández, J.R., Alarcón, J.M., Abanades, J.C., (2016). Investigation of a fixed-reactor for the calcination of $CaCO_3$ by the simultaneous reduction of CuO with a fuel gas. Industrial & Engineering Chemistry Research, 55, 5128-5132.

IV. Alarcón, J.M., Fernández, J.R., Abanades, J.C., (2017). Study of a chemical loop for the calcination of $CaCO_3$ in a fixed bed reactor. Enviado a Chemical Engineering Journal.

LISTA DE FIGURAS

LISTA DE TABLAS

CAPÍTULO I

INTRODUCCIÓN

1. INTRODUCCIÓN

1.1. Cambio climático, emisiones de CO_2 y energía

Es un hecho probado que el clima está cambiando a gran velocidad como consecuencia de la influencia del ser humano. Estos cambios se evidencian por el incremento de la temperatura media del planeta y los océanos, la disminución del volumen de nieve y hielo, así como el aumento del nivel del mar en este último siglo (IPCC, 2014). Estas alteraciones, a pesar de poder estar también en parte causadas por fenómenos naturales tales como la actividad volcánica o la variación en la intensidad de la energía solar que llega al planeta, tienen su principal causa en el aumento de las emisiones de gases de efecto invernadero (GEI) de origen antropogénico desde el comienzo de la revolución industrial.

El aumento progresivo de la población mundial y el crecimiento económico han dado lugar a un sustancial incremento de la demanda mundial de energía. Desde 1970 las emisiones antropogénicas totales de GEI (CO_2, CH_4, N_2O, HFCs, PFCs y SF_6-) se han incrementado en más de un 80%, alcanzando 49 Gteq CO_2 en 2014 (Green house gas inventory, octubre 2016)[1].

A nivel global, los GEI que se emiten en mayor medida son CO_2, CH_4 y N_2O siendo el CO_2 el principal y el de mayor influencia sobre el cambio climático. La curva Keeling que se muestra en la figura 1.1 representa la evolución de la concentración de CO_2 en los últimos 60 años[2]. Se observa como el nivel de CO_2 atmosférico ha experimentado un aumento continuado sobrepasando los 400 ppm en varias ocasiones desde mayo de 2013 y manteniéndose por encima de estos niveles en la actualidad.

El aumento de las emisiones de CO_2 tiene su principal causa en la tendencia al alza en el uso de combustibles fósiles, representando actualmente en torno al 80% de la energía primaria (IEA, 2016). Uno de los sectores más dependientes de este tipo de combustibles es el energético, el cual es el responsable de aproximadamente dos tercios de las emisiones globales de GEI (IEA, 2016). Por tanto, a la vista de los datos,

[1] https://www.bafu.admin.ch/bafu/en/home/topics/climate/state/data/greenhouse-gas-inventory.html (visitado en abril de 2017).

las acciones que se lleven a cabo en este sector son claves en la lucha contra el cambio climático.

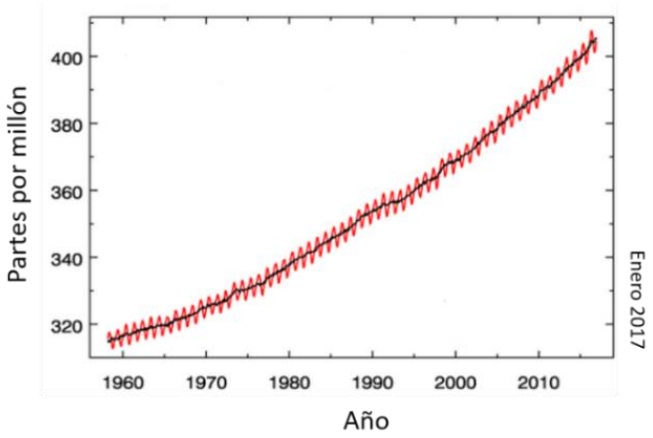

Figura 1.1: concentración global de CO_2 en la atmósfera (1960-actualidad) medida en el observatorio de Mauna Loa (Hawai) (Fuente: Maunaloa, Hawai observatory website[2]).

En los últimos años se ha logrado un creciente consenso a nivel mundial sobre la necesidad de reducir las emisiones de GEI, acelerando la transición hacia un sistema energético más limpio y eficiente (IEA, 2016). En la conferencia internacional sobre el cambio climático (COP 21) celebrada en París a finales de 2015, se alcanzó un acuerdo casi universal que establece como objetivo fundamental que la temperatura media global no supere los 2ºC respecto a niveles preindustriales. Se busca, además, promover esfuerzos adicionales que hagan posible que el calentamiento global no supere los 1,5ºC. Este acuerdo es más ambicioso que el asociado al Protocolo de Kioto, pero por ahora cada país establece sus compromisos de reducción de emisiones de acuerdo a sus realidades, a diferencia del Protocolo de Kioto en el que se intentó una reducción de emisiones legalmente vinculante que muchos países decidieron no ratificar.

La Agencia Internacional de la Energía define tres posibles escenarios del sector energético en su informe anual hasta 2040 (IEA, 2016). Estos escenarios se basan en la evolución en el uso de los recursos energéticos, el número de habitantes y su estilo

[2] Maunaloa, Hawai observatory, sitio web: https://www.esrl.noaa.gov/gmd/obop/mlo/ (visitado en enero de 2017).

de vida. En primer lugar, está el escenario de políticas actuales, que describe el camino del sistema energético actual con las políticas aprobadas hasta mediados de 2016. En este escenario, para el año 2040 las emisiones llegarían a 42 Gt CO_2. En segundo lugar, está el escenario 450, cuyo objetivo es limitar la concentración de CO_2 en la atmósfera en 450 ppm, y no sobrepasar la temperatura media global en 2ºC para 2100 (en una probabilidad del 50%) con respecto a niveles preindustriales. En este caso, para 2020 las emisiones de CO_2 tendrán que haber alcanzado su máximo y decrecer hasta 18 Gt CO_2 para 2040 suponiendo emisiones netas negativas. Finalmente, está el escenario de nuevas políticas, que son las dirigidas a cumplir el acuerdo de París, reafirmado en la COP 22 celebrada en noviembre de 2016, en Bab Ighli, Marrakech (Marruecos). Bajo estos acuerdos se prevé que las emisiones para 2040 sean de 36 Gt CO_2. La reducción necesaria de las emisiones de CO_2 para alcanzar los objetivos climáticos globales conlleva las siguientes medidas: la mejora de la eficiencia energética en los procesos de producción, distribución y uso, el aumento en el uso de energías renovables, combustibles y vehículos alternativos, la utilización de energía nuclear, así como el desarrollo de tecnologías de captura y almacenamiento de CO_2 eficientes (IEA, 2016a). En la figura 1.2 se muestra la contribución de las distintas opciones de reducción de emisiones globales de CO_2 en los escenarios de nuevas políticas y 450.

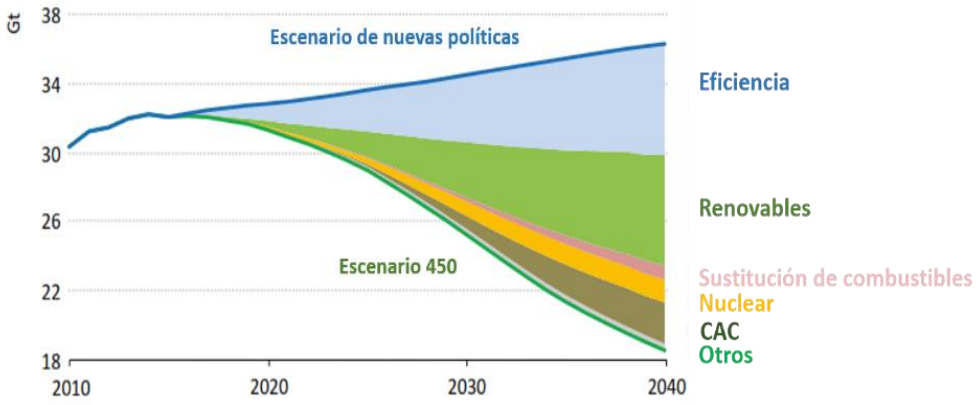

Figura 1.2: contribución de las distintas opciones de reducción de emisiones globales de CO_2 en el escenario de nuevas políticas y 450 (Fuente: IEA 2016).

El escenario de nuevas políticas prevé un incremento en la demanda de energía primaria del 31% para 2040, aumentando las emisiones de CO_2 en el sector energético en un 13%. En la figura 1.3 se presenta la contribución en la demanda de energía primaria por tipo de combustible. Se observa que en general aumentará el consumo

de todas las fuentes de energía, aunque las renovables serán las que más lo hagan en el mix energético global, seguidas del gas natural. Sin embargo, a pesar de los grandes progresos realizados en los últimos años, los combustibles fósiles seguirán primando en el mix energético global (IEA, 2016).

Las tecnologías de captura y almacenamiento de CO_2 (CAC) se presentan como una solución factible para reducir significativamente las emisiones de CO_2 procedentes de la combustión de combustibles fósiles, y poder lograr los objetivos de París (COP 21). Además, en el sector industrial (acero, hierro, cemento y procesamiento del gas natural), que contribuye en un 26% de las emisiones de CO_2 (IEA, 2016), la CAC se presenta como la única alternativa para su descarbonización, ya que, en muchos casos, el uso de combustibles fósiles es intrínseco del proceso productivo. Se prevé que la CAC contribuya en una reducción de las emisiones del 12% (94 Gt hasta 2050) situándose en tercer lugar en importancia después de la eficiencia energética (38%) y las energías renovables (figura 1.2) (32%) (IEA, 2016d).

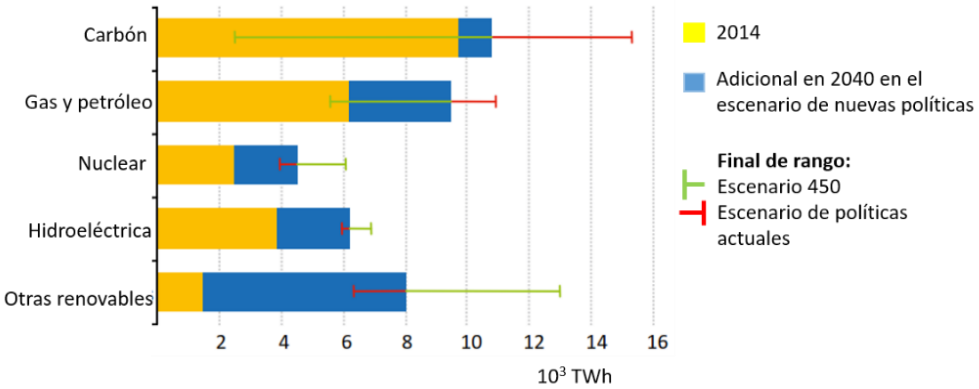

Figura 1.3: demanda de energía primaria mundial por tipo de recurso energético en el escenario de políticas actuales, 450 y nuevas políticas. Fuente: (IEA, 2016).

Dentro de los avances de la CAC cabe destacar la puesta en marcha en 2014 de la primera central térmica de carbón con captura de CO_2 (Boundary Dam unit 3, con 120 MW_e de capacidad), que posteriormente se transporta y es usado para la extracción mejorada de petróleo (de sus siglas en inglés, Enhanced Oil Recovery, EOR). Además, hay más de 20 proyectos a gran escala, tanto en operación como en construcción, representando en la actualidad en torno a 40 Mt de CO_2 al año capturados (Global CCS, 2016b).

1.2. Captura y almacenamiento de CO_2

Los procesos de captura, transporte y almacenamiento de CO_2, se describen en esta sección basados en el informe del IPCC 2005 y una edición especial conmemorando su décimo aniversario (Gale et al., 2015).

El objetivo de cualquier tecnología de CAC es generar una corriente concentrada de CO_2 adecuada para su posterior compresión, transporte y almacenamiento permanente. Esta tecnología es susceptible de ser aplicada en grandes fuentes estáticas de emisión de CO_2 tales como centrales térmicas, cementeras, refinerías, acerías, etc…(IPCC, 2005). Fuentes emisoras de CO_2 procedentes del sector residencial o el transporte se consideran fuera del alcance de la CAC, por su pequeño tamaño o carácter móvil, aunque estos sectores podrían también abordarse con CAC de forma indirecta, a través de vectores como la electricidad o el hidrógeno de plantas de CAC.

1.2.1. Captura de CO_2

La etapa de captura de CO_2 representa aproximadamente el 75% del coste total del proceso total de CAC (IPCC, 2005). Aunque la estimación de costes diez años después es más precisa, debido a pequeños cambios en el precio de la electricidad, incremento del capital de equipos industriales, etc, no ha habido cambios significativos en el mismo (Rubin et al., 2015). Dependiendo del punto del proceso donde se separa el CO_2, se distinguen fundamentalmente tres tipos de tecnologías: post-combustión, oxicombustión y pre-combustión. En la figura 1.4 se esquematizan los distintos procesos de captura atendiendo a este criterio.

Post-combustión: esta tecnología tiene como objetivo separar el CO_2 que se encuentra diluido en el resto de componentes de un gas de combustión, procedente de quemar combustibles fósiles o biomasa en presencia de aire. Este proceso presenta la ventaja de ser de fácil implantación en centrales ya existentes. Sin embargo, el sistema completo de captura requiere de grandes flujos de calor para su operación, lo que reduce considerablemente el rendimiento energético del sistema.

Dentro de esta familia de tecnologías, la absorción química con aminas es la más desarrollada. En este proceso se emplea una torre de absorción, donde tiene lugar la separación del CO_2 de los gases de combustión, y un regenerador donde se recupera el solvente, obteniéndose una corriente concentrada de CO_2. Entre las principales limitaciones de este sistema, se encuentra la degradación de las aminas, los

problemas de corrosión que acarrean los solventes ricos en CO_2 y el elevado consumo energético para su regeneración (Rochelle, 2016).

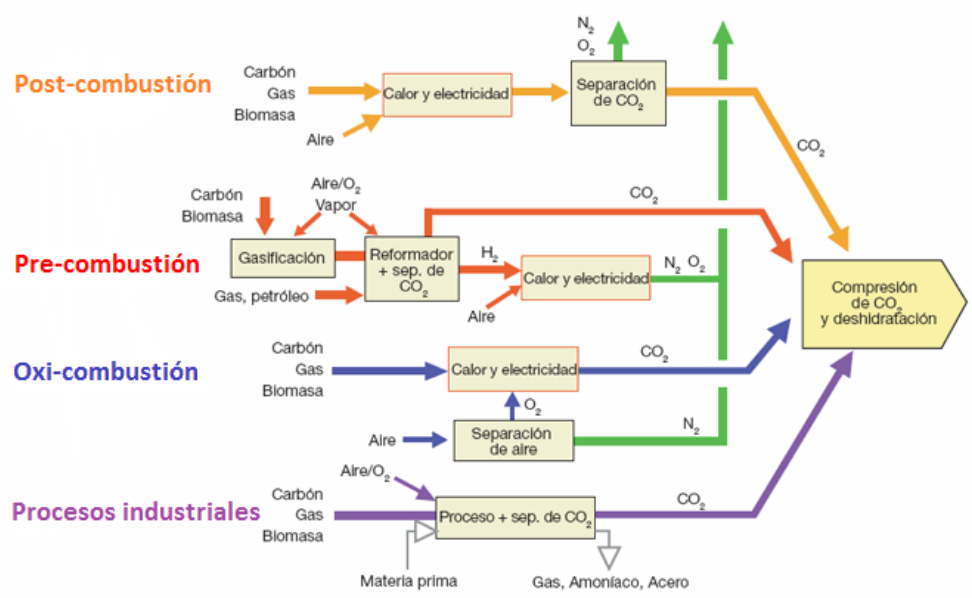

Figura 1.4*:* esquema general de las distintas tecnologías de captura (Fuente: IPCC 2005).

Como tecnologías menos desarrolladas, se encuentran los sistemas de separación basados en membranas y las reacciones de adsorción/desorción mediante sólidos regenerables.

Oxicombustión: esta tecnología consiste en llevar a cabo la combustión en presencia de oxígeno diluido en CO_2 (para controlar la temperatura de combustión) en lugar de aire. De este modo, el gas efluente es muy rico en CO_2, lo que facilita su separación final antes del almacenamiento. La principal problemática de esta tecnología es el alto coste de la unidad de separación de aire para obtener el O_2 con la pureza adecuada. Este proceso se suele llevar a cabo mediante métodos criogénicos, lo que supone una elevada penalización energética. Debido a que se necesitan modificaciones en la caldera para trabajar con O_2 en lugar de aire, estas tecnologías son más adecuadas para plantas de nueva construcción (Stanger et al., 2015).

Como tecnología emergente dentro de este grupo cabe resaltar la que hace uso de transportadores sólidos de oxígeno (Chemical Looping Combustion), la cual se explica con detalle en la sección 1.3.2.

Pre-combustión: En este caso, la captura de CO_2 es previa a la combustión. Esta tecnología se basa en la transformación del combustible en una mezcla de H_2 y CO (gas de síntesis), mediante un proceso de gasificación (si el combustible es carbón o biomasa) o reformado (para gas natural u otros hidrocarburos). Posteriormente el CO se hace reaccionar con vapor en un reactor catalítico donde se produce la reacción de desplazamiento gas-agua (más conocida por su nombre inglés Water Gas Shift, WGS) para producir más H_2 y CO_2. La conversión de CO a CO_2 hace que se alcancen presiones parciales de CO_2 mayores que en post-combustión, lo que facilita la separación de CO_2 y su posterior purificación. Para llevar a cabo la separación del CO_2 se pueden usar los procesos comerciales de absorción física usando rectisol o selexol, donde el CO_2 se pone en contacto con el solvente a baja temperatura y alta presión, y éste es posteriormente regenerado invirtiendo las condiciones, o también los procesos de absorción química con aminas (Jansen et al., 2015).

Tras la separación de CO_2 se obtiene un gas rico en H_2 que puede ser usado en procesos químicos o como combustible en turbinas de gas para la producción de electricidad. En las últimas décadas, la demanda de hidrógeno como materia prima en la industria química, de refino, vidrio y acero ha ido creciendo continuamente. Además, se prevé que su uso como combustible en turbinas de gas, pilas de combustible y motores de combustión aumente de medio a largo plazo una vez que se demuestren estas tecnologías recientes a gran escala (IEA, 2015). Hoy día la mayor parte del hidrógeno que se produce es a partir de gas natural, mediante procesos de reformado de metano con vapor (del inglés, Steam Methane Reforming, SMR), oxidación parcial y reformado autotérmico, siendo el SMR la principal tecnología, contribuyendo en torno al 48% (IEA, 2015). Por ello, muchas de las tecnologías de captura de CO_2 que se están desarrollando en la actualidad están dirigidas a acoplarse a plantas de reformado de gas natural.

1.2.2. Transporte de CO_2

Una vez separado el CO_2 mediante alguna de las tecnologías descritas anteriormente, se procede a una etapa de acondicionamiento para reducir el contenido de incondensables (N_2, H_2, O_2 y CH_4) hasta un máximo del 4% vol., aunque se permite hasta un 10% para distancias cortas, y así facilitar el posterior transporte y almacenamiento de CO_2 (Boot-Handford et al., 2014). Es fundamental eliminar el agua para evitar problemas de corrosión de tuberías durante el transporte, así como para evitar la formación de hidratos (taponamientos) o formación de gotas de agua que dañarían los equipos de compresión. Otras impurezas presentes que tienen que

dañarían los equipos de compresión. Otras impurezas presentes que tienen que guardar unos límites de seguridad y salud según su límite de exposición de corta duración (de sus siglas en inglés, STELs) son el H_2S, CO, SO_x y NO_x, con un máximo de 200 ppm para el H_2S o 2000 ppm para el CO (Boot-Handford et al., 2014).

Una vez purificado el CO_2 gaseoso, se comprime a una presión superior a 80 bar con objeto de aumentar su densidad y de esta forma facilitar y abaratar su transporte (Boot-Handford et al., 2014). Dentro de las opciones disponibles para el transporte de CO_2, se distingue el uso de gaseoductos (marítimo o terrestre), barcos, ferrocarriles o camiones cisterna (IPCC, 2005).

La forma más habitual de transporte es mediante gaseoducto (marítimo o terrestre). En este caso, se necesitan estaciones de compresión que permiten comprimir el gas para compensar la pérdida de carga a lo largo de la tubería. Se trata de una tecnología madura, ya que en el transporte de CO_2 destinado a la recuperación mejorada de pozos de petróleo (EOR) se lleva haciendo en Estados Unidos y Canadá desde los años 70. Solo Estados Unidos cuenta con una red de gaseoductos terrestre de más de 7500 km que transportan alrededor de 68 Mt de CO_2 (Global CCS, 2016b). La construcción del primer gaseoducto marítimo, asociado con el proyecto Snøhvit (Noruega), cuenta con 153 km de conducción y opera desde 2008 (Global CCS, 2016a).

1.2.3. Almacenamiento de CO_2

La etapa final del proceso de captura comprende su almacenamiento definitivo de forma segura y permanente. La opción más común es su confinamiento en formaciones geológicas profundas, para lo que es necesario que el emplazamiento se encuentre por debajo de 800 m de profundidad. A estas profundidades, el CO_2 alcanza las condiciones de estado supercrítico, con una densidad similar a la de un líquido (entre el 50 y 80% de la densidad del agua), mientras que mantiene la viscosidad propia de un gas. En estas condiciones el volumen ocupado por 1 tonelada de CO_2 es 400 veces menor que en la superficie (IPCC 2005).

De entre las opciones posibles de almacenamiento geológico, destacan los yacimientos de petróleo agotados o en su última fase de producción, acuíferos salinos profundos y yacimientos de carbón no explotables. La inyección directa en los fondos oceánicos también se presenta como una opción factible, aunque problemas medioambientales tales como la acidificación y la eutrofización de los océanos, probablemente limitará su aplicación.

Hoy en día en más de 150 emplazamientos se está inyectando CO_2 en el subsuelo, bien para la extracción mejorada de petróleo o con el propósito de almacenarlo (Global CCS, 2016b). Los yacimientos agotados de gas y petróleo son una opción muy atractiva, dado que son formaciones sedimentarias que han tenido almacenados durante varios millones de años fluidos a altas presiones, y existe una gran infraestructura disponible. Los acuíferos salinos presentan la mayor capacidad de almacenamiento, estando repartidos por todo el mundo, aunque su geología y distribución son menos conocidos (Bachu, 2015). En los últimos 20 años varios proyectos a escala piloto y comercial han sido puestos en marcha en acuíferos salinos. El proyecto Sleipner en el mar del Norte, almacena 1 Mt de CO_2 al año procedente del gas natural extraído desde que empezara a operar en 1996 (Global CCS, 2016a). En 2008, el proyecto Snøhvit (Mar de Barents) comenzó a inyectar CO_2 en una formación salina marítima de roca arenisca porosa, habiendo inyectado en torno a 3 Mt de CO_2 para el año 2016 (Global CCS, 2016a). El proyecto Illinois (Estados Unidos), con su puesta en marcha prevista a lo largo de 2017, es capaz de inyectar 1 Mt/año de CO_2 (Global CCS, 2016a).

1.3. Tecnologías emergentes de captura de CO_2

Las tecnologías de captura anteriores son lo suficientemente maduras para ser escaladas a nivel demostración, ya que los procesos de separación que incorporan ya están implementados en la industria a escala cercana a lo necesario en CAC (IPCC, 2005). Sin embargo, con el objetivo de mejorar la eficiencia y disminuir los costes de captura, surgen tecnologías emergentes capaces de competir con las más maduras (Gale et al., 2015). Éstas incluyen:

- Sistemas de ciclos de sólidos a alta temperatura: estos procesos se basan en reacciones reversibles gas-sólido que tienen lugar a alta temperatura con O_2 (combustión mediante transportadores de oxígeno, más conocido por su nombre en inglés Chemical Looping Combustion, CLC) o con CO_2 (procesos empleando óxidos de calcio, en inglés Ca-looping). En estos sistemas, la separación del gas tiene lugar a alta temperatura (entre 600ºC y 1200ºC) lo que permite una integración térmica eficiente con ciclos de vapor. Estos sistemas han experimentado un desarrollo importante en los últimos años, con varios proyectos en curso a escala piloto y demostración en todo el mundo (Abanades et al., 2015; Boot-Handford et al., 2014).

- Sorbentes sólidos: esta tecnología se basa en la adsorción del CO_2 sobre un sorbente sólido (principalmente zeolitas, geles de sílice, carbón activo, alúmina) a bajas temperaturas, entre 25-40ºC, quedando el gas retenido por medio de interacciones superficiales. Posteriormente el sólido es regenerado mediante variaciones de presión (del inglés Pressure Swing Adsortion, PSA) o temperatura (del inglés Temperature Swing Adsortion, TSA) lo que permite que sea usado en un proceso cíclico. Aunque los materiales adsorbentes presentan gran estabilidad con el número de ciclos, esta tecnología no está indicada para concentraciones de CO_2 elevadas, debido al alto consumo energético empleado en la regeneración. Además, en muchos casos se requiere un intenso pretratamiento del gas previo a la captura para proteger al material de impurezas y en algunos casos de humedad, con su consiguiente penalización energética (Lee y Park, 2015).

Membranas: en este caso el proceso de separación se basa en la permeabilidad selectiva del gas que se quiere separar hacia el otro lado de la membrana. Actualmente se aplicada en procesos industriales, tales como la separación de CO_2 del gas natural o la producción de N_2 puro a partir de aire. Sin embargo, existe un consumo energético para generar la diferencia de presión a ambos lados, y se requiere que el gas de entrada sea limpio para evitar la degradación del material. Esta tecnología se puede emplear tanto en procesos en pre-combustión como en post-combustión, aunque estos últimos tienen la limitación de necesitar membranas de alta selectividad para extraer concentraciones relativamente bajas de CO_2 (Sreedhar et al., 2017). Las membranas poliméricas han experimentado un gran desarrollo en los últimos 10 años para la separación de CO_2 del gas natural, aunque cabe destacar los avances alcanzados con membranas inorgánicas para la separación de CO_2 de H_2 en sistemas en pre-combustión (Pera-Titus, 2014) y membranas de transporte de oxígeno (Kelly, 2014).

A continuación, dentro de los sistemas de ciclos de sólidos a alta temperatura, se explican con detalle los procesos que emplean óxidos de calcio (Ca-looping), transportadores de oxígeno (chemical looping combustion) y finalmente el proceso Ca-Cu, que es la base de esta tesis doctoral.

1.3.1. Tecnologías basadas en óxidos de calcio "Ca-looping"

Estas tecnologías emplean CaO como sorbente sólido que reacciona reversiblemente con CO_2 de acuerdo a la siguiente reacción:

$$CaO(s) + CO_2(g) \leftrightarrow CaCO_3(s) \quad \Delta H_{r,298K} = -178.8\frac{kJ}{mol} \qquad (1.1)$$

La reacción de carbonatación-calcinación se basa en el equilibrio $CaO/CaCO_3$, por tanto, dado su carácter reversible, está sujeta a restricciones termodinámicas que limitan la conversión en función de la temperatura. De este modo, con objeto de obtener altas conversiones y eficiencias de captura, la temperatura óptima para la carbonatación del CaO en contacto con gases de combustión a presión atmosférica está entre los 600-700ºC. Estas condiciones permiten alcanzar una baja concentración de CO_2 en el gas de salida (entre el 0.5 y 3.5%), a la vez que se consigue una cinética de carbonatación rápida (lo que permite trabajar con reactores compactos y tiempos de residencia cortos). En el caso de la calcinación, para descomponer el $CaCO_3$ en una atmósfera concentrada de CO_2, es necesario alcanzar temperaturas en torno a 900ºC (Baker, 1962).

Los sistemas de Ca-looping se han planteado tanto para procesos de captura en post-combustión como en pre-combustión, estando los primeros en un estado de madurez superior. En lo que se refiere a procesos de producción de hidrógeno, el uso del CaO como sorbente de CO_2 fue propuesto en varios procesos durante el siglo XIX, pero es en los años 60 cuando este concepto se demostró con éxito en una planta de gasificación de carbón para el desarrollo del "CO_2 acceptor gasification process" (Curran et al., 1967). En este proceso, el CaO reacciona con el CO_2 procedente de la gasificación del carbón con un doble propósito. Por un lado, suministrar el calor necesario para la reacción de gasificación, y por otro, incrementar el poder calorífico del gas obtenido aumentando el contenido en H_2. La finalidad de este proceso no era obtener una corriente concentrada de CO_2, ya que la regeneración del sorbente se llevaba a cabo quemando un combustible con aire, dando lugar a una corriente diluida de CO_2. Estudios posteriores empiezan a considerar la necesidad de reducir las emisiones de CO_2 empleando la reacción reversible de carbonatación-calcinación, generando una corriente concentrada de CO_2 (Silaban y Harrison, 1995). En 1999 se propuso aplicar este concepto a la captura del CO_2 presente en gases de combustión, haciendo uso de un sistema de dos lechos fluidizados interconectados (carbonatador y calcinador), donde la regeneración del sorbente se hacía quemando un combustible

con una mezcla de O_2/CO_2, obteniendo de esta forma una corriente muy concentrada en CO_2 (Shimizu et al., 1999). El material empleado habitualmente como precursor de CaO, caliza o dolomita natural, se caracteriza por su bajo coste, abundancia y amplia distribución geográfica. El CaO reacciona con el SO_2 además de con el CO_2, por lo que su aplicación a gases de combustión de una central térmica de carbón podría evitar la necesidad de una unidad de desulfuración de gases, con la consiguiente disminución de costes. Además, el CaO purgado puede ser usado como materia prima para la fabricación de cemento. Sin embargo, una debilidad de este proceso es la rapidez con la que disminuye la actividad de los materiales de CaO naturales tras ser sometidos a sucesivos ciclos de carbonatación-calcinación. Este fenómeno se debe a un cambio estructural del sólido, el cual pierde porosidad, evolucionando hacia una estructura con poros de mayor diámetro y menor área superficial para la absorción de CO_2 (Alvarez y Abanades, 2005a, b). Numerosos estudios coinciden en que partículas de CaO procedentes de caliza natural o dolomita ven reducida su capacidad para absorber CO_2 llegando a actividades residuales entre 7-9% tras un número elevado de ciclos (Grasa y Abanades, 2006; Sun et al., 2008; Zhen-shan et al., 2008). Se ha demostrado que temperaturas de calcinación superiores a 950ºC aceleran este proceso de desactivación (González et al., 2008; Grasa y Abanades, 2006; Valverde et al., 2014), por lo que la temperatura de calcinación es un parámetro a controlar en todo proceso de Ca-looping. Para contrarrestar la pérdida de actividad con el número de ciclos, en los últimos años se han propuesto distintos métodos entre los que se encuentran la inclusión de una etapa de hidratación, que se realiza después de la calcinación alimentando una corriente de vapor (Arias et al., 2010; Manovic et al., 2008) y la recarbonatación, que consiste en someter el material parcialmente carbonatado a una corriente de CO_2 puro a alta temperatura (en torno a 800ºC) (Arias et al., 2012; Grasa et al., 2014). Otra alternativa es el empleo de sorbentes sintéticos. En literatura aparecen diferentes rutas de síntesis de materiales de calcio (coprecipitación, sol-gel, impregnación, dopado o hidratación, entre otros), que dan lugar a sorbentes con un contenido activo de más del 30% incluso después de numerosos ciclos de carbonatación-calcinación (Kierzkowska et al., 2013; Luo et al., 2013; Manovic y Anthony, 2009; Zhao et al., 2014).

En los procesos en post-combustión se emplean principalmente reactores de lecho fluidizado circulantes. Esta elección se debe al elevado flujo de gases a tratar en una central térmica (del orden de 300 Nm^3/s para una central de 1000 MWt). Los lechos fluidizados circulantes permiten operar con altas velocidades de gas (3-6 m/s), lo que permite reducir la sección transversal de los reactores. En este sistema, los gases

procedentes de la combustión de una central térmica con cierto contenido en CO_2 (10-15% vol. CO_2) se alimentan a uno de los reactores, que actúa como carbonatador, donde el CO_2 reacciona con las partículas de CaO en torno a 650ºC, formando $CaCO_3$. A continuación, la corriente de sólidos, tras ser separada del gas de salida en un ciclón, circula hacia un segundo reactor, que actúa como calcinador, donde se quema un combustible (generalmente carbón) en condiciones de oxi-combustión para generar la energía necesaria para la calcinación del $CaCO_3$. El concepto de Ca-looping para la captura de CO_2 fue demostrado inicialmente en ensayos multiciclo en un reactor de combustión de lecho burbujeante localizado en CANMET (Canadá) (Abanades et al., 2004). Estudios posteriores en plantas piloto que incluían lechos circulantes interconectados confirmaron los resultados satisfactorios. En las plantas del INCAR-CSIC de 30 kWt (Abanades et al., 2009; Alonso et al., 2010) y del IFK (Stuttgart, Alemania) de 10 kWt (Charitos et al., 2010), se han contabilizado más de 800 horas de operación en continuo entre ambas, alcanzando eficacias de captura superiores al 90% (Abanades et al., 2015). Basándose en la experiencia adquirida en estas plantas piloto a TRL4[3], se diseñó y construyó la planta de 1,7 MW_t situada en la central térmica de La Pereda (Asturias), a través de un consorcio entre el INCAR-CSIC, HUNOSA, ENDESA y otros actores. Esta planta piloto trata alrededor del 1% del gas de salida de la térmica y acumula en torno a 3500 h de operación, alcanzando eficacias de captura en torno al 90% (Arias, 2016; Sanchez- Bienzma, 2012; Sánchez-Biezma et al., 2013). Otras instalaciones construidas y operadas recientemente en otras partes del mundo son la planta de Darmstadt de 1 MW_t, en Alemania (Galloy et al., 2011; Kremer et al., 2013; Plötz, 2012), y la construida en Taiwan por el ITRI (Industrial Technology Research Institute) de 1.9 MW_t, pero que no ha generado todavía resultados experimentales.

El concepto de “Ca-looping” aplicado a sistemas de pre-combustión, se describe en mayor detalle a continuación, dado que constituye una parte importante de esta tesis doctoral.

Como se ha explicado anteriormente, el uso de CaO en procesos de pre-combustión comenzó con el “CO_2 acceptor gasification process” propuesto por Curran et. al, (1967). En este sistema, la etapa de gasificación de carbón se realizaba con vapor

[3] Nivel de madurez de la tecnología 4 (del inglés Technology Readiness Level 4 (TRL4)): Tecnología validada a escala de laboratorio (plantas piloto operadas en continuo <50kWth).

operando a alta presión y temperatura (a 20 bar y 815ºC, respectivamente). Para regenerar el $CaCO_3$ se quemaba carbón con aire a 20 bar, lo que obligaba a alcanzar temperaturas de 1060ºC para garantizar una rápida calcinación debido a la elevada presión parcial de CO_2 en el regenerador (4 bar). Este concepto se demostró experimentalmente a escala piloto, tratando 40 t/día de carbón sin captura de CO_2. Los graves problemas de circulación de sólidos observados al operar a alta presión han dificultado el escalado de este proceso.

La gasificación de biomasa en presencia de CaO para producir un combustible rico en H_2 se estudió en una planta de 8 MWt situada en Gussing (Austria) (Hofbauer, 2003). Se trata de un sistema de lechos fluidizados interconectados que operan a presión atmosférica. Se han propuesto también otras tecnologías de producción de hidrógeno donde se pretende obtener una corriente concentrada de CO_2 para su transporte y almacenamiento. En el proceso ZEC (de sus siglas en inglés, Zero Emissions Carbon) se pretende generar electricidad en una pila de combustible haciendo uso de parte del H_2 producido en un gasificador, y la regeneración del $CaCO_3$ se lleva a cabo empleando el gas de combustión a alta temperatura procedente de la pila de combustible (principalmente vapor de agua) (Ziock, 2001). También surgen en esta línea otros procesos, como el HyPr-RING (de sus siglas en inglés, Hydrogen production by reaction-integrated novel gasification) (Lin et al., 2002), el proceso LEGS (de sus siglas en inglés, Lime Enhanced Gasification) (Weimer et al., 2008) o el CLP (de sus siglas en inglés, Calcium Looping Process) (Ramkumar et al., 2011), en los que bajo diferentes condiciones de operación de presión y temperatura se lleva a cabo la gasificación de carbón en presencia de CaO para mejorar la producción de H_2, regenerando el sorbente quemando el char activo u otro combustible con oxígeno.

Se ha propuesto también el uso de CaO en el reformado mejorado de gas natural (en inglés, sorption enhanced reforming, SER). Hay varias patentes al respecto, entre las que se encuentran las de Texaco de 2005, en la que se propone un reactor catalítico para llevar a cabo el proceso SER (Stevens y Rovner, 2005), u otra posterior de 2008, en la que se incluye además una etapa de hidratación para mantener la actividad del material de calcio estable después de numerosos ciclos de reformado-carbonatación/calcinación (Stevens et al., 2008). En la figura 1.5 se muestra un esquema simplificado del proceso SER. La presencia de CaO junto con el catalizador de reformado (habitualmente soportado en Níquel) hace que en una única etapa tengan lugar la reacción de reformado (reacción 1.2), la WGS (reacción 1.3) y la carbonatación (reacción 1.1).

$$CH_4 + H_2O \leftrightarrow CO + 3\,H_2 \qquad \Delta H_{298K} = +206.2\frac{kJ}{mol} \qquad (1.2)$$

$$CO + H_2O \leftrightarrow CO_2 + H_2 \qquad \Delta H_{298K} = -41.5\frac{kJ}{mol} \qquad (1.3)$$

$$CaO + CO_2 \leftrightarrow CaCO_3 \qquad \Delta H_{298K} = -178.8\frac{kJ}{mol} \qquad (1.1)$$

La reacción de carbonatación elimina el CO_2 de la fase gas tan pronto como se forma, desplazando el equilibrio termodinámico de las reacciones de reformado y WGS hacia la producción de H_2, lo que permite obtener concentraciones en base seca de H_2 de en torno al 96% vol. (Harrison, 2008). En el reformado mejorado se pueden lograr conversiones elevadas de metano (>80%) operando entre 650-700ºC, lo que supone una rebaja sustancial respecto a la temperatura de operación del reformado convencional (entre 850-950ºC). Además, se evita la necesidad de llevar a cabo la reacción WGS en dos reactores adicionales, el de alta y el de baja temperatura. De esta forma el proceso se simplifica y disminuye el coste de inversión. Además, la energía liberada por las reacciones exotérmicas de carbonatación y WGS es suficiente para llevar a cabo la reacción de reformado sin necesidad de un aporte externo de energía. De hecho, la entalpía global de proceso es ligeramente exotérmica ($\Delta H_{r,298K}$=-14.1 kJ/mol).

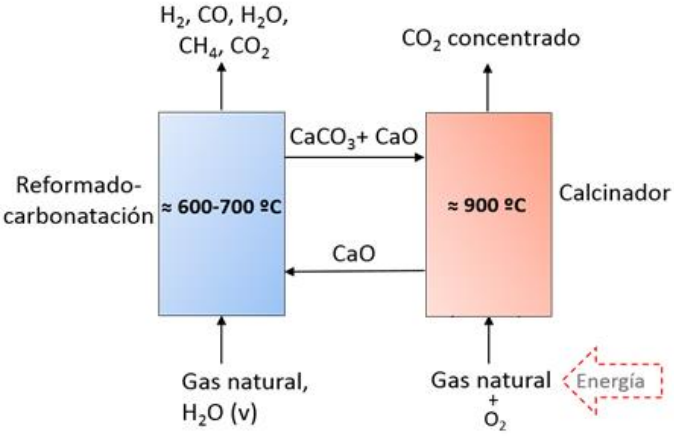

Figura 1.5: Esquema simplificado del proceso SER.

El reformado mejorado de metano se ha estudiado principalmente en reactores de lecho fijo (Aloisi et al., 2017; García-Lario et al., 2015a; Li et al., 2006; Martínez et al.,

2013c; Ochoa-Fernández et al., 2005), al igual que ocurre en el reformado de metano convencional. Esta configuración permite producir H_2 a presión elevada, lo que facilita el posterior uso del H_2 en procesos químicos o en generación de energía. Sin embargo, existen varias limitaciones que han dificultado hasta la fecha el escalado del reformado mejorado en lechos fijos. Puesto que la etapa de regeneración del sorbente de CO_2 ha de llevarse a cabo a presión atmosférica para evitar temperaturas de calcinación superiores a 920ºC, son necesarias etapas intermedias de presurización y despresurización que pueden incrementar el número de reactores necesarios para el proceso (Boon et al., 2015). La existencia de reacciones muy exotérmicas y/o muy endotérmicas hace también necesario el desarrollo de estrategias para gestionar los calores involucrados y poder así evitar cambios excesivos de temperatura en los frentes de reacción. Asimismo, son necesarias válvulas que operen a muy altas temperaturas para poder dirigir las transiciones entre etapas del proceso, y este tipo de válvulas aún no han alcanzado un alto grado de desarrollo. El uso de lechos fluidizados interconectados es otra opción propuesta en la literatura (Martínez et al., 2013c). Esta configuración presenta ciertas ventajas tales como facilitar la buena mezcla entre los sólidos, mejorando el control de la temperatura y permitiendo el aporte de sólidos frescos al sistema y la purga de los que se hayan desactivado. Sin embargo, cuenta con la limitación de tener que operar a presiones cercanas a la atmosférica, puesto que es difícil controlar la circulación de sólidos a alta presión entre lechos fluidizados. Presiones bajas de operación favorecen la producción de H_2 de acuerdo al equilibrio de reformado de metano, pero la inmensa mayoría de los usos industriales del H_2 requieren presión alta, por lo que es necesario enfriar y comprimir la corriente rica en H_2 obtenida en el reformador-carbonatador. Ello supone un consumo energético adicional y por tanto una mayor penalización energética en el proceso (Martínez et al., 2013c).

Existe algún ejemplo de reformado mejorado en lechos fluidizados a escala piloto, tales como las plantas pilotos construidas en Hynor Lillestrøm (Noruega). Una de ellas alimentada con biogás y con 40 kWt de capacidad (Meyer et al., 2014), y otra llamada Bio-ZEG (de sus siglas en inglés zero emissions gas power) de coproducción de H_2 y electricidad mediante una pila de combustible (SOFC, de sus siglas en inglés solid oxide fuel cell) alimentada con biometano y con una capacidad de 50kWt (Andresen et al., 2014).

Como se ha dicho con anterioridad, para la descomposición de $CaCO_3$ en CaO y CO_2 se ha propuesto generalmente la oxi-combustión de combustible adicional (metano,

char o el gas de rechazo generado en la etapa de purificación de H_2 aguas abajo del reactor de reformado)(Chen et al., 2011; Martínez et al., 2013c; Weimer et al., 2008). Sin embargo, este proceso requiere una costosa unidad de separación de aire (en inglés Air Separation Unit, ASU) que conlleva un consumo elevado de electricidad para generar O_2 puro de forma criogénica. Se han propuesto recientemente diferentes alternativas para aportar la energía necesaria para la calcinación evitando el uso de una unidad de separación de aire, tales como transferir el calor indirectamente a través de una pared metálica desde un reactor a mayor temperatura (Abanades et al., 2005; Junk et al., 2013), introducir en el calcinador una corriente de sólidos a alta temperatura que proceden de una cámara de combustión (Abanades et al., 2005) o alimentar al calcinador gases de combustión procedentes de una pila de combustible (Meyer et al., 2011). Otra alternativa reciente es usar el calor sensible de sólidos calientes (óxidos metálicos) que llegan al calcinador a temperaturas mayores a 1000ºC procedentes de una etapa de oxidación de un proceso de "Chemical Looping Combustion" (Fernández y Abanades, 2016; Wolf y Yan, 2005). De combinar el Ca-Looping y el Chemical Looping Combustion nace la propuesta reciente de emplear el calor generado en la reducción exotérmica de CuO con un combustible gaseoso para calcinar simultáneamente $CaCO_3$ (proceso Ca-Cu) (Abanades y Murillo, 2009; Fernández et al., 2012). Tanto los procesos de Chemical Looping Combustion como el proceso Ca-Cu, se describen en mayor detalle en las secciones 1.3.2 y 1.3.3, ya que constituyen el principal objeto de estudio en esta tesis doctoral.

1.3.2. Captura de CO_2 mediante transportadores de oxígeno

La combustión mediante transportadores de oxígeno (Chemical Looping Combustion en inglés, CLC) se basa en la transferencia del oxígeno del aire a un combustible mediante el uso de un transportador sólido de oxígeno, que suele ser un óxido metálico. De esta forma se evita el contacto directo entre aire y combustible, con lo que la separación del CO_2 es inherente al proceso y se reduce la penalización energética. El uso de transportadores de oxígeno para producir una corriente pura de CO_2 fue propuesto por primera vez por Lewis et. al (Lewis, 1951). Más tarde Richter y Knoche (1983) propusieron el concepto de CLC para mejorar la eficiencia energética en centrales térmicas (Richter y Knoche, 1983). Sin embargo, no es hasta finales de los años ochenta y principios de los noventa cuando se planteó el "Chemical Looping Combustion" como tecnología de captura de CO_2 (Ishida y Jin, 1994; Ishida et al., 1987). También se ha propuesto el uso de transportadores de oxígeno para la producción de H_2 con captura de CO_2, lo que se conoce como reformado mediante

transportadores de oxígeno (en inglés Chemical Looping Reforming, CLR) (Rydén y Lyngfelt, 2006).

Los sistemas de CLC requieren un mínimo de dos reactores, uno para la oxidación del transportador de O_2 (reactor de oxidación), y otro para la reducción del mismo (reactor de reducción). La figura 1.6 muestra un esquema simplificado del proceso.

En el reactor de reducción, el óxido metálico reacciona con el combustible y es reducido a metal o a una de sus formas reducidas (reacción 1.4). El combustible se oxida a CO_2 y $H_2O(v)$, y una vez separado el $H_2O(v)$ por condensación, se obtiene fácilmente una corriente de CO_2 concentrado.

$$(2n+m)Me_xO_y + C_nH_{2m} \rightarrow (2n+m)Me_xO_{y-1} + mH_2O + nCO_2 \qquad (1.4)$$

En el reactor de oxidación, el sólido es oxidado con aire según la reacción 1.5., quedando en condiciones para iniciar un nuevo ciclo.

$$Me_xO_{y-1} + \frac{1}{2}O_2 \rightarrow Me_xO_y \qquad (1.5)$$

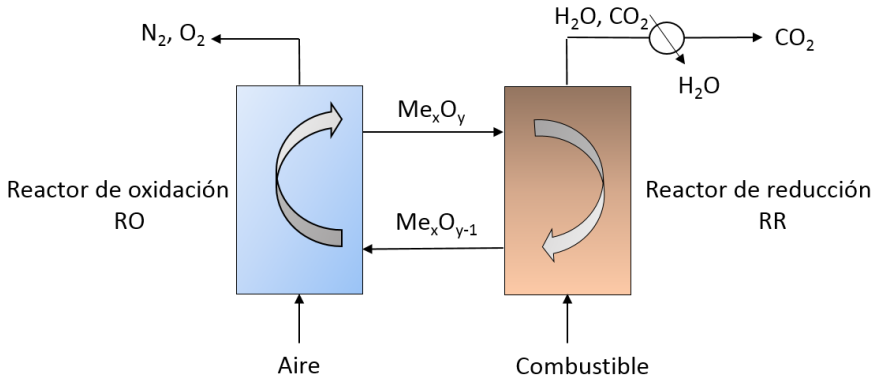

Figura 1.6: esquema simplificado del proceso CLC.

Dependiendo del combustible y del óxido metálico empleado, la reacción de reducción puede ser endotérmica o exotérmica, mientras que la reacción de oxidación es siempre exotérmica, siendo la energía total del sistema equivalente a la producida en la combustión convencional.

En CLC se pueden emplear combustibles sólidos, líquidos o gaseosos (Adanez et al., 2012; Lyngfelt, 2013). En el caso de combustibles gaseosos, el óxido metálico reacciona directamente con el combustible (gas natural, de refinería, etc). Cuando se trata de combustibles sólidos (generalmente carbón o biomasa), el transportador de oxígeno oxida los productos de la gasificación del combustible (H_2 y CO principalmente), la cual puede producirse fuera o dentro del sistema de CLC (gasificación in-situ). Otra opción reciente es el CLC con desacomplamiento de oxígeno (Chemical looping with oxygen uncoupling del inglés, CLOU)(Mattisson et al., 2009), en el que se opera en unas condiciones de temperatura que hacen que el óxido metálico libere oxígeno en fase gas, el cual reacciona directamente con el combustible sólido.

Lyngfelt et al. (2001) realizaron el primer diseño conceptual de reactores de CLC en el que el reactor de oxidación operaba como un lecho circulante y el reactor de reducción como un lecho burbujeante (Lyngfelt et al., 2001). En los últimos 10 años se han construido y ensayado más de 20 plantas piloto experimentales de CLC, que han demostrado este concepto a escala entre 0.3-3MWt empleando óxidos de Fe, Cu, Mn, Ni y Co (Abanades et al., 2015). El tiempo total de operación excede de las 7000 h (Adanez et al., 2012; Fan, 2010; Lyngfelt, 2011, 2015). De entre las plantas piloto construidas, cabe destacar la instalación de la universidad tecnológica de Chalmers (Suecia) de 10kWt, donde se realizó la primera demostración experimental de la tecnología (Lyngfelt y Thunman, 2005), la del CSIC de 10kWt (Adánez et al., 2006; de Diego et al., 2007) o la de KIER (Korea Institute of Energy Research) de 50kWt (Ryu et al., 2004) las cuales emplean gas natural. Otras más recientes son las unidades del CSIC de 50 kWt (Adánez et al., 2014), la de Darmstadt (Germany) de 1MWt (Ströhle et al., 2014) o la de Alstom en Windsor (USA) de 3MWt (Abdulally et al., 2012) que operan con carbón.

En los últimos años la investigación se ha centrado en el desarrollo de transportadores de oxígeno (Adánez et al., 2004; Berdugo et al., 2017; Cho et al., 2004; Hossain y de Lasa, 2008) y la demostración de esta tecnología empleando la configuración citada anteriormente (Lyngfelt, 2011). A la hora de seleccionar los óxidos metálicos, se buscan una serie de aspectos tales como elevada reactividad con el combustible y el oxígeno, conversiones elevadas del combustible a CO_2 y H_2O, suficiente capacidad transportadora de oxígeno, baja tendencia a la deposición de carbono, baja tendencia a la fragmentación, atrición y aglomeración, así como bajo coste y riesgo para la salud y el medio ambiente (Adanez et al., 2012). En literatura se han propuesto diferentes

óxidos metálicos como buenos candidatos para su uso en CLC tales como: Fe_2O_3, NiO, Mn_2O_3, CuO, CoO and CdO. Estos materiales se suelen combinar con un inerte, como Al_2O_3, SiO_2, ZrO_2 o TiO_2, el cual proporciona mayor área superficial para la reacción, resistencia mecánica y por tanto resistencia a la atrición. Los óxidos de cobre y niquel, son los que presentan mayor capacidad de transferencia de oxígeno, con 0.20 y 0.21 (kg O_2 transferido/Kg óxido metálico), respectivamente (Adanez et al., 2012). Además, son muy reactivos con gas natural y gas de síntesis, poseen una buena estabilidad química con el número de ciclos, y apenas tienen restricciones termodinámicas para alcanzar la conversión completa a CO_2 y H_2O. Sin embargo, cuentan con algunas desventajas. En el caso de los óxidos de níquel, son materiales caros, con baja resistencia a la deposición de carbono y peligrosos para la salud y el medio ambiente. En el caso de los materiales de cobre, el problema está en su relativamente bajo punto de fusión (en torno a 1085ºC), lo que obliga a trabajar a temperaturas inferiores a 900ºC para evitar su desactivación (con la consiguiente pérdida de eficiencia energética aguas abajo del sistema de CLC) (Cho et al., 2004; de Diego et al., 2004). Los materiales naturales (minerales de hierro, manganeso, ilmenita, entre otros), presentan la ventaja de su bajo coste, en torno a 0.1$/kg la ilmenita si se compara con los materiales sintéticos, sobre 9$/kg en el caso del Ni (Mineral commodity survey 2016[4]), aunque presentan menor capacidad de transporte de oxígeno. El uso de ilmenita, principalmente compuesta de $FeTiO_3$ ($FeO.TiO_2$), es una opción muy atractiva, dada su disponibilidad, una reactividad razonable, buena estabilidad química y mecánica a altas temperaturas (1200ºC), y baja tendencia a la deposición de carbono.

El uso de lechos fluidizados interconectados en sistemas de CLC presenta también algunos inconvenientes. Para integrar de forma eficiente el sistema CLC en un ciclo combinado, se requiere trabajar a alta presión (Brandvoll y Bolland, 2004). Aunque el uso de lechos fluidizados interconectados a presión aplicados a CLC se ha estudiado en varios trabajos (Bischi et al., 2011; Naqvi y Bolland, 2007; Xiao et al., 2010), a día de hoy, no se ha resuelto la dificultad de mantener una circulación estable de los sólidos entre los reactores presurizados, lo que impide el desarrollo de esta configuración a gran escala. Por otro lado, los lechos fluidizados requieren un complejo sistema de filtración a alta temperatura para retener los finos resultantes de la atrición de los sólidos, y así preservar el buen funcionamiento de la turbina de gas aguas abajo del sistema de CLC (Adanez et al., 2012).

[4] https://minerals.usgs.gov/minerals/pubs/commodity/ (visitado en marzo 2017)

Como alternativa a los lechos fluidizados, se ha planteado el uso de lechos fijos a presión operados de forma dinámica (Noorman et al., 2011a; Noorman et al., 2007; Noorman et al., 2010b). En estos sistemas el transportador de oxígeno permanece estacionario, mientras que la alimentación del gas se va alternando (combustible y aire, respectivamente) para llevar a cabo las etapas de reducción y oxidación. El uso de al menos dos reactores de lecho fijo operando en paralelo asegura por un lado la producción continua de una corriente de gas a alta presión y temperatura, que va dirigida a una turbina de gas para la producción de electricidad, y por otro la obtención de una corriente concentrada de CO_2 en condiciones adecuadas para su transporte y almacenamiento. En la figura 1.7 se muestra un esquema simplificado del proceso con lechos fijos.

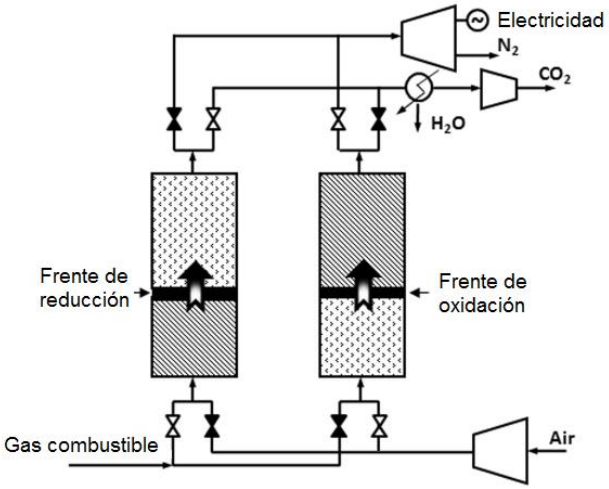

Figura 1.7: esquema simplificado de un sistema CLC en lechos fijos para generación de electricidad (Fernández y Alarcón, 2015).

En los sistemas de CLC en lechos fijos no es necesario el uso de filtros y ciclones a la salida del sistema, y el aprovechamiento del transportador de oxígeno es mejor, ya que permite un mayor grado de conversión entre la forma oxidada y reducida. Sin embargo, requieren el desarrollo de estrategias complejas para gestionar los cambios de temperatura en el interior de los lechos y también válvulas de alta temperatura, tal y como se ha explicado anteriormente.

Desde el punto de vista experimental, el CLC en lechos fijos se ha validado parcialmente a escala de laboratorio (Hamers et al., 2014; Hamers et al., 2015; Noorman et al., 2010a; Noorman et al., 2011a) en el ámbito del proyecto europeo DEMOCLOK[5], en el que además se estudiaron diferentes estrategias para la gestión del calor operando a 10 bar de presión y temperaturas máximas de 1200ºC (Hamers et al., 2015; Spallina et al., 2013). El empleo de esta tecnología de lechos fijos alternantes a alta temperatura, forma parte del objeto principal de esta tesis doctoral, por lo que es analizada en mayor profundidad en el capítulo III.

1.3.3. Proceso de producción de H_2 y/o electricidad con captura insitu de CO_2 usando ciclos de Ca-Cu.

Esta tecnología se basa en el concepto de reformardo sin mezcla (más conocido por su nombre en inglés "unmixed reforming") propuesto por Kumar y colaboradores (Kumar et al., 2002), en el que se emplea un ciclo adicional de óxidos metálicos (de Fe o Ni), cuya oxidación con aire proporciona la energía necesaria para descomponer el $CaCO_3$ formado durante la etapa SER. Sin embargo, dicho proceso no es un proceso de captura de CO_2, ya que el CO_2 resultante de la regeneración del sorbente está muy diluido en N_2 y por tanto no cumple las condiciones adecuadas para su compresión, transporte y almacenamiento.

En el proceso Ca-Cu la energía necesaria para la calcinación del $CaCO_3$ la proporciona la reducción exotérmica del CuO con CH_4 o gas de síntesis produciendo una corriente concentrada de CO_2. El concepto ha sido patentado por el CSIC (Abanades y Murillo, 2009). Con este método se debería alcanzar una alta eficiencia energética, dado que el acoplamiento de ambas reacciones (endotérmica y exotérmica) en un mismo lecho, permite que el calor sea directamente transferido de las partículas del óxido metálico a las de $CaCO_3$, sin necesidad de ninguna etapa intermedia de intercambio de calor. Aunque el proceso Ca-Cu puede ser adaptado para sistemas de captura en post-combustión (Abanades y Murillo, 2009; Duhoux et al., 2016), la mayor parte de los estudios realizados sobre este proceso se centran en la producción de H_2 y/o energía. El proceso se puede llevar a cabo en reactores de lecho fluidizado interconectados o en lechos fijos operando en paralelo (Abanades y Murillo, 2009). Como se ha comentado en las secciones anteriores, el uso de lechos fijos permite operar a

[5] https://www.sintef.no/projectweb/democlock/ (visitada en febrero 2017)

presiones elevadas y por lo tanto alcanzar mayores eficiencias energéticas, por lo que esta memoria se centra en el uso de los mismos para la producción de H_2. En la figura 1.8 se muestra el esquema básico de esta tecnología, donde se representa la secuencia de reacciones que tienen lugar: SER, oxidación de Cu y reducción de CuO/calcinación de $CaCO_3$ simultáneas.

En la primera etapa de SER se produce una corriente rica en H_2 (> 90% vol. en base seca) a presión elevada (hasta 35 bar), en presencia de un catalizador de Ni, CaO y Cu en su estado reducido (el cual actúa como inerte en esta etapa).

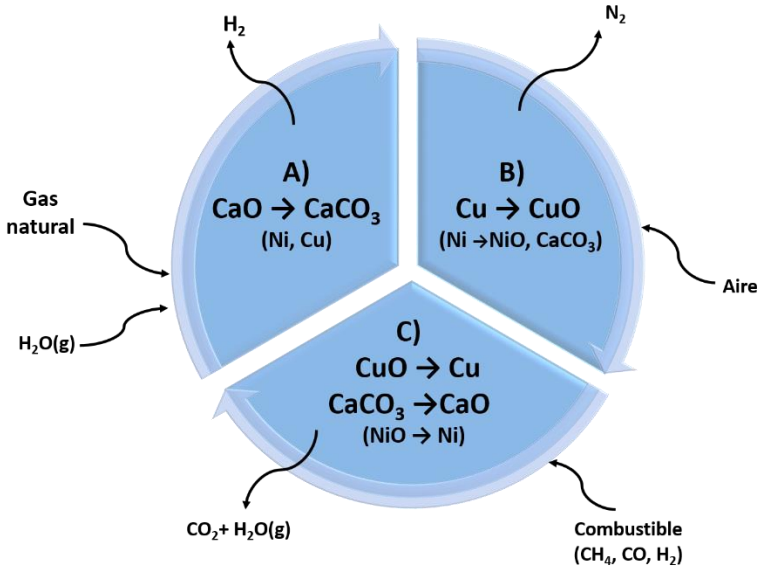

Figura 1.8: diagrama conceptual del proceso Ca-Cu para producción de H_2 a partir de metano con captura de CO_2 (Abanades y Murillo, 2009).

En la siguiente etapa se lleva a cabo la oxidación del material de cobre con aire a alta presión. Dado que la oxidación del cobre es muy exotérmica (reacción 1.6), el incremento de temperatura debe de ser controlado para evitar la descomposición parcial del $CaCO_3$ y así mantener una elevada eficacia de captura de CO_2. Para ello, se alimenta un bajo contenido de O_2, en torno al 3-4%, que se consigue mediante la recirculación de gran parte del gas producto de esta etapa (que es N_2 puro), y se disminuye la temperatura de alimentación del gas entre 150-300ºC. Ambas condiciones permiten moderar el aumento de temperatura en el frente de oxidación y alcanzar una temperatura máxima en torno a 830ºC (Fernandez et al., 2014;

Fernández et al., 2013). El nitrógeno obtenido a presión y no recirculado puede ser enviado a una turbina de gas para la producción de electricidad. Si el proceso está orientado únicamente a la producción de electricidad, el H_2 generado en la etapa SER se quema con aire y se expande en una turbina de gas (Abanades et al., 2010).

$$Cu + \frac{1}{2}\, O_2 \rightarrow CuO \qquad \Delta H_{298K} = -156.1 \frac{kJ}{mol} \qquad (1.6)$$

En la tercera etapa tiene lugar la calcinación del $CaCO_3$ a presión atmosférica mediante el calor desprendido por la reducción exotérmica del CuO formado en la etapa previa. Como gas reductor se puede emplear CH_4, CO, H_2 o mezclas entre ellos (reacciones 1.7, 1.8, 1.9). La proporción de $CuO/CaCO_3$ en el lecho ha de ser tal que el calor desprendido en la reducción de CuO sea suficiente para llevar a cabo la calcinación completa del $CaCO_3$ y sin sobrepasar los 900ºC (Alarcón y Fernández, 2015). De este modo si se emplea como gas reductor CH_4, el ratio molar sería de 3.1, en el caso de H_2 sería 1.8 y con CO sería de 1.3. En varios trabajos se plantea en esta etapa el uso del gas de rechazo procedente de la unidad PSA de purificación del H_2 de la etapa SER (principalmente compuesta por H_2 y CO) y/o el gas de síntesis obtenido en una etapa de reformado posterior (etapa C') (Fernández et al., 2012; Martínez et al., 2014; Ridha et al., 2015), por lo que se reduce el ratio Cu/Ca debido a la alta entalpía de reducción del CuO con CO y H_2.

$$4\, CuO + CH_4 \rightarrow Cu + CO_2 + 2H_2O \qquad \Delta H_{298K} = -195.3 \frac{kJ}{mol} \qquad (1.7)$$

$$CuO + CO \rightarrow Cu + CO_2 \qquad \Delta H_{298K} = -131.9 \frac{kJ}{mol} \qquad (1.8)$$

$$CuO + H_2 \rightarrow Cu + H_2O \qquad \Delta H_{298K} = -89.6 \frac{kJ}{mol} \qquad (1.9)$$

El primer estudio sobre el proceso Ca-Cu en el que se incluyen los balances básicos de materia y energía y las condiciones de operación en cada etapa, fue propuesto por Abanades et al. (2010). En un trabajo posterior, Fernández et. al (2012) desarrolla el primer diseño conceptual del proceso empleando un sistema de reactores de lecho fijo operando en paralelo. Se detallan las condiciones de operación de una forma más precisa, así como las composiciones requeridas de los materiales. El estudio se lleva a cabo empleando un modelo básico de reactor en el que se asume que las reacciones son lo suficientemente rápidas para ocurrir en un frente de reacción muy estrecho (es

decir, cinéticas muy elevadas). Fernández et al. (2012) identificaron la necesidad de incluir etapas intermediadas de intercambio de calor y de reacción para gestionar adecuadamente el calor, lograr la conversión completa de los sólidos en cada etapa de reacción y evitar de paso la formación de puntos calientes en las etapas exotérmicas. En trabajos posteriores se desarrollan modelos dinámicos más elaborados para predecir con mayor exactitud los perfiles de temperatura y concentración de gases y sólidos, similares a los propuestos para sistemas de CLC en reactores de lecho fijo (Hamers et al., 2014; Noorman et al., 2011b). En dichos trabajos sobre el proceso Ca-Cu, se llevan cabo análisis de sensibilidad de los principales parámetros de operación para la etapa SER (Fernandez et al., 2012a; Fernandez et al., 2012b), la oxidación del Cu (Fernandez et al., 2014; Fernández et al., 2013) y la reducción de CuO/calcinación de $CaCO_3$ (Qin et al., 2015). El modelado de esta última etapa se describe en detalle en la Publicación II, ya que constituye una parte importante del trabajo desarrollado en esta tesis doctoral. En el ámbito del proyecto europeo ASCENT,[6] se han desarrollado esquemas avanzados del proceso Ca-Cu en lechos fijos. Para ello, se ha simulado el comportamiento dinámico en cada etapa durante un ciclo completo considerando que las condiciones iniciales de cada etapa son el resultado de la previa (Fernández y Abanades, 2017; Martini et al., 2016a; Martini et al., 2016b). Se han evaluado nuevas condiciones de operación para tratar de reducir el número de reactores necesarios (y por tanto reducir los costes de instalación y el número de válvulas) (Fernández y Abanades, 2017), incrementar la eficacia de captura de CO_2 (Martini et al., 2016a) y evitar posibles reacciones secundarias (como la hidratación del CaO en la etapa SER) que puedan deteriorar las propiedades mecánicas de los materiales (Fernández y Abanades, 2017).

Aparte de la simulación dinámica del proceso Ca-Cu, también se han publicado trabajos que incluyen integraciones térmicas detalladas del proceso a gran escala (Martínez et al., 2013a; Martínez et al., 2013b; Martínez et al., 2014; Martini et al., 2016a), demostrando que teóricamente se pueden alcanzar altas eficacias de captura de CO_2 con penalizaciones energéticas moderadas si se comparan con las tecnologías comerciales sin captura. Martínez et al. (2014) llevó a cabo la integración del proceso Ca-Cu en un ciclo combinado de gas natural, asumiendo el modelo básico de reactores empleado por Fernández et al. (2012). Los resultados muestran que una eficiencia energética del 51% es posible (8 puntos porcentuales por debajo comparado con un ciclo combinado sin captura) junto con una reducción del 90% de las emisiones de

[6] http://ascentproject.eu

CO_2. En un trabajo posterior, se llevó a cabo la integración energética del proceso Ca-Cu en una planta de producción de H_2 (Martínez et al., 2014), obteniendo eficiencias en la producción de H_2 del 77% con eficacias de captura de CO_2 del 94%. Estos valores son 6 y 9 puntos porcentuales por encima, respectivamente, de los calculados para una planta de producción de H_2 mediante reformado de metano con vapor que emplea absorción con aminas para capturar el CO_2.

A nivel experimental a escala de laboratorio, Navarro et al. (2017) estudiaron la etapa de reformado mejorado de metano (SER) empleando mezclas de catalizador de reformado y material de CaO sometidos a múltiples ciclos de oxidación y reducción, tal y como ocurre en el proceso Ca-Cu (Navarro et al., 2017). Se demostró que para las condiciones de este proceso los materiales estudiados permiten alcanzar purezas de H_2 en el gas producto cercanas a las predichas por el equilibrio SER. El INCAR-CSIC ha llevado a cabo estudios de viabilidad de las etapas de reducción del CuO/Calcinación del $CaCO_3$ y de oxidación de Cu en un reactor pseudo-adiabático de lecho fijo de 1 m de longitud y 38 mm de diámetro interno. El estudio realizado se detalla en las Publicaciones III y IV de la presente Tesis Doctoral.

La aplicación de los ciclos Ca-Cu en sistemas en post-combustión también ha sido estudiada recientemente (Ozcan et al., 2015; Duhoux et al., 2016). Aunque estos trabajos han estimado penalizaciones energéticas de este proceso ligeramente inferiores a otros sistemas de captura en postcombustión más desarrollados, como la absorción con aminas, el uso de gran cantidad de gas natural para la reducción/calcinación pone en cuestión la viabilidad del sistema. El proceso Ca-Cu también ha sido estudiado para ser implementado en procesos industriales. Fernández et al., (2017) han planteado descarbonizar una parte importante del gas procedente del alto horno de una acería, de sus siglas en inglés Blast Furnace Gas, BFG, (alrededor del 27%), compuesto principalmente por CO, CO_2, H_2 y H_2O, mediante la reacción WGS en presencia de CaO (de sus siglas en inglés, Sorption Enhanced Water Gas Shift, SEWGS), y llevando a cabo posteriormente la calcinación de $CaCO_3$ con el calor desprendido en la reducción de CuO con gas de coquería (de sus siglas en inglés Coke Oven Gas, COG), rico en H_2 y CH_4 (Fernández et al., 2017). Martínez et al. (2017) han planteado la integración del proceso Ca-Cu en una planta de producción de amoniaco (Martínez et al., 2017). Este proceso presenta la gran ventaja de producir corrientes separadas de H_2 y N_2 fácilmente purificables que permiten teóricamente producir NH_3 ahorrando un 4% de energía y evitando alrededor del 85% de las emisiones de CO_2.

En cuanto al desarrollo de materiales de calcio y de cobre susceptibles de ser utilizados en el proceso de Ca-Cu, se han llevado avances significativos en los últimos años en relación a mejorar su reactividad en ciclos de carbonatación/calcinación y de oxidación/reducción, respectivamente. Trabajos recientes muestran materiales sintéticos de CaO capaces de mantener al menos un 30% en peso activo tras un número elevado de ciclos de carbonatación/calcinación (descrito en sección 1.3.1) (Blamey et al., 2011; Kierzkowska et al., 2013). En relación a los materiales de cobre, se han desarrollado sólidos con hasta un 60% en peso de Cu, que presentan gran reactividad en ciclos de oxidación/reducción y que mantienen su elevada capacidad de transporte de O_2 a largo plazo (Chuang et al., 2008; Imtiaz et al., 2012). Aunque mezclas a nivel de partícula de CaO y CuO se han probado con éxito experimentalmente (Fernández et al., 2016; Ridha et al., 2015) existe interés en desarrollar materiales mixtos de Ca-Cu y de Ca-Ni con el fin de disminuir la cantidad de material inerte en los reactores y favorecer la transferencia de materia y de calor durante la etapa de reducción/calcinación (Manovic et al., 2011; Qin et al., 2012), y durante la etapa de reformado mejorado de metano (García-Lario et al., 2015b; Kierzkowska et al., 2013; Martavaltzi y Lemonidou, 2010).

CAPÍTULO II

OBJETIVOS Y JUSTIFICACIÓN DE LA TESIS

2. OBJETIVOS Y JUSTIFICACIÓN DE LA TESIS

La presente tesis se ha desarrollado dentro del marco del proyecto del plan nacional BES-2013-063835, con título "*Producción de hidrogeno con captura de CO_2 mediante nuevos ciclos de reformado Ca-Cu*" y del proyecto europeo ASCENT, "*Advance solids cycles with efficient novel technologies"*, financiando por el séptimo programa marco de la Unión Europea, FP7.

Como se ha discutido en la sección anterior, el uso de reactores de lecho fijo en sistemas de Ca-looping y de CLC, se presenta como una opción de gran potencial para la producción de H_2 y de electricidad, respectivamente, reduciendo gran parte de las emisiones de CO_2 a la atmósfera. La posibilidad de trabajar a alta presión facilita la integración de estos sistemas en un ciclo combinado de manera eficiente, lo que reduciría significativamente la penalización energética ligada a la separación de CO_2. El objetivo principal de esta tesis es por tanto avanzar en el desarrollo de sistemas combinados de Ca-Cu y demostrar experimentalmente a escala de laboratorio (TRL3-4) estas tecnologías.

Para alcanzar el objetivo global, se han llevado a cabo una serie de trabajos de investigación con objetivos particulares, que se han agrupado en tres bloques en esta memoria, con sus correspondientes resultados publicados en forma de artículos científicos en revistas internacionales, los cuales se resumen a continuación:

En primer lugar, el bloque 1 (capítulo III) tiene como principal objetivo el diseño a nivel conceptual de un proceso a alta presión de combustión (CLC) que emplea ilmenita como transportador de oxígeno y metano como fuente de energía. Como resultado de esta investigación se incluye una publicación (I). En este trabajo se emplea un modelo básico de reactor que ha permitido diseñar una estrategia para gestionar los calores involucrados en las reacciones de oxidación y de reducción de ilmenita. Se ha determinado la ventana de condiciones de operación que permite llevar a cabo el proceso sin gradientes de temperatura excesivos y con un número mínimo de reactores operando en continuo. El modelo de reactor planteado en este bloque se utiliza como herramienta para los bloques 2 y 3.

El objetivo del segundo bloque (capítulo IV) es el desarrollo de modelos de reactor de lecho fijo más elaborados que permitan obtener estimaciones más precisas de los perfiles de temperatura y composición de gases y sólidos, durante la etapa de

reducción de CuO y calcinación de $CaCO_3$ simultáneas del proceso Ca-Cu. Como objetivos concretos, se evalúa la influencia teórica de parámetros clave en esta etapa tales como el ratio Ca/Cu en el lecho, la composición del gas de alimentación y la temperatura inicial de los sólidos y del gas a la entrada (Publicación II).

Finalmente, el objetivo del último bloque (capítulo V), es el estudio experimental mediante ensayos a escala de laboratorio en un reactor de lecho fijo de las etapas de oxidación de Cu y de reducción/calcinación simultáneas del proceso Ca-Cu. El efecto de variables de operación esenciales en ambas etapas, tales como la proporción de Ca y Cu en el lecho, temperatura inicial de los sólidos, y composición y temperatura del combustible (en reducción/calcinación), y la concentración de O_2 en el gas de entrada (para la oxidación de Cu) han sido evaluados experimentalmente. Asimismo, el modelo matemático desarrollado previamente ha sido validado satisfactoriamente con los resultados experimentales obtenidos en ambas etapas. Los resultados obtenidos se recogen en dos publicaciones (III y IV).

CAPÍTULO III

DISEÑO CONCEPTUAL DE UN NUEVO PROCESO DE CLC EN REACTORES DE LECHO FIJO A ALTA PRESIÓN

3. DISEÑO CONCEPTUAL DE UN NUEVO PROCESO DE CLC EN REACTORES DE LECHO FIJO A ALTA PRESIÓN.

Como parte del trabajo desarrollado en esta tesis doctoral, en este capítulo se realiza el análisis conceptual de un sistema de CLC en reactores de lecho fijo adiabáticos, empleando ilmenita como transportador de oxígeno y metano como combustible.

En este estudio se desarrolla una estrategia para gestionar el calor producido y/o consumido en cada etapa del proceso, de forma que los gradientes de temperatura generados en los frentes de reacción, se moderan mediante la recirculación de una fracción de los gases producto obtenidos en las etapas de reducción y de oxidación de ilmenita. Además, se ha llevado a cabo un diseño conceptual del proceso empleando un modelo básico de reactor y resolviendo los balances de materia y energía en cada etapa del proceso.

Forma parte de este capítulo la publicación I que se adjunta en la sección 3.1.1, en la que se detallan el modelo de reactor, la configuración del proceso, las condiciones de operación, y se discuten los resultados obtenidos, mostrando la influencia de las distintas variables.

3.1. Descripción del proceso y principales resultados

Como se ha explicado con anterioridad, la combustión mediante transportadores de oxígeno (CLC) en lechos fijos es una tecnología prometedora para la producción de energía con captura de CO_2. El uso de ilmenita ($FeTiO_3$) como transportador de oxígeno resulta particularmente interesante en este tipo de procesos, debido a que presenta una buena reactividad frente a CO y H_2 (moderada frente a CH_4), alta estabilidad mecánica y química a altas temperaturas (hasta 1200ºC) y bajo coste en comparación con otros materiales (0.1 $/kg frente a 9 $/kg de Ni) (Mineral commodity summaries 2016).

El proceso de CLC propuesto en este trabajo requiere un sistema de reactores de lecho fijo dispuestos en paralelo y que operan de forma dinámica (un sistema de válvulas dirige las transiciones entre etapas) para producir de forma continua por un lado un gas producto (principalmente N_2) a alta presión y temperatura, que es expandido en un ciclo combinado para la generación de energía, y por otro lado una corriente

concentrada de CO_2 en condiciones adecuadas para su posterior transporte y almacenamiento. Únicamente dos reactores no son suficientes para operar el proceso, puesto que las condiciones al final de una etapa (especialmente en lo que se refiere a los perfiles de temperatura) no son adecuadas para llevar a cabo directamente la siguiente. Por ello, se plantean etapas intermedias entre la de oxidación y reducción, de forma que se puedan acomodar las temperaturas de gases y sólidos, se favorezcan las reacciones involucradas en el proceso y se satisfagan las necesidades energéticas en cada una de ellas. Una secuencia de cuatro etapas: reducción de ilmenita, reformado de metano con vapor, oxidación de ilmenita y eliminación del calor, se propone para llevar cabo el proceso de forma continua.

Con el objetivo de describir cada una de las etapas que tienen lugar en el proceso, se emplea un modelo básico de reactor, previamente propuesto en otros trabajos donde se han estudiado sistemas similares de CLC (Fernández et al., 2012; Noorman et al., 2007). En dicho modelo de reactor se asume que las reacciones son suficientemente rápidas como para que tengan lugar en un frente nítido de reacción, el cual avanza a lo largo del lecho dejando atrás sólidos completamente convertidos. Asimismo, se considera flujo de pistón sin dispersión axial y ausencia de resistencia a la transferencia de materia y energía, lo que supone que no habrá diferencia de temperatura entre el sólido y el gas a lo largo del lecho. Las elevadas velocidades de gas (2-3 m/s) en cada etapa necesarias para maximizar la capacidad de los reactores por unidad de sección transversal y así lograr un sistema compacto, hacen que el régimen sea altamente turbulento y sean asumibles altos coeficientes de trasferencia de materia y energía. En aquellas etapas en las que las reacciones que tienen lugar no son térmicamente neutras y/o cuando la temperatura de los sólidos y del gas en contacto son distintas, se forman frentes de intercambio de calor. Tanto los frentes de reacción como los de intercambio de calor, avanzan a medida que transcurre la operación con velocidades diferentes. Tal y como se explica en la publicación I, estas velocidades dependen principalmente de la estequiometría de las reacciones, de la velocidad del gas, de la concentración de los reactivos y de las capacidades caloríficas de los gases y los sólidos. Las variaciones de temperatura en los frentes de reacción se calculan resolviendo los balances de energía en cada frente.

Para estudiar el proceso de CLC propuesto se define un caso de referencia en el que se alimenta un flujo másico de 10 kg/s de CH_4 (equivalente a 500 MWt) y se emplea como transportador de oxígeno un sólido que contiene un 35% en peso de ilmenita y un 5% en peso de Ni soportados sobre alúmina. La presencia de Ni mejora la

reactividad de la ilmenita y permite introducir una etapa de reformado de metano. La operación es llevada a cabo a una presión de 20 bar. A continuación, se describen brevemente las distintas etapas que constituyen el proceso.

En la primera etapa del proceso se lleva a cabo la reducción del sólido (de Fe_2TiO_5 a $FeTiO_3$) alimentando gas de síntesis procedente de una etapa posterior de reformado de CH_4 con vapor. Como consecuencia de una etapa previa a la de reducción, parte del lecho (40%) está inicialmente a una temperatura de 1200ºC y otra parte (60%) a 370ºC. El gas de síntesis se alimenta por la parte del lecho a 1200ºC, lo que facilita la reducción del sólido y la oxidación completa del gas a CO_2 y $H_2O(v)$. La reducción de la ilmenita con el gas de síntesis es moderadamente endotérmica, lo que provoca un ligero descenso en la temperatura en el frente de reducción. Se forman dos frentes de intercambio de calor: uno en la transición entre la parte del lecho que está a 1200ºC y la que está a 370ºC y otro como resultado de la reacción de reducción del sólido. Debido a la alta concentración de CO y de H_2 en el gas de síntesis y el relativamente bajo contenido de ilmenita en el sólido, el frente de reducción avanza muy rápido en relación a los frentes de intercambio de calor presentes en el lecho. La recirculación de parte del gas producto permite acelerar el avance de los frentes de intercambio de calor (debido a que hay mayor flujo de gas a través del lecho) y así poder llevar a cabo la etapa de reducción con una menor proporción de lecho a 1200ºC. Esto significa que una mayor parte del calor generado en la etapa posterior de oxidación de la ilmenita puede extraerse del lecho y ser transformado en electricidad. La recirculación de gas en este sistema se ha diseñado de tal forma que el frente de reducción alcanza el frente de intercambio de calor que limita las zonas de 1200ºC y 370ºC justo al final del reactor. La recirculación del 40% del gas producto permite llevar a cabo la reducción del sólido en un frente de reacción que mientras avanza encuentra sólidos a 1200ºC (nunca a 370ºC, porque el frente de intercambio correspondiente siempre avanza por delante), dejando atrás parte del lecho a 1187ºC debido al consumo de calor que requiere la reacción de reducción. En la Publicación I se estudia el efecto de la recirculación en el avance de los frentes de intercambio y en la caída de temperatura en el frente de reducción.

El hecho de que la oxidación de la ilmenita sea exotérmica y que gran parte del lecho reducido quede a una temperatura de 1187ºC (cerca del límite máximo admisible de 1200ºC), hace que en este trabajo se proponga la introducción de una etapa adicional de reformado de metano con vapor (fuertemente endotérmica) con un doble objetivo: por un lado reducir el exceso de temperatura almacenado en el lecho y por

otro lado usar dicho calor para transformar el metano de entrada en una mezcla principalmente de CO y H_2 que presenta una cinética más rápida para la etapa de reducción. Se asume que al final de esta etapa el lecho queda a una temperatura de 550ºC, que corresponde a la dada por el equilibrio de reformado de metano en condiciones de 20 bar y ratio vapor/metano en la alimentación de 1.

En la etapa de oxidación de ilmenita se genera una gran cantidad de calor que posteriormente se transforma en electricidad en un ciclo combinado. La temperatura de 550ºC en el lecho es suficientemente alta para iniciar de forma rápida la oxidación del sólido con aire. La ilmenita presenta una capacidad de transporte de oxígeno relativamente modesta (0.05 kg O_2/kg ilmenita frente a 0.2 k gO_2/kg Ni o Cu), que hace que su entalpía de oxidación sea menor que las de otros transportadores de O_2 (como Ni o Cu). Para las condiciones de referencia de este trabajo, la oxidación directamente con aire (21% vol. O_2) daría lugar a un incremento máximo de temperatura en el frente de oxidación de 600ºC (en condiciones adiabáticas). Por tanto, la temperatura máxima alcanzada en el lecho sería de 1150ºC, por debajo del límite máximo admisible de 1200ºC. La recirculación de parte del producto de salida (N_2 puro) permite disminuir el contenido de O_2 y aumentar el flujo de entrada al reactor de oxidación. La dilución de O_2 en la alimentación hace que el frente de oxidación y el de intercambio de calor resultante avancen hacia la salida del reactor más cerca uno del otro (es decir, a velocidades más parecidas). Por tanto, hay menos sólidos entre ellos que absorban el calor generado en el frente de oxidación y el aumento de temperatura es mayor.

El efecto de la recirculación en el aumento de la temperatura en el frente de oxidación se evalúa en la Publicación I para seleccionar el valor óptimo de acuerdo a los requerimientos del proceso. Para las condiciones de referencia estudiadas, la recirculación de aproximadamente el 30% del N_2 de salida, diluye el O_2 en la alimentación hasta el 16% vol. O_2 dando lugar a una temperatura máxima en el frente de oxidación de 1200ºC. Resulta de gran importancia alcanzar las temperaturas máximas admisibles en el sistema de CLC para luego lograr una mayor eficiencia en el ciclo combinado. El hecho de que el frente de oxidación avance por delante del de intercambio durante la etapa de oxidación, hace que durante dicha etapa el gas de salida se emita a una temperatura relativamente baja (550ºC, correspondiente a la temperatura inicial del lecho) y todo el calor generado en la oxidación quede almacenado en el lecho fijo. Por ello, es necesario incluir una etapa final de eliminación del calor, donde se alimenta aire comprimido a 20 bar y 370ºC (temperatura alcanzada por el aire a la salida del compresor). El aire va enfriando el

lecho a su paso (hasta 370ºC) y a su vez adquiere a la salida la temperatura de 1200ºC, siendo posteriormente expandido en un ciclo combinado para la generación de electricidad. No todo el calor acumulado resultante de la oxidación puede ser extraído para la generación de electricidad. Como se ha dicho anteriormente, parte del lecho ha de quedar a 1200ºC (40% en el caso de referencia estudiado en la publicación I) para poder llevar a cabo una nueva etapa de reducción. El efecto de la recirculación de N_2 en el avance de los frentes de oxidación e intercambio de calor se evalúa en la Publicación I.

En el presente trabajo se ha llevado a cabo un diseño básico de proceso con el fin de determinar el número mínimo de reactores en paralelo necesarios para asegurar una operación continua con el menor coste en equipamiento. Cada reactor debe acomodar el flujo de gas a una velocidad razonable para evitar caídas de presión excesivas. Se han considerado como razonables tiempos para cada etapa de 10 minutos, pérdidas máximas de presión por etapa del 6% y un ratio mínimo de longitud/diámetro de reactor de 1.5. Para las condiciones del caso de referencia, se ha calculado un mínimo de 5 reactores (uno de reducción, uno de reformado, uno de oxidación y dos para la eliminación de calor), con una longitud de 10 m y un diámetro interno de 6.7 m.

En la publicación I se muestra un esquema detallado de la configuración propuesta con los equipos auxiliares necesarios y el modo de accionamiento de las válvulas para controlar la alimentación en cada etapa. Los resultados obtenidos en este estudio muestran el potencial teórico de esta nueva tecnología para la generación de electricidad con captura de CO_2. Debido al estado preliminar en el que se encuentra dicha tecnología, se requiere un importante trabajo de modelado y de validación experimental para demostrar su viabilidad a gran escala.

3.1.1. Publicación I

Chemical looping combustion process in fixed-Reactors using ilmenite as oxygen carrier: Conceptual design and operation strategy.

Publicado en:

Chemical Engineering Journal

Volumen 264

Páginas 797-806

Año 2015

Chemical Engineering Journal 264 (2015) 797–806

Contents lists available at ScienceDirect

Chemical Engineering Journal

journal homepage: www.elsevier.com/locate/cej

Chemical looping combustion process in fixed-bed reactors using ilmenite as oxygen carrier: Conceptual design and operation strategy

J.R. Fernández *, J.M. Alarcón

Spanish Research Council, CSIC-INCAR, Instituto Nacional del Carbón, C/ Francisco Pintado Fe, 26, 33011 Oviedo, Spain

HIGHLIGHTS

- The feasibility of fixed-bed CLC with methane and ilmenite as carrier is assessed.
- A conceptual design has determined operating windows for each stage of the system.
- Suitable recycles allow the advance of the fronts along the beds to be controlled.
- A steam reforming stage enhances the reduction of the carrier and the combustion efficiency.
- Results show technical viability of fixed-bed CLC and its potential for further development.

ARTICLE INFO

Article history:
Received 9 October 2014
Received in revised form 4 December 2014
Accepted 5 December 2014
Available online 12 December 2014

Keywords:
CO_2 capture
Chemical looping combustion
Adiabatic fixed-bed
Ilmenite
Reforming
Heat management

ABSTRACT

A process scheme based on fixed-bed reactors is presented as a possible alternative for carrying out the chemical looping combustion of methane at high pressure with ilmenite as oxygen carrier. The operation at high pressure permits the use of highly efficient power cycles. However, complex heat management strategies and switching valves able to function at very high temperatures are required. The continuous cyclic operation of a packed-bed chemical looping combustion process is described using a basic reactor model. A sequence of four stages: reduction, steam reforming, oxidation and heat removal ensures the production of a continuous high temperature and high pressure gas able to efficiently drive a gas turbine for power generation in combination with a steam cycle. At the same time, a concentrated stream of CO_2 suitable for transport and storage is also produced. The use of suitable recycles of product gases makes it possible to control the progression of the reaction and the heat exchange fronts, which improves the heat management of the CLC process. The inclusion of steam methane reforming in the process allows the conversion of the ingoing methane to syngas, which enhances the reduction kinetics of the ilmenite and the overall combustion efficiency of the process. A preliminary conceptual design for an inlet flow of 10 kg/s of methane (500 MWt) has shown that a minimum of five reactors, 10 m long, with an inner diameter of 6.7 m, would be required to fulfil the overall process assuming cycles of 10 min with maximum pressure drops per stage of less than 6%. These results demonstrate the potential of this novel technology for power generation in combination with CO_2 capture.

1. Introduction

The potential increase in world energy demand over the next few decades and the alarming signs of global warming make it necessary to drastically reduce greenhouse gas emissions from anthropogenic sources [1]. Of the different strategies directed at mitigating CO_2 emissions developed in recent years, carbon capture and storage (CCS) is considered as a valid mid-term solution [2]. CO_2 capture is nowadays the most energy-intensive step in CCS, and as a result, there is growing interest in the development of new CO_2 capture technologies, especially in large-scale power production in order to address the problem of energy penalties and the cost of existing equipment [3].

Of the different technologies proposed in the literature, chemical looping combustion (CLC) represents one of the most promising alternatives for achieving a very high CO_2 capture efficiency with reduced energy penalties [4]. This concept consists in the transfer of oxygen from air to the fuel by using a solid oxygen carrier (typically a metal oxide) and so avoiding any direct contact between the fuel and air. The dilution of the combustion products

* Corresponding author at: CSIC-INCAR, Spanish Research Council, Francisco Pintado Fe, 26, 33080 Oviedo, Spain. Tel.: +34 985119090; fax: +34 985297662.
E-mail address: jramon@incar.csic.es (J.R. Fernández).

http://dx.doi.org/10.1016/j.cej.2014.12.022
1385-8947/

Nomenclature

c_{pi}	specific heat capacity of component i (kJ/mol °C)
ΔH_r	enthalpy of the reaction (kJ/mol)
M_i	molecular weight of component i (kg/mol)
P	pressure (bar)
t	time (s)
T_{gin}	inlet gas temperature (°C)
T_{max}	maximum temperature (°C)
T_{s0}	initial temperature of bed reactor (°C)
ΔT_{max}	maximum adiabatic temperature variation (°C)
u_e	heat exchange front velocity (m/s)
u_g	gas velocity (m/s)
u_r	reaction front velocity (m/s)
x_i	weight fraction of component i (dimensionless)

Greek letters

ρ_i	density of component i (kg/m^3)
ε	porosity (dimensionless)
φ	stoichiometric factor (dimensionless)

with nitrogen is avoided and the resulting gas is highly concentrated in CO_2. CLC was firstly conceived in the 1950s [5], but it was not until the 1990s when it was proposed as a CO_2 capture system [6]. Most of the CLC configurations proposed consist of interconnected fluidized-bed reactors, where the oxygen carrier is reduced in the fuel reactor and rapidly transported to the air reactor to be regenerated [7–14]. The small size of the particles used in fluidized beds ensures that there is good contact between the gas and solids, as a result of which the kinetics of the reactions involved in the process are considerably enhanced. Furthermore, rapid mixing of the solids ensures an adequate control of the temperature, which is of fundamental importance in the energy-intense reactions characteristic of CLC processes. The application of the CLC concept in fluidized-beds has been widely studied in recent years in several experimental units at different pilot scales [13–20]. However, the use of interconnected fluidized-beds in CLC has several drawbacks. Operation at high pressure is required to enable a CLC system to be integrated in a combined cycle to increase the energy efficiency [21]. Several works have been published in recent years about CLC performed in fluidized-beds at high pressure [22–24], but this concept still faces critical challenges, such as the difficulty in maintaining a stable circulation of solids between the pressurized reactors, in order to demonstrate its feasibility on a large scale. Moreover, a high-temperature and high-pressure solids filtering system is required to eliminate the fines resulting from particle attrition, since the presence of particles in the exiting gas from the CLC unit could have a negative effect on the performance of the downstream gas turbine [4].

An alternative for CLC applications at high pressure is the use of configurations based on dynamically operated fixed-bed reactors, where the oxygen carrier remains stationary and the gas feed (fuel gas and air, respectively) is periodically alternated in order to perform the reduction and oxidation stages. As can be seen from Fig. 1, the use of at least two reactors operating in parallel ensures: (1) the production of a continuous high-temperature and high-pressure stream of gas, that is able to drive a gas turbine for power generation, and (2) a concentrated stream of CO_2 suitable for transport and subsequent geological storage. In fixed-bed systems, attrition in the oxygen carriers can be expected to be negligible, and therefore, cyclones and filters downstream are not required. Moreover, the oxygen carrier can be better utilized, because operating in fixed-beds allows a larger degree of conversion between the reduced and oxidized forms. In contrast, heat management strategies for controlling the changes in temperature as the reaction fronts advance through the bed and switching valves able to function with gases at high temperature are required in fixed-bed systems. The high temperature valves required are one of the major drawbacks of this technology. There are commercial valves designed to operate at very high pressures and temperatures for over thousands of cycles, but further investigation is

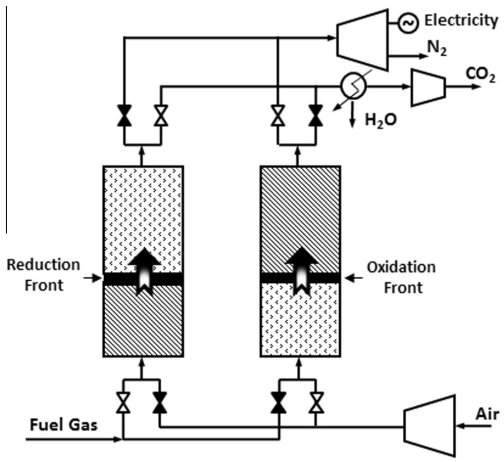

Fig. 1. Representation of a CLC system with alternating fixed-bed reactors for power generation.

needed to improve their performance under the CLC operating conditions. Although there is a wide experience in industry with pressure and temperature swing adsorption systems, there are very few works that deal with the feasibility of CLC in fixed-bed configurations [25–28]. Early works on chemical looping processes carried out in fixed-beds [25] showed that the oxidation and reduction reactions involved can proceed very fast in narrow reaction fronts. During chemical looping combustion, both reaction and heat exchange fronts are formed and move forward at different velocities depending mainly on the concentration and molecular weights of the reactants and on the stoichiometry of the reactions [26], which is a similar phenomenon to the catalytic oxidation of a fuel gas when it is carried out at different operating temperatures [29]. Several heat management strategies have been proposed in the literature in relation with CLC for controlling the increase in temperature in the reaction fronts, while the product gas is discharged at nearly constant temperature and mass flow rate to protect the gas turbine from thermal and mechanical stress, and also to ensure that the temperature profiles of the solids are sufficiently high to allow fast reaction rates and total gas and solids conversion from the very beginning of the operation.

One option is to use an oxygen carrier with a sufficiently low content of active phase that allows the oxidation stage to be accomplished without exceeding the maximum allowable temperature (i.e. up to 1200 °C depending on the oxygen carrier in order

to avoid solids deactivation). Under these circumstances, the reaction front proceeds very quickly along the reactor, leaving behind the solid/gas heat exchange front. A large amount of inert material makes it possible to separate the advance of the reaction and heat exchange fronts so that there will be a larger mass of solids between them able to absorb the heat released from the oxidation reaction. When oxygen carriers with a high carrying capacity and a high oxidation enthalpy, such as Ni or Cu, are used, very low metal loadings (lower than 20 wt.%) are required to limit the increase in temperature during the operation, which means that larger high-pressure reactors are required for a given flow of fuel gas fed into the system. This option has been studied assuming methane [26–28,30,31] and syngas [32–34] to be the fuel gas. Another alternative is to control the increase in temperature during the oxidation stage by recycling a large amount of the cooled N_2 product gas in order to dilute the O_2 fed into the air reactor [35,36]. In these conditions, the reaction front advances at a slower velocity than the heat exchange front, which allows the oxidation stage to be carried out with a higher amount of active oxygen carrier content without exceeding the maximum allowable temperature in the reaction front. This alternative permits a more compact reactor design at the expense of a higher energy requirement and equipment cost due to the recirculation of part of the product gas to the air reactor inlet.

Many materials have been evaluated as oxygen carriers for CLC, including synthetic materials, mixed oxides, minerals and waste materials [37–47]. Ni-based and Cu-based carriers have been the most extensively studied materials in the literature because of their favourable characteristics for chemical looping applications, such as their high oxygen carrying capacity, high reactivity with methane and syngas, good chemical stability after multiple redox cycles at high temperatures and also few thermodynamic restrictions for allowing the complete fuel conversion to CO_2 and H_2O [37–42,46]. Despite these advantages, Ni-based materials are expensive oxygen carriers (see Fig. 2), they have a low resistance to carbon deposition and emissions of their trace compounds must at all costs be avoided because of their potential risks to human health and the environment. With regards to Cu-based materials, they have a relatively low melting point (1085 °C) and therefore cannot be used at the highest temperature range for CLC (1100–1200 °C) in order to prevent their deactivation through agglomeration [39,40].

The main advantage of using natural materials as oxygen carriers is their lower cost in comparison to synthetic materials, though at the expense of a lower oxygen transport capacity (see Fig. 2). Several studies have been published on the suitability of using these materials (iron ore, ilmenite, manganese ore, etc.) in CLC applications [43–48]. Manganese ore is reasonably cheap and has a relatively high reactivity with methane and syngas, but after repeated redox cycles it shows poor mechanical stability [47]. Iron-based materials are most stable at high temperatures but their oxygen carrying capacity is very limited and their reactivity with methane is moderate [47,48]. In general, oxygen carriers with a low oxygen transport capacity require a large amount of active phase in fixed-bed CLC configurations in order to reach a sufficiently high temperature in the oxidation front that allows the generation of power at a high efficiency [26]. However, active contents greater than 60 wt.% can cause a drastic reduction in mechanical stability after multiple redox cycles [4]. Moreover, the extremely low carrying capacity of many iron-based materials makes the CLC operation unfeasible in a single oxidation stage [33]. Therefore, the use of low-cost carriers in fixed-bed CLC systems requires a substantial effort to find appropriate heat management strategies for this technology to be feasible on a large scale. Ilmenite is a common mineral found in metamorphic and igneous rocks that is mainly composed of iron and titanium oxides. The reduced form of ilmenite in CLC applications is $FeTiO_3$, whereas the most oxidized form is Fe_2TiO_5. Of all the natural materials studied for CLC, ilmenite is one of the most attractive options because of its low price (around 0.3 $/kg) [49], its reasonably effective oxygen transport capacity (up to 0.05 kg/kg), its good chemical and mechanical stability at temperatures up to 1200 °C and its poor tendency towards carbon deposition during the reduction stage [43]. Although ilmenite reacts rapidly with CO and H_2, several works have demonstrated that it allows a moderate conversion of CH_4 to CO_2 and H_2O [43,48,50]. A previous calcination [45] and the addition of a small amount of Ni (lower than 5 wt.%) [51,52] to the ilmenite have been proposed in the literature as a way to improve its reactivity with methane in order to achieve combustion efficiencies close to 100%.

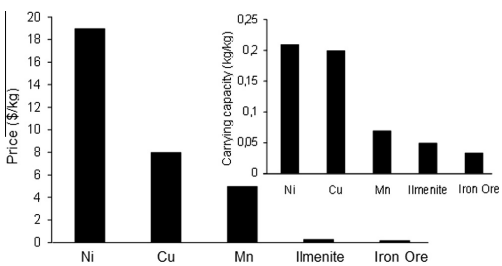

Fig. 2. Approximate cost and carrying capacity of the main oxygen carriers used in chemical looping combustion.

This study proposes a fixed-bed process scheme as a valid alternative to carry out the chemical looping combustion of methane using ilmenite as oxygen carrier. We outline a heat management strategy in which the gradients of temperature at the different reaction stages are controlled by suitable gas recycles. Moreover, a steam reforming stage is incorporated to the system as a source of syngas that promotes the reduction kinetics of ilmenite and enhances the combustion efficiency of the overall process. The process design proposed envisages a compact system with a minimum number of reactors able to carry out the entire synchronized operation.

2. Reactor design and process description

The process proposed in this work requires a system of fixed-bed reactors dynamically operated in order to produce a continuous gas stream at a sufficiently high temperature and pressure to efficiently drive a gas turbine for power generation. Only two reaction stages are not sufficient to complete this novel CLC configuration because the conditions at the end of one stage (especially in terms of temperature profiles) do not satisfactorily meet the requirements to carry out the next stage. Additional stages are needed between the oxidation and reduction steps in order to accommodate the temperature of the solids and gases present in the process, to carry out the reactions involved and fulfil the energy requirements of the process.

A basic reactor model is adopted to represent the performance of the fixed-beds in each stage of the process. Reaction rates are assumed to be sufficiently fast to take place in narrow reaction fronts that move forward as the oxygen carrier is converted. Moreover, an ideal plug flow pattern and negligible axial gas dispersion are considered to approximately represent the cyclic operation of the CLC system. Relatively high gas velocities are required in each stage of the CLC process to maximize the reactor capacities per unit

of cross sectional area, which will lead to a high turbulent regime and therefore high heat transfer coefficients between gas and solids. Sharp reaction and heat transfer fronts moving along a fixed-bed reactor, that are typical of many fixed-bed catalytic systems [53–55], have also been adopted to describe the performance of dynamically operated fixed-bed systems in CLC [26,27,36,56] and sorption enhanced reforming applications [35,56–58]. Recent works about CLC in fixed beds [31,34] have given experimental evidences about the formation of sharp temperature profiles during the operation, which confirm that the assumption of plug flow with very low axial dispersion is perfectly realistic. Heat exchange fronts are formed when the process is not thermally neutral and/or when the temperatures of the gases and solids in contact are different. Both the reaction fronts and heat exchange fronts advance during the operation at different velocities (u_r and u_e, respectively), that can be estimated by solving the heat balances in each front, Eqs. (4) and (5) in Table 1. The variation of temperature in the reaction front (ΔT_{max}) can be calculated from Eq. (2) assuming that heat (released or consumed depending on whether the reaction is exothermic or endothermic, respectively) is taken by or from the solids when the gas reacts with them [26]. The reactor model equations considered in this work are listed in Table 1.

Fig. 3 shows the fixed-bed CLC process proposed in this work. Assuming an intense heat transfer between the gases and solids, the temperature of the gases and solids will be similar at any point of the beds, and therefore, the dynamic behaviour of each stage of the process can be represented by using a single axial temperature profile. A base case with a reference inlet flow of 10 kg/s of methane (equivalent to 500 MWt), stream 1 in Fig. 3, is examined to show the feasibility of this CLC process on a large scale. An ilmenite-based oxygen carrier with an active content of about 35 wt.% has been chosen as being an intermediate value for the ilmenite contents of most oxygen carriers studied in the literature for CLC applications [43–45]. Around 5 wt.% of Ni in the packed-bed composition is assumed in order to promote ilmenite reactivity and allow a steam reforming stage. The contribution of the Ni-based material in the mass and heat balances is assumed to be negligible at every stage of the CLC process.

A maximum temperature of 1200 °C is assumed in order to maintain the chemical and mechanical stability of the carrier after multiple redox cycles [43–45]. An operating pressure of about 20 bar has been selected in order to achieve the highest energy efficiency in the downstream gas turbine [21]. At the beginning, the fixed beds are assumed to contain the oxygen carrier in its reduced form. A certain amount of energy must be spent to heat the solids up to a minimum temperature of about 550 °C. At this temperature, the oxidation of the ilmenite can be initiated by feeding in pressurized air. During this first oxidation stage, the exothermicity of this reaction and the suitable recirculation of part of the product gas will make most of the bed achieve a very high temperature. In a subsequent heat removal stage, part of the heat will be blown out of the bed, leaving a fraction of the solids at the maximum temperature, which is needed to carry out effectively the next reduction stage, as explained below. The temperature profiles obtained from

Table 1
Equations used in the model.

Energy balance	$\frac{\rho_g u_g x_g}{M_g}(-\Delta H_r) = \varepsilon \rho_s c_{p,s}(u_r - u_e)(T_{max} - T_0)$	(1)
Variation of temperature in the reaction front	$\Delta T_{max} = \frac{-\Delta H_r}{\frac{c_{pg} M_g}{x_g \varphi} - \frac{c_{pg} M_g}{x_g}}$	(2)
Maximum temperature	$T_{max} = T_{s0} + \Delta T_{max}$	(3)
Velocity of reaction front	$u_r = \frac{\rho_g u_g x_g M_s}{\varepsilon \rho_s x_s M_g \varphi}$	(4)
Velocity of heat exchange front	$u_e = \frac{\rho_g u_g c_{pg}}{\varepsilon \rho_s c_{p,s}}$	(5)

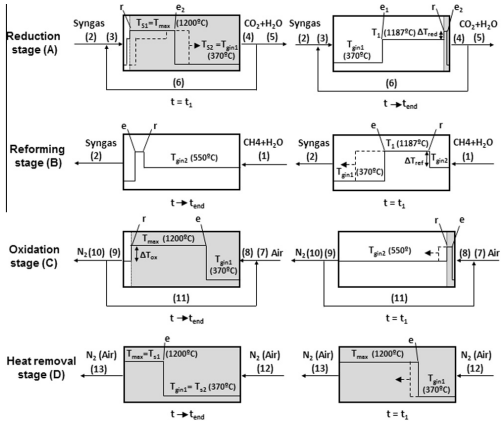

Fig. 3. Evolution of the temperature profiles during the stages of the proposed fixed-bed CLC process (*r*, reaction front; e_i, heat exchange front; white zone, reduced oxygen carrier; grey zone, oxidized oxygen carrier). The temperatures achieved for the reference case study are indicated in brackets.

Table 2
Input operating conditions and reactor characteristics for the reference case study.

Parameters	Values
Inlet CH_4 mass flow (kg/s)	10
Pressure (bar)	20
Inlet gas temperature (°C)	370
Ilmenite content (wt.%)	35
Ni content (wt.%)	5
Particle size (m)	0.005
Bed porosity	0.5
Bed bulk density (kg/m^3)	1950
$\Delta H_{red\_H_2}$ (kJ/mol)	10.5
ΔH_{red_CO} (kJ/mol)	−12.2
$\Delta H_{red\_CH_4}$ (kJ/mol)	95.4
ΔH_{ox} (kJ/mol)	−440.2
ΔH_{ref} (kJ/mol)	193.4

the model correspond to a cyclic steady state, which is assumed to be achieved after a few initial cycles. Table 2 summarizes the input operating conditions chosen for the case study and Table 3 indicates the temperature, flow rate and composition of the gas streams obtained by solving the mass and heat balances at each stage of the CLC process.

2.1. Reduction stage

At the beginning of the reduction stage (stage A in Fig. 3), it is assumed that the active phase of the ilmenite-based oxygen carrier is completely oxidized (Fe_2TiO_5) and that the bed is divided into two parts at different temperatures, as a result of the preceding stage explained below. A part of the packed bed is at 1200 °C (T_{s1} in Fig. 3), while the rest of the solids are at 370 °C (T_{s2} in Fig. 3). A stream of syngas (stream 2 in Fig. 3) of about 2.4 kmol/s is fed in at the part of the bed that is at 1200 °C, which is a sufficiently high temperature to ensure the fast and complete oxidation of the syngas to CO_2 and steam from the very beginning of the process [43–45]. The syngas, which is mainly composed of H_2 (73 vol.%) and CO (24 vol.%), is obtained from a subsequent steam methane reforming stage (B) that is described below. It is assumed that the Fe_2TiO_5 contained in the bed is reduced to $FeTiO_3$ during stage (A) and that there is no total reduction to $FeTiO_2$ (Fe + TiO_2).

Table 3
Estimated temperatures, flow rates and compositions of the gas streams involved in each stage of the CLC process for the operating conditions listed in Table 2.

Streams	1	2	3	4	5	6	7	8	9	10	11	12	13
T (°C)	550	370	370	370	370	370	370	370	550	550	370	370	1200
Flow (kmol/s)	1.25	2.42	4.0	4.10	2.50	1.58	5.94	7.84	6.59	4.69	1.90	13.21	13.21
Composition (vol.%)													
CH_4	50	2	1	–	–	–	–	–	–	–	–	–	–
CO	–	24	15	–	–	–	–	–	–	–	–	–	–
H_2	–	72	44	–	–	–	–	–	–	–	–	–	–
CO_2	–	–	10	25	25	25	–	–	–	–	–	–	–
H_2O	50	2	30	75	75	75	–	–	–	–	–	–	–
N_2	–	–	–	–	–	–	79	84	100	100	100	100	100
O_2	–	–	–	–	–	–	21	16	–	–	–	–	–

The presence of pure Fe would reduce the selectivity of syngas to CO_2 and steam, resulting in a higher carbon slip and therefore a lower CO_2 capture efficiency. Moreover, the formation of pure Fe would cause the partial deactivation of the oxygen carrier because Fe tends to agglomerate at the usual temperatures of CLC [32]. Side reactions of the syngas during the reduction stage (carbon deposition by the Boudouard reaction and WSG) are assumed to be negligible. When the syngas comes into contact with oxidized solids, it rapidly reacts to form a narrow reduction front (r) that will move forward at a velocity (u_r) (indicated in Fig. 3 as the transition between the white and grey zones). For the syngas composition of this reference case the reduction of the ilmenite is slightly endothermic, and therefore, a small drop in temperature (ΔT_{red} in Fig. 3) is produced at the reduction front. This value can be calculated from Eq. (2) in Table 1. As the stage starts with the solids bed being at two different temperatures (T_{s1} and T_{s2}) and the syngas is also fed in at another temperature ($T_{gin,1}$), two heat exchange fronts (e_1) and (e_2) are formed, and they move forward at velocities (u_{e1}) and (u_{e2}), respectively. Under the conditions chosen for the reduction stage (A), Eqs. (4) and (5) predict the reduction front moves forward faster than the heat exchange fronts ($u_r/u_e > 1$), and consequently, a heat plateau (at T_1) forms in the bed. In this situation, the syngas arrives at the reaction front already preheated by the reduced solids, which in turn have been cooled down from T_{s1} to T_1 because of the heat consumed in the endothermic reduction of the ilmenite with the syngas. Downstream of the reduction front (r), the intense heat transfer between gases and solids causes the product gas to be emitted at the initial temperature of the solids located near the reactor exit (T_{s2} = 370 °C). In the conditions listed in Table 2, a product gas (stream 5 in Fig. 3) of around 2.5 kmol/s is emitted during stage (A), which is composed of 75 vol.% of H_2O and 25 vol.% of CO_2.

The recirculation of a part of the product gas (stream 6 in Fig. 3) will increase the flow rate into the reduction stage (stream 3 in Fig. 3), which will accelerate the advance of the heat exchange fronts (e_1 and e_2) along the bed (bringing u_r/u_e closer to 1). Moreover, the presence of a large amount of steam and CO_2 in the feed will prevent carbon deposition and the over-reduction of Fe_2TiO_5 to pure Fe will be kept to a minimum during stage (A) [32]. The recirculation of gas can be designed in a manner such that both the reaction front (r) and the heat exchange front (e_2) reach the reactor exit at the same time. This will allow the reduction stage (A) to be initiated with only a portion of the bed at 1200 °C (T_{s1} in Fig. 3), and therefore, a higher amount of the heat generated in the subsequent oxidation stage (C) can be used for power generation (as explained below). However, the shorter distance between the advance of the reaction front (r) and the heat exchange front (e_1) will cause a higher drop in temperature in the reduction front (ΔT_{red}), because there will be fewer solids at 1200 °C (T_{s1} in Fig. 3) to supply the necessary heat for the endothermic reduction of the ilmenite (see Fig. 3). Furthermore, a reasonable recirculation ratio must be chosen in order to avoid the excessive dilution of the syngas that would lead to a dramatic decrease in the reduction rate. H_2 and/or CO contents lower than 30 vol.% in the feed will significantly reduce ilmenite reactivity [50], and therefore the assumption of narrow reduction fronts during stage (A) would be erroneous. Fig. 4 shows the effect of the recirculation ratio on these variables for the conditions chosen in this case study.

As can be seen in Fig. 4, the recirculation of around 40% of the product gas to the reactor inlet (recirculation ratio of around 0.4) causes the reaction front (r) to advance only 1.7 times faster than the heat exchange front (e_2), predicted by Eqs. (4) and (5) that are listed in Table 1. It will therefore be possible to completely reduce the solids bed by initiating the reduction stage with around 40% of the bed at 1200 °C (T_{s1}) and the remaining 60% of the bed at 370 °C (T_{s2}). Under these conditions, the decrease in temperature in the reduction front will be around 13 °C, Eq. (2), and therefore the reduced solids will be left behind the reaction front at 1187 °C (T_1 in Fig. 3). At this recirculation ratio, the inlet flow rate (stream 3 in Fig. 3) will increase to 4 kmol/s, with a composition of 43 vol.% of H_2 and 14 vol.% of CO. Once the solids bed has been completely reduced ($t = t_{end}$ in Fig. 3), the part of the bed that has been traversed by all the fronts will be left at the temperature of the inlet gas (370 °C). This section of the bed is around 60 wt.% for the conditions of the reference case and a recirculation ratio of 0.4. The rest of the bed (around 40 wt.%) will remain at 1187 °C (T_1 in Fig. 2).

2.2. Reforming stage

Since the oxidation of ilmenite with air is moderately exothermic, the fact that much of the bed is initially at a very high temperature (1187 °C) may cause the temperature to rise above the maximum allowable value during the oxidation stage, which would have a negative effect on the properties of the oxygen carrier [32]. We therefore propose for this study the addition of a steam reforming stage (B), which would allow the solids bed to cool down to a suitable temperature before the next oxidation stage (C) begins. The excess of sensible heat stored in the solids after the reduction step is used to convert the inlet flow of methane and steam (stream 1 in Fig. 3) fed into the system into a product gas (stream 2) that contains a large amount of H_2 and CO. This stream (2) can then be used as reducing gas in stage (A), which will enhance the kinetics of the reduction of Fe_2TiO_5 to $FeTiO_3$, while ensuring at the same time the total conversion of the syngas to CO_2 and steam. As mentioned above, the reactivity of ilmenite with methane is slower, even at very high temperatures and gives a moderate conversion to CO_2 and H_2O, resulting a carbon slip during the reduction stage. A flow of methane of about 0.625 kmol/s (10 kg/s of CH_4) with steam is supplied at 550 °C (T_{gin2} in Fig. 3) and 20 bar to stage (B) through the part of the reactor where the solids are at the highest temperature, 1187 °C (T_1 in Fig. 3). Under these conditions, the steam methane reforming reaction (SMR) will be favoured [59], and therefore, a narrow reaction front will be

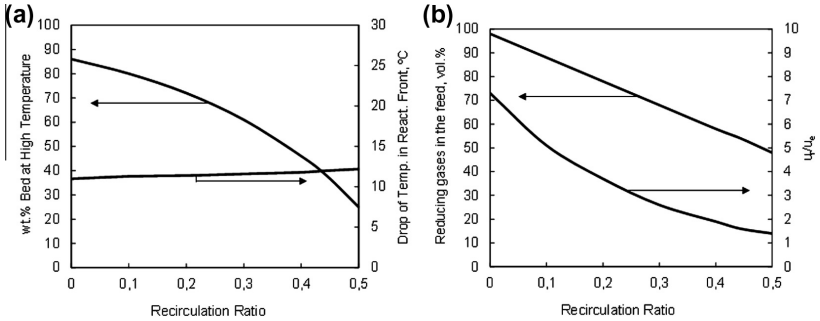

Fig. 4. Effect of the recirculation ratio on: (a) the amount of solids at high temperature initially required for the reduction stage and drop in temperature at the reduction front, (b) the dilution of syngas and the ratio between the reaction and heat exchange front velocity.

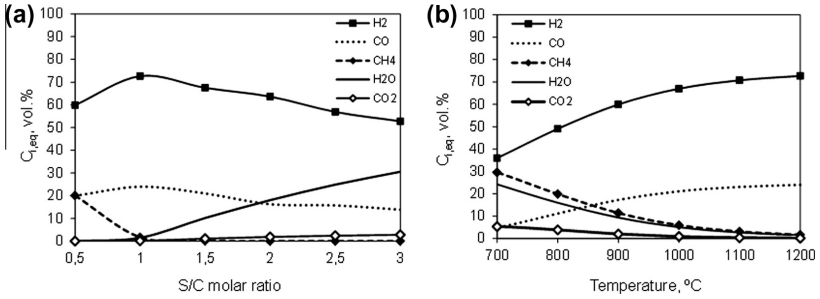

Fig. 5. Equilibrium compositions at 20 bar in steam methane reforming as a function of the *S/C* molar ratio (a) and as a function of the temperature, *S/C* = 1 (b).

formed. Since the reforming reaction is highly endothermic, the solids at the highest temperature will supply the heat needed to maintain the advance of the reaction front (*r*) through the bed, causing a dramatic drop in temperature (ΔT_{ref} = 637 °C in Fig. 3). As the reaction front moves forward, the solids will be left behind at the temperature of the incoming gas, 550 °C (T_{gin2} in Fig. 3). At this temperature, the kinetics of steam methane reforming will be too slow [59,61], and therefore, the conversion of methane to syngas behind the reaction front (*r*) will be negligible.

The composition of the syngas (stream 2) will be determined by the SMR equilibrium at the temperature of the reaction front (1187 °C) and it will strongly depend on the steam-to-carbon (S/C) molar ratio fed into stage (B). As shown in Fig. 5, the S/C molar ratio fed into stage (B) must be around 1 in order to promote the conversion of methane to H_2 (which will accelerate the reduction kinetics of the ilmenite in stage (A) and minimize the consumption of steam in the process. Under the conditions selected for stage (B), the reaction front (*r*) will advance much faster than the heat exchange front (*e*), labelled in Fig. 3 as the transition T_1/T_{gin1}. As a result, the reaction front will catch up with the heat exchange front before it reaches the reactor exit. The syngas produced during stage (B) therefore can be assumed to be discharged at a constant temperature of 370 °C (T_{gin1} in Fig. 3). At the end of stage (B), the entire bed will have cooled down to 550 °C, which is still a sufficiently high temperature to start a rapid oxidation of the ilmenite-based carrier in the following stage (C) [50].

2.3. Oxidation and heat removal stages

Once stage (B) has finished, the subsequent oxidation stage (C) is initiated by feeding in air (stream 7 in Fig. 3), which is supplied by the compressor of the turbine at 20 bar. The air is introduced into the process at 370 °C (T_{gin1} in Fig. 3), as a result of its compression. A flow rate of about 5.9 kmol/s of air (stream 7) is assumed to be sufficient for the complete oxidation of the solids bed in a similar cycle time as that needed for the reaction stages (A) and (B) with only a moderate pressure drop. Given the operating conditions listed in Table 2, the reaction front (*r*) will advance much faster than the heat exchange front (e) and the solids located between both fronts will absorb the heat released in the reaction front, resulting in an increase in their temperature. Under these conditions, the air stream will arrive at the reaction front already preheated by the oxidized solids up to the maximum temperature reached in the reaction front (T_{max} in Fig. 3). This temperature will allow the solids and oxygen to achieve a complete conversion in a narrow reaction front, and consequently, the product gas will contain pure nitrogen (stream 9 in Fig. 3). Meanwhile, the solids that have already been oxidized are left behind at the inlet gas temperature (370 °C). As happened in the previous reaction stages, the fast solid/gas heat transfer will allow the nitrogen produced in stage (C) to be discharged at the temperature of the solids situated closest to the reactor exit (T_{gin2} = 550 °C).

As explained above, ilmenite is an oxygen carrier with a moderate carrying capacity and its oxidation enthalpy is lower than that of other common carriers used in CLC applications, such as Ni or Cu. For the reference case of this work (35 wt.% of active phase in the oxygen carrier), the increase in temperature in the oxidation front (ΔT_{ox} in Fig. 3) can be calculated from Eq. (2) and it will be around 600 °C. Since the temperature of the solids ahead of the reaction front (T_{gin2} in Fig. 3) is 550 °C, the maximum temperature achieved during the oxidation stage (T_{max}) are obtained from Eq. (3) and it will be around 1150 °C, which is lower than the

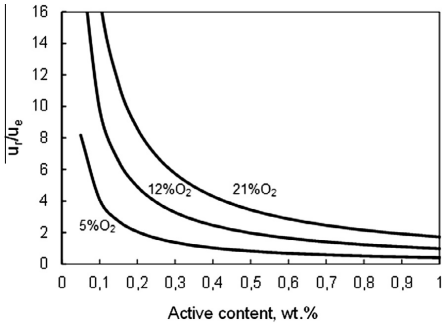

Fig. 6. Reaction and heat exchange front velocity ratio as a function of the ilmenite content in the oxygen carrier and the O_2 content in the feed during the oxidation stage.

maximum limit (1200 °C) that can be reached without the performance of the ilmenite-based material being affected. As a result, the flue gas generated in the subsequent heat removal stage (D) will be sent to the gas turbine at 1150 °C (well below the nominal inlet temperature of modern combined cycles), and therefore, the efficiency of the CLC process will diminish. As can be seen in Fig. 6, the ratio between the reaction and heat exchange front (u_r/u_e) mainly depends on the contents of ilmenite and O_2 in the solids bed and in the gas feed, respectively. The dilution of the O_2 fed into stage (C) will allow the reaction and heat exchange fronts to approach each other (u_r/u_e closer to 1). Consequently, there will be a smaller mass of solids located between them to absorb the heat released from the oxidation reaction, which will cause the temperature in the reaction front to increase. A suitable gas recycle (stream 11 in Fig. 3) in the oxidation stage (C) will permit the desired temperature increase in the oxidation front even in fixed-bed CLC systems that use oxygen carriers with a low carrying capacity and/or low oxidation enthalpy (such as many manganese and iron-based oxygen carriers).

The effect of the recirculation ratio on the increase of temperature in the oxidation front (see Table 1) and on the dilution of O_2 in the feed is illustrated in Fig. 7. For the reference case of this study, a

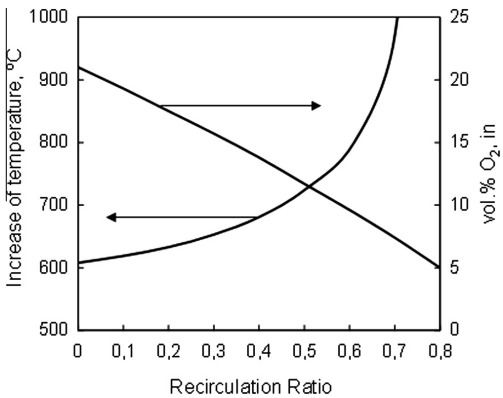

Fig. 7. Influence of the recirculation ratio on the increase in temperature in the oxidation front and on the dilution of O_2 in the feed (in the conditions of the reference case).

recirculation ratio of around 0.3 will increase the inlet flow rate (stream 8 in Fig. 3) up to 7.8 kmol/s, with an O_2 content of around 16 vol.%, which means that the reaction front (r) will advance approximately 4 times faster than the heat exchange front (e), Eqs. (4) and (5). In these conditions, the maximum increase in temperature in the oxidation front, Eq. (2), will be around 650 °C, and therefore, the resulting maximum temperature reached during the oxidation stage will be 1200 °C, Eq. (3). The approach of the reaction and heat exchange fronts during the operation will decrease the amount of bed that is left at the maximum temperature once the oxidation has finished ($t = t_{end}$ in Fig. 3). For a recirculation ratio of about 0.3, the part of the bed that is left at 1200 °C will be around 76 wt.%. The rest of the bed (around 24 wt.%) will remain at 370 °C (T_{gin1} in Fig. 3).

Once the oxidation stage (C) has finished, the heat stored in the solids bed will be removed in a subsequent heat removal stage (D) by a gas flow (stream 12 in Fig. 3), which will be released at 1200 °C and later expanded in a combined cycle for power generation. The inlet gas will be supplied to stage (D) at 20 bar and 370 °C. For this purpose, air from the compressor of the turbine can be used. Another option would be to recirculate and re-compress a large fraction of the exhaust gas (N_2) from the HRSG of the combined cycle, which is a similar operation to the partial recirculation of the flue gas that is employed in NGCC to increase the concentration of CO_2 in the exit gas before it enters postcombustion capture systems [60]. During stage (D), the solids bed will gradually cool down from 1200 °C (T_{max}) to 370 °C (T_{gin1}) as the heat exchange front (e) moves forward. However, not all the heat stored in the bed can be blown out of the reactor for power generation. As explained above, a sufficient amount of bed needs to be left at a very high temperature (T_{s1} in Fig. 3) so that a new reduction stage (A) can be initiated. For the conditions of the reference case, stage (D) will finish when around 40 wt.% of the bed is at 1200 °C and the remaining 60 wt.% of the bed at 370 °C. A flow rate of about 13.2 kmol/s of nitrogen (stream 12) is considered to be necessary to carry out stage (D) for a reasonable cycle duration and pressure drop.

2.4. Process design

The CLC process proposed in this work needs to ensure the production of a continuous stream of nitrogen at high temperature and high pressure for its expansion in a combined cycle. This stream must be generated at a nearly constant temperature and mass flow rate in order to protect the gas turbine expander from thermal and mechanical stress [32]. The number of reactors required for the complete process (following the sequence of four stages explained above) must be kept to a minimum in order to minimize the equipment cost. However, a larger number of reactors may be needed, since the gas flow rates calculated for every stage must be accommodated at reasonable gas velocities in order to avoid excessive pressure drops. Taking into account the operating conditions listed in Table 2 and the inlet flow rates calculated for each stage (see Table 3), a total of five reactors operating in synchronized mode will be required, i.e., one reactor for stage (A), one reactor for stage (B), one reactor for stage (C) and two reactors for stage (D). Very short rinse/purge steps can be introduced to remove traces of unconverted species after the oxidation and reduction stages in order to avoid unwanted reactions during the transition periods. The duration of the purges can be considered negligible in relation to the duration of each stage of the process because from industrial experience only five times the total reactor volume of inert gas will be required for a complete rinse [61]. The operational diagram of the proposed CLC system is represented in Fig. 8, which is similar to other configurations used in sorption enhanced reforming (SER) and other CLC applications [61–64].

Reactor Number					
1	A	B	C	D	D
2	D	A	B	C	D
3	D	D	A	B	C
4	C	D	D	A	B
5	B	C	D	D	A

Fig. 8. Operational diagram of the proposed fixed-bed reactor configuration for the chemical looping combustion of methane using an ilmenite-based carrier with nitrogen recycling (the dotted line represents a snapshot of the process at a specific point in time as shown in Fig. 9).

The overall flow diagram of the proposed CLC configuration (see Fig. 9) comprises elements that are common to conventional natural gas combined cycles (NGCC), such as an air compressor (101), a gas turbine (107), a heat recovery steam generator (HRSG, 108 in Fig. 9) and a compressor (109) for the recirculation (to the oxidation and heat removal stages) of the N_2 discharged downstream of the HRSG. A topping cycle can also be introduced in order to maximize the efficiency of the gas turbine. A small flow of methane and pressurized air can be burned to increase the temperature of the gas sent to the combined cycle up to the optimum value (1400–1450 °C), at the expense of a slightly lower CO_2 capture efficiency [65]. Moreover, additional elements are introduced to ensure optimal performance in each stage of the CLC process. Blowers (102) and (105) are required to re-compress the recycled streams of CO_2 with steam and N_2, respectively. Heat exchangers (100), (103) and (106) are needed to condition the temperature of the inlet feed of methane and the temperature of the inner recycles incorporated into the process.

A valve set-up is necessary to synchronize the operation of the five reactors. For the instant represented in Fig. 8 by a dotted line, valve (9) is open to introduce the methane required to carry out the reforming stage (B), while the valves responsible for feeding air/N_2 into this reactor are closed. Downstream of the reactor that is performing as stage (B), valves (46) and (42) are open in order to allow the syngas produced in (B) to be fed into the reactor that is operating as stage (A). Subsequently, valves (31), (26) and (21) are also open to regulate the fraction of the CO_2 and H_2O produced in stage (A) that is destined for transport and storage and the fraction that is recirculated into the process. Meanwhile, valve (8) is open in order to allow air to be fed into the reactor that is operating as stage (C). Downstream of stage (C), valve (39) is open to allow the recirculation of the N_2 produced during the oxidation. The heat exchanger (106) removes the excess of sensible heat from this stream before it is recompressed (no blowers operate at high

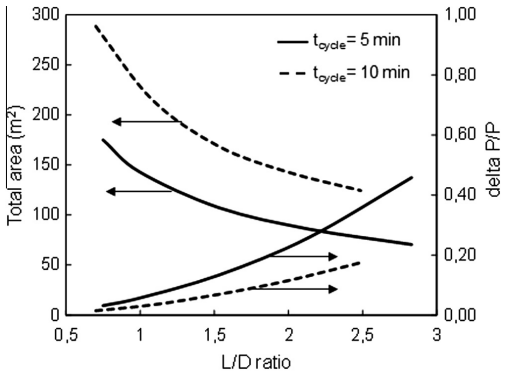

Fig. 10. Effect of cycle duration on the reactor geometry and pressure drop.

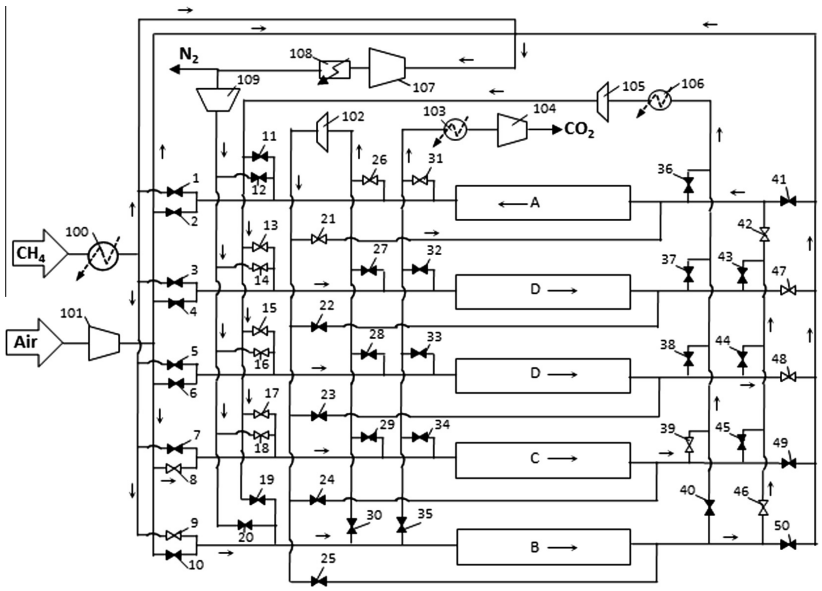

Fig. 9. Process flow diagram of the proposed fixed-bed system for the chemical looping combustion of methane using an ilmenite-based oxygen carrier with nitrogen recycling (white valves are open and black valves are closed for a specific point in time).

temperature in this system). Moreover, valves (13–16) are open to allow the recirculated N_2 to be fed into the reactors that are performing as stage (D). Finally, valves (47) and (48) are open so that the outlet N_2 (that is being discharged from stage (D) at 1200 °C) can be sent to the combined cycle while part of the exhaust N2 is being recirculated to the system via the compressor (109).

The reactor geometry and the duration of a single stage are also defined for the operating conditions listed in Table 2. As mentioned above, the cross-sectional area and the minimum time for accomplishing each single stage must be able to accommodate the inlet gas flows at reasonable gas velocities in order to avoid excessive pressure drops. The effect of the cycle duration on the geometry of the reactor and pressure drop has been studied assuming a maximum inlet flow per stage of 7.8 kmol/s (i.e., the inlet flow calculated for stage C), a pellet size of 0.005 m, a void fraction of 50% and a bed density of 1950 kg/m^3 when the ilmenite-based carrier is completely oxidized.

As can be seen in Fig. 10, shorter cycle durations makes it possible to convert the same amount of gas fed into the system using smaller cross-sectional areas. Larger reactor lengths combined with smaller diameters (i.e. higher L/D ratios) also reduce the total area required. However, these conditions will cause higher pressure drops, resulting in an increase in the energy needed to recompress the gas streams involved in the process. For the operating conditions and reactor characteristics assumed in the reference case, a minimum duration of about 10 min can be considered as a reasonable time for each single stage of the CLC process. Taking into consideration that five reactors are required to fulfil the process, a total cycle time of about 50 min will be needed. Assuming a minimum L/D ratio of about 1.5 and a maximum pressure drop of about 6% in each stage, the full process scheme to convert 10 kg/s of methane fed into the system will require 5 reactors, 10 m long with an inner diameter of 6.7 m (with a total area of around 175 m^2).

3. Conclusions

A fixed-bed process scheme for carrying out the chemical looping combustion of methane using ilmenite as oxygen carrier has been described assuming a set of reasonable operating conditions. The possibility of producing a gas stream at high pressure and at high temperature makes this technology feasible and easy to integrate into a highly efficient natural gas combined cycle. CLC based on fixed-bed reactors are shown to be a competitive mid-term alternative to pressurized fluidized beds, which are handicapped by problems in relation with the circulation of solids at high pressures. However, fixed-bed systems require more complex heat management strategies and high-temperature switching valves that represent a formidable challenge from a technical point of view. A basic reactor model has shown that with reasonable flue gas recycles it is possible to control the advance of reaction and heat exchange fronts, which enhances considerably the heat management of the CLC process. The partial recirculation of the CO_2 and H_2O produced in the reduction stage brings the advance of the fronts closer, which means that the operation can be initiated with a smaller fraction of solids at high temperature. Consequently, a higher proportion of the heat generated during the oxidation stage can be used for power generation in the gas turbine. By means of the same procedure, the recirculation of the nitrogen produced in the oxidation stage under suitable conditions allows the required increase in temperature in the oxidation front to be reached. The partial recirculation of N_2 will dilute the O_2 content in the feed, but at the expense of a higher total gas flow through the reactor. The gas velocity will be then higher, which will accelerate the advance of the heat exchange front, while the velocity of the oxidation front remains unchanged. As a result, the heat exchange front will move closer to the reaction front and therefore, there will be fewer solids between both fronts that can absorb the heat released from the oxidation reaction, which will facilitate the increase in temperature in the oxidation front to 1200 °C, and therefore result in a more efficient generation of power. Moreover, a steam methane reforming stage is incorporated to the system as a source of syngas that will promote the reduction kinetics of the ilmenite, enhancing the combustion efficiency of the process. A preliminary design of this configuration for an inlet flow of 10 kg/s of methane shows that a minimum of five reactors (10 m long with an inner diameter of 6.7 m) operating in cycles of 10 min are required for the successful completion of the process. The results of this study demonstrate the potential of this novel technology for power generation with CO_2 capture, although a substantial effort to experimentally validate the performance of the reactors is required for its development at a large scale. A detailed heat integration of this configuration lies outside the scope of this work, but the absence of process stages with a large energy penalty (apart from the purification and compression of CO_2 as in other capture technologies) is an indication of the high energy efficiency that can be expected of this novel system.

Acknowledgements

This work has been financed through the project ENE2012-37936-C02-02, funded under the R+D Spanish National Program organised by the Spanish Ministry of Economy and Competitiveness.

References

[1] B. Metz, Controlling Climate Change, Cambridge University Press, 2010.
[2] IPCC, Climate change, in: T. Stocker, D. Qin, G. Plattner, M. Tignor, S. Allen, J. Boschung, A. Nauels, Y. Xia, B. Bex, B. Midgley (Eds.), The Physical Science Basis. Contribution of Working Group I to the Fifth Assessment Report of the Intergovernmental Panel on Climate Change, Cambridge University Press, 2013.
[3] M.E. Boot-Handford, J.C. Abanades, E.J. Anthony, M.J. Blunt, S. Brandani, N. Mac Dowell, J.R. Fernandez, M.C. Ferrari, R. Gross, J.P. Hallett, R.S. Haszeldine, P. Heptonstall, A. Lyngfelt, Z. Makuch, E. Mangano, R.T.J. Porter, M. Pourkashanian, G.T. Rochelle, N. Shah, J.G. Yao, P.S. Fennell, Carbon capture and storage update, Energy Environ. Sci. 7 (2014) 130–189.
[4] J. Adanez, A. Abad, F. Garcia-Labiano, P. Gayan, L.F. de Diego, Progress in chemical-looping combustion and reforming technologies, Prog. Energy Combust. Sci. 38 (2012) 215–282.
[5] W.K. Lewis, E.R. Gilliland, W.P. Sweeney, Gasification of carbon – metal oxides in a fluidized powder bed, Chem. Eng. Prog. 57 (1951) 251–257.
[6] M. Ishida, H. Jin, A new advanced power-generation system using chemical-looping combustion, Energy 19 (1994) 415–422.
[7] A. Lyngfelt, B. Leckner, T. Mattisson, A fluidized-bed combustion process with inherent CO_2 separation; application of chemical-looping combustion, Chem. Eng. Sci. 56 (2001) 3101–3113.
[8] M. Ishida, M. Yamamoto, T. Ohba, Experimental results of chemical-looping combustion with $NiO–NiAl_2O_4$ particle circulation at 1200 (degree) C, Energy Convers. Manage. 43 (2002) 1469–1478.
[9] B. Kronberger, A. Lyngfelt, G. Löffler, H. Hofbauer, Design and fluid dynamic analysis of a bench-scale combustion system with CO_2 separation – chemical-looping combustion, Ind. Eng. Chem. Res. 44 (2005) 546–556.
[10] A. Abad, T. Mattisson, A. Lyngfelt, M. Rydén, Chemical-looping combustion in a 300 W continuously operating reactor system using a manganese-based oxygen carrier, Fuel 85 (2006) 1174–1185.
[11] E. Johansson, T. Mattisson, A. Lyngfelt, H. Thunman, A 300 W laboratory reactor system for chemical-looping combustion with particle circulation, Fuel 85 (2006) 1428–1438.
[12] L.F. de Diego, F. García-Labiano, P. Gayán, J. Celaya, M.J. Palacios, J. Adánez, Operation of a 10 kWth chemical-looping combustor during 200 h with a $CuO–Al_2O_3$ oxygen carrier, Fuel 86 (2007) 1036–1045.
[13] C. Linderholm, A. Abad, T. Mattisson, A. Lyngfelt, 160 h of chemical-looping combustion in a 10 kW reactor system with a NiO-based oxygen carrier, Int. J. Greenhouse Gas Control 2 (2008) 520–530.
[14] L.S. Fan, L. Zeng, W. Wang, S. Luo, Chemical looping processes for CO_2 capture and carbonaceous fuel conversion – prospect and opportunity, Energy Environ. Sci. 5 (2012) 7254–7280.
[15] A. Lyngfelt, H. Thunman, Construction and 100 h of operational experience of a 10-kW chemical-looping combustor, in: D.C. Thomas (Ed.), Carbon Dioxide

Capture for Storage in Deep Geologic Formations, Elsevier Science, Amsterdam, pp. 625–645.
[16] J. Adánez, P. Gayán, J. Celaya, L.F. de Diego, F. García-Labiano, A. Abad, Chemical looping combustion in a 10 kWth prototype using a CuO/Al_2O_3 oxygen carrier: effect of operating conditions on methane combustion, Ind. Eng. Chem. Res. 45 (2006) 6075–6080.
[17] C.R. Forero, P. Gayán, L.F. de Diego, A. Abad, F. García-Labiano, J. Adánez, Syngas combustion in a 500 Wth chemical-looping combustion system using an impregnated Cu-based oxygen carrier, Fuel Process. Technol. 90 (2009) 1471–1479.
[18] P. Kolbitsch, J. Bolhàr-Nordenkampf, T. Pröll, H. Hofbauer, Operating experience with chemical looping combustion in a 120 kW dual circulating fluidized bed (DCFB) unit, Int. J. Greenhouse Gas Control 4 (2010) 180–185.
[19] A. Lyngfelt, Oxygen carriers for chemical looping combustion 4000 h of operational experience, Oil Gas Sci. Technol. 66 (2011) 161–172.
[20] S.P. Sit, A. Reed, U. Hohenwarter, V. Horn, K. Marx, T. Proell, Cenovus 10 MW CLC field pilot, Energy Proc. 37 (2013) 671–676.
[21] O. Brandvoll, O. Bolland, Inherent CO_2 capture using chemical looping combustion in a natural gas fired power cycle, J. Eng. Gas Turbines Power 126 (2004) 316–321.
[22] R. Naqvi, O. Bolland, Multi-stage chemical looping combustion (CLC) for combined cycles with CO_2 capture, Int. J. Greenhouse Gas Control 1 (2007) 19–30.
[23] R. Xiao, Q. Song, M. Song, Z. Lu, S. Zhang, L. Shen, Pressurized chemical-looping combustion of coal with an iron ore-based oxygen carrier, Combust. Flame 157 (2010) 1140–1153.
[24] A. Bischi, Ø. Langørgen, I. Saanum, J. Bakken, M. Seljeskog, M. Bysveen, J.X. Morin, O. Bolland, Design study of a 150 kWth double loop circulating fluidized bed reactor system for chemical looping combustion with focus on industrial applicability and pressurization, Int. J. Greenhouse Gas Control 5 (2011) 467–474.
[25] R. Kumar, R. Lyon, J. Cole, Unmixed reforming: a novel autothermal cyclic steam reforming process, in: C.E.L. Grégoire Padró, Francis (Eds.), Adv. Hydrogen Energy, Springer, US, 2002. pp. 31–45.
[26] S. Noorman, M. van Sint Annaland, J.A.M. Kuipers, Packed bed reactor technology for chemical-looping combustion, Ind. Eng. Chem. Res. 46 (2007) 4212–4220.
[27] S. Noorman, F. Gallucci, M. van Sint Annaland, J.A.M. Kuipers, A theoretical investigation of CLC in packed beds. Part 2: Reactor model, Chem. Eng. J. 167 (2011) 369–376.
[28] S. Noorman, F. Gallucci, M. van Sint Annaland, J.A.M. Kuipers, Experimental investigation of a CuO/Al_2O_3 oxygen carrier for chemical-looping combustion, Ind. Eng. Chem. Res. 49 (2010) 9720–9728.
[29] D. Dissanayake, M.P. Rosynek, K.C.C. Kharas, J.H. Lunsford, Partial oxidation of methane to carbon monoxide and hydrogen over a Ni/Al_2O_3 catalyst, J. Catal. 132 (1991) 117–127.
[30] S. Noorman, F. Gallucci, M. van Sint Annaland, J.A.M. Kuipers, A theoretical investigation of CLC in packed beds. Part 1: Particle model, Chem. Eng. J. 167 (2011) 297–307.
[31] S. Noorman, F. Gallucci, M. van Sint Annaland, J.A.M. Kuipers, Experimental investigation of chemical-looping combustion in packed beds: a parametric study, Ind. Eng. Chem. Res. 50 (2011) 1968–1980.
[32] V. Spallina, F. Gallucci, M.C. Romano, P. Chiesa, G. Lozza, M. van Sint Annaland, Investigation of heat management for CLC of syngas in packed bed reactors, Chem. Eng. J. 225 (2013) 174–191.
[33] H.P. Hamers, F. Gallucci, P.D. Cobden, E. Kimballc, M. van Sint Annaland, A novel reactor configuration for packed bed chemical-looping combustion of syngas, Int. J. Greenhouse Gas Control 16 (2013) 1–12.
[34] H.P. Hamers, F. Gallucci, P.D. Cobden, E. Kimball, M. van Sint Annaland, CLC in packed beds using syngas and CuO/Al_2O_3: model description and experimental validation, Appl. Energy 119 (2014) 163–172.
[35] J.R. Fernández, J.C. Abanades, R. Murillo, G. Grasa, Conceptual design of a hydrogen production process from natural gas with CO_2 capture using a Ca–Cu chemical loop, Int. J. Greenhouse Gas Control 6 (2012) 126–141.
[36] J.R. Fernández, J.C. Abanades, Conceptual design of a Ni-based chemical looping combustion process using fixed-beds, Appl. Energy 135 (2014) 309–319.
[37] R. Villa, C. Cristiani, G. Groppi, L. Lietti, P. Forzatti, U. Cornaro, S. Rossini, Ni based mixed oxide materials for CH_4 oxidation under redox cycle conditions, J. Mol. Catal. A: Chem. 204–205 (2003) 637–646.
[38] M. Johansson, T. Mattisson, A. Lyngfelt, Investigation of Fe_2O_3 with $MgAl_2O_4$ for chemical-looping combustion, Ind. Eng. Chem. Res. 43 (2004) 6978–6987.
[39] L.F. de Diego, F. Garcıa-Labiano, J. Adánez, P. Gayán, A. Abad, B.M. Corbella, M.J. Palacios, Development of Cu-based oxygen carriers for chemical-looping combustion, Fuel 83 (2004) 1749–1757.
[40] P. Cho, T. Mattisson, A. Lyngfelt, Comparison of iron-, nickel-, copper- and manganese-based oxygen carriers for chemical-looping combustion, Fuel 83 (2004) 1215–1225.
[41] T. Mattisson, M. Johansson, A. Lyngfelt, The use of NiO as an oxygen carrier in chemical-looping combustion, Fuel 85 (2006) 736–747.
[42] M. Johansson, T. Mattisson, A. Lyngfelt, Investigation of Mn_3O_4 with stabilized ZrO_2 for chemical-looping combustion, Chem. Eng. Res. Des. 84 (2006) 807–818.
[43] H. Leion, A. Lyngfelt, M. Johansson, E. Jerndal, T. Mattisson, The use of ilmenite as an oxygen carrier in chemical-looping combustion, Chem. Eng. Res. Des. 86 (2008) 1017–1026.
[44] H. Leion, T. Mattisson, A. Lyngfelt, Use of ores and industrial products as oxygen carriers in chemical-looping combustion, Energy Fuels 23 (2009) 2307–2315.
[45] J. Adánez, A. Cuadrat, A. Abad, P. Gayán, L.F. de Diego, F. García-Labiano, Ilmenite activation during consecutive redox cycles in chemical-looping combustion, Energy Fuels 24 (2010) 1402–1413.
[46] E. Jerndal, T. Mattisson, I. Thijs, F. Snijkers, A. Lyngfelt, Investigation of $NiO/NiAl_2O_4$ oxygen carriers for chemical-looping combustion produced by spray-drying, Int. J. Greenhouse Gas Control 4 (2010) 23–35.
[47] R. Xiao, L. Chen, C. Saha, S. Zhang, S. Bhattacharya, Pressurized chemical-looping combustion of coal using an iron ore as oxygen carrier in a pilot-scale unit, Int. J. Greenhouse Gas Control 10 (2012) 363–373.
[48] A. Fossdal, E. Bakken, B.A. Øye, C. Schøning, I. Kaus, T. Mokkelbost, Y. Larring, Study of inexpensive oxygen carriers for chemical looping combustion, Int. J. Greenhouse Gas Control 5 (2011) 483–488.
[49] U.S.G. Survey, Mineral Commodity Summaries 2013, U.S. Geological Survey, Reston, VA, 2013.
[50] A. Abad, J. Adánez, A. Cuadrat, F. García-Labiano, P. Gayán, L.F. de Diego, Kinetics of redox reactions of ilmenite for chemical-looping combustion, Chem. Eng. Sci. 66 (2011) 689–702.
[51] M. Johansson, T. Mattisson, A. Lyngfelt, Creating a synergy effect by using mixed oxides of iron- and nickel oxides in the combustion of methane in a chemical-looping combustion reactor, Energy Fuels 20 (2006) 2399–2407.
[52] M. Rydén, M. Johansson, E. Cleverstam, A. Lyngfelt, T. Mattisson, Ilmenite with addition of NiO as oxygen carrier for chemical-looping combustion, Fuel 89 (2010) 3523–3533.
[53] D. Vortmeyer, W. Jahnel, Moving reaction zones in fixed bed reactors under the influence of various parameters, Chem. Eng. Sci. 27 (1972) 1485–1496.
[54] G. Kolios, J. Frauhammer, G. Eigenberger, Autothermal fixed-bed reactor concepts, Chem. Eng. Sci. 55 (2000) 5945–5967.
[55] R.M. Navarro, M.A. Pena, J.L. Fierro, Hydrogen production reactions from carbon feedstocks: fossil fuels and biomass, Chem. Rev. 107 (2007) 3952–3991.
[56] J.R. Fernández, J.C. Abanades, R. Murillo, Modeling of Cu oxidation in adiabatic fixed-bed reactor with N_2 recycling in a Ca/Cu chemical loop, Chem. Eng. J. 232 (2013) 442–452.
[57] J.R. Fernández, J.C. Abanades, R. Murillo, Modeling of sorption enhanced steam methane reforming in an adiabatic fixed bed reactor, Chem. Eng. Sci. 84 (2012) 1–11.
[58] J.R. Fernandez, J.C. Abanades, G. Grasa, Modeling of sorption enhanced steam methane reforming—Part II: Simulation within a novel Ca/Cu chemical loop process for hydrogen production, Chem. Eng. Sci. 84 (2012) 12–20.
[59] J. Xu, G.F. Froment, Methane steam reforming, methanation and water-gas shift: I. Intrinsic kinetics, AIChE J. 35 (1989) 88–96.
[60] K. Jonshagen, N. Sipöcz, M. Genrup, A novel approach of retrofitting a combined cycle with post combustion CO_2 capture, J. Eng. Gas Turbines Power 133 (2010) 011703.
[61] I. Martínez, M.C. Romano, J.R. Fernández, P. Chiesa, R. Murillo, J.C. Abanades, Process design of a hydrogen production plant from natural gas with CO_2 capture based on a novel Ca/Cu chemical loop, Appl. Energy 114 (2014) 192–208.
[62] E.R. van Selow, P.D. Cobden, R.W. van den Brink, J.R. Hufton, A. Wright, Performance of sorption-enhanced water–gas shift as a pre-combustion CO_2 capture technology, Energy Proc. 1 (2009) 689–696.
[63] A.D. Wright, V. White, J.R. Hufton, R. Quinn, P.D. Cobden, E.R. van Selow, CAESAR: development of a SEWGS model for IGCC, Energy Proc. 4 (2011) 1147–1154.
[64] I. Martínez, R. Murillo, G. Grasa, J.R. Fernández, J.C. Abanades, Integrated combined cycle from natural gas with CO_2 capture using a Ca–Cu chemical loop, AIChE J. 59 (2013) 2780–2794.
[65] S. Consonni, G. Lozza, G. Pelliccia, S. Rossini, F. Saviano, Chemical-looping combustion for combined cycles with CO_2 capture, J. Eng. Gas Turbines Power 128 (2006) 525–534.

CAPÍTULO IV

MODELO DE REACTOR PROCESO Ca-Cu

4. MODELO DE REACTOR DEL PROCESO Ca-Cu.

Como se ha explicado en el capítulo II, uno de los objetivos de investigación de esta tesis es llevar a cabo el modelado de la etapa clave y novedosa del proceso Ca-Cu: la calcinación de $CaCO_3$ mediante la reducción simultánea de CuO con un gas combustible. Para ello, se ha resuelto un modelo más elaborado que el explicado en el capítulo anterior aplicado a un reactor de lecho fijo adiabático, que ha permitido estudiar las principales variables de diseño de esta etapa y así determinar condiciones de operación razonables para llevarla a cabo.

Forma parte de este capítulo la publicación II, que se adjunta en la sección 4.2.1, en la que se detallan el modelo de reactor, las condiciones de operación, y se discuten los resultados obtenidos mostrando la influencia de las distintas variables evaluadas.

4.1. Descripción del modelo de reactor desarrollado

Puesto que tanto el CuO como el $CaCO_3$ reaccionan de forma progresiva a lo largo del lecho, se requiere un modelo de reactor dinámico para describir esta operación no estacionaria. Se ha propuesto un modelo de reactor pseudo-homogéneo unidimensional con las siguientes características, comunes a otros modelos aplicados a sistemas de CLC en lechos fijos (Hamers et al., 2014; Noorman et al., 2007):

- Dispersión de materia y energía en la dirección axial
- Gradientes de concentración y temperatura en la dirección radial despreciables
- Gradientes de concentración y temperatura entre partículas despreciables
- Porosidad constante a lo largo del lecho
- Tamaño de partícula uniforme
- Mezcla perfecta de los sólidos en el lecho

Estas suposiciones son razonables operando en condiciones industriales. Las altas velocidades de gas en el interior del reactor a gran escala (alrededor de 3 m/s) implican operar bajo un régimen altamente turbulento, lo que permite una dispersión axial moderada y que los perfiles radiales sean despreciables. Por otro lado, el tamaño de partícula en un reactor industrial ha de ser elevado (entre 5 y 10 mm de diámetro equivalente) para evitar caídas de presión excesivas. Para considerar el efecto de posibles resistencias difusionales a nivel de partícula se han introducido en el modelo

matemático factores de eficacia para las reacciones gas-sólido involucradas en el proceso.

Las reacciones que tienen lugar en esta etapa se muestran en la sección 1.3.3. Los balances de materia y energía, las ecuaciones correspondientes a la dispersión axial y las cinéticas de reacción consideradas, se encuentran detalladas en la Publicación II.

Para la resolución del modelo, se ha creado un código en el programa Matlab donde se incluyen las ecuaciones que definen los balances de materia y de energía, las cinéticas de reacción (suponiendo modelo de núcleo decreciente para cada reacción) y las condiciones de contorno del proceso, obteniendo como resultado los perfiles de concentración y de temperatura para gases y sólidos en la dirección axial con el tiempo. Los detalles de la definición del mismo se encuentran en la Publicación II.

4.2. Principales resultados obtenidos

En primer lugar, se ha empleado el modelo explicado anteriormente para estudiar únicamente la reducción de CuO con H_2 (es decir, sin presencia de $CaCO_3$ en el lecho). El hidrógeno es el gas mayoritario si se lleva a cabo la etapa de reducción/calcinación alimentando como combustible el gas de síntesis generado en una etapa posterior de reformado de metano, o si se emplea como reductor el gas de rechazo obtenido en la etapa de purificación de H_2 aguas abajo del reactor de SER. Diferentes composiciones de H_2 en el gas de entrada y de CuO en el lecho modifican el avance de los frentes de reducción y de intercambio de calor correspondiente, influyendo decisivamente en los perfiles longitudinales de temperatura, puesto que los sólidos que haya entre ambos frentes son los que absorben el calor desprendido de la reacción. Operando con una concentración alta de H_2 en la alimentación (75% en volumen) y un contenido de CuO en el lecho relativamente bajo (15% en masa), el frente de reducción avanza a mayor velocidad que el de intercambio de calor. La gran cantidad de sólido inerte en el lecho permite moderar el incremento de temperatura hasta un valor cercano a 920ºC.

Si se diluye la cantidad de H_2 en la alimentación hasta el 50% vol. manteniendo el mismo caudal total de gas y la misma concentración de Cu en el lecho, el frente de reacción avanza a menor velocidad. Por tanto, los frentes de reducción y de intercambio de calor avanzan a lo largo del lecho más próximos entre sí y por tanto habrá menos sólidos para absorber el calor de reducción. Como resultado la temperatura máxima alcanzada será mayor (alrededor de 950ºC). Si se incrementa la

cantidad de Cu en el lecho (del 15% al 25%), manteniendo la misma composición y flujo de gas con respecto al caso base, el frente de reducción también avanza a menor velocidad. Aunque en este tercer caso la relación de velocidades entre ambos frentes es la misma que en el segundo caso, el incremento de temperatura alcanzado en el frente de reducción es mucho mayor (hasta alrededor de 1120ºC). Esto se debe a que mayores concentraciones de CuO y de H_2 favorecen la cinética de reducción del sólido y por tanto se genera una mayor cantidad de calor por unidad de tiempo.

Una vez estudiada la reducción de CuO por separado, se llevó a cabo el modelo de la reducción/calcinación simultáneas con el fin de estudiar los principales parámetros del proceso: la proporción de $CuO/CaCO_3$ en el lecho, la temperatura inicial de los sólidos y la composición del gas reductor. Como se ha explicado en la sección 1.3.3, debe existir una proporción adecuada entre CuO y $CaCO_3$ en el lecho de forma que se opere bajo condiciones térmicamente neutras, logrando conversiones completas de los sólidos y a la misma vez evitando la formación de puntos calientes en los frentes de reacción que pudiesen conducir a una degradación de los sólidos. Si se emplea H_2 como gas reductor es necesaria una proporción molar $CuO/CaCO_3$ de 1.8 en el lecho para operar de forma neutra. Tal y como se describe en la publicación II, bajo estas condiciones de operación la reducción de CuO tiene lugar en un frente nítido de reacción. La temperatura máxima alcanzada será en torno a 900ºC, lo que permite la calcinación simultánea de $CaCO_3$. Ambos frentes de reacción avanzarán juntos a lo largo del lecho, dejando atrás sólidos completamente convertidos y generando como gas producto vapor de agua y CO_2 procedente de la descomposición del $CaCO_3$. Si se opera con una mayor proporción de CuO habrá un exceso de calor generado en el frente de reducción, y se alcanzarán temperaturas superiores a 900ºC. Si por el contrario se trabaja con defecto de CuO en el lecho, no se generará suficiente calor en el frente de reducción y parte del $CaCO_3$ quedará por detrás sin calcinar.

Para evaluar el efecto de la temperatura de partida del lecho se llevaron a cabo simulaciones con diferentes temperaturas iniciales (entre 500ºC y 800ºC) considerando una composición de sólidos con un ratio $CuO/CaCO_3$ de 1.8 y un gas reductor con el 75% vol. de H_2 (es decir, condiciones para operar de forma neutra en los frentes de reacción). Se realizaron estudios partiendo de un lecho con temperatura uniforme, así como también partiendo de fracciones de lecho a temperaturas diferentes en semejanza a lo que ocurre en condiciones reales del proceso Ca-Cu. El modelo indica que incluso partiendo de temperaturas bajas (en torno a 500ºC), la reducción de CuO tiene lugar de forma rápida y se consigue una conversión completa

del sólido a Cu y del gas a H_2O desde un primer momento. El calor que desprende la reducción de CuO hace que la temperatura del lecho vaya subiendo progresivamente a medida que avanza el frente de reducción a lo largo del reactor. Sin embargo, sólo cuando se alcanzan temperaturas próximas a 850ºC tiene lugar una calcinación efectiva del $CaCO_3$, quedando hasta ese momento gran parte de los sólidos sin calcinar por detrás. De ahí en adelante, ambos frentes de reducción y de calcinación avanzan juntos hasta el final del reactor convirtiendo completamente los sólidos presentes en esa parte del lecho.

La reducción de CuO es exotérmica cuando se lleva a cabo con CH_4, CO, H_2 o una mezcla de ellos. Sin embargo, dependiendo de la proporción de cada uno en el gas reductor, la cantidad de CuO necesaria para lograr la calcinación completa del carbonato de calcio sin aporte externo de energía es diferente. La reducción de CuO con CO es la que presenta mayor entalpía de reacción (-126.9 KJ/molCuO) y por ello se requiere una menor proporción molar $CuO/CaCO_3$ en el lecho (en torno a 1.3). La reducción de CuO con metano es la que presenta menor entalpía de reducción (-44.5 KJ/mol CuO) y por eso es el caso que requiere una mayor proporción de $CuO/CaCO_3$ en el reactor (3.1). Por este motivo, el uso de un gas de síntesis o el rechazo de la PSA como gases reductores es preferible, ya que se reduce sustancialmente la cantidad de CuO requerida para llevar a cabo la calcinación. Estas consideraciones teóricas han sido corroboradas con los resultados obtenidos en las simulaciones llevadas a cabo en la publicación II con CH_4, CO y H_2.

4.2.1. Publicación II

$CaCO_3$ calcination by the simultaneous reduction of CuO in a Ca/Cu chemical looping process

Publicado en:

Chemical Engineering Science

Volumen 137

Páginas 254-267

Año 2015

Chemical Engineering Science 137 (2015) 254–267

Contents lists available at ScienceDirect

Chemical Engineering Science

journal homepage: www.elsevier.com/locate/ces

$CaCO_3$ calcination by the simultaneous reduction of CuO in a Ca/Cu chemical looping process

J.M Alarcón, J.R. Fernández *

Spanish Research Council, CSIC-INCAR, Instituto Nacional del Carbón, C/Francisco Pintado Fe, 26, 33011 Oviedo, Spain

HIGHLIGHTS

- The reduction of CuO can supply the energy required for $CaCO_3$ calcination in a same bed.
- A dynamic model predicts the evolution of the reaction and heat exchange fronts.
- Calcination modifies the advance of the heat exchange front.
- Changes in Cu/Ca ratio and in fuel composition have a substantial effect on bed performance.

ARTICLE INFO

Article history:
Received 26 February 2015
Received in revised form
8 May 2015
Accepted 6 June 2015
Available online 2 July 2015

Keywords:
CO_2 capture
$CaCO_3$ calcination
CuO reduction
Chemical looping combustion
Adiabatic fixed bed

ABSTRACT

The exothermic reduction of CuO to Cu using a fuel gas as a source of heat to carry out the simultaneous calcination of $CaCO_3$ in a fixed bed is evaluated. The absence of apparent large energy penalties, as in other chemical looping processes, is an indication that there is great potential for achieving a high level of energy efficiency with this Ca/Cu looping concept. A dynamic pseudo-homogeneous model has been developed to describe in detail the transient behavior of this operation in a fixed-bed reactor under adiabatic conditions. A sensitivity analysis of the main operating parameters (i.e. the $CuO/CaCO_3$ molar ratio, starting temperature and fuel gas composition) confirms the theoretical viability of this operation. A balanced $CuO/CaCO_3$ ratio ensures a suitable bed performance allowing the reduction and calcination fronts to advance together, reach moderate maximum temperatures of around 900 °C and leave behind totally converted solids. The use of CO as fuel gas significantly reduces the $CuO/CaCO_3$ ratio required for the $CaCO_3$ calcination. A careful adjustment to bed composition must be carried out, since an excess of CuO in the bed will generate more heat than required for the calcination, and consequently hot spots higher than 1000 °C will form along the bed. In contrast, an excess of $CaCO_3$ will increase the energy demand and part of the bed will be left uncalcined.

1. Introduction

The increase in carbon dioxide emissions related to human activities is extensively recognized as one of the most important causes of climate change. The consumption of fossil fuels for power generation is expected to rise due to an increment in the world energy demand in the coming years and therefore, there is an urgent need to reduce greenhouse gas emissions from anthropogenic sources (Metz, 2010; Metz et al., 2005). Carbon capture and storage (CCS) has been proposed as a feasible mid-term solution to drastically reduce CO_2 emissions (Stocker et al., 2013). For the implementation of CCS in a process, the CO_2 capture step is the most energy intense, accounting for about 75% of the overall CCS costs (Feron and Hendriks, 2005). For this reason, there is a growing interest in developing new CO_2 capture technologies in order to minimize the energy penalties and the costs associated with existing equipment (Boot-Handford et al., 2014).

Hydrogen, which is an important raw material in the chemical and petroleum industries, can also be considered as the most promising clean source of energy. Steam reforming of methane (SR) is still the most common hydrogen production method in commercial use (Rostrup-Nielsen, 2009). Steam reforming that must be carried out in multiple steps and severe operating conditions, consumes high amounts of energy because of the high endothermicity of the overall reaction. Combining reaction with separation in order to simplify the process, enhance efficiency and improve the hydrogen yield has gained in importance in recent years. In the sorption enhanced reforming (SER), the CaO-based material present in the reformer removes the CO_2 as soon as it is produced, shifting the equilibrium to the formation of H_2,

* Corresponding author. Tel.: +34 985119090; fax: +34 985297662.
E-mail address: jramon@incar.csic.es (J.R. Fernández).

http://dx.doi.org/10.1016/j.ces.2015.06.030
0009-2509/

according to Le Chatelier's principle. As a result, an almost complete conversion of methane and CO and a higher H_2 yield can be achieved under relatively mild conditions of pressure and temperature (Harrison, 2008). The carbonation of the CaO-sorbent is strongly exothermic and provides in situ the energy required to accomplish the reforming reaction. Therefore, no external heating is required by the reforming process. However, $CaCO_3$ formed by the CO_2 removal reaction must be subsequently regenerated by calcination to allow multicycle operation in the SER process. This regeneration is highly endothermic and needs to be performed under a CO_2-rich atmosphere if the process is aimed at zero CO_2 emissions. Several alternatives have been proposed in the literature as a means of providing the heat required for the calcination of $CaCO_3$. These mainly include oxy-fuel combustion in a regenerator (Martínez et al., 2013b; Weimer et al., 2008; Wolf and Yan, 2005), indirect heating by hot solids (Wolf and Yan, 2005) or by hot gases (Johnsen et al., 2006; Li and Cai, 2007; Stevens et al., 2007) obtained from additional fuel combustion, or the use of the waste heat from a fuel cell coupled to the SER process (Boshu et al., 2008; Meyer et al., 2011).

In order to attain a high energy efficiency and reduce the equipment cost, a Ca–Cu chemical looping process was recently proposed (Abanades et al., 2010; Fernández et al., 2012b), which is based on the "unmixed combustion" concept (Kumar et al., 2002). In this process, the heat needed for calcination is supplied by the exothermic reduction of CuO with CH_4, CO or H_2. The Ca–Cu process consists of a sequence of five stages (see Fig. 1), that are carried out in adiabatic fixed-bed reactors, where the temperature and pressure are modified to enhance H_2 production while a CO_2-rich stream is obtained suitable for transport and storage. Several reactors operating in parallel are required to carry out every stage simultaneously. A valve set-up will synchronize the operation of each reactor in order to obtained continuous flows of H_2 in the SER stage, high temperature gas in the oxidation stage able to drive a gas turbine for power generation, and a concentrated stream of CO_2 in the reduction/calcination stage. Previous works have demonstrated the feasibility of this novel concept for hydrogen production (Martínez et al., 2014) and for power generation (Martínez et al., 2013a) with moderate efficiency penalties.

The first stage of the process (step A in Fig. 1) comprises the production of a hydrogen-rich stream by means of the sorption enhanced reforming of CH_4 with steam and the simultaneous carbonation of the CaO with the CO_2 generated in the reforming reaction. High pressures in the range of 15–35 atm, steam to carbon ratios of around 3–5 and temperatures of around 700 °C are required to achieve a good balance between the H_2 production yield and capture efficiency (Fernandez et al., 2012; Fernández et al., 2012a). In the next reaction step (stage B), the oxidation of Cu to CuO is carried out by feeding in pressurized diluted air under conditions of minimal decomposition of the $CaCO_3$ formed during step A (temperatures lower than 830 °C). A low oxygen content in the feed and a low inlet gas temperature allow the maximum temperature in the oxidation front to be controlled (Fernandez et al., 2014; Fernández et al., 2013). Since the oxidation front moves behind the heat exchange front during the oxidation of Cu, at the end of stage B, the solids bed is left at a sufficiently low temperature to initiate the subsequent reduction of CuO with a fuel gas. For this reason, it is necessary to include an additional heat exchange step (B′ in Fig. 1) to raise the temperature of the oxidized bed to a value that allows the reduction of CuO by extracting the excess sensible heat from the portion of the product gas that must be recirculated to perform the stage B. The stage C involves the regeneration of the $CaCO_3$ formed in stage A by means of the reduction of the CuO produced in stage B. With a suitable $CuO/CaCO_3$ molar ratio, the heat generated in the reduction of CuO will provide the energy required to carry out the endothermic $CaCO_3$ calcination without the need for an additional energy supply (Fernández et al., 2012b). The operating pressure must decrease to atmospheric pressure to facilitate calcination at reasonable temperatures (around 900 °C). Once calcination is completed, most of the solids are left at around 900 °C, which is a too high temperature for an optimal performance of another SER stage, as pointed out above. In the final stage C′, a steam methane reforming process is carried out by using part of the sensible heat of the solids and leaving the bed at a suitable temperature for the SER operation. Moreover, a stream mainly composed of CO and H_2, will be produced, that can be used in stage C to reduce the $CuO/CaCO_3$ molar ratio required and also to accelerate the reduction of CuO to Cu (Fernández et al., 2012b).

The main objective of the present work is to simulate in detail the calcination of $CaCO_3$ by the simultaneous reduction of CuO in an adiabatic fixed-bed reactor. A dynamic model that incorporates existing knowledge on kinetics and basic assumptions about gas flow and heat transfer has been developed in order to study the effect of the key design variables on this operation, such as the $CuO/CaCO_3$ molar ratio, the starting temperature and the composition of the inlet gas. This work is essentially focused on the boundary conditions of the Ca–Cu looping process, but some of the

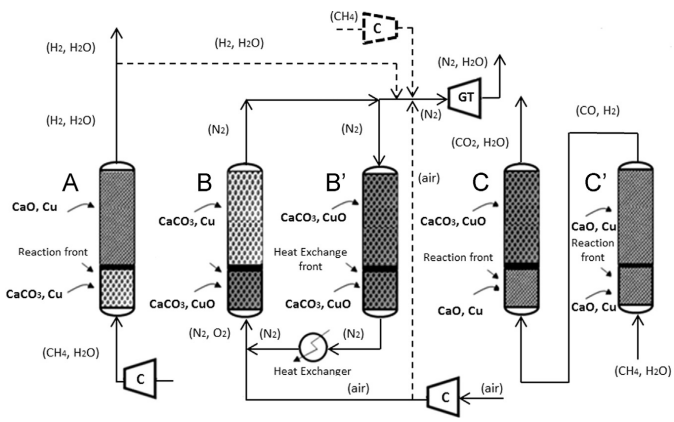

Fig. 1. Scheme of the Ca/Cu looping process for power generation and/or hydrogen production using CH_4 as energy source (Fernández et al., 2012b).

observed trends may be valid for other calcium looping systems that use a second chemical loop to carry out the calcination step.

2. Mathematical model description

A pseudo-homogenous model was developed to describe the progressive reduction of CuO with a fuel gas and the simultaneous decomposition of $CaCO_3$ in an adiabatic fixed bed. A dynamic model was employed to describe this process, since CuO and $CaCO_3$ are gradually converted during the course of the stage C of the process. The following assumptions were adopted: mass and thermal dispersion in the axial direction, negligible radial temperature and concentration gradients, negligible intra-particle mass and temperature gradients, ideal gas behavior, a constant bed void fraction, a uniform particle size in the bed and a perfect mixing of the solids. At industrial scale, these assumptions may be considered quite reasonable. The high velocities expected (around 3 m/s) will allow the reactor to perform with a high turbulent flow, and therefore, there will be moderate axial dispersion throughout the reactor and negligible radial gradients (Fernández et al., 2012a, 2013). The principal chemical reactions that take place in the reduction/calcination stage C under the boundary conditions of a Ca–Cu looping process are as follows:

$$CuO\ (s)+H_2\ (g)\rightarrow Cu\ (s)+H_2O\ (g)\ \Delta H_{298\ K}=-85.8\ kJ/mol \quad (I)$$

$$CuO\ (s)+CO\ (g)\rightarrow Cu\ (s)+CO_2\ (g)\ \Delta H_{298\ K}=-126.9\ kJ/mol \quad (II)$$

$$4CuO\ (s)+CH_4\ (g)\rightarrow 4Cu\ (s)+CO_2\ (g)+2H_2O(g)\ \Delta H_{298\ K}=-44.5\ kJ/mol \quad (III)$$

$$CaCO_3\ (s)\rightarrow CaO\ (s)+CO_2\ (g)\ \Delta(_{298\ K}=-178.8\ kJ/mol \quad (IV)$$

Furthermore, it is assumed that the fuel gas is fully converted to CO_2 and H_2O, which means that carbon deposition is negligible. The literature on chemical looping combustion with Cu-based materials supports this affirmation, since no carbon deposition has been found during the reduction of CuO with a syngas, specially, in the presence of large amounts of steam in the feed (Abad et al., 2010; de Diego et al., 2004; Hamers et al., 2014; Mattisson et al., 2003). Moreover, the presence of calcium avoids carbon formation, even at high temperatures (Bellido et al., 2009; Choudhary et al., 1998). An overview of the mass and energy balances is given in Table 1. The axial mass and heat dispersion coefficients are calculated by the equations listed in Table 2.

Table 3 summarizes the set of operating conditions and reactor characteristics chosen for this study. A reference inlet flow of 1000 mol/s for the reduction/calcination stage has been assumed, which is equivalent to the flow required in the stage C of a Ca–Cu looping process of 500 MW (10 kg/s of CH_4 in the SER stage) (Fernández et al., 2012a). The reactor geometry (i.e., 8 m length and 5.3 inner diameter) has been defined for the operating conditions listed in Table 3 and assuming a minimum L/D ratio of about 1.5 and a maximum pressure drop of about 6% in the stage, which are usual design constraints in packed-bed reactors for CLC applications (Fernández and Abanades, 2014; Fernández and Alarcón, 2015; Spallina et al., 2014).

A shrinking core model (SCM) with cylindrical geometry was employed to represent the kinetics of CuO reduction, which is a generally accepted model in the literature for CLC applications. Although a more elaborate model has recently been published (Chuang et al., 2010), the kinetics model obtained by García-Labiano et al. (2004) was selected for its simplicity and its accuracy in the range of the operating conditions assumed in this study. The kinetic parameters considered in this work are listed in Table 4. Assuming that the chemical reaction is the main resistance to the global reaction, the equation that describes this model for cylinders is the following, Eq. (1):

$$\frac{t}{\tau}=1-(1-X_{red})^{1/2};\quad \tau=\frac{\rho_{m,CuO}L_{CuO}}{k_{red}C_g^n} \quad (1)$$

where the kinetic constant follows an Arrhenius type dependence with temperature, Eq. (2).

$$k_{red}=k_0e^{\frac{-E_a}{RT}} \quad (2)$$

According to Eqs. (1) and (2), the reduction rate of CuO to Cu can be calculated as follows,

$$r_{red}=\frac{\rho_{CuO}}{M_{CuO}}\frac{1000}{}\frac{dX_{red}}{dt} \quad (3)$$

To describe the calcination kinetics of the calcium carbonate, the shrinking core model proposed by Martínez et al. (2012) was chosen:

$$\frac{dX_{cal}}{dt}=k_{cal}(1-X_{cal})^{2/3}(C_{CO_{2,eq}}-C_{CO_2}) \quad (4)$$

Table 1
Mass and energy balances used in the model.

Component mass balances
$\varepsilon\frac{\partial C_i}{\partial t}=-u_g\frac{\partial C_i}{\partial z}+\frac{\partial}{\partial z}(D_{eff}\frac{\partial C_i}{\partial z})+\eta(1-\varepsilon)r_i$
Energy balance
$((1-\varepsilon)\rho_sC_{ps}+\varepsilon\rho_gC_{pg})\frac{\partial T}{\partial t}=-u_g\rho_gC_{pg}\frac{\partial T}{\partial z}+\frac{\partial}{\partial z}(\lambda_{eff}\frac{\partial T}{\partial z})-\Sigma\eta_i(1-\varepsilon)H_{ri}r_i$
Momentum balance, Ergun equation (Ergun, 1952)
$\frac{dP}{dz}=-150\frac{u_g(1-\varepsilon)^2}{d_p^2\varepsilon^3}+1.75\frac{u_g^2\rho_g(1-\varepsilon)}{d_p\varepsilon^3}$

Table 2
The axial mass and heat dispersion coefficients.

Axial mass dispersion coefficient
$D_{eff}=\left[\frac{0.73}{R_eS_c}+\frac{0.5}{\varepsilon+\frac{9.7\varepsilon}{R_eS_c}}\right]u_gd_p$ (Edwards and Richardson, 1968)
Effective axial heat dispersion
$\lambda_{eff}=\lambda_{0bed}+\frac{R_gP_rk_g}{Pe_{az}}+\frac{R_s^2P_r^2k_s^2}{6(1-\varepsilon)N_u}$; (Vortmeyer and Berninger, 1982) where λ_{0bed} is calculated according to (Krupiczka, 1967)
$\lambda_{0bed}=\left(\frac{k_s}{k_g}\right)^{0.28-0.757\log(\varepsilon)-0.057\log\left(\frac{k_s}{k_g}\right)}$
in which Pe_{az} is calculated according to (Gunn and Misbah, 1993)
$Pe_{az}=\frac{2p}{1-p}$; $p=0.17+0.29e^{\left[\frac{-2d}{d_p}\right]}$
Gas-to-particle heat transfer coefficient
$N_u=2+1.8R_e^{0.5}P_r^{0.33}$ (Gunn, 1987)

Table 3
Operating conditions and reactor characteristics.

Parameters	Values
Inlet gas temperature, T_{gin}	700 °C
Initial solids temperature, T_{s0}	700 °C
Pressure, P	1 atm
Inlet molar flow velocity	1000 mol s^{-1}
effectiveness factor (reduction) η_{red}	0.8
effectiveness factor (calcination) η_{calc}	1
Particle size, d_p	0.005 m
Reactor length, L	8 m
Reactor diameter, D_r	5.3 m
Bed porosity, ε	0.5
Bed density, ρ_s	2330 kg m^{-3}

Table 4
Kinetic parameters of the reactions involved in this work.

Parameters	Values
$\rho_{m,\ CuO}$, mol m^{-3}	80,402
L_{CuO}, m	0.4×10^{-9}
$k_{0,H2}$, m s^{-1}	1.0×10^{-4}
$E_{a,H2}$, kJ mol^{-1}	33
$k_{0,CO}$, m s^{-1}	5.9×10^{-6}
$E_{a,CO}$, kJ mol^{-1}	14
$k_{0,CH4}$, m s^{-1}	4.5×10^{-4}
$E_{a,CH4}$, kJ mol^{-1}	60
$k_{0,Cal}$, m^3 mol s^{-1}	252.015
$E_{a,Cal}$, kJ mol^{-1}	91.7

The equilibrium concentration of CO_2 (mol/m^3) can be calculated using Eq. (5) (Baker, 1962).

$$C_{CO_{2,eq}} = \frac{5.045\ x\ 10^{11}}{T} exp\left(\frac{-20.474}{T}\right) \tag{5}$$

The molar rate of CO_2 released per unit volume of sorbent, r_{CO_2}(mol/m^3 s), can be calculated from Eq. (6):

$$r_{cal} = r_{CO_2} = \frac{\rho_{CaCO_3}}{M_{CaCO_3}} \frac{1000}{} \frac{dX_{cal}}{dt} \tag{6}$$

In fixed-bed reactors, where large particles (generally in pellet form) must be used to moderate the pressure drop during the operation, the effect of intraparticle mass-(and heat-) transfer limitations may be considerable. As mentioned above, the reduction/calcination stage performs with a high turbulent flow, and therefore, these effects can be considered negligible. Internal diffusion limitations may also appear, especially as a consequence of Knudsen diffusion (Noorman et al., 2011). However, Cu-based materials undergo important changes in morphology after successive oxidation/reduction cycles carried out at high temperatures (> 700 °C). The average pore size increases, and therefore, the effect of diffusion limitations is partially reduced (Noorman et al., 2010). Nevertheless, since the Ca–Cu looping process on a large scale requires relatively large pellets, an effectiveness factor (η) was included in the model (see Table 1). The value of the effectiveness factor is approximately constant during the reduction of CuO to Cu for a specific particle size, but it can decrease considerably as the solid approaches its total conversion point (Noorman et al., 2011). In this work, an average effectiveness factor of about 0.8 was assumed in order to tackle possible diffusion resistance in the Cu-based particles. This assumption is in agreement with the results recently published on Cu reduction with a syngas for chemical looping applications (Hamers et al., 2014). However, the effectiveness factor for the $CaCO_3$ calcination was assumed to be 1, as the temperature is the main limiting factor in this reaction, being negligible possible diffusional effects.

As shown above, the mathematical model is mainly composed of partial differential equations, algebraic equations, and initial and boundary conditions. The model was implemented and solved by MATLAB programming software. The partial differential equations for each gas component (H_2, CO, CO_2, H_2O) were converted to a set of ordinary differential equations with initial conditions by discretizing the spatial derivative in axial direction (z) using finite differences both for the first and for the second order.

The initial and boundary conditions in the equations listed in Table 1 are as follows:

$$C_i = C_{i,0} \quad T = T_{s_0} \quad \text{at} \quad t = 0$$

$$C_i = C_{i,n} \quad T = T_{g_{in}} \quad P = P_{in} \quad \text{at} \quad z = 0$$

The initial concentrations of the gas species in the reactor should be set to zero. However, in order to avoid errors in the calculation (i.e., denominators equal to zero), these concentrations were actually considered to be equal to 10^{-6} in the MATLAB programme. The system formed by the differential and algebraic equations was simultaneously solved using a MATLAB tool called "ode15s.m", which is a function implemented to calculate initial value problems in stiff differential equations.

3. Dynamic analysis during CuO reduction to Cu in an adiabatic fixed-bed reactor: effect of solids bed and fuel gas compositions on reactor performance

The model described in the previous paragraphs was developed to analyze the dynamic evolution of the concentrations of the gases involved in the process (H_2, CO, CO_2, H_2O), the solids conversion and the temperature with time along the axial direction of a fixed bed reactor. By means of this model and assuming the operating conditions listed in Table 3, it is possible to predict the breakthrough time, which is when the solids (CuO and $CaCO_3$) have been almost completely converted.

First of all, the reduction of CuO to Cu with H_2 (without the presence of $CaCO_3$) was investigated in order to evaluate the effect of the fuel gas composition and the CuO content in the bed on the reactor performance. Fig. 2 shows the dynamic profiles obtained under the operating conditions outlined in Table 3 and for an inlet gas containing 75 vol% H_2 and 25 vol% H_2O, which is fed into a fixed bed with an initial CuO content of 15 wt%. Fig. 2a and c shows that, as the gas stream goes through the bed, the concentration of H_2 decreases rapidly while the solids approach total reduction. A starting temperature of 700 °C allows the rapid and total conversion of the CuO in a narrow reduction front from the very beginning. The temperature of the solids rises due to the exothermic reduction of CuO to Cu with H_2 and a heat plateau at around 920 °C appears in the bed (see Fig. 2d). Because of the low content of CuO in the solids and the high concentration of H_2 in the feed, the reaction front advances faster than the heat exchange front and the solids located between both fronts absorb the heat released by the reduction reaction (Noorman et al., 2007). Under these circumstances, the fuel gas arrives at the reaction front having been already preheated by the reduced solids. Meanwhile, the solids that are left behind are cooled down by the inlet gas to 700 °C (in the heat exchange front). These results confirm the general trends observed in recent works about CLC in fixed beds using Cu-based materials as oxygen carriers (Hamers et al., 2013, 2014). As can be seen in Fig. 2, after approximately 8 min of operation, the reaction front will approach the reactor exit, and therefore, the solids bed will be close to its total conversion. However, at this point, only a small part of the bed will be

traversed by the heat exchange front, which means that most of the solids will still be at the maximum temperature reached by the reduction front (around 920 °C).

As shown in Fig. 3, the reduction stage can be divided into three periods according to the evolution of the outlet temperature and gas composition with time. During the prebreakthrough period ($t < 8$ min), the inlet H_2 is totally converted in the reduction front, and therefore, the product gas is only composed of H_2O. During this period of time, the reaction and heat exchange fronts are still inside the reactor and the product gas is discharged at the temperature of the solids situated closest to the reactor exit (700 °C). When the reduction front approaches the reactor exit, the bed is close to its total conversion (breakthrough), resulting in an increase in the H_2 content in the product gas from 0 vol% to 75 vol%, i.e., its composition in the inlet gas. The temperature profile also increases until it reaches a maximum of around 920 °C. Due to the rapid reduction of CuO with H_2, a very short breakthrough period (around 1 min) is observed. This situation is highly favorable because a high degree of solids conversion may be achieved at the cost of a minimum slip of fuel gas during the reduction operation.

Once the CuO has been completely converted, the heat generated during the reduction stage will remain inside the reactor. During the postbreakthrough period ($t > 9$ min), the inlet gas will remove the stored heat producing a gas stream at a high temperature. While the heat exchange front is relatively far away from the reactor exit (9 min $< t <$ 28 min), the product gas will be discharged at almost constant temperature (around 920 °C), which corresponds to the maximum temperature achieved in the reduction front. As the heat exchange front approaches the reactor exit, the temperature profile will gradually decrease until it reaches the temperature of the inlet gas (700 °C), that is, after approximately 60 min of operation (Fig. 3b).

The effect of key design variables such as the solids bed and fuel gas compositions on reactor performance was also

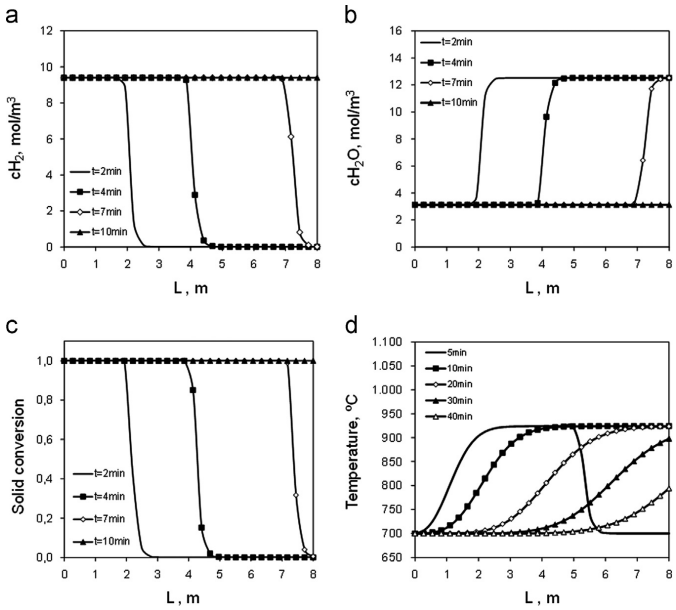

Fig. 2. Dynamic profiles during the reduction of CuO to Cu with H_2 along the bed (15 wt% CuO, 75 vol% H_2): (a) evolution of H_2 concentration; (b) evolution of H_2O concentration; (c) evolution of solids conversion; (d) evolution of temperature.

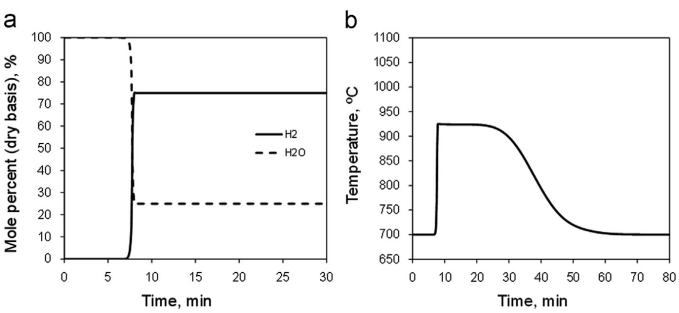

Fig. 3. Product gas composition (a) and temperature (b) evolution of the outlet gas with time during the reduction of CuO with H_2 (15 wt% CuO, 75 vol% H_2).

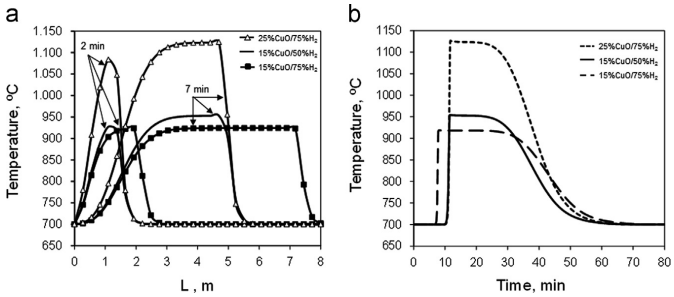

Fig. 4. Effect of solid and inlet gas compositions on temperature profiles during the CuO reduction with H_2: (a) along the bed; (b) at the reactor exit.

investigated. Both parameters decisively affect the advance of the reaction and heat exchange fronts, causing significant changes in the temperature profile and in the duration of the reduction stage. The velocities of both the reaction and heat exchange fronts (u_r and u_e, respectively) can be estimated by solving the mass and heat balances in each front following the expressions formulated by Noorman et al. (2007). Fig. 4 shows the dynamic behavior during the Cu reduction stage for different CuO contents in the bed (15 wt% and 25 wt%) and concentrations of H_2 in the fuel gas (50 vol% and 75 vol%) at the operating conditions summarized in Table 3. Taking as reference case the reduction of a solids bed with a CuO content of 15 wt% with a fuel gas containing 75 vol% H_2 (explained above), the dilution of the H_2 in the feed to 50 vol% will decelerate the advance of the reaction front, extending the duration of the prebreakthrough period from 8 min to approximately 11 min. Since the total gas flow is maintained at 1000 mol/s, the velocity of the heat exchange front through the bed will not change, and therefore, both fronts will approach each other (see Fig. 4a). Consequently, there will be a smaller amount of solids located between them to absorb the heat released from the reduction reaction, which will increase the temperature in the reaction front from 920 °C to 950 °C.

The increase in the CuO content in the bed from 15 to 25 wt% (while maintaining 75 vol% H_2 in the feed) will also make the reaction front advance at a slower velocity, extending the CuO operation to 11 min and increasing the maximum temperature up to 1125 °C. This increase of temperature will be considerably higher than that obtained by operating with 15 wt% CuO and 50 vol% H_2 (see Fig. 4). This effect will happen despite the fact that the ratio of velocities at which the reaction and the heat exchange fronts are moving forward will be similar in both cases (u_r/u_e around 3). The reasons for this increase in temperature during the operation are: (1) the higher contents of H_2 and CuO reacting in the reduction front that will cause a greater release of heat per unit of time, and (2), the higher H_2 content in the feed that will favor the reduction kinetics (García-Labiano et al., 2004).

4. $CaCO_3$ calcination by the simultaneous reduction of CuO with a syngas

4.1. Effect of the Cu/$CaCO_3$ molar ratio on reactor performance

As mentioned above, the reduction of CuO to Cu with a fuel gas can be used to provide the heat required to carry out the calcination of $CaCO_3$ in a same matrix bed. The pseudo-homogeneous model developed in this work was used to study the effect of key design variables, such as the CuO/$CaCO_3$ molar ratio in the bed, operating temperature and composition of the fuel gas, on the dynamic behavior of this system under the boundary conditions of a Ca–Cu looping process. A suitable CuO/$CaCO_3$ ratio is needed to ensure the complete calcination of $CaCO_3$. Moreover, excessive hot spots in the reaction front must be avoided in order to maintain the chemical and mechanical stability of the solids involved in the process (García-Labiano et al., 2004; González et al., 2008). This study has been carried out for the operating conditions and reactor characteristics listed in Table 3 and for a fuel gas containing 75 vol% H_2 and 25 vol% H_2O, that is fed into a fixed bed with a CuO content of 30 wt% and different contents of $CaCO_3$ (from 5 to 30 wt%). The rest of the bed composition is assumed to be inert that acts as a support for both CuO- and Ca-based materials and inert CaO, which is generally present in different proportions in Ca-based sorbents.

When this stage is carried out with a very low content of $CaCO_3$ in the bed (5 wt%), the temperature profiles along the reactor will be very similar to those obtained in a conventional Cu reduction stage without $CaCO_3$ (as described in the previous section). The temperature of the bed will rise due to the exothermic reduction of CuO and a heat plateau at around 1150 °C will form (Fig. 5a). At this temperature, the $CaCO_3$ will be rapidly calcined and from the very beginning of the operation, the product gas will contain H_2O and increasing quantities of CO_2 (given by the equilibrium for the calcination reaction) up to 9 vol% until just before reaching the breakthrough at $t=15$ min (Fig. 5c). Although the contents of CuO and H_2 chosen for this case study theoretically make the reaction front advance faster than the heat exchange front, it can be observed in Fig. 5b, that the temperature of the product gas will gradually rise from 700 °C (initial temperature of the solids closest to the reactor exit) to approximately 750 °C just before the breakthrough. This phenomenon, as explained previously, does not occur in a conventional reduction stage without $CaCO_3$ in the bed, where the temperature of the product gas remains constant during the prebreakthrough period (see Fig. 3b).

As the proportion of $CaCO_3$ in the bed increases (15 wt%), the temperature profiles will change considerably. As can be seen in Fig. 6a, the maximum temperature reached will be significantly lower (around 1000 °C) because a large part of the heat released from the reduction reaction will be used to carry out the calcination of the $CaCO_3$. Two different heat plateaus will be formed, one at 1000 °C because of the CuO reduction, and the other at approximately 840 °C because of the $CaCO_3$ calcination. The transition between them will be determined by the position of both the reduction front (R in Fig. 6a) and the calcination front (C in Fig. 6a). While the heat exchange front formed as a result of the reduction reaction (HR) will move behind the reduction front (R), the heat exchange front resulting from the calcination (HC) will advance first leaving behind the calcination front (C). This may be due to the increase in the molar flow rate resulting from the $CaCO_3$

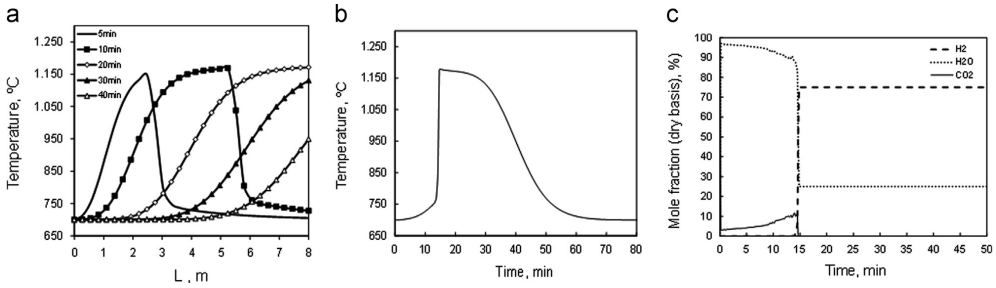

Fig. 5. Dynamic profiles during $CaCO_3$ calcination with simultaneous CuO reduction (30 wt% CuO, 5 wt% $CaCO_3$ in the solids bed, 75 vol% H_2 in the feed): (a) axial temperature; (b) temperature at the reactor exit; (c) composition of the product gas at the reactor exit.

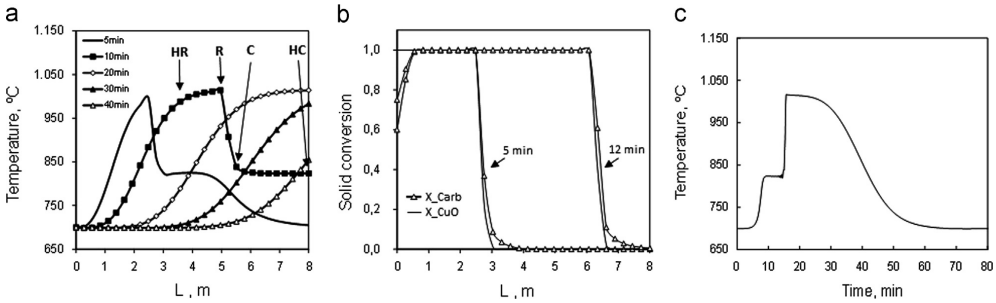

Fig. 6. Dynamic profiles during $CaCO_3$ calcination with simultaneous CuO reduction (30 wt% CuO, 15 wt% $CaCO_3$ in the solids bed, 75 vol% H_2 in the feed): (a) axial temperature; (b) axial solids conversion; (c) temperature at the reactor exit.

calcination (Eq. IV), which will accelerate the heat exchange front (HC). As can be seen in Fig. 6b, the reduction reaction will occur in a narrow reaction front that will advance behind the calcination zone, which is much wider. Moreover, part of the $CaCO_3$ at the reactor inlet will be left uncalcined once it has been traversed by all the heat exchange and reaction fronts.

According to the evolution of the temperature of the product gas, the reduction/calcination operation can be divided into different periods (Fig. 6c). In the first stage ($t < 8$ min), the heat exchange front (HC) will still be inside the reactor exit, and therefore, the product gas will be discharged at the initial temperature of the solids bed (700 °C). When the heat exchange front (HC) approaches the reactor exit, the temperature will rise rapidly until it reaches approximately 840 °C (about $t = 10$ min). In the subsequent period, which will take place between $t = 10$ min and $t = 14$ min, the temperature of the product gas will remain constant, corresponding to the first temperature plateau formed in the bed as a result of the $CaCO_3$ calcination. When the calcination front (C) reaches the reactor exit ($t = 14$ min), the temperature profile will rise dramatically to a maximum of around 1000 °C. There will be a very short breakthrough period (of around 1 min) until the reduction front (R) reaches the exit ($t = 15$ min), which means that the solids bed has been totally converted. During the first part of the postbreakthrough period (15 min $< t <$ 25 min), the product gas will be emitted at almost constant temperature (around 1000 °C), corresponding to the second heat plateau formed in the bed as a result of the CuO reduction. As the heat exchange front (HR in Fig. 6a) approaches the reactor exit, the outlet temperature will gradually drop until it reaches the temperature of the inlet gas (700 °C) after around 65 min of operation.

An increase in the $CaCO_3$ content to 21 wt% means that the bed contains the theoretical $CuO/CaCO_3$ proportion required to carry out the reduction/calcination stage, i.e., a $CuO/CaCO_3$ molar ratio of 1.8. Although the relative position of the reaction and heat exchange fronts along the bed will be the same, the temperature profiles will be flatter than in the previous case (see Fig. 7a). The maximum temperature in the reduction front (R) will be significantly lower (around 900 °C) due to the fact that a substantial part of the heat released from the Cu reduction will be simultaneously consumed to carry out the calcination of the $CaCO_3$. This temperature will favor both reduction and calcination reactions, and the chemical and mechanical properties of the solids will be maintained in the long term (Fernández et al., 2012b). The higher content of $CaCO_3$ in the bed will allow a higher amount of CO_2 to be generated by calcination. Therefore, there will be an increase in the total flow rate and the heat exchange front (HC) will advance even faster, reaching the reactor exit after 4 min of operation (Fig. 7b). Until that time, the degree of calcination in the bed will still be low, and therefore, the CO_2 content in the product gas will be around 4 vol% (Fig. 7c). Subsequently, the temperature profile will rapidly rise up to 850 °C (temperature of the first heat plateau) and it will remain constant until the reduction front reaches the reactor exit ($t = 14$ min). Under these conditions, the calcination will be highly favoured, allowing the product gas to reach a maximum CO_2 content of around 30 vol% (given by the calcination equilibrium).

The balanced amounts of CuO and $CaCO_3$ in the bed will make both reaction fronts advance together and they will reach their respective breakthroughs at around the same time, i.e., about $t = 15$ min (Fig. 7d). During the breakthrough, a peak of temperature at around 900 °C will be observed resulting from the fast increase in temperature produced during this period. At this point, the bed will be close to its total reduction, resulting in a rapid increase in the H_2 content in the outlet gas from 0 vol% to 75 vol%.

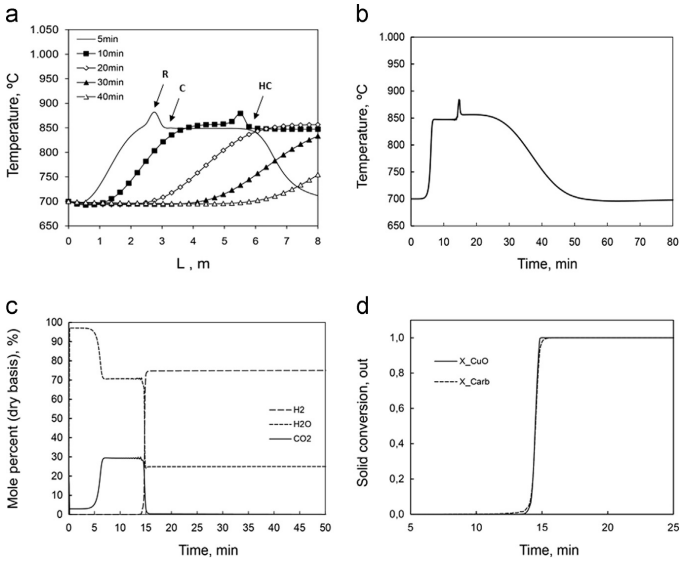

Fig. 7. Dynamic profiles during $CaCO_3$ calcination with simultaneous CuO reduction (30 wt% CuO, 21 wt% $CaCO_3$ in the solids bed, 75 vol% H_2 in the feed): (a) axial temperature; (b) temperature at the reactor exit; (c) composition of the product gas at the reactor exit; (d) solids conversion at the reactor exit.

The calcination will also be completed since there will be no CO_2 present in the product gas during the postbreakthrough (Fig. 7c). In this period, the outlet temperature will drop until it becomes stable at around 850 °C between $t=16$ min and $t=25$ min, as a consequence of the second heat plateau formed in the bed. As the heat exchange front (HR) approaches the end of the reactor, the temperature profile will progressively fall until it reaches 700 °C (after 60 min of operation).

An excess of $CaCO_3$ in the bed, as occurs in Fig. 8 (30 wt% CuO and 30 wt% $CaCO_3$), will hinder the reduction/calcination operation. Although the maximum temperature achieved in the reduction front will stay close to 900 °C, the shape of the temperature profiles will change significantly. As in the previous cases, the heat exchange front resulting from the calcination (HC in Fig. 8a) will advance first, leaving behind the reduction front (C). However, no heat plateau due to the CuO reduction will form because all the heat generated in the reduction front will be simultaneously consumed in the calcination of $CaCO_3$. Therefore, the solids will be left behind at around 700 °C (temperature of the inlet gas), which is a too low temperature for the calcination of the bed to be completed. Once the breakthrough of the CuO reduction is reached ($t=15$ min), the temperature of the product gas will dramatically drop (Fig. 8 b). The presence of a relatively high content of CO_2 in the flue gas during the first part of the postbreakthrough (Fig. 8c) indicates that some of the solids are still undergoing their calcination despite the fact that the CuO reduction has already been completed. At $t>15$ min, most of the bed will be at 700 °C, which will strongly hinder the calcination of the remaining $CaCO_3$. The CO_2 content in the product gas will gradually decrease to around 1 vol% and a significant part of the bed will be left uncalcined even after 80 min of operation (Fig. 8d).

4.2. Effect of the operating temperature on reactor performance

The influence of the initial temperature of the bed (T_{s0}) on the temperature profiles and on the product gas composition has been also analyzed. This study has been carried out for initial temperatures from 500 °C to 800 °C, assuming the operating conditions listed in Table 3, for a fuel gas containing 75 vol% H_2 and 25 vol% H_2O, that is fed into a fixed bed with a CuO content of 30 wt% and 21 wt% of $CaCO_3$. As shown in Fig. 9, the temperature profiles formed during the operation will significantly change. A starting temperature of 800 °C will allow from the very beginning a rapid reduction of CuO with H_2, and consequently, the temperature in the reduction front (R) will escalate to a maximum of around 900 °C. At these conditions, the calcination of $CaCO_3$ will be highly favoured, and therefore, a large amount of CO_2 will be released. As a result, there will be a significant increase in the molar flow rate, which will accelerate the heat exchange front resulting from the calcination reaction (HC), as explained above. As T_{s0} decreases, the heat exchange front (HC) will advance at a slower velocity and closer to the reduction front (R). Although the maximum temperature achieved will stay around 900 °C, all the heat generated in the reduction front will be rapidly consumed and the solids bed will not contain sufficient sensible heat to maintain very high temperatures behind the reduction front. As can be seen in Fig. 9c and d (i.e., for initial temperatures of 600 °C and 500 °C, respectively), no heat plateau behind the reduction front will form and the solids will be left at around 700 °C, which is the temperature of the inlet gas. Moreover, the heat plateau formed downstream of the reduction front will tend to disappear, which indicates a lower CO_2 release by calcination.

As can be seen in Fig. 10, higher starting temperatures will increase the degree of calcination achieved during the operation and consequently the amount of CO_2 generated by calcination. The great increase in the total flow rate at a T_{s0} of 800 °C will accelerate the advance of the heat exchange front resulting from the calcination (HC), reaching the reactor exit after 3 min of operation (Fig. 10a). From the very beginning, the calcination will be highly favoured and a CO_2 content in the product gas of around 15 vol% will be obtained. During the rest of the pre-breakthrough period, the product gas will be emitted at around 850 °C with a CO_2 content of approximately 30 vol% (given by the calcination equilibrium). An initial temperature of 500 °C (see Fig. 10d) will allow

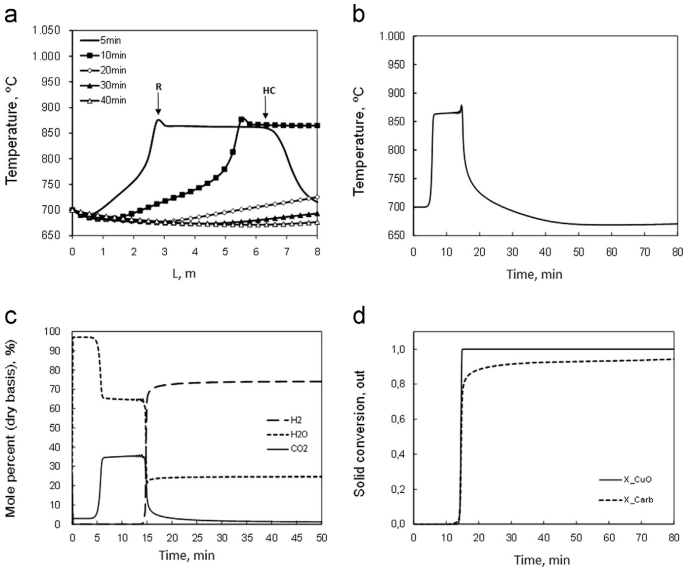

Fig. 8. Dynamic profiles during $CaCO_3$ calcination with simultaneous CuO reduction (30 wt% CuO, 30 wt% $CaCO_3$ in the solids bed, 75 vol% H_2 in the feed): (a) axial temperature; (b) temperature at the reactor exit; (c) composition of the product gas at the reactor exit; (d) solids conversion at the reactor exit.

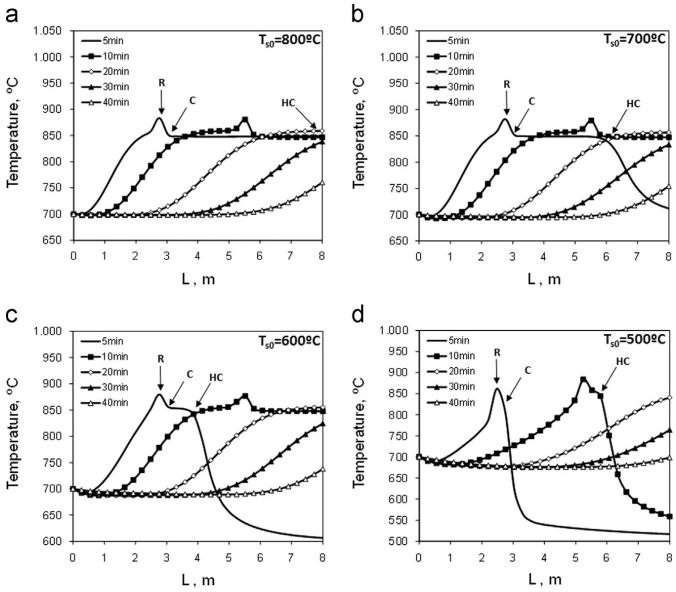

Fig. 9. Effect of starting temperature on the temperature profiles during reduction/calcination operation (30 wt% CuO, 21 wt% $CaCO_3$ in the solids bed, 75 vol% H_2 in the feed): (a) at 800 °C; (b) at 700 °C; (c) at 600 °C, (d) at 500 °C.

the complete reduction of CuO to Cu to be achieved, but a significant part of the $CaCO_3$ will be left uncalcined (only 50% of solids conversion at the reactor inlet). The generation of CO_2 by calcination will dramatically drop (less than 1 vol% of CO_2 in the product gas in the first 6 min) and therefore, the heat exchange front (HC) will advance significantly slower, reaching the reactor exit after 10 min of operation. Only in the last 2 min before reaching the breakthrough, the temperature of the flue gas will achieve 850 °C, allowing the product gas to reach a maximum CO_2 content of 30 vol%.

Under the boundary conditions of the Ca–Cu looping process, the reduction/calcination operation may start with a no uniform

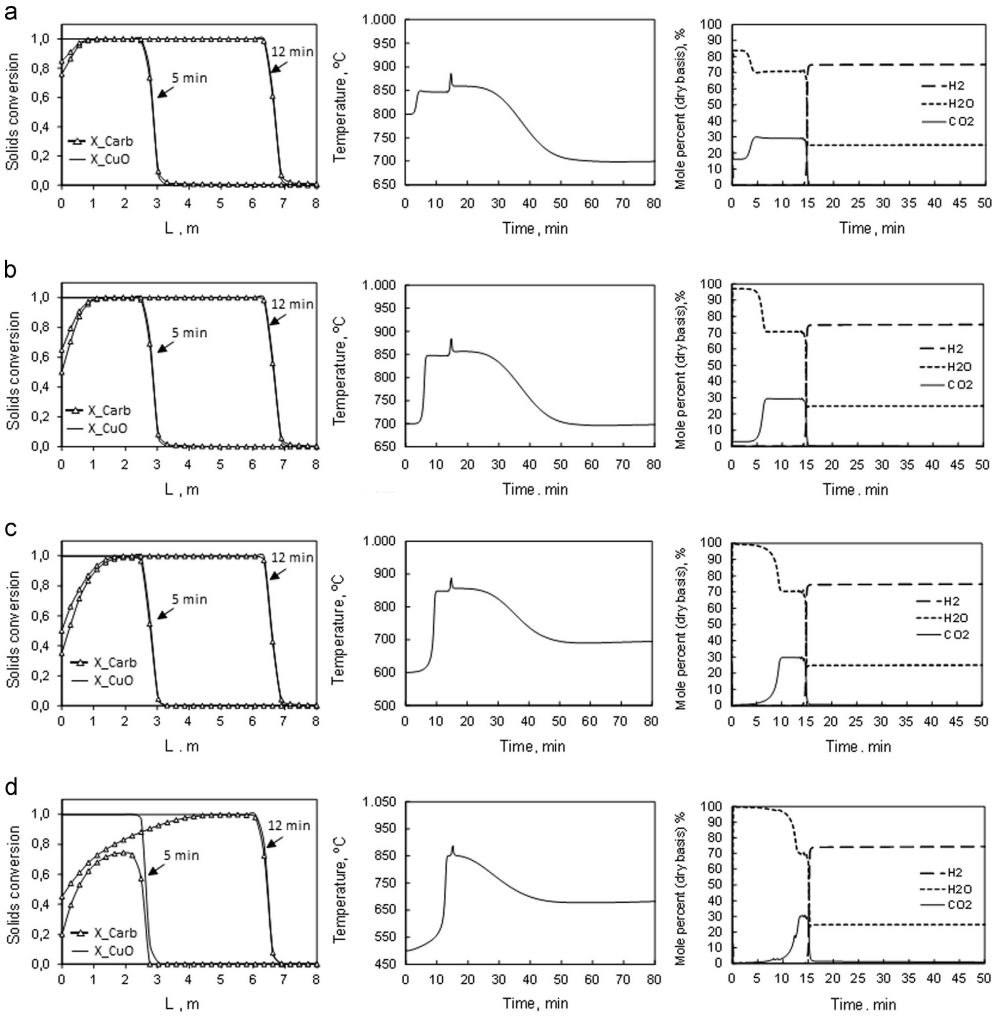

Fig. 10. Dynamic profiles during reduction/calcination operation for different starting temperatures (30 wt% CuO, 21 wt% $CaCO_3$ in the solids bed, 75 vol% H_2 in the feed): (a) at 800 °C; (b) at 700 °C; (c) at 600 °C, (d) at 500 °C.

temperature profile (between 700 °C and 830 °C), resulting from a previous stage of the process (Fernández et al., 2012b; Fernandez et al., 2013). The performance of the reactor where two different temperatures are present at the beginning of the reaction stage has been also studied. The operating conditions listed in Table 3, a fuel gas containing 75 vol% H_2 and 25 vol% H_2O, and a bed (30 wt% and 21 wt% of $CaCO_3$) with 50 wt% of the solids initially at 800 °C and the other 50 wt% at 700 °C were assumed. The feed of the fuel gas by the part of the reactor at the highest temperature (800 °C) was also considered. As can be seen in Fig. 11, the evolution of the temperature profile will be very similar to that obtained when the operation begins with the entire bed at 800 °C. In both cases, the temperature of the solids will rapidly rise due to the exothermic reduction of CuO to Cu with H_2 until it reaches a maximum close to 900 °C. The solids downstream of the reduction front will gradually be heated by the effect of the heat exchange front resulting from the calcination (HC), as explained above. Only during the first 4 min, while the heat exchange front (HC) remains inside the bed, the temperature of the product gast will be different (see Fig. 11b), since it will be emitted at the temperature of the solids situated closest to the end of the bed (800 °C and 700 °C, respectively). However, for longer operation times the temperature profiles will match each other until the end of the reduction/calcination operation.

4.3. Effect of the fuel gas composition on reactor performance

The calcination of $CaCO_3$ by the simultaneous reduction of CuO to Cu can be carried out with a fuel gas composed of CH_4, H_2, CO or a mixture of them. The composition of the reducing gas will

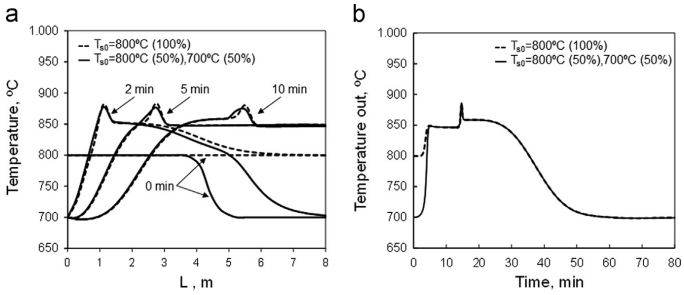

Fig. 11. Effect of initial temperature profile on reactor performance (30 wt% CuO, 21 wt% $CaCO_3$ in the solids bed, 75 vol% H_2 in the feed): (a) axial temperature profiles; (b) temperature at the reactor exit.

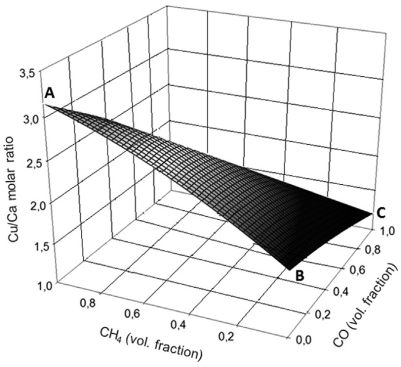

Fig. 12. Effect of fuel gas composition on the Cu/Ca molar ratio required for the process (gas compositions balanced with H_2).

strongly affect the proportion of CuO and $CaCO_3$ required in the bed in order to ensure a suitable performance. A Cu/Ca molar ratio of 3.1 would be needed in case of using pure CH_4 (point A in Fig. 12) to reach neutral conditions in the reaction fronts, taking into account the enthalpies of reaction (III) and reaction (IV) at 900 °C. Given the higher reduction enthalpy of CuO with H_2, the theoretical Cu/Ca molar ratio would decrease to 1.8 (point B in Fig. 12). If CO is used as reducing gas, the Cu/CaO molar ratio would be the minimum required (around 1.3, point C in Fig. 12).

Fig. 13 shows the dynamic behavior during the reduction/calcination operation when methane is used as reducing gas (75 vol% CH_4 and 25 vol% H_2O) for different Cu/Ca molar ratios, at the operating conditions summarized in Table 3. When the bed contains the theoretical CuO/$CaCO_3$ proportion needed (i.e., a Cu/Ca molar ratio of 3.1), the increase of temperature in the reduction front (R) will be moderate, reaching a maximum temperature close to 870 °C. Under these conditions, both reduction and calcination will be highly favoured and the reaction fronts (R and C) will advance together, reaching their respective breakthroughs at the same time. The content of CuO in the bed is the same as the previous cases with H_2 in the feed (30 wt%) and due to the different stoichiometry of the reduction of CuO with methane (one mole of gas will react with 4 mol of solid, see reaction III), the stage will become shorter and the total bed conversion will be achieved after approximately 3 min of operation (see Fig. 13a). A too low Cu/Ca molar ratio in the bed (around 1.8) will hamper the calcination of the $CaCO_3$. Although a maximum temperature of around 870 °C will be achieved in the reduction front (R), the heat released from this exothermic reaction will be insufficient to accomplish the simultaneous calcination of the $CaCO_3$ present in the bed. As a result, no heat plateau will form behind the reduction front and a large part of the bed will be left uncalcined. The presence of a high content of CO_2 in the product gas during the postbreakthrough ($t > 3$ min) shows that a part of the bed will continue its calcination once the CuO reduction has finished (Fig. 13b).

Fig. 14a shows that a CuO/$CaCO_3$ molar ratio of around 1.3 is large enough to carry out this reaction stage when CO is used as fuel gas (75 vol% CO and 25 vol% H_2O). The temperature profiles will evolve along the bed without exceeding maximum temperatures than could cause a certain degree of agglomeration and/or deactivation in the materials involved in the process. Moreover, both reduction and calcination fronts will move forward together leaving behind solids at a sufficiently high temperature (around 920 °C) to ensure the complete calcination of the bed. However, higher Cu/$CaCO_3$ ratios in bed composition will generate more heat than required for the operation. These conditions will favor the formation of very high temperature profiles from the very beginning (see Fig. 14b), promoting the calcination of $CaCO_3$. The heat exchange front resulting from the calcination (HC) will advance faster and a heat plateau at around 900 °C will form downstream. Under these circumstances, some of the $CaCO_3$ will be calcined ahead of the reduction front (R). This will lead to a lower energy demand in the reduction/calcination front, which combined with the high exothermicity of the CuO reduction with CO, will cause a dramatic increase in temperature to around 1250 °C.

This work theoretically demonstrates that the reduction of CuO to Cu with a fuel gas can provide the thermal energy required to accomplish the $CaCO_3$ calcination in the same matrix bed while at the same time a CO_2-rich product gas is obtained ready for its transport and geological storage. Further investigation is needed to develop and test suitable materials, to experimentally validate their behavior under the Ca–Cu chemical looping conditions and to improve the reactor models that allow the optimization of the process. The absence of steps with significant energy penalties (as in other chemical looping processes) indicates that this concept offers the possibility of achieving a very high level of energy efficiency.

5. Conclusions

The calcination of $CaCO_3$ by the simultaneous reduction of CuO to Cu with a fuel gas in an adiabatic fixed-bed reactor has been described using a dynamic pseudo-homogeneous model. With a suitable CuO/$CaCO_3$ ratio, the heat generated by the exothermic reduction of CuO is sufficient to carry out the endothermic $CaCO_3$

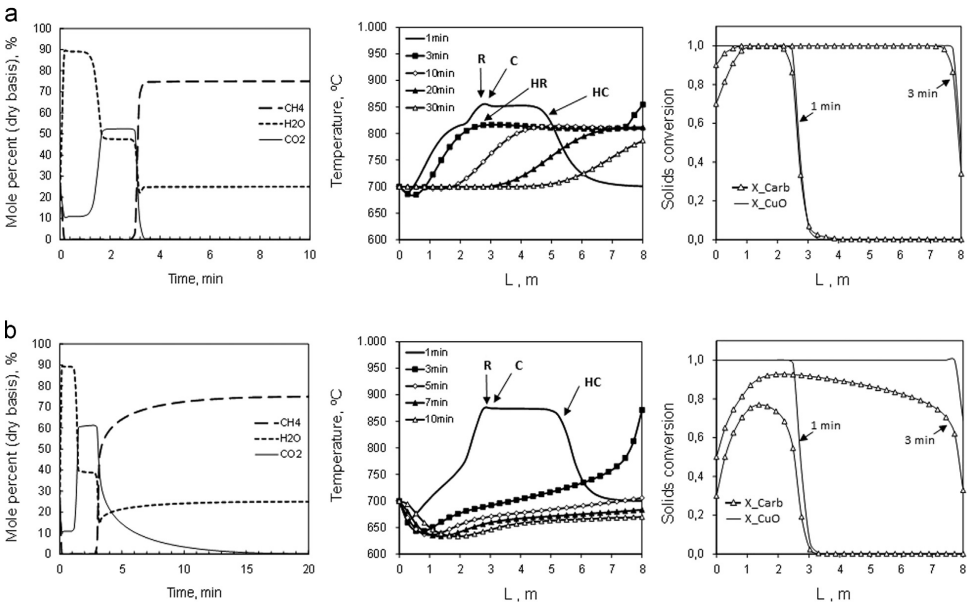

Fig. 13. Dynamic profiles (gas composition, temperature and solids conversion) during reduction/calcination operation when CH_4 is used as fuel gas: (a) for a Cu/Ca molar ratio of 3.1; (b) for a Cu/Ca molar ratio of 1.8.

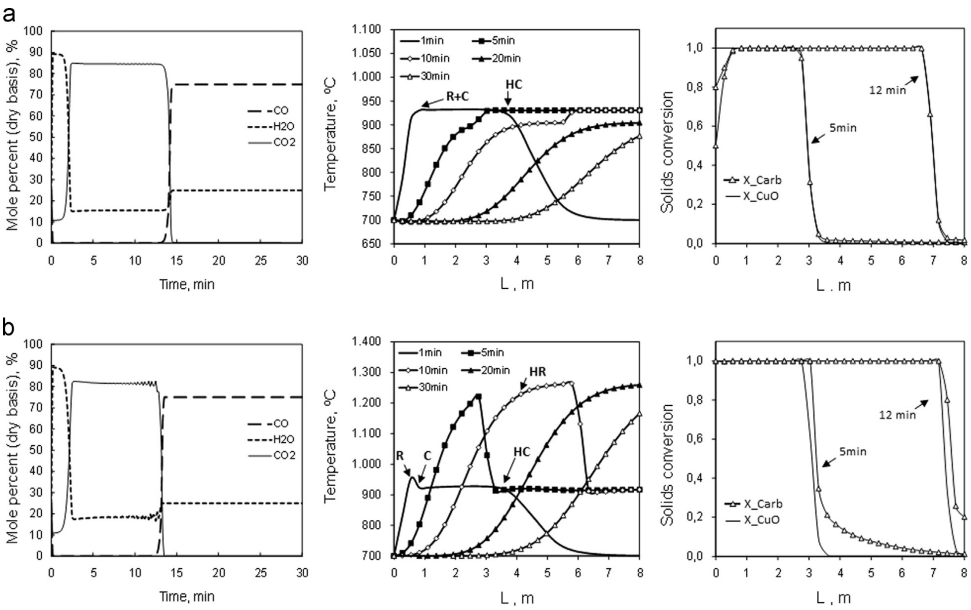

Fig. 14. Dynamic profiles (gas composition, temperature and solids conversion) during reduction/calcination operation when CO is used as fuel gas: (a) for a Cu/Ca molar ratio of 1.3; (b) for a Cu/Ca molar ratio of 1.8.

calcination without the need for supplementary energy, while a rich stream of CO_2 for disposal is obtained as product gas. The operating conditions required in the Ca–Cu looping process make the CuO reduction take place in a narrow reaction front that advances behind the calcination zone, which is in general wider. Two heat plateaus are formed along the bed because of the

reduction and calcination reactions. While the heat exchange front resulting from the CuO reduction moves behind the reduction front, the heat exchange front formed due to the $CaCO_3$ calcination advances first, leaving behind the calcination front. The increase in the molar flow rate because of the calcination significantly accelerates the advance of the heat exchange front. The $CuO/CaCO_3$ ratio in the bed and the composition of the fuel gas strongly affect the axial temperature and conversion profiles of the solids during the operation. Balanced amounts of CuO and $CaCO_3$ in the bed (e.g. a $CuO/CaCO_3$ molar ratio of 1.8 when H_2 is used as fuel gas) make both reaction fronts move forward together with moderate maximum temperatures of around 900 °C. An excess of CuO in the bed will generate more heat than that required for the calcination. Consequently, hot spots higher than 1000 °C may occur along the bed, that might cause irreversible loss of activity in the Cu- and Ca-based materials. In contrast, an excess of $CaCO_3$ will impede the reduction/calcination operation and part of the bed will be left uncalcined. The use of CO as fuel gas significantly reduces the $CuO/CaCO_3$ ratio required for the $CaCO_3$ calcination. The absence of large energy penalties and the results obtained in this study confirm the potential of the proposed process.

Nomenclature

C_{CO_2}	concentration of CO_2 in the gas phase, kmol m^{-3}
$C_{CO_{2eq}}$	equilibrium concentration of CO_2, kmol m^{-3}
C_i	concentration of component *i* in the reactor, kmol m^{-3}
C_{in}	concentration of component *i* in the feed, kmol m^{-3}
C_g	concentration of the gas, kmol m^{-3}
C_{pg}	specific heat capacity of the gas, kJ kg^{-1} K^{-1}
C_{ps}	specific heat capacity of the solid, kJ kg^{-1} K^{-1}
D_{eff}	axial mass dispersion coefficient, m^2 s^{-1}
D_r	Inner diameter of the reactor, m
d_p	particle diameter, m
$E_{a,Calc}$	activation energy calcination reaction, kJ mol^{-1}
$E_{a,CO}$	activation energy reduction reaction with CO, kJ mol^{-1}
E_{a,H_2}	activation energy reduction reaction with H_2, kJ mol^{-1}
H_{ri}	Enthalpy reaction of gas component *i*, kJ mol^{-1}
$k_{0,Calc}$	preexponential factor of the $CaCO_3$ calcination reaction, mol^{1-n} m^{3n-3} s^{-1}
$k_{0,CO}$	preexponential factor of the CuO reduction reaction with CO, mol^{1-n} m^{3n-3} s^{-1}
k_{0,H_2}	preexponential factor of the CuO reduction reaction with H_2, mol^{1-n} m^{3n-3} s^{-1}
k_{cal}	reaction rate constant of the $CaCO_3$ calcination, mol^{1-n} m^{3n-3} s^{-1}
k_{red}	reaction rate constant of the CuO reduction, mol^{1-n} m^{3n-3} s^{-1}
K_g	thermal conductivity of the gas, W K^{-1} m^{-1}
K_s	thermal conductivity of the solids, W K^{-1} m^{-1}
L	reactor length, m
L_{CuO}	layer thickness of CuO, m
M_{CaCO_3}	molar mass of CaCO3, kg kmol^{-1}
M_{CuO}	molar mass of CuO, kg kmol^{-1}
N_u	Nusselt number, dimensionless
P	pressure, MPa
Pe_{az}	Peclet number, dimensionless
P_{in}	pressure at the reactor entrance, MPa
P_r	Prandt number, dimensionless
R_e	Reynolds number, dimensionless
r_i	reaction rate of component *i*,
r_{cal}	reaction rate of calcination, mol m^{-3} s^{-1}
r_{CO_2}	reaction rate of CO_2 formation, mol m^{-3} s^{-1}
r_{red}	reaction rate of CuO reduction, mol m^{-3} s^{-1}
S_c	Schmidt number, dimensionless
T	Temperature, K
T_{in}	Temperature at the reactor entrance, K
T_{s0}	initial temperature of the solids in the fixed bed, K
T_w	reference temperature, K
X_{red}	fractional reduction conversion of CuO, dimensionless
X_{cal}	fractional calcination conversion of $CaCO_3$, dimensionless

Greek letters

E	bed void fraction, dimensionless
ρ_g	gas phase density, kg m^{-3}
$\rho_{m,CuO}$	molar density of Cu, mol m^{-3}
ρ_s	apparent density of the mixed solids in reactor, kg m^{-3}
λ_{eff}	effective axial heat dispersion coefficient, W m^{-2} K^{-1}
λ_{0bed}	effective axial heat dispersion with no flow conditions, W m^{-2} K^{-1}
η_{red}	effectiveness factor of reduction, dimensionless
η_{cal}	effectiveness factor of calcination, dimensionless
τ	time for complete solid conversion, dimensionless
μ_g	gas viscosity, MPa s

Acknowledgments

The authors acknowledge the grant awarded by the Spanish Ministry of Economy and Competiveness (Grant number BES-2013-063835), financed under the R+D Spanish National Program within the Project ENE2012-37936-C02-02 and the financial support from the ASCENT (Advanced solid cycles with efficient novel technologies) Project coordinated by the European Union Seventh Framework Programme FP7 under Grant agreement no. 608512.

References

Abad, A., Adánez, J., García-Labiano, F., de Diego, L.F., Gayán, P., 2010. Modeling of the chemical-looping combustion of methane using a Cu-based oxygen-carrier. Combust. Flame 157, 602–615.
Abanades, J.C., Murillo, R., Fernandez, J.R., Grasa, G., Martínez, I., 2010. New CO_2 capture process for hydrogen production combining Ca and Cu chemical loops. Environ. Sci. Technol. 44, 6901–6904.
Baker, E., 1962. The calcium oxide–carbon dioxide system in the pressure range 1–300 atm. J. Chem. Soc. (Resumed), 464–470.
Bellido, J.D.A., De Souza, J.E., M'Peko, J.C., Assaf, E.M., 2009. Effect of adding CaO to ZrO_2 support on nickel catalyst activity in dry reforming of methane. Appl. Catal. A: Gen. 358, 215–223.
Boot-Handford, M.E., Abanades, J.C., Anthony, E.J., Blunt, M.J., Brandani, S., Mac Dowell, N., Fernandez, J.R., Ferrari, M.C., Gross, R., Hallett, J.P., Haszeldine, R.S., Heptonstall, P., Lyngfelt, A., Makuch, Z., Mangano, E., Porter, R.T.J., Pourkashanian, M., Rochelle, G.T., Shah, N., Yao, J.G., Fennell, P.S., 2014. Carbon capture and storage update. Energy Environ. Sci. 7, 130–189.
Boshu, H., Mingyang, L., Xin, W., Ling, Z., Lili, W., Jiwei, X., Zhenxing, C., 2008. Chemical kinetics-based analysis for utilities of ZEC power generation system. Int. J. Hydrog. Energy 33, 4673–4680.
Choudhary, V.R., Rajput, A.M., Mamman, A.S., 1998. NiO-alkaline earth oxide catalysts for oxidative methane-to-syngas conversion: influence of alkaline earth oxide on the surface properties and temperature-programmed reduction/reaction by H_2 and methane. J. Catal. 178, 576–585.
Chuang, S.Y., Dennis, J.S., Hayhurst, A.N., Scott, S.A., 2010. Kinetics of the oxidation of a co-precipitated mixture of cu and Al $_2O_3$ by O_2 for chemical-looping combustion. Energy Fuels 24, 3917–3927.
de Diego, L.F., García-Labiano, F., Adánez, J., Gayán, P., Abad, A., Corbella, B.M., Palacios, M.J., 2004. Development of Cu-based oxygen carriers for chemical-looping combustion. Fuel 83, 1749–1757.
Edwards, M.F., Richardson, J.F., 1968. Gas dispersion in packed beds. Chem. Eng. Sci. 23, 109–123.
Ergun, S., 1952. Fluid flow through packed columns. Chem. Eng. Prog. 48, 89–94.
Fernández, J.R., Abanades, J.C., 2014. Conceptual design of a Ni-based chemical looping combustion process using fixed-beds. Appl. Energy 135, 309–319.
Fernandez, J.R., Abanades, J.C., Grasa, G., 2012. Modeling of sorption enhanced steam methane reforming – Part II: simulation within a novel Ca/Cu chemical loop process for hydrogen production. Chem. Eng. Sci. 84, 12–20.
Fernández, J.R., Abanades, J.C., Murillo, R., 2012a. Modeling of sorption enhanced steam methane reforming in an adiabatic fixed bed reactor. Chem. Eng. Sci. 84, 1–11.

Fernández, J.R., Abanades, J.C., Murillo, R., 2013. Modeling of Cu oxidation in adiabatic fixed-bed reactor with N_2 recycling in a Ca/Cu chemical loop. Chem. Eng. J. 232, 442–452.
Fernández, J.R., Abanades, J.C., Murillo, R., Grasa, G., 2012b. Conceptual design of a hydrogen production process from natural gas with CO_2 capture using a Ca–Cu chemical loop. Int. J. Greenh. Gas Control 6, 126–141.
Fernandez, J.R., Abanades, J.C., Murillo, R., 2014. Modeling of Cu oxidation in an adiabatic fixed-bed reactor with N_2 recycling. Appl. Energy 113, 1945–1951.
Fernández, J.R., Alarcón, J.M., 2015. Chemical looping combustion process in fixed-bed reactors using ilmenite as oxygen carrier: conceptual design and operation strategy. Chem. Eng. J. 264, 797–806.
Feron, P., Hendriks, H.M., C., A., 2005. CO_2 capture process principles and costs. Oil Gas Sci. Technol – Rev. IFP 60, 451–459.
García-Labiano, F., de Diego, L.F., Adánez, J., Abad, A., Gayán, P., 2004. Reduction and oxidation Kinetics of a copper-based oxygen carrier prepared by impregnation for chemical-looping combustion. Ind. Eng. Chem. Res. 43, 8168–8177.
González, B., Grasa, G.S., Alonso, M., Abanades, J.C., 2008. Modeling of the deactivation of CaO in a carbonate loop at high temperatures of calcination. Ind. Eng. Chem. Res. 47, 9256–9262.
Gunn, D.J., 1987. Axial and radial dispersion in fixed beds. Chem. Eng. Sci. 42, 363–373.
Gunn, D.J., Misbah, M.M.A., 1993. Bayesian estimation of heat transport parameters in fixed beds. Int. J. Heat Mass Transf. 36, 2209–2221.
Hamers, H.P., Gallucci, F., Cobden, P.D., Kimball, E., van Sint Annaland, M., 2013. A novel reactor configuration for packed bed chemical-looping combustion of syngas. Int. J. Greenh. Gas Control 16, 1–12.
Hamers, H.P., Gallucci, F., Cobden, P.D., Kimball, E., van Sint Annaland, M., 2014. CLC in packed beds using syngas and CuO/Al_2O_3: model description and experimental validation. Appl. Energy 119, 163–172.
Harrison, D.P., 2008. Sorption-enhanced hydrogen production: a review. Ind. Eng. Chem. Res. 47, 6486–6501.
Johnsen, K., Ryu, H.J., Grace, J.R., Lim, C.J., 2006. Sorption-enhanced steam reforming of methane in a fluidized bed reactor with dolomite as CO_2-acceptor. Chem. Eng. Sci. 61, 1195–1202.
Krupiczka, R., 1967. Analysis of thermal conductivity in granular materials. Int. Chem. Eng. 7, 122–144.
Kumar, R., Lyon, R., Cole, J., 2002. Unmixed reforming: a novel autothermal cyclic steam reforming process. In: Padró, Grégoire, C.E.L., Francis (Eds.), Advances in Hydrogen Energy. Springer, US, pp. 31–45.
Li, Z.-s., Cai, N.-s., 2007. Modeling of multiple cycles for sorption-enhanced steam methane reforming and sorbent regeneration in fixed bed reactor. Energy Fuels 21, 2909–2918.
Martínez, I., Grasa, G., Murillo, R., Arias, B., Abanades, J.C., 2012. Kinetics of calcination of partially carbonated particles in a Ca-looping system for CO_2 capture. Energy Fuels 26, 1432–1440.
Martínez, I., Murillo, R., Grasa, G., Fernández, J.R., Abanades, J.C., 2013a. Integrated combined cycle from natural gas with CO_2 capture using a Ca–Cu chemical loop. AIChE J. 59, 2780–2794.
Martínez, I., Romano, M.C., Chiesa, P., Grasa, G., Murillo, R., 2013b. Hydrogen production through sorption enhanced steam reforming of natural gas: thermodynamic plant assessment. Int. J. Hydrog. Energy 38, 15180–15199.
Martínez, I., Romano, M.C., Fernández, J.R., Chiesa, P., Murillo, R., Abanades, J.C., 2014. Process design of a hydrogen production plant from natural gas with CO_2 capture based on a novel Ca/Cu chemical loop. Appl. Energy 114, 192–208.
Mattisson, T., Järdnäs, A., Lyngfelt, A., 2003. Reactivity of some metal oxides supported on alumina with alternating methane and oxygen application for chemical-looping combustion. Energy Fuels 17, 643–651.
Metz, B., 2010. Controlling Climate Change. Cambridge University Press.
Metz, B., Davidson, O., De Coninck, H., Loos, M., Meyer, L., 2005. IPCC Special report on carbon dioxide capture and storage. Prepared by working group III of the intergovernamental panel on climate change.
Meyer, J., Mastin, J., Bjørnebøle, T.K., Ryberg, T., Eldrup, N., 2011. Techno-economical study of the zero emission gas power concept. Energy Procedia 4, 1949–1956.
Noorman, S., Gallucci, F., van Sint Annaland, M., Kuipers, H.J.A.M., 2010. Experimental investigation of a CuO/Al_2O_3 oxygen carrier for chemical-looping combustion. Ind. Eng. Chem. Res. 49, 9720–9728.
Noorman, S., Gallucci, F., van Sint Annaland, M., Kuipers, J.A.M., 2011. Experimental investigation of chemical-looping combustion in packed beds: a parametric study. Ind. Eng. Chem. Res. 50, 1968–1980.
Noorman, S., Van Sint Annaland, M., Kuipers, J.A.M., 2007. Packed bed reactor technology for chemical-looping combustion. Ind. Eng. Chem. Res. 46, 4212–4220.
Rostrup-Nielsen, J.R., 2009. Steam reforming and chemical recuperation. Catal. Today 145, 72–75.
Spallina, V., Romano, M.C., Chiesa, P., Gallucci, F., van Sint Annaland, M., Lozza, G., 2014. Integration of coal gasification and packed bed CLC for high efficiency and near-zero emission power generation. Int. J. Greenh. Gas Control 27, 28–41.
Stevens, J.F., Krishnamurthy, B., Atanassova, P., Spilker, K., 2007. Development of 50 kW fuel processor for stationary fuel cell applications. Final report, DOE/GO/13102-1. Chevron Techology Ventures, LLC.
Stocker, T., Qin, D., Plattner, G., Tignor, M., Allen, S., Boschung, J., Nauels, A., Xia, Y., Bex, B., Midgley, B., 2013. IPCC, climate change, The physical science basis. Contribution of working group I to the fifth assessment report of the intergovernmental panel on climate change, Cambridge University Press.
Vortmeyer, D., Berninger, R., 1982. Comments on the paper, theoretical prediction of effective heat transfer parameters in packed beds by Anthony Dixon and D. L. Cresswell (AIChE J., 25, 663 (1979)). AIChE J. 28, 508-510.
Weimer, T., Berger, R., Hawthorne, C., Abanades, J.C., 2008. Lime enhanced gasification of solid fuels: examination of a process for simultaneous hydrogen production and CO_2 capture. Fuel 87, 1678–1686.
Wolf, J., Yan, J., 2005. Parametric study of chemical looping combustion for tri-generation of hydrogen, heat, and electrical power with CO_2 capture. Int. J. Energy Res. 29, 739–753.

CAPÍTULO V

PRUEBA DE CONCEPTO DEL PROCESO Ca-Cu

5. PRUEBA DE CONCEPTO DEL PROCESO Ca-Cu

Como parte de esta tesis doctoral, se ha diseñado y construido un dispositivo experimental a escala de laboratorio con el objetivo de validar experimentalmente las etapas de oxidación de cobre y de reducción de CuO/calcinación de $CaCO_3$ simultáneas, presentes en el proceso Ca-Cu. Los experimentos se han realizado en unas condiciones similares a las esperadas a escala industrial y han servido para validar el modelo dinámico de reactor explicado en el capítulo anterior. Forman parte de este capítulo las publicaciones III y IV, mostradas en las secciones 5.3.1 y 5.3.2, donde se describen en detalle las condiciones de operación en cada caso y se discuten los resultados obtenidos.

5.1. Descripción de la instalación

En la figura 5.1 se muestra una fotografía del dispositivo experimental empleado (en las publicaciones III y IV se incluye un esquema detallado). El elemento principal es un reactor de lecho fijo fabricado en inconel de 38 mm de diámetro interno y 0.92 m de longitud. Con el objetivo de operar en condiciones pseudo-adiabáticas, el reactor está recubierto con un espesor de 80 mm de lana de roca que actúa como aislante térmico. Tanto el reactor como el recubrimiento de lana de roca se ubican dentro de un horno tubular refractario de 14 kW de potencia, que es el encargado de compensar las pérdidas de calor al exterior.

Se emplean controladores de flujo másico Bronkhorst para alimentar al reactor H_2, CO, CH_4, N_2 y aire en rangos de 0 a 30 lN/min. El aire es suministrado por un compresor a una presión de 4 bar. El resto de los gases proceden de botellas comerciales. Un sistema de precalentamiento de gases compuesto por dos cintas térmicas de 450 W y 780 W de potencia, respectivamente, permiten incrementar la temperatura de los gases de entrada hasta aproximadamente 500ºC. Una vaina fabricada en inconel de termopares tipo K con 14 puntos de medida dispuesta axialmente permite medir los perfiles longitudinales de temperatura dentro del reactor. Un lecho de gel de sílice a la salida del reactor es el encargado de eliminar el vapor de agua generado en la operación. Analizadores SICK GM800 permiten medir en continuo la concentración en base seca del gas producto. Un módulo de infrarrojo mide CO en un rango de 0-50% vol., CO_2 en dos rangos de medida de 0-10% vol. y de 0-100% vol. y CH_4 en dos rangos de 0-50% vol. y 0-100% vol. El H_2 se mide por conductividad térmica en un rango de 0-100% y el O_2 mediante un analizador paramagnético en un rango de 0-21%. Un

equipo de adquisición de datos Agilent 34972A con 66 canales permite registrar las temperaturas y las concentraciones de gases en continuo a la salida del reactor.

Por otro lado, se ha empleado una termobalanza que opera a presión atmosférica diseñada por el grupo de captura de CO_2 para estudiar la capacidad de absorción de CO_2 del material de calcio a lo largo de múltilples ciclos de carbonatación/calcinación. Dicho equipo consiste principalmente en una microbalanza colocada en la parte superior (cabeza) y un reactor de cuarzo de 25 mm situado en un horno con dos zonas de calentamiento que puede trabajar hasta 1000ºC y a diferente temperatura en cada zona. Los ensayos termogravimétricos para determinar la capacidad de transporte de O_2 del material de cobre se realizaron en una termobalanza comercial CI Electronics Ltd (a presión atmosférica) realizando múltiples ciclos de oxidación/reducción. Las condiciones de operación de estos ensayos se detallan en la Publicación IV. Asimismo, se han realizado análisis de difracción de Rayos X empleando un difractómetro Siemens D500/501 para muestras en polvo, con objeto de determinar las fases cristalinas presentes en ambos materiales antes y después de llevar a cabo ensayos multiciclo. Para ello las muestras se tamizaron para obtener un tamaño inferior a 200 µm, seleccionándose tamaños y tiempos de paso de 0.025º y 0.8 s respectivamente, con un intervalo de escaneo entre 20º y 70º 2θ.

Respecto a los sólidos empleados, Johnson Matthey ha suministrado el material de cobre, el cual tiene una composición en peso del 60% de Cu soportado sobre sílice. Carmeuse ha suministrado el material cálcico con un 99% en peso de CaO. También se ha empleado alúmina suministrada por Sigma Aldrich (3 mm de diámetro) como sólido inerte para llevar a cabo las pruebas de transmisión de calor, así como para rellenar la parte inferior del reactor durante los experimentos de reacción.

Figura 5.1: Fotografía del equipo experimental del INCAR. Incluye: sistema de alimentación y precalentamiento de gases, reactor tubular, horno, vaina de termopares, analizadores de gases y equipo de adquisición de datos.

5.2. Metodología experimental

Tras realizar ensayos previos de reacción en el reactor de lecho fijo, se decidió trabajar con tamaños de partícula de 3 mm para los materiales de cobre y de calcio, y así disminuir las resistencias difusionales y lograr frentes de reacción más nítidos. El material cálcico suministrado por Carmeuse presentaba inicialmente una distribución de tamaños muy amplia por lo que fue necesario llevar a cabo un proceso de tamizado. El material de cobre de Johnson Matthey fue suministrado en forma de pellets de 5 mm de longitud y 4.5 mm de diámetro. Se procedió a partir dichos pellets para lograr un tamaño aproximado a los 3 mm requeridos. Los experimentos de reacción se llevaron a cabo con una carga de sólidos mezclados de aproximadamente 1 kg.

Para llevar a cabo los experimentos de reacción fue necesario precalentar el lecho de sólidos hasta conseguir un perfil de temperatura estable. Debido a la gran inercia

térmica del sistema, los precalentamientos se iniciaron en cada experimento entre 16 y 18 horas antes. Dada la longitud del reactor y la existencia de un único termopar de control en el horno, no se lograron perfiles de temperatura longitudinales homogéneos (especialmente para temperaturas de partida mayores a 600ºC). Sin embargo, esta limitación del sistema permitió estudiar la influencia de la temperatura inicial de los sólidos en las reacciones involucradas en cada ensayo.

Antes del comienzo de cada experimento se procedió al calibrado de los analizadores ajustando para cada gas el cero y una concentración de referencia, que varió dependiendo de las concentraciones empleadas en cada experimento.

En los experimentos de reducción/calcinación el precalentamiento se realizó con aire para oxidar el material de cobre y una vez alcanzadas temperaturas en el lecho cercanas a 650ºC, se alimentaron mezclas de CO_2 en aire para carbonatar el material cálcico. De acuerdo a los ensayos realizados en termobalanza, se seleccionó el tiempo de carbonatación necesario para alcanzar la conversión requerida del material de calcio y lograr así una determinada proporción $CuO/CaCO_3$ en el lecho (diferente según la composición del gas reductor, tal y como se ha explicado en el capítulo anterior).

En los ensayos de reducción/calcinación se partió de temperaturas máximas del lecho en torno a 680ºC. Se ajustaron los caudales de alimentación para lograr la conversión del lecho en un tiempo aproximado de 10 minutos, aunque cada ensayo se prolongó durante 60 min para evaluar también la transmisión de calor sin reacción. En los ensayos de oxidación se partió de temperaturas en el lecho en torno a 400ºC y los experimentos se prolongaron entre 30 y 60 minutos. Las condiciones de operación de estos ensayos se detallan en las publicaciones III y IV.

5.3. Principales resultados obtenidos y validación del modelo

En primer lugar, se llevaron a cabo experimentos de transmisión de calor sin reacción química para determinar el coeficiente global de transferencia de calor del sistema (U). Para ello, se introdujo en el reactor una masa en torno a 1 kg de alúmina con un tamaño de partícula de 3 mm. Este estudio consistió en calentar el lecho de sólidos, inicialmente a temperatura ambiente, alimentando un caudal de 40 lN/min de N_2 precalentado a 475ºC durante 60 minutos. Asimismo, se realizaron ensayos de enfriamiento del lecho, inicialmente a 600ºC, alimentando igualmente un caudal de

40 lN/min de N_2 a 475ºC. Para determinar el coeficiente global de transferencia de calor (U) se hizo uso del modelo dinámico desarrollado en Matlab (descrito en el capítulo anterior) aplicando el balance de energía al sistema sin reacción química, e introduciendo un programa de optimización para la determinación de dicho coeficiente mediante un ajuste por mínimos cuadrados entre los valores predichos por el modelo y los datos experimentales. El valor obtenido del ajuste fue de 5 W/m^2K, suficientemente bajo para suponer que el sistema puede operar en condiciones pseudo-adiabáticas. Los resultados de estos ensayos se detallan en la Publicación III.

Para realizar los primeros ensayos de reducción/calcinación se eligió como gas reductor una corriente concentrada de H_2 (50% vol. H_2 en N_2) por los siguientes motivos: (1) el hidrógeno posee una gran reactividad frente al CuO (lo que permite ver frentes de reducción nítidos incluso a bajas temperaturas), (2) el H_2 es el gas mayoritario en un gas de síntesis generado bajo condiciones del proceso Ca-Cu (etapa C`) o en el gas de rechazo de una PSA, y (3) el CO_2 del gas producto en una reducción/calcinación llevada a cabo con H_2 corresponde únicamente al generado en la descomposición de $CaCO_3$ a CaO. Bajo esta premisa, los experimentos se realizaron con un contenido inicial en el lecho del 14% en peso de $CaCO_3$ y 21% de CuO (el resto era CaO inerte y SiO_2 que sirve de soporte al CuO). Es decir, un ratio molar $CuO/CaCO_3$ en torno a 1.8, que es el necesario para trabajar en condiciones térmicamente neutras cuando se emplea H_2 como gas reductor.

Se partió de un perfil de temperatura no homogéneo (entre 400ºC en la parte inferior del reactor hasta 700ºC en la superior). Se alimentó el gas reductor precalentado a 400ºC por la parte inferior del reactor, y de esta forma se estudió el efecto de la temperatura inicial del lecho en la reducción/calcinación. Siguiendo la evolución de los perfiles de temperatura a lo largo del reactor se observó un rápido incremento de temperatura desde un primer momento, lo que confirmó la elevada reactividad del H_2 frente al CuO, incluso a bajas temperaturas. Durante la parte de los experimentos en que la temperatura no superó los 800ºC, la calcinación de $CaCO_3$ no estaba favorecida y no se detectaron cantidades apreciables de CO_2 en el gas de salida. Sólo cuando se alcanzaron temperaturas cercanas a 850ºC se detectaron grandes cantidades de CO_2 en el gas producido (hasta un 40% en volumen).

Operando con relativamente bajo contenido de CuO en el lecho y alta concentración de H_2 en la alimentación, la evolución de los perfiles de temperatura confirma que el frente de reducción avanza más rápido que el frente de intercambio de calor

resultante, por lo que los sólidos reducidos quedan aguas arriba a alta temperatura. Como resultado, el gas llega al frente de reducción precalentado por dichos sólidos. La generación de CO_2 procedente de la calcinación de $CaCO_3$ incrementa el flujo molar de gas a través del lecho. El frente de intercambio de calor resultante de la calcinación avanza por delante, lo que hace que los sólidos aguas abajo vean incrementada ligeramente su temperatura. Estos resultados confirman las predicciones teóricas obtenidas a partir del modelo matemático desarrollado en Matlab y explicado en la publicación II. Éste ajusta razonablemente bien tanto las concentraciones de salida como los perfiles axiales de temperatura, tal y como se detalla en la Publicación III.

En un primer momento se detectaron a la salida concentraciones pequeñas de CO que inicialmente se creyeron fruto de interferencias en el analizador de gases entre el CO_2 y el CO y no se asumió ninguna reacción secundaria que diera lugar a la presencia de este gas. Ensayos posteriores confirmaron que la presencia de CO era debida a la reacción inversa gas-agua (en inglés Reverse Water Gas Shift, RWGS). La elevada temperatura en el frente de reducción y las altas concentraciones de CO_2 alcanzadas por la calcinación de $CaCO_3$ hacen que parte del H_2 reaccionara con CO_2 para producir CO y $H_2O(v)$. Esta reacción secundaria se contempló en el modelo matemático desarrollado en la Publicación IV, obteniendo una mejor descripción de los datos experimentales.

Para estudiar el efecto de la composición del gas reductor en la etapa de reducción/calcinación se realizaron experimentos alimentando H_2 con concentraciones crecientes de CO (hasta un 20% en volumen de CO). Tal y como se ha explicado con anterioridad, el uso de CO permite reducir la cantidad de CuO necesaria para calcinar simultáneamente $CaCO_3$ (es decir, reducir el ratio $CuO/CaCO_3$ en el lecho). Se empleó la misma carga de sólidos, pero aumentando el tiempo de carbonatación previo de acuerdo a los experimentos realizados en termobalanza. De esta forma, para los experimentos llevados a cabo con 10% vol. de CO y 40% vol. de H_2 el ratio inicial de $CuO/CaCO_3$ en el lecho fue de 1.7, y para los experimentos con 20% vol. de CO y 30% vol. de H_2 en la alimentación el ratio se redujo a 1.6. Al igual que en los experimentos realizados con H_2, desde el principio se observó un rápido incremento de la temperatura que confirma la alta reactividad del material de cobre con H_2 y CO a temperaturas relativamente bajas, aunque la cinética de reducción del CuO con H_2 es ligeramente más rápida que con CO, viendo la pendiente de las curvas de ruptura de los gases de salida.

Aunque el modelo matemático predijo correctamente la evolución de los perfiles de temperatura y las curvas de ruptura de H_2 y CO, la cantidad de CO_2 medida en el gas de salida fue significativamente mayor a la predicha teóricamente por el modelo. Este fenómeno, no observado inicialmente en la reducción/calcinación con H_2, se repitió en sucesivos experimentos realizados con H_2 y con mezclas de CO y H_2. Análisis de difracción de rayos X realizados con muestras de sólidos de cobre y de calcio altamente ciclados en el reactor, mostraron cambios de cristalinidad y de composición química en los mismos. Aparte de CuO y de CaO se detectaron en muestras calcinadas óxidos mixtos de cobre y calcio, que eran capaces de formar carbonatos en presencia de CO_2. Estos resultados concuerdan con los obtenidos por Kierzkowska y Müller (2013), que previamente habían demostrado que la formación de estos óxidos mixtos podía modificar la capacidad de absorción de CO_2 de estos materiales.

Respecto a la etapa de oxidación de Cu, se realizaron varios ensayos modificando el caudal total de gas y el contenido de O_2 a la entrada del reactor, para estudiar el efecto de estas variables de operación. En todos ellos, el material de calcio permaneció en estado calcinado para evitar interferencias del $CaCO_3$ en el estudio de la oxidación de Cu. Se empleó la misma carga de sólidos, lo que supuso operar con una concentración de material de cobre en el lecho cercana al 20% en peso.

Partiendo de cobre reducido y de un lecho a una temperatura inicial en torno a 400ºC, se alimentó un caudal de 8 lN/min de aire precalentado también a 400ºC. Bajo estas condiciones de operación se observó un rápido incremento de temperatura en el frente de oxidación, lo que confirma la gran facilidad para la oxidación del cobre incluso a temperaturas tan bajas. Bajo estas condiciones de operación, el frente de oxidación avanza a gran velocidad dejando atrás sólidos a gran temperatura fruto del calor desprendido por la reacción de oxidación. Se alcanzó una temperatura máxima de casi 900ºC en el frente de oxidación, que coincide con el incremento de temperatura teórico predicho por Noorman et al. (2007) en condiciones adiabáticas para estas condiciones de operación.

Estos resultados experimentales demuestran que la oxidación de Cu con aire en un lecho fijo con contenidos de cobre iguales o mayores al 20% en peso conlleva alcanzar temperaturas mayores a 900ºC, las cuales podrían conducir a una rápida degradación del sólido, tal y como se ha explicado en la introducción de la presente tesis doctoral. El control del aumento de la temperatura es aún más delicado durante la etapa de oxidación en el proceso Ca-Cu, puesto que en el lecho habrá material de calcio

parcialmente carbonatado en una etapa previa de reformado de metano, y su calcinación ha de minimizarse para mantener una eficacia elevada de captura de CO_2 en el proceso.

Para moderar la temperatura máxima del frente de oxidación a valores cercanos a 800ºC manteniendo una concentración de cobre en el lecho en torno al 20% en peso, es necesario recircular gran parte del N_2 obtenido a la salida y así disminuir significativamente el contendido de O_2 en la alimentación, tal y como propusieron Abanades et al. (2010). Para demostrar experimentalmente este caso se llevó a cabo un nuevo ensayo alimentando un flujo mucho mayor de gas (24 lN/min) con un contenido en oxígeno del 3% en volumen partiendo de un perfil de temperaturas en el lecho cercano a 400ºC, y precalentando la alimentación a 400ºC. Bajo estas condiciones de operación el frente de intercambio de calor resultante de la oxidación de Cu avanza muy por delante del frente de reacción. El gas llega al frente de oxidación a su temperatura de entrada y se calienta rápidamente gracias al calor desprendido de la oxidación. El caudal de gas tan elevado transporta este calor aguas abajo y de esta forma se modera la temperatura máxima del lecho. A pesar de partir de un lecho a tan baja temperatura y alimentar una concentración de O_2 muy diluida, la cinética de oxidación fue suficientemente rápida como para convertir todo el oxígeno, de forma que para tiempos previos al periodo de ruptura sólo se observó N_2 a la salida del reactor. Los resultados experimentales han validado razonablemente el modelo matemático desarrollado en Matlab, tal y como se muestra en la Publicación IV.

Con el objetivo de mejorar el perfil inicial de temperatura en el lecho y poder evaluar otras condiciones de operación a nivel experimental, se están realizando mejoras en el equipo experimental construido en el INCAR. Con ello se pretende continuar con estos ensayos partiendo de un perfil de temperatura más homogéneo, poder ampliar el análisis de sensibilidad incluyendo metano en la alimentación, así como profundizar en el estudio sobre la formación de óxidos mixtos de cobre y calcio tras múltiples ciclos de carbonatación/calcinación y reducción/oxidación.

5.3.1. Publicación III

Investigation of a fixed-reactor for the calcination

$CaCO_3$ by the simultaneous reduction of CuO With a fuel gas

Publicado en:

Industrial & Engineering Chemistry Research

Volumen 55

Páginas 5128-5132

Año 2016

I&EC research
Industrial & Engineering Chemistry Research

Article
pubs.acs.org/IECR

Investigation of a Fixed-Bed Reactor for the Calcination of $CaCO_3$ by the Simultaneous Reduction of CuO with a Fuel Gas

José R. Fernández,* Juana M. Alarcón, and J. Carlos Abanades

Spanish Research Council, INCAR-CSIC, C/Francisco Pintado Fe, 26, 33011, Oviedo, Spain

ABSTRACT: The exothermic reduction of CuO to Cu using a fuel gas as a source of heat to carry out the simultaneous calcination of $CaCO_3$ in a fixed bed has been evaluated. A dynamic pseudohomogeneous model has been developed to describe in detail the transient behavior of this operation. The experimental tests have been performed in a lab scale packed-bed reactor (i.d. × L = 38 mm × 920 mm) containing a mixture of CaO- and CuO-based particles (with 12 and 60 wt % of active phase, respectively). Preliminary heat-transfer studies have been carried out using inert gases at different temperatures to estimate the overall heat transfer coefficient of the system. An overall heat transfer coefficient of around 5 W/m^2 K has been obtained, which is a sufficiently low value to claim an operation close to adiabatic conditions. Hydrogen has been chosen as reducing gas. A Cu/Ca molar ratio of 1.8 in the bed allows both the reduction and calcination fronts to advance together, with moderate maximum temperatures of around 870 °C, leaving behind totally converted solids. The effect of the solids temperature on the operation has also been evaluated. A rapid and complete reduction of CuO with H_2 has been achieved, even with starting temperatures slightly higher than 400 °C. However, the calcination of $CaCO_3$ was complete only in those zones of the bed where the temperature profile reached 870 °C.

INTRODUCTION

The increase in carbon dioxide emissions related to human activities is widely recognized as one of the most important causes of climate change. Among the various strategies proposed, carbon capture and storage (CCS) is considered a feasible midterm solution to drastically reduce the CO_2 emissions generated in activities, which nowadays are great consumers of fossil fuels (i.e., power generation, cement production, refineries, steel industry, etc.).[1] The purpose of CO_2 capture is to obtain a concentrated stream that can be readily transported to a CO_2 storage site. CO_2 capture is currently considered the most energy intensive step in CCS (around 75% of the overall cost), and therefore, there is a great interest worldwide in developing new technologies focused on minimizing the energy penalties, the environmental impact, and the cost of the equipment traditionally associated with the CO_2 capture process.[2] Hydrogen, which has long been an important raw material in the chemical and petroleum industries, is also considered to be a clean source of energy for sustainable consumption. Steam methane reforming (SMR) is still the most common route for the industrial production of hydrogen. This heterogeneous catalyzed process requires multiple steps that must be performed under severe operating conditions and consumes a large amount of energy because of the high endothermicity of the overall reforming reaction.[3] In the sorption enhanced reforming (SER), the combination of a Ca-based material with the reforming catalyst allows the CO_2 to be removed as soon as it is produced. The separation of CO_2 from the gas phase shifts the equilibrium to the production of H_2, with the result that almost complete conversion of methane and CO can be achieved in one step under relatively mild operating conditions. Moreover, the carbonation of the Ca-sorbent is strongly exothermic and provides directly the energy required to carry out the reforming reaction without the need for external heating.[4−7] However, the $CaCO_3$ formed by the carbonation of the CO_2-sorbent needs to be subsequently regenerated by calcination to allow a multicycle operation in the SER process. The calcination of $CaCO_3$ is highly endothermic and needs to be carried out under a CO_2-rich atmosphere and at a very high temperature (above 850 °C) if the objective is a high CO_2 capture efficiency. Several proposals have been reported in the literature. These mainly involve oxy-fuel combustion in a regenerator,[8,9] indirect heating by hot solids,[10,11] or by hot gases obtained from additional fuel combustion.[12,13] Another alternative that has recently been proposed is the use of a Ca−Cu chemical loop system to supply the energy required to regenerate the Ca-based sorbent,[14] based on the "unmixed reforming" concept originally conceived by Kumar et al.[15] This concept involves the use of a metal/metal oxide chemical loop (Fe- or Ni-based material) to generate the heat required for the decomposition of $CaCO_3$ to CaO by means of the oxidation of the metal with air. With this method, a high energy efficiency can be achieved since the heat is directly transferred from the metal particles, which are being reduced, to the $CaCO_3$ particles arranged in the same bed. However, the CO_2 resulting from the calcination is emitted highly diluted by nitrogen, and therefore, the problem of the emissions of CO_2 to atmosphere remains unsolved. In the Ca−Cu looping process, the heat needed for the calcination is supplied by the exothermic reduction of CuO with a fuel gas (CH_4, CO, or H_2), which produces a gas stream rich in CO_2 and easily separable H_2O. The Ca/Cu looping process consists

Special Issue: International Conference on Chemical and Biochemical Engineering 2015

Received: October 28, 2015
Revised: December 18, 2015
Accepted: December 20, 2015
Published: December 31, 2015

DOI: 10.1021/acs.iecr.5b04073
Ind. Eng. Chem. Res. 2016, 55, 5128−5132

of a sequence of three main reaction stages (see Figure 1), that are carried out in adiabatic fixed-bed reactors operating in

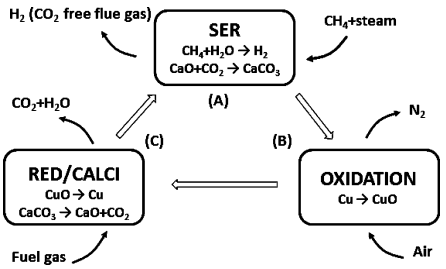

Figure 1. General scheme of the Ca/Cu looping process.

parallel to ensure that every stage is carried out simultaneously. The first step (A) comprises the production of H_2 by means of a SER process using steam and methane as feedstock in the presence of a reforming catalyst, a Ca-based sorbent, and a Cu-based material in its reduced form.[16] In the next reaction step (B), the oxidation of Cu to CuO is carried out by feeding diluted air under conditions of minimal decomposition of the $CaCO_3$ formed during step A.[17]

In the last stage (C), the calcination of the $CaCO_3$ formed in stage A is performed by means of the simultaneous reduction of the CuO produced in stage B. With a suitable $CuO/CaCO_3$ molar ratio, the heat generated in the reduction of CuO with a fuel gas will provide the energy required for the endothermic $CaCO_3$ calcination without the need for an additional energy supply.[18] At the same time, a CO_2-rich product gas is obtained ready for its transport and geological storage. The composition of the fuel gas strongly affects the Cu/Ca molar ratio required to ensure a suitable bed performance. If pure CH_4 is used, a Cu/Ca molar ratio of 3.1 will be needed to reach neutral conditions in the reaction fronts, taking into account the enthalpies of both CuO reduction and $CaCO_3$ calcination reactions given at 900 °C. The reduction enthalpy of CuO with H_2 is higher, which reduces the Cu/Ca molar ratio needed to 1.8. If pure CO is used as fuel gas, the Cu/Ca molar ratio will be the minimum required (i.e., around 1.3). Some recent works have been done on the conceptual design of the Ca−Cu looping process[19] and the development of Ca/Cu based sorbents that could be potentially applied.[20−24] However, any work to date has been focused on experimentally demonstrating under the boundary conditions of a Ca/Cu looping system the viability of the reduction/calcination stage, which is the key reaction step of this process. The modeling work and preliminary heat-transfer and reaction tests presented in this work demonstrate that the exothermic reduction of CuO with a fuel gas is able to support the calcination of $CaCO_3$ in a same fixed-bed reactor under pseudoadiabatic conditions.

■ EXPERIMENTAL SECTION

An experimental setup was specifically designed and constructed to study the reduction/calcination operation. The fixed-bed reactor consists of an Inconel tube (i.d. × L = 38 mm × 920 mm) that contains a mixture of CaO- and CuO-based materials (with 12 and 60 wt % of active phase, respectively). A thick coating of insulating material (quartz wool) surrounds the reactor tube, which in turn is installed inside a ceramic oven to minimize heat losses. Inside the bed, a multipoint K-type thermocouple measures the temperature at different axial positions. A schematic overview of the experimental setup, including a representation of the reactor cross section, is shown in Figure 2. The flow rate and gas composition are controlled

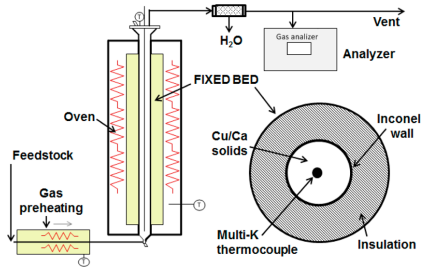

Figure 2. Schematic overview of the fixed-bed reactor setup.

by mass flow controllers. The feed gas is preheated before it enters the reactor by means of two heating tapes. A bed of silica gel downstream of the fixed bed allows the steam present in the product gas to be removed. The dry composition of the product gas is measured by IR and thermal conductivity analyzers.

■ REACTOR MODEL

A pseudohomogenous model was developed to describe the progressive reduction of CuO with a fuel gas and the simultaneous decomposition of $CaCO_3$ in the fixed bed. A dynamic model is required to describe this process, since CuO and $CaCO_3$ are gradually converted during the course of the operation. The following assumptions were adopted: mass and thermal dispersion in the axial direction, negligible radial temperature and concentration gradients, negligible intraparticle mass and temperature gradients, ideal gas behavior, a constant bed void fraction (ε = 0.5), a uniform particle size in the bed (dp = 0.003 m) and a perfect mixing of the solids. For the incorporation of heat losses, the environment was assumed to have a constant temperature (T_w) and the heat transferred between the reactor and the oven was evaluated using an overall heat transfer coefficient (U), which was experimentally estimated.

The fuel gas was assumed to be fully converted to CO_2 and H_2O, which means that carbon deposition is negligible. The literature on chemical looping combustion with Cu-based materials supports this affirmation.[25] Moreover, the presence of calcium minimizes carbon formation, even at high temperatures.[26] An overview of the mass and energy balances is given in Table 1. Internal diffusion limitations may also appear. An average effectiveness factor (η) of about 0.5 is assumed in order to tackle possible diffusion resistance in the Cu-based particles. This assumption is in agreement with the results recently published on Cu reduction with a syngas for chemical looping applications.[27] However, the effectiveness factor for the $CaCO_3$ calcination is assumed to be 1, as temperature is the main limiting factor in this reaction, there being negligible possible diffusional effects. A shrinking core model (SCM) was used to represent the kinetics of CuO reduction and $CaCO_3$ calcination, which is a generally accepted model in the literature. More details about the kinetics and the implementa-

DOI: 10.1021/acs.iecr.5b04073
Ind. Eng. Chem. Res. 2016, 55, 5128−5132

Table 1. Mass and Energy Balances Used in the Model

Component mass balances

$$\varepsilon\frac{\partial C_i}{\partial t} = -u_g\frac{\partial C_i}{\partial Z} + \frac{\partial}{\partial Z}\left(D_{eff}\frac{\partial C_i}{\partial Z}\right) + \eta(1-\varepsilon)r_i$$

Energy balance

$$((1-\varepsilon)\rho_s C_{ps} + \varepsilon\rho_g C_{pg})\frac{\partial T}{\partial t} = -u_g\rho_g C_{pg}\frac{\partial T}{\partial Z} + \frac{\partial}{\partial Z}\left(\lambda_{eff}\frac{\partial T}{\partial Z}\right) - \Sigma\eta_i(1-\varepsilon)H_{ri}r_i - U(4/dr)(T - Tw)$$

Momentum balance

$$\frac{dP}{dZ} = -150\frac{\mu_g u_g(1-\varepsilon)^2}{d_p^2\varepsilon^3} + 1.75\frac{\rho_g u_g^2(1-\varepsilon)}{d_p\varepsilon^3}$$

Axial mass dispersion coefficient

$$D_{eff} = \left[\frac{0.73}{R_e S_c} + \frac{0.5}{\varepsilon + \frac{9.7\varepsilon^2}{R_e S_c}}\right]u_g d_p$$

$$\lambda_{eff} = \lambda_{0bed} + \frac{R_e P k_g}{Pe_{az}} + \frac{R_e^2 P_r^2 k_g^2}{6(1-\varepsilon)N_u};$$

$$\lambda_{0bed} = \left(\frac{k_s}{k_g}\right)^{0.28-0.757\log(\varepsilon)-0.057\log(k_s/k_g)}$$

$$Pe_{az} = \frac{2p}{1-p}; \quad p = 0.17 + 0.29e^{[-24/R_e]}; \; N_u = 2 + 1.8R_e^{0.5}P_r^{0.33}$$

Reaction rates

$$\frac{t}{\tau} = 1 - (1 - X_{red})^{1/2}; \quad \tau = \frac{\rho_{m,CuO}L_{CuO}}{k_{red}C_g^n}$$

$$r_{red} = \frac{\rho_{CuO}1000}{M_{CuO}}\frac{dX_{red}}{dt}; \quad k_{red} = k_0 e^{-E_a/(RT)}$$

$$\frac{dX_{cal}}{dt} = k_{cal}(1 - X_{cal})^{2/3}(C_{CO_2,eq} - C_{CO_2}); \quad r_{cal} = \frac{\rho_{CaCO_3}1000}{M_{CaCO_3}}\frac{dX_{cal}}{dt}$$

tion of the model in order to find a numerical solution have been provided elsewhere.[18]

RESULTS AND DISCUSSION

First, heat-transfer experiments without any chemical reaction were carried out by feeding pure N_2 (40 lN/min) into the fixed bed, which only contained alumina (d_p = 0.003 m) in order to estimate the overall heat transfer coefficient (U) of the system. This study consisted in heating the solids bed, initially at ambient temperature, by feeding preheated N_2 at 475 °C. The cooling of the fixed bed (initially at 600 °C) by the feed of N_2 to a lower temperature was also carried out. A value of U of about 5 W/(m^2 K) was calculated, which allows a good adjustment between the experimental results and the temperature profiles predicted by the model. Figure 3 shows the results obtained during the solids bed heating test.

For the study of the calcination of $CaCO_3$ by the simultaneous reduction of CuO, the fixed bed was loaded with a mixture of CaO- and CuO-based particles (d_p = 3 mm). As reported in previous works on Ca/Cu looping process,[14,19] the fuel gas fed into the reduction/calcination stage is obtained in a subsequent steam reforming stage. This stream is mainly composed of H_2 (up to 75 vol %) and CO. For this reason, hydrogen was chosen as reducing gas in this work. The solids bed consisted of a mass of 920 g with an active weight content of 20.6 wt % CuO and 13.5 wt % of $CaCO_3$. The rest of the bed was mainly inert CaO and inert support of the CuO-based material. In these conditions, a Cu/Ca molar ratio of around 1.8 was present in the bed, which is the composition needed to theoretically reach neutral conditions in the reaction fronts during the reduction/calcination operation with H_2.[18] A flow rate of 15 lN/min (50 vol % H_2 and 50 vol % of N_2) preheated at 400 °C was used as fuel gas. In this study, the operation was carried out with an initial solids temperature that ranged from 415 °C at the bottom of the reactor to around 700 °C at the top. The fuel gas was fed in at the bottom (at the lowest temperature) in order to study the effect of the initial temperature on the reactions involved in the process. From the moment that the fuel gas is fed into the reactor, a rapid increase in temperature is observed due to the exothermic reduction of CuO with H_2. During the first minutes (t < 2 min), the temperature achieved in the reduction front (R) is lower than 800 °C. In these conditions, the calcination of $CaCO_3$ is not favored, and therefore, during this period of time, the product gas contains a very small amount of CO2 (less than 1 vol %, as can be seen in Figure 4). Because of the low content of CuO in the bed and the high concentration of H_2 in the feed, the reduction front (R) advances faster than the heat exchange front resulting from the reduction of CuO. Consequently, the reduced solids are left behind at high temperature, which allows

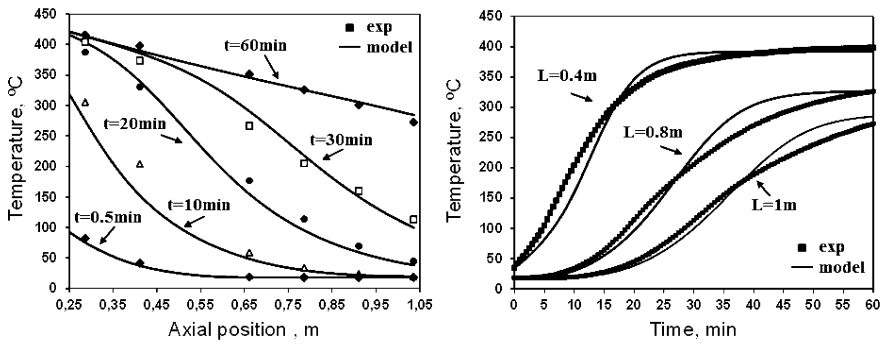

Figure 3. Comparison between temperature profiles obtained in heat-transfer experiments and the profiles predicted by the model for U = 5 W/(m^2 K) (inlet gas temperature = 475 °C, starting bed temperature = 25 °C).

DOI: 10.1021/acs.iecr.5b04073
Ind. Eng. Chem. Res. 2016, 55, 5128−5132

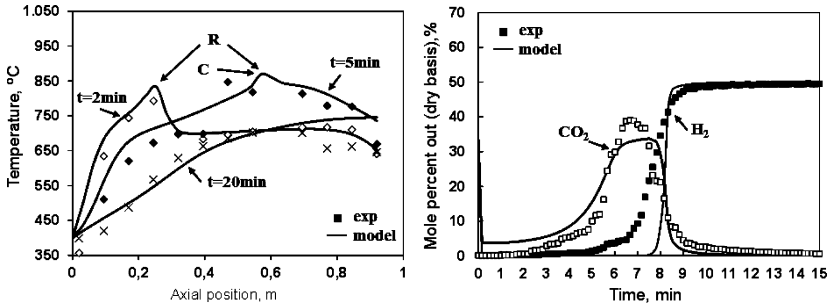

Figure 4. Axial temperature profiles and outlet gas composition during the reduction/calcination operation.

the fuel gas to arrive at the reduction front preheated by these solids. As the reduction front moves forward, the temperature profile progressively increases until it reaches a maximum of around 870 °C (t = 5 min). At this temperature, $CaCO_3$ is rapidly calcined, resulting in increasing quantities of CO_2 in the product gas up to 40 vol % (on a dry basis). The evolution of the temperature and gas composition during the operation is described very accurately by the model, as shown in Figure 4.

The generation of CO_2 by calcination causes a significant increase in the total flow rate, and therefore, the heat exchange front resulting front calcination advances faster than both the reduction (R) and calcination (C) fronts. Under these circumstances, part of the heat generated in the reduction front is blown downstream and is used to increase the temperature of the still unconverted solids. These results confirm the general trends observed in a recent work.[18] After 6 min of operation, increasing amounts of H_2 in the product gas are observed that indicate the reduction front is approaching the reactor exit (breakthrough period). At t = 9 min, the H_2 content in the product gas reaches 50 vol %, which means the bed has been totally reduced. However, a lower amount of CO_2 than expected for the total bed calcination is observed in the product gas during the operation.

Figure 5 shows the axial solids conversions predicted by the model. A starting temperature of 415 °C at the reactor inlet

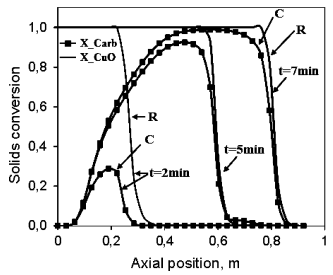

Figure 5. Evolution of axial solids conversions given by the model.

allows from the very beginning the rapid and total conversion of the CuO in a narrow reduction front (R). However, the maximum temperature achieved during the first 5 min is too low to favor the calcination and, therefore, part of the bed is left uncalcined. By the time the temperature profile achieves a maximum of 870 °C (see Figure 4), the reduction and calcination fronts advance together (see t > 5 min in Figure 5), leaving the second half of the reactor totally converted. At these conditions, around 25% of the $CaCO_3$ present in the bed is left uncalcined. Nongenerated $CaCO_3$ would act as inert in a subsequent SER stage. A lower amount of H_2 would be produced for the same cycle duration, and therefore, the overall energy efficiency of the process would decrease. A suitable process design is required in order to leave the solids bed after the oxidation stage (B in Figure 1) at a sufficiently high temperature to allow from the very beginning the simultaneous reduction/calcination during the stage C.[14,18] The results obtained in this work confirm that the reduction of CuO to Cu with H_2 can provide the thermal energy required to carry out the calcination of $CaCO_3$ in the same fixed-bed reactor. Future work will include a detailed study of the key design variables of this operation, that is, the Cu/Ca molar ratio, the temperature, and the composition of the fuel gas. Alternative fuel gases (CH_4, CO) and other materials for the Ca/Cu looping process will be also investigated.

■ CONCLUSIONS

The viability of $CaCO_3$ calcination by the simultaneous reduction of CuO in a fixed-bed reactor has been demonstrated. The dynamic model developed in this work gives a good description of this operation. A suitable Cu/Ca molar ratio in the bed (around 1.8 when H_2 is used as fuel gas) allows both the reduction and calcination fronts to move forward together at a moderate maximum temperature of 870 °C, leaving behind solids totally converted. Temperatures in the bed lower than 800 °C allow a rapid reduction of CuO with H_2, but the calcination is not favored under these conditions and part of the bed may be left uncalcined.

■ AUTHOR INFORMATION

Corresponding Author

*Tel.: +34 985 11 90 90. E-mail: jramon@incar.csic.es.

Notes

The authors declare no competing financial interest.

■ ACKNOWLEDGMENTS

The authors gratefully acknowledge the support from Johnson Matthey and Carmeuse for supplying the Cu- and Ca-based materials in this work. This work was financed by the Spanish National Program (ENE2012-37936-C02-02) and by the EU Seventh Framework Programme (ASCENT project, n° 608512). Financial support for the Ph.D. of Juana M. Alarcón

DOI: 10.1021/acs.iecr.5b04073
Ind. Eng. Chem. Res. 2016, 55, 5128−5132

is provided by the FPI Spanish National Programme (Grant No. BES-2013-063835).

REFERENCES

(1) Metz, B. *Controlling Climate Change*; Cambridge University Press: 2010.

(2) Boot-Handford, M. E.; Abanades, J. C.; Anthony, E. J.; Blunt, M. J.; Brandani, S.; Mac Dowell, N.; Fernandez, J. R.; Ferrari, M. C.; Gross, R.; Hallett, J. P.; Haszeldine, R. S.; Heptonstall, P.; Lyngfelt, A.; Makuch, Z.; Mangano, E.; Porter, R. T. J.; Pourkashanian, M.; Rochelle, G. T.; Shah, N.; Yao, J. G.; Fennell, P. S. Carbon capture and storage update. *Energy Environ. Sci.* **2014**, *7*, 130−189.

(3) Rostrup-Nielsen, J. R. Steam reforming and chemical recuperation. *Catal. Today* **2009**, *145*, 72−75.

(4) Hufton, J. R.; Mayorga, S.; Sircar, S. Sorption-enhanced reaction process for hydrogen production. *AIChE J.* **1999**, *45* (2), 248−256.

(5) Lopez Ortiz, A.; Harrison, D. P. Hydrogen production using sorption-enhanced reaction. *Ind. Eng. Chem. Res.* **2001**, *40* (23), 5102−5109.

(6) Johnsen, K.; Grace, J. R.; Elnashaie, S. S. E. H.; Kolbeinsen, L.; Eriksen, D. Modeling of sorption-enhanced steam reforming in a dual fluidized bubbling bed reactor. *Ind. Eng. Chem. Res.* **2006**, *45* (12), 4133−4144.

(7) Harrison, D. P. Sorption-enhanced hydrogen production: a review. *Ind. Eng. Chem. Res.* **2008**, *47*, 6486−6501.

(8) Weimer, T.; Berger, R.; Hawthorne, C.; Abanades, J. C. Lime enhanced gasification of solid fuels: Examination of a process for simultaneous hydrogen production and CO_2 capture. *Fuel* **2008**, *87*, 1678−1686.

(9) Martínez, I.; Romano, M. C.; Chiesa, P.; Grasa, G.; Murillo, R. Hydrogen production through sorption enhanced steam reforming of natural gas: Thermodynamic plant assessment. *Int. J. Hydrogen Energy* **2013**, *38*, 15180−15199.

(10) Wolf, J.; Yan, J. Parametric study of chemical looping combustion for tri-generation of hydrogen, heat, and electrical power with CO_2 capture. *Int. J. Energy Res.* **2005**, *29*, 739−753.

(11) Fernández, J. R.; Abanades, J. C. CO_2 capture from the calcination of $CaCO_3$ using iron oxide as heat carrier. *J. Cleaner Prod.* **2016**, *112*, 1211−1217.

(12) Johnsen, K.; Ryu, H. J.; Grace, J. R.; Lim, C. J. Sorption-enhanced steam reforming of methane in a fluidized bed reactor with dolomite as CO_2-acceptor. *Chem. Eng. Sci.* **2006**, *61*, 1195−1202.

(13) Stevens, J. F.; Krishnamurthy, B.; Atanassova, P.; Spilker, K. *Development of 50 kW Fuel Processor for Stationary Fuel Cell Applications*; Final report, DOE/GO/13102-1; Chevron Techology Ventures, LLC: 2007.

(14) Fernández, J. R.; Abanades, J. C.; Murillo, R.; Grasa, G. Conceptual design of a hydrogen production process from natural gas with CO_2 capture using a Ca−Cu chemical loop. *Int. J. Greenhouse Gas Control* **2012**, *6*, 126−141.

(15) Kumar, R.; Lyon, R.; Cole, J. Unmixed reforming: A novel autothermal cyclic steam reforming process. In *Advances in Hydrogen Energy*; Springer, US: 2000; pp 31−45.

(16) Fernandez, J. R.; Abanades, J. C.; Grasa, G. Modeling of sorption enhanced steam methane reforming—Part II: Simulation within a novel Ca/Cu chemical loop process for hydrogen production. *Chem. Eng. Sci.* **2012**, *84*, 12−20.

(17) Fernández, J. R.; Abanades, J. C.; Murillo, R. Modeling of Cu oxidation in adiabatic fixed-bed reactor with N_2 recycling in a Ca/Cu chemical loop. *Chem. Eng. J.* **2013**, *232*, 442−452.

(18) Alarcón, J. M.; Fernández, J. R. $CaCO_3$ calcination by the simultaneous reduction of CuO in a Ca/Cu chemical looping process. *Chem. Eng. Sci.* **2015**, *137*, 254−267.

(19) Martinez, I.; Romano, M. C.; Fernandez, M. C.; Chiesa, P.; Murillo, R.; Abanades, J. C. Process design of a hydrogen production plant from natural gas with CO_2 capture based on a novel Ca/Cu chemical loop. *Appl. Energy* **2014**, *114*, 192−208.

(20) Manovic, V.; Anthony, E. J. Integration of calcium and chemical looping combustion using composite CaO/CuO-based materials. *Environ. Sci. Technol.* **2011**, *45*, 10750−10756.

(21) Qin, C.; Yin, J.; Liu, W.; An, H.; Feng, B. Behavior of CaO/CuO based composite in a combined calcium and copper chemical looping process. *Ind. Eng. Chem. Res.* **2012**, *51*, 12274−12281.

(22) Kierzkoska, A.; Muller, C. R. Development of calcium-based, copper functionalized CO_2 sorbents to integrate chemical looping combustion into calcium looping, Energ. *Energy Environ. Sci.* **2012**, *5*, 6061−6065.

(23) García-Lario, A. L.; Martínez, I.; Murillo, R.; Grasa, G.; Fernández, J. R.; Abanades, J. C. Reduction Kinetics of a High Load Cu-based Pellet Suitable for Ca/Cu Chemical Loops. *Ind. Eng. Chem. Res.* **2013**, *52*, 1481−1490.

(24) Qin, C.; Feng, B.; Yin, J.; Ran, J.; Zhang, L.; Manovic, V. Matching of kinetics of $CaCO_3$ decomposition and CuO reduction with CH_4 in Ca−Cu chemical looping. *Chem. Eng. J.* **2015**, *262*, 665−675.

(25) Adanez, J.; Abad, A.; Garcia-Labiano, F.; Gayan, P.; de Diego, L. F. Progress in chemical-looping combustion and reforming technologies. *Prog. Energy Combust. Sci.* **2012**, *38*, 215−282.

(26) Bellido, J. D. A.; De Souza, J. E.; M'Peko, J. C.; Assaf, E. M. Effect of adding CaO to ZrO_2 support on nickel catalyst activity in dry reforming of methane. *Appl. Catal., A* **2009**, *358*, 215−223.

(27) Hamers, H. P.; Gallucci, F.; Cobden, P. D.; Kimball, E.; van Sint Annaland, M. A novel reactor configuration for packed bed chemical-looping combustion of syngas. *Int. J. Greenhouse Gas Control* **2013**, *16*, 1−12.

DOI: 10.1021/acs.iecr.5b04073
Ind. Eng. Chem. Res. 2016, 55, 5128−5132

5.3.2. Publicación IV

Study of a Cu-CuO chemical loop for the calcination of $CaCO_3$ in a fixed-bed reactor

Pendiente de publicación en:

Chemical Engineering Journal

Elsevier Editorial System(tm) for Chemical Engineering Journal
Manuscript Draft

Manuscript Number:

Title: Study of a Cu-CuO chemical loop for the calcination of CaCO3 in a fixed bed reactor

Article Type: Research Paper

Section/Category: Chemical Reaction Engineering

Keywords: CO2 capture; CaCO3 calcination; CuO reduction; Cu oxidation, chemical looping combustion

Corresponding Author: Dr. Jose Ramon Fernandez,

Corresponding Author's Institution: CSIC-INCAR

First Author: Juan Maria Alarcon

Order of Authors: Juan Maria Alarcon; Jose Ramon Fernandez; Juan Carlos Abanades

Abstract: The use of a Cu/CuO chemical loop to supply the heat required to carry out the calcination of CaCO3 in a fixed-bed reactor is experimentally evaluated. The effects of the fuel gas composition, the Cu/Ca molar ratio, the temperature of the solids bed and possible side reactions on the reduction/calcination stage are studied under pseudo-adiabatic conditions in a fixed-bed reactor (i.d. × L = 0.038 m × 0.92 m) using commercial Ca- and Cu-based materials. It was observed that initial temperatures in the solids bed of more than 650 °C make it possible to achieve the complete calcination of CaCO3. Suitable Cu/Ca molar ratios, depending on the composition of the gaseous fuel used to reduce CuO, can moderate the increase in temperature in the reduction front and allow the simultaneous calcination of CaCO3. The multicycle operation at high temperature modifies the chemical composition of the functional materials and leads to the formation of mixed Ca-Cu oxides that are able to capture CO2, which affect the CO2 sorption capacity of these materials. Moreover, the influence of O2 dilution in the inlet gas upon the temperature profiles during the Cu oxidation stage was assessed. The recirculation of a large part of the product gas resulting from the oxidation stage moderates the temperature profile and the complete conversion of the Cu-based solids is achieved in a relatively sharp oxidation front despite the low O2 content in the feed (i. e., 3 vol.% O2). The experimental results are in close agreement with the predictions of a one-dimensional reactor model that incorporates existing information taken from the literature on the kinetics, fluid dynamics and heat transfer

Suggested Reviewers: Stefano Stendardo
Department of Advanced Technologies for Energy and Industry, ENEA
stefano.stendardo@enea.it
Expert in catalysis and CO2 capture processes

Angeliki Lemonidou
Department of Chemical Engineering, University of Thessaloniki

Study of a Cu-CuO chemical loop for the calcination of $CaCO_3$ in a fixed bed reactor

Juana María Alarcón, José Ramón Fernández*, Juan Carlos Abanades

Spanish Research Council, INCAR-CSIC. C/ Francisco Pintado Fe, 26, 33011, Oviedo. Spain.

*corresponding author: jramon@incar.csic.es

Abstract

The use of a Cu/CuO chemical loop to supply the heat required to carry out the calcination of $CaCO_3$ in a fixed-bed reactor is experimentally evaluated. The effects of the fuel gas composition, the Cu/Ca molar ratio, the temperature of the solids bed and possible side reactions on the reduction/calcination stage are studied under pseudo-adiabatic conditions in a fixed-bed reactor (i.d. × L = 0.038 m × 0.92 m) using commercial Ca- and Cu-based materials. It was observed that initial temperatures in the solids bed of more than 650 ºC make it possible to achieve the complete calcination of $CaCO_3$. Suitable Cu/Ca molar ratios, depending on the composition of the gaseous fuel used to reduce CuO, can moderate the increase in temperature in the reduction front and allow the simultaneous calcination of $CaCO_3$. The multicycle operation at high temperature modifies the chemical composition of the functional materials and leads to the formation of mixed Ca-Cu oxides that are able to capture CO_2, which affect the CO_2 sorption capacity of these materials. Moreover, the influence of O_2 dilution in the inlet gas upon the temperature profiles during the Cu oxidation stage was assessed. The recirculation of a large part of the product gas resulting from the oxidation stage moderates the temperature profile and the complete conversion of the Cu-based solids is achieved in a relatively sharp oxidation front despite the low O_2 content in the feed (i. e., 3 vol.% O_2). The experimental results are in close agreement with the predictions of a one-dimensional reactor model that incorporates existing information taken from the literature on the kinetics, fluid dynamics and heat transfer.

Keywords: CO_2 capture; chemical looping combustion; $CaCO_3$ calcination; CuO reduction; Cu oxidation; fixed-bed reactor

1. Introduction

The increasing concentration of greenhouse gases in the atmosphere resulting from anthropogenic emissions is generally accepted as one of the main factors of climate change [1]. Carbon capture and storage (CCS) remains a promising alternative for drastically reducing CO_2 emissions from industries and large-scale power generation [2]. The development of pre-combustion CO_2 capture technologies is an attractive option for producing hydrogen with a potentially low-carbon footprint [2]. The demand for hydrogen as a feedstock in chemical, refining, glass and steel industries has grown

in the last few decades [3]. Moreover, its use as a fuel for gas turbines, fuel cells and combustion engines is expected to increase further in the medium-to-long term once the viability of these recent technologies has been demonstrated on a large scale [3]. Although hydrogen can be obtained from many primary energy sources, Steam Methane Reforming (SMR) remains the most widely used and economical technology for producing H_2 on a commercial scale [3]. This heterogeneous catalytic process requires multiple steps performed under severe operating conditions (i. e. temperatures between 800 and 900 ºC and pressures of up to 35 bar) to overcome the thermodynamic limitations imposed by the reforming reactions and to facilitate the conversion of the fuel to H_2 [4]. Although SMR is a highly efficient route compared to other alternatives [3], it is an energy-intensive process since the main reactions involved are highly endothermic. Moreover, the CO_2 emissions caused by the steam reforming are significantly high (about 9 kg CO_2/kg H_2 produced) due not only to the CO_2 generated inside the tubular reformers but also to the CO_2 produced by firing additional fuel in external burners in order to supply the heat required for the process [4].

In the Sorption Enhanced Reforming (SER), the CO_2 is removed "in situ" in the reforming reactor by a CO_2-sorbent (typically a CaO-based material) in combination with the reforming catalyst [5]. The CO_2 sorption reaction (i. e. CaO carbonation) shifts the equilibrium of the steam reforming and water-gas-shift (WGS) reactions towards the production of hydrogen, with the result that almost pure H_2 (higher than 90 vol.% on a dry basis) can be obtained in a single stage under relatively mild operating conditions (between 600-700 ºC) [5, 6]. In the SER, the carbonation of CaO (a highly exothermic reaction) supplies the heat to sustain the process directly, avoiding the need for an external energy supply. Additional WGS stages are not required and the downstream H_2 purification procedure is significantly simplified (or even eliminated depending on the final application of the H_2). Considerable progress has recently been made in the field of SER in fixed beds [7-11] and in the development of CaO-based materials in order to improve their sorbent capacity and durability [12-14]. However, the main obstacle to the development of the SER technology is to find a procedure to supply the heat required for the calcination of $CaCO_3$ under CO_2-rich atmospheres (a necessary condition to facilitate the subsequent purification, compression and storage of CO_2) with the minimum energy penalty. Several process schemes envisaged for this purpose are described in literature, such as heating by using high-temperature solids that come from a separate combustion chamber [15, 16], oxy-fuel combustion in a regenerator [17-19] and indirect heating through heat transfer surfaces [20-22]. The use of chemical looping combustion (CLC) systems [23] has also been proposed to carry out the thermal decomposition of $CaCO_3$. General Electric originally calcined $CaCO_3$ by means of the simultaneous oxidation of nickel-based particles with air in the same reactor [24]. Direct heating without the need for intermediate devices should lead to greater energy efficiency, but the CO_2 generated is highly diluted with nitrogen (from the air), making it necessary to include downstream steps for the capture of CO_2. More recently CLC configurations have been designed to supply the heat needed for calcination by

exploiting the large heat-transfer capacity of oxygen carriers that come from an oxidation reactor at temperatures above 1000 ºC [25, 26].

A Ca-Cu looping process has recently been proposed to enhance the production of H_2 with CO_2 capture (on the basis of the SER concept). In this process, a Cu/CuO chemical loop directly supplies the heat needed to regenerate the Ca-based sorbent [27, 28]. The heat is generated by the exothermic reduction of CuO with gaseous fuels (CH_4, CO, H_2 present in the process), thereby producing a highly concentrated stream of CO_2 and H_2O(v). The basic Ca-Cu looping concept comprises a sequence of three reaction steps, which are represented in Fig. 1. An enriched stream of hydrogen is produced at a moderate temperature and at high pressure in a first stage of sorption enhanced reforming of methane in the presence of a reforming catalyst, a calcium-based sorbent and a reduced copper-based material (that acts as inert solid in this step) [29]. In the following stage, the Cu-based solids are oxidized by diluted air at high pressure. A low oxygen content and a low temperature in the feed moderate the increase in temperature during the Cu oxidation, thereby minimizing the decomposition of $CaCO_3$ through partial calcination [30]. In the next step, a suitable CuO/$CaCO_3$ ratio in the composition of the bed ensures that the heat released from the reduction of CuO is enough to simultaneously calcine the $CaCO_3$ without the need for an external energy supply [31-33].

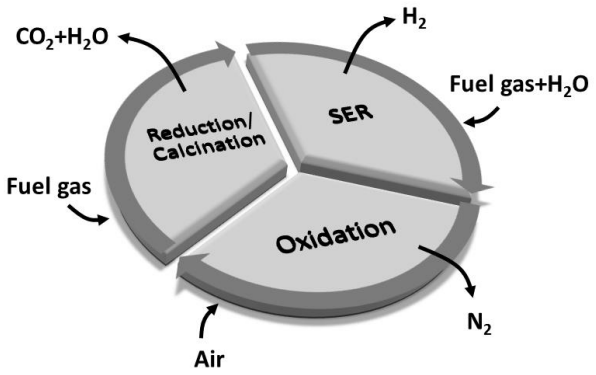

Fig. 1. Main reaction stages involved in the Ca-Cu looping process.

Although interconnected fluidized bed reactors have also been considered for this purpose [34, 35], most studies on the Ca-Cu looping process propose systems composed of packed beds [28-31, 33, 36, 37] since they facilitate operation at the high pressures required for energy efficient natural gas or H_2 energy systems. As in other fixed-bed CLC systems [38-44], energy-intensive reactions will take place in relatively narrow reaction zones, which makes it necessary to develop suitable heat management strategies to approach the complete conversion of the solids, while at the same time

avoiding the formation of hot spots during the operation [29-31, 37]. Preliminary model simulations including the thermal integration of the Ca-Cu looping process with power systems [36, 45] have shown that high CO_2 capture efficiencies with competitive energy penalties are possible when compared with benchmark power generation technologies without CO_2 capture. The application of the Ca-Cu looping process in post-combustion capture systems has also been evaluated [35, 46], but the consumption of a large amount of natural gas in the reduction/calcination stage (i. e. methane burnt at atmospheric pressure with an efficiency tipical of a steam cycle) makes the process less viable compared to other CO_2 capture technologies suited for natural gas. Accordingly, novel materials with suitable characteristics for application in the Ca-Cu looping process have recently been developed. Apart from the substantial progress made in the field of calcium-based CO_2 sorbents using different synthesis routes [12-14], copper-based oxygen carriers with active contents higher than 60 wt.% have been successfully tested over multiple oxidation/reduction cycles [47-49]. Even combinations of CaO/CuO materials [50-53] and hybrid CaO/reforming catalysts [54-56] have been shown to be resistant to agglomeration and deactivation in the long term.

In a previous paper [57], we reported the first experimental demonstration of the viability of the simultaneous CuO reduction/$CaCO_3$ calcination in a pseudo-adiabatic fixed-bed reactor. In the present work, the effects of the fuel gas composition, the Cu/Ca ratio, the temperature of the solids bed and possible side reactions on the reduction/calcination stage are experimentally investigated under pseudo-adiabatic conditions. Moreover, the influence of O_2 dilution in the inlet gas on the temperature profiles during Cu oxidation has been tested. The experimental results obtained have also been compared to the predictions of a one-dimensional reactor model that includes information taken from the literature on kinetics, fluid dynamics and heat transfer.

2. Experimental section

The experiments were carried out using a Cu-based catalyst (60 wt.% Cu over SiO_2 with a diameter of 3 mm) supplied by Johnson Matthey and a pre-calcined calcium-based material (99 wt% CaO with a particle size of 3 mm) from Carmeuse. The simultaneous CuO reduction/$CaCO_3$ calcination and the Cu oxidation stages were studied using an experimental setup specifically constructed at INCAR-CSIC (see Fig. 2). The packed-bed reactor consisted of a 920 mm long Inconel tube (OD x ID= 42 x 38 mm) loaded with a mixture of Ca- and Cu-based particles. Inside the reactor, a multipoint K-type thermocouple (14 points) was installed to measure the evolution of the axial temperature profile. The tube was surrounded by a thick layer of insulating material (quartz wool) to reduce heat loss. Both the reactor and the insulating coating were placed inside a ceramic oven with a capacity of 14 kW. The feed gases were preheated before entering the reactor by means of two heating tapes. The flow rate and composition of inlet gas were regulated by mass flow controllers. The steam generated in the process was removed by passing the product gas through a bed of silica placed

downstream of the reactor. The dry composition of the product gas was measured by infrared and thermal conductivity analysers.

Preliminary oxidation/reduction and carbonation/calcination tests were carried out in thermo-gravimetric analysers (TGA) in-house designed by the INCAR-CSIC and described in detail elsewhere [58, 59] in order to study the behaviour (in terms of O_2 carrying and CO_2 sorption capacities) of the CuO- and CaO-based materials, respectively, over multiple reaction cycles. The procedures followed in the TGA analysis are described below in section 4. X-Ray diffraction (XRD) measurements (obtained in a Siemens D500/501 diffractometer using Cu Kα radiation) were used to determine the crystalline phases present in the CuO- and CaO-based solids after the multi-cycling operation. The samples were scanned in the 2θ range of 20-70º using a step size of 0.025º and a scan time per step of 0.8 s.

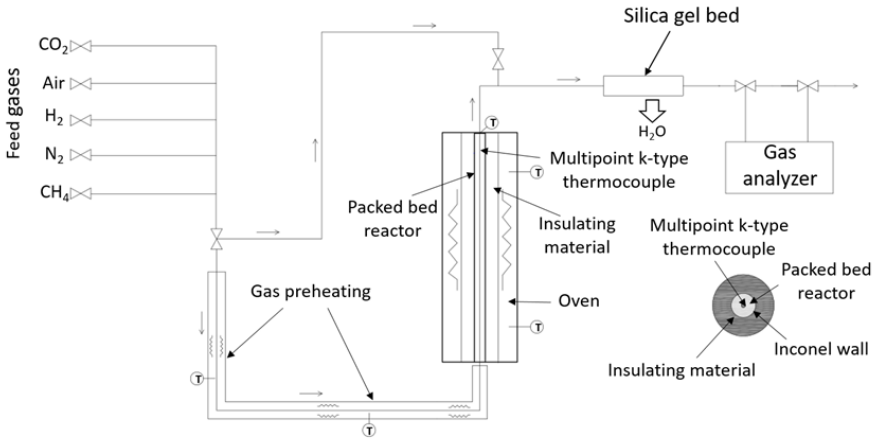

Fig. 2. Simplified scheme of the experimental setup at INCAR-CSIC.

3. Model description

The evolution of the product gas composition and the temperature profiles obtained from the experiments carried out in the fixed-bed reactor have been validated using a one-dimensional pseudo-homogenous reactor model. To dynamically simulate the simultaneous CuO reduction/$CaCO_3$ decomposition and the oxidation of Cu in the fixed bed, a multi-component system has been modelled, adopting the following assumptions for all reaction stages: ideal gas behavior, plug flow with a moderate axial mass and thermal dispersion, a negligible radial concentration and radial temperature gradients, the absence of inter-particle concentrations and internal temperature gradients, a constant bed void fraction (ε=0.5), a uniform particle size (d_p=0.003 m) and a uniform distribution of all the active species in the solids bed. During the reduction of CuO, total conversion of the gaseous fuels to CO_2 and H_2O is assumed. Hence negligible carbon

deposition is assumed in this model. This is consistent with results reported in the literature on CLC with Cu-based materials [23, 60]. Moreover, the presence of Ca-based particles also helps to reduce the formation of carbon, even at high temperatures [61, 62]. The water gas shift (WGS) reaction (or its reverse reaction depending on the temperature and gas composition) is also included in the model. The copper-based particles may catalyze the WGS reaction, which is favoured by the availability of CO, H_2, CO_2 and H_2O in the same reaction zone during the reduction/calcination stage [40]. The model also takes into account the variation of physical properties with temperature and composition. Heat transfer between the reactor and the oven is incorporated into the energy balance by means of an overall heat transfer coefficient (U=5 W/m^{2}s), which was experimentally estimated for this setup in a previous work [57]. The mass and energy balances together with the mass and heat dispersion descriptions included in the reactor model are outlined in Table 1.

Table 1. Mass and energy balances used in the model.

Component mass balances

$$\varepsilon\frac{\partial C_i}{\partial t} = -u_g\frac{\partial C_i}{\partial Z} + \frac{\partial}{\partial Z}(D_{eff}\frac{\partial C_i}{\partial Z}) + \eta(1-\varepsilon)\rho ir_i$$

Energy balance

$$\left((1-\varepsilon)\rho_s C_{ps} + \varepsilon\rho_g C_{pg}\right)\frac{\partial T}{\partial t} = -u_g\rho_g C_{pg}\frac{\partial T}{\partial Z} + \frac{\partial}{\partial Z}(\lambda_{eff}\frac{\partial T}{\partial Z}) - \Sigma\eta_i(1-\varepsilon)H_{ri}\rho ir_i - U(4/Dr)(T-Tw)$$

Momentum balance

$$\frac{dP}{dZ} = -150\frac{\mu_g u_g(1-\varepsilon)^2}{{d_p}^2\varepsilon^3} + 1.75\frac{\rho_g {u_g}^2(1-\varepsilon)}{d_p\varepsilon^3}$$

Axial mass dispersion coefficient [63-67]

$$D_{eff} = \left[\frac{0.73}{R_e S_c} + \frac{0.5}{\varepsilon + \frac{9.7\varepsilon^2}{R_e S_c}}\right]u_g d_p$$

$$\lambda_{\mathrm{eff}} = \lambda_{\mathrm{0bed}} + \frac{\mathrm{R_e P_r k_g}}{\mathrm{Pe_{az}}} + \frac{\mathrm{R_e}^2\mathrm{P_r}^2\mathrm{k_g}^2}{6(1-\varepsilon)\mathrm{N_u}};\quad \lambda_{\mathrm{0bed}} = \left(\frac{\mathrm{k_s}}{\mathrm{k_g}}\right)^{0.28-0.757\log(\varepsilon)-0.057\log\left(\frac{\mathrm{k_s}}{\mathrm{k_g}}\right)}$$

$$Pe_{az} = \frac{2p}{1-p}\ ;\ p = 0.17 + 0.29e^{\left[\frac{-24}{R_e}\right]};\quad N_u = 2 + 1.8{R_e}^{0.5}{P_r}^{0.33}$$

A shrinking core model (SCM) under chemical reaction control is assumed in order to calculate the kinetics of Cu oxidation, CuO reduction and $CaCO_3$ calcination, which is a commonly accepted model for CLC and calcium looping applications [68, 69]. The kinetics reported by Xu and Froment [70] were assumed in order to model the WGS reaction. Average effectiveness factors (η) have been incorporated into the kinetic equations to deal with possible internal diffusion resistances during the Cu/CuO chemical loop [37, 39, 40]. The equations and parameters that describe the kinetic

models are summarized in Table 2. A detailed explanation of the implementation of the model in order to obtain a numerical solution can be found elsewhere [29-31].

Table 2. Kinetic equations and parameters included in the reactor model.

Cu/CuO chemical loop (oxidation/reduction kinetics) [68]

$$\frac{t}{\tau} = 1 - (1 - X_i)^{1/2} \qquad \tau = \frac{\rho_{m,i} L_i}{b k_i C_g}$$

$$r_i = \frac{\rho_i 1000}{M_i} \frac{dX_i}{dt}$$

Calcination of $CaCO_3$ [69]

$$\frac{dX_{cal}}{dt} = k_{cal}(1 - X_{cal})^{\frac{2}{3}} \left(C_{CO_{2,eq}} - C_{CO_2}\right); \; r_{cal} = \frac{\rho_{CaCO_3} 1000}{M_{CaCO_3}} \frac{dX_{cal}}{dt}$$

$$C_{CO_{2,eq}} = \frac{5.045 \, x \, 10^{11}}{T} exp\left(\frac{-20.474}{T}\right)$$

Water gas shift [70]

$$r_{WGS} = \frac{1}{DEN^2} \frac{k_3}{p_{H_2}} \left(p_{co} p_{H_2O} - \frac{p_{H_2} p_{co_2}}{K_3}\right)$$

$$DEN = 1 + K_{co} p_{co} + K_{H_2} p_{H_2} + K_{CH_4} p_{CH_4} + K_{H_2O} \frac{p_{H_2O}}{p_{H_2}}$$

Kinetic parameters [68, 69]

	H_2	CO	O_2	Calcination
ρ_m, mol m^{-3}	80402	80402	140252	-
L_{Cu}, m	4.0 x 10^{-10}	4.0 x 10^{-10}	2.3 x 10^{-10}	-
k_{0i}, m s^{-1}	1.0 x 10^{-4}	5.9 x 10^{-6}	4.7 x 10^{-6}	252.02*
E_{ai}, kJ mol^{-1}	33	14	15	91.7
b	1	1	2	-
η	0.2	0.2	0.3	1

* m^3 mol s^{-1}

4. Results and discussion

Standard characterisation tests on small samples from the solids using TGA at atmospheric pressure were carried out in order to confirm O_2 carrying capacity of the CuO-based material and the CO_2 uptake of the CaO-based solid used in the experiments. In the case of the redox experiments, an individual CuO-based pellet of 123 mg was placed in a platinum basket and heated up to 870 ºC under a flow of 13 Nl/h N_2. The temperature and total gas flow were kept constant during the successive reduction/calcination tests. To reduce CuO to Cu, an inlet stream containing 20 vol.% H_2 in N_2 was introduced for 200 s. Afterwards, the feed of H_2 was stopped and air was introduced for 500 s to oxidize Cu back to CuO. The reduction/oxidation cycle was

repeated five times. Fig. 3a shows the change in weight of the CuO-based material as measured by TGA. During the reduction stage, there is a rapid decrease in mass from 123 mg to 104 mg, indicating that full conversion of CuO of Cu (60 wt.% of Cu in the oxidized solid) has been achieved. In the subsequent oxidation step, there is a fast increase in mass until it reaches the initial value of the oxidized pellet. The results show an oxygen transport capacity (OTC) of about 0.154, calculated as the difference in mass between the oxidized and the reduced sample divided by the mass of the oxidized sample [23]. The evolution of the OTC as a function of the number of cycles is represented in Fig. 3b. As can be seen, the O_2 transport capacity remains stable over five redox cycles, which is consistent with the high chemical stability of the Cu-based solid reported by other authors for these materials [23].

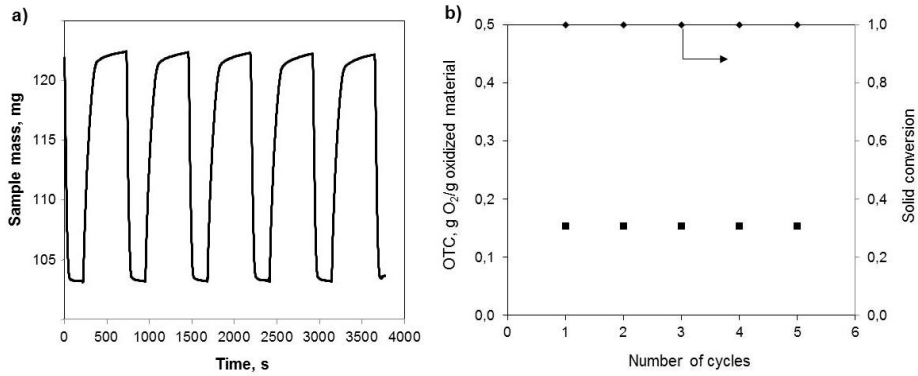

Fig 3. Mass changes, O_2 carrying capacity and solids conversion during the redox cycles in TGA. Reduction: 20 vol.% H_2 in N_2 at 870 ºC; Oxidation: 100 vol.% air at 870 ºC.

For the carbonation/calcination tests, a small sample (<15 mg) of pre-calcined Ca-based material was used. The experimental procedure consisted in the carbonation of the material at 650 ºC with 10 vol.% CO_2 in N_2 for 600 s. The calcination of the solid was carried out with 100 vol.% air at 900 ºC for 600 s. During the cyclic operation the inlet gas flow introduced into the TGA was maintained constant at 26 Nl/h. From Fig. 4a, it can be seen that during the carbonation step there is initially a rapid increase in the weight of the sample (due to the CaO carbonation under a kinetically limited regime) followed by a second period at a lower carbonation rate (limited by diffusion through the product layer) [71]. At 900 ºC, there is a sharp decrease in the weight of the sample due to the decomposition of the $CaCO_3$. The CO_2 carrying capacity of the Ca-based material (expressed as CaO molar conversion in Fig. 4b) is relatively low (12 mol.%) but close to the residual activity typically observed in natural limestones, which are known to be very stable over hundreds of cycles [58].

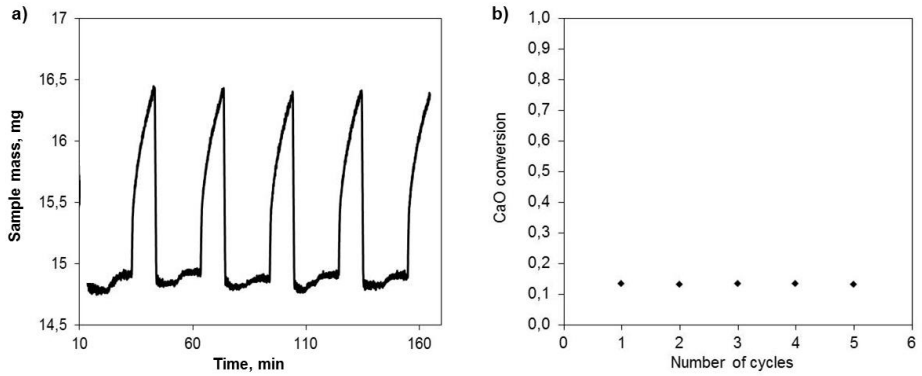

Fig. 4. Evolution of the sample weight and CaO conversion during the carbonation/calcination cycles in TGA. Carbonation: 10 vol.% CO_2 in N_2 at 650 ºC; Calcination: 100 vol.% air at 900 ºC.

The fixed-bed reactor described above was loaded with 953 g of CuO- and Ca-based solids (with a particle diameter of 3 mm) mixed homogeneously in order to study in detail the calcination of $CaCO_3$ by means of a Cu-CuO chemical loop under relevant conditions for the Ca-Cu looping process. First of all, the fixed bed was heated up in air until a temperature profile in the bed of between 400 and 700 ºC was obtained. Then, a flow of 15 Nl/min (10 vol.% CO_2 in N_2 preheated at 350 ºC) was fed in for 10 minutes in order to partially carbonate the calcium-based material assuming a final CaO conversion to $CaCO_3$ of 12% according to the TGA test results shown in Fig. 4. Under these conditions, the solids bed would contain around 21 wt.% of CuO and 14 wt.% of $CaCO_3$ (i. e. a Cu/Ca molar ratio of about 1.85), which is close to the theoretical bed composition required to perform the reduction/calcination stage with H_2 under neutral conditions [31]. A flow rate of 15 Nl/min (50 vol.% H_2 in nitrogen) was chosen to carry out the reduction/calcination operation within a reasonable period of time (i. e. a breakthrough time of around 8 minutes). The reducing gas was preheated at a temperature of 350 ºC and then fed in at the bottom of the bed, which is the part of the reactor at the lowest temperature, in order to evaluate the effect of the bed temperature on the reduction/calcination stage. The evolution of the axial temperature profile and the temperature and composition of the experimentally obtained outlet gas are represented in Fig. 5 and Fig. 6 and compared with the results predicted by the reactor model.

Once the fuel gas has been fed into the fixed bed, the temperature of the solids rapidly increases because of the exothermic reduction of the CuO particles even at low starting temperatures, which demonstrates the high reactivity of H_2 with CuO. During the first 2 minutes of operation, the temperature profile achieves a maximum value of around 800 ºC (see Fig. 5a). The high concentration of H_2 in the gaseous fuel and the relatively low CuO content in the bed make the reduction front (R) advance very quickly, leaving the solids upstream at a high temperature. Because of this, the reducing gas arrives at the reaction front preheated by the reduced solids. After 5 minutes of operation, the temperature profile achieves a maximum of around 870 ºC, which is a suitable

temperature to ensure the complete calcination of the $CaCO_3$ present in this part of the bed. The CO_2 emitted by the decomposition of calcium carbonate increases the gaseous flow rate inside the reactor. As result of this, the heat exchange front resulting from the calcination moves ahead of the reduction/calcination front and a fraction of the heat released from the CuO reduction is transported downstream by the product gas increasing the temperature of the still unconverted particles. Small differences between the model predictions and experimental temperature profiles along the bed were found as a consequence of an insufficiently homogenous distribution of the solids in the reactor.

From Fig. 5b, it can be seen that during the first 3 minutes of operation the temperature of the product gas remains stable at around 700 ºC (i. e., the initial temperature of the solids located in the second half of the fixed bed). From then on, the outlet temperature rises rapidly to reach a maximum value of 850 ºC (t=5 min). The model predicts the temperature of the outlet gas reasonably well during the period of time in which the reduction/calcination operation takes place (t<9 min). Nevertheless, the experimental data are in general slightly lower than the model prediction (e. g. the maximum temperature achieved at the end of the bed is 25 ºC lower than the theoretical value). These discrepancies may be due to the position of the thermocouple that measures the exit gas, which is located at the edge of the ceramic oven where the heat loss is greater.

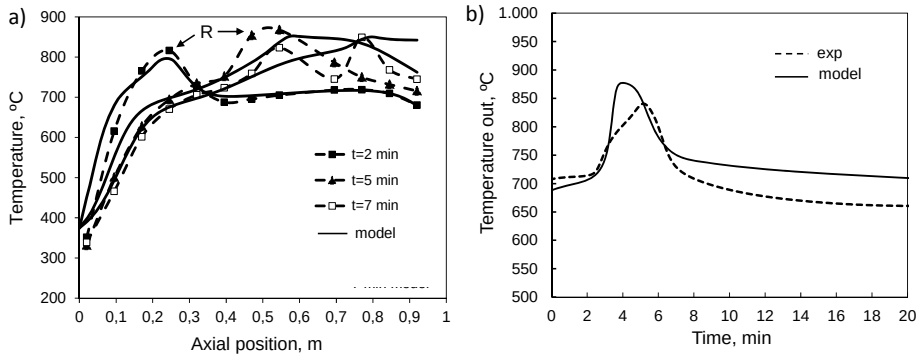

Fig 5. Evolution of the temperature profiles during the reduction/calcination operation carried out with H_2 as reducing gas (R is the reduction front).

Fig. 6 shows the composition of the product gas during the reduction/calcination step with hydrogen. During the first 2 minutes of operation, the temperature achieved in the bed is too low to favour the calcination of $CaCO_3$, and therefore, the outlet gas contains less than 2 vol.% CO_2 (on a dry basis). Once the temperature of the bed approaches 870 ºC (t>4 min), the calcination proceeds very quickly and a rapid increase in the CO_2 content up to 36 vol.% (on a dry basis) is observed. As can be seen in Fig. 6, during the pre-breakthrough period (t<7 min) all of the H_2 is converted to $H_2O(v)$. From that point onwards, the H_2 content in the product gas rises rapidly, which means that the particles of CuO are on the point of being totally reduced. The sharp breakthrough curve in Fig. 6

confirms the high reactivity of CuO with H_2. A small amount of CO (up to a maximum of 9 vol.% CO) was detected in the product gas during the breakthrough period. This is because high temperatures and a high CO_2 content in the atmosphere favour the reaction of some of the H_2 with CO_2 to form CO and $H_2O_{(v)}$ by means of the reverse water gas shift (RWGS) reaction, catalyzed by the Cu-based particles [72, 73]. After 15 minutes of operation, the temperature of the solids bed is sufficiently low to minimize both the $CaCO_3$ calcination and RWSG reactions, resulting in a product gas mainly composed of H_2 and N_2 (i.e. the composition of the feed).

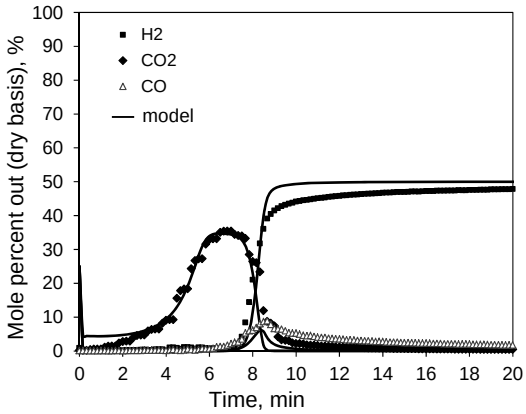

Fig 6. Gas composition at the outlet of the reactor during the reduction/calcination step with hydrogen.

The amount of CO_2 released during the reduction/calcination test is significantly lower than expected taking into account the $CaCO_3$ present in the bed at the beginning, which means that a fraction of the carbonated particles is left uncalcined. The evolution of the solids conversion along the bed can be theoretically described by the reactor model. As can be seen in Fig. 7, starting temperatures in the solids of about 400 ºC are sufficiently high to allow the total reduction of the CuO particles in a sharp reduction front (R). However, only when the temperature profile approaches 850 ºC (t>5 min), is the calcination of $CaCO_3$ highly favoured (the calcination front is represented as C in Fig. 7). From that moment onwards, both the reduction and calcination fronts move forward together until they reach the end of the bed after 9 min of operation. In these operating conditions, the copper-based particles are totally reduced but only 65 wt% of the $CaCO_3$ has been calcined, which corresponds with the amount of CO_2 experimentally measured at the reactor exit during the reduction/calcination test. These results demonstrate that a sufficiently high temperature (T>700 ºC) is required in the bed at the beginning of the reduction/calcination step in order to ensure the complete calcination of $CaCO_3$.

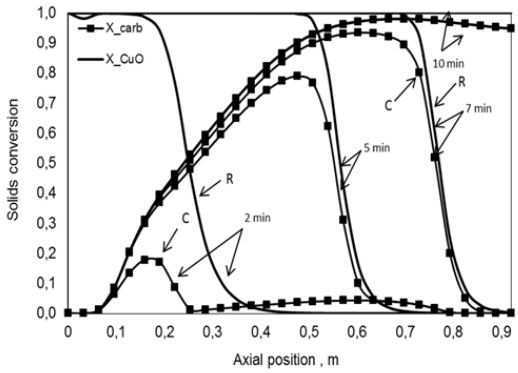

Fig. 7. Theoretical axial solids conversion during the reduction/calcination step with H_2.

Additional experiments were carried out by feeding into the fixed bed mixtures of CO and H_2 with similar compositions to what would be expected if the PSA off-gas resulting from the H_2 purification step downstream of the SER reactor and/or the syngas obtained in a steam reforming stage were used as reducing gas, as proposed by some works on the Ca-Cu looping process [28, 33, 36]. Due to the higher reduction enthalpy of CuO with CO, lower $CuO/CaCO_3$ molar ratios in bed composition are required in order to maintain neutral conditions in the reduction/calcination front during the operation. The reversibility of the CaO carbonation reaction allows a high solid conversion to be achieved after long carbonation times [71]. Therefore, higher amounts of $CaCO_3$ in the reactor (i. e., lower $CuO/CaCO_3$ molar ratios) can be achieved with the initial load of solids by prolonging the carbonation step before the reduction/calcination test.

In order to study the effect of the fuel composition on reactor performance, a gaseous feed composed of 10 vol.% CO and 40 vol.% H_2 in N_2 was used to carry out the reduction/calcination operation. First of all, the reactor was heated in air until a temperature profile similar to that attained in the reduction/calcination test with H_2 was obtained. Then, a flow of 15 Nl/min (10 vol.% CO_2 in N_2 preheated at 350 ºC) was introduced for 15 minutes in order to achieve a solids conversion in the Ca-based particles of 13%, according to the results obtained in the TGA (not shown here for the sake of simplicity). In these conditions, the solids bed contains around 21 wt.% of CuO and 16 wt.% of $CaCO_3$ (i. e. a $CuO/CaCO_3$ molar ratio of about 1.7), which is the theoretically required bed composition for the reduction/calcination under neutral conditions. Another experiment was carried out by feeding in a fuel gas composed of 20 vol.% CO and 30 vol.% H_2 in N_2. In this case, the same flow of CO_2 in N_2 was introduced into the reactor for 20 minutes in order to carbonate up to 14% the Ca-based particles, corresponding a $CuO/CaCO_3$ molar ratio of 1.6. A total flow rate of 14 Nl/min was selected for both experiments with CO and H_2 in order to achieve the breakthrough period within a reasonable period (i. e., around 10 minutes of operation).

Fig. 8 shows the evolution of the axial temperature profiles and product gas composition measured at the reactor exit compared to the results predicted by the reactor model for the experiments with mixtures of CO and H_2 in the feed. As in the previous reduction/calcination test using only H_2, there is a rapid increase in the temperature profiles because of the reduction of CuO even at low starting temperatures (Fig. 8a and Fig. 8c), which confirms the high reactivity of the CuO-based material with CO and H_2. As the bed contains in each case a suitable $CuO/CaCO_3$ molar ratio, the maximum temperatures achieved in the reaction fronts are moderate (around 870 ºC). The reactor model describes reasonably well the advance of the reduction fronts (R in Fig. 8a and Fig. 8c) during the operation. Only at the reactor exit are the experimental temperature profiles below the temperature predicted by the model. This is probably due to the high heat losses at this part of the reactor. As can be seen in Fig. 8b and Fig. 8d, the breakthrough curves for CO at the reactor exit are less steep than the H_2 curves, which indicates that the reduction kinetics of the CuO-based material with CO are slightly slower in these experimental conditions.

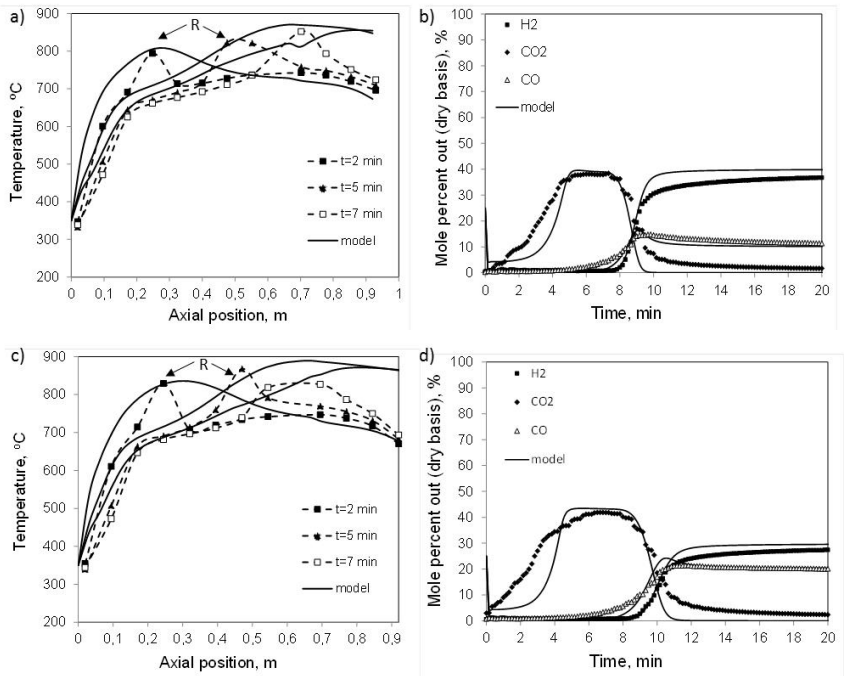

Fig. 8. Axial temperature profile and composition of the product gas at the reactor exit obtained during the reduction/calcination operation carried out with CO and H_2 as reducing gas (R is the reduction front): a) and b) 10 vol.% CO, 40 vol.% H_2 in N_2; c) and d) 20 vol.% CO, 30 vol.% H_2 in N_2.

The reactor model predicts the tendency of the CO_2 composition in the product gas reasonably well. However, the amount of CO_2 measured at the reactor exit is slightly higher than the theoretical CO_2 profile predicted by the model (see Fig. 8b and Fig. 8d),

which was not observed in the initial experiment carried out with H_2 using fresh Ca- and Cu-based materials (see Fig. 6). Additional tests carried out in the same conditions with only H_2 as reducing agent were conducted, and higher amounts of CO_2 than expected were measured at the reactor exit (not shown here for the sake of simplicity). XRD analyses were carried out to determine possible changes in crystallinity and chemical composition of the Ca- and Cu-based materials after several carbonation/calcination and oxidation/reduction cycles. Fig. 9a shows the XR difractogram obtained with a Ca-based solid taken from the upper part of the reactor and subsequently calcined in a muffle furnace at 900 ºC for 15 minutes. As can be seen, apart from CaO and CuO mixed Ca-Cu oxides were detected in the material, which confirms that the multicycle operation at high temperature produced some modifications in the CO_2 sorbent. To determine whether the mixed Ca-Cu oxides present in the material were able to capture CO_2 and form carbonates, a previously carbonated Ca-based solid was also analyzed using XRD. Fig. 9b confirms that the mixed Ca-Cu oxides are able to form carbonates, in agreement with the results obtained by Kierzkowska and Muller [74] using combined Ca-Cu materials for CO_2 capture.

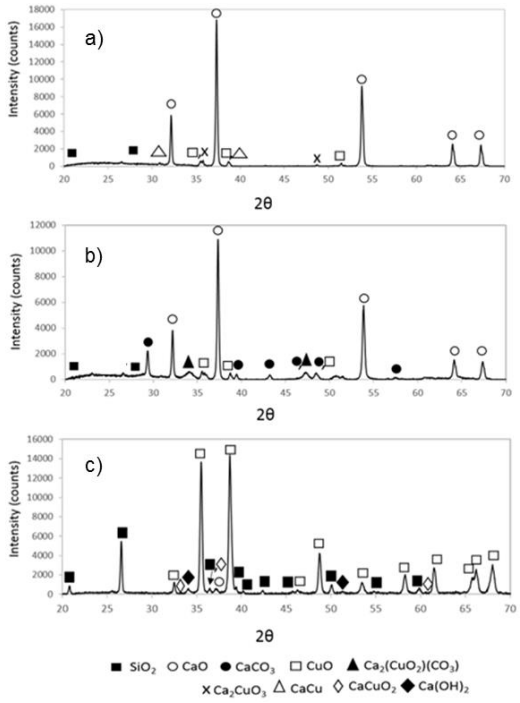

Fig. 9. XRD measurements of Ca- and Cu-based materials after a multicyle operation: a) a calcined Ca-based solid, b) a carbonated Ca-based solid, c) a Cu-based solid.

XRD measurements carried out with Cu-based solids also showed the presence of mixed Ca-Cu phases in the material (see Fig. 9c), although subsequent TGA carbonation tests demonstrated that a negligible amount of carbonates were formed. In view of these results, the differences obtained in experimental CO_2 breakthrough curves

with respect to the analytical solution can be attributed to the substantial changes observed in the composition of the solids after multiple cycles, which affect the CO_2 sorption capacity of these materials.

The oxidation of Cu to CuO under conditions relevant to the Ca-Cu looping process was also studied. Once the copper-based particles were completely reduced, a flow of 8 Nl/min of N_2 preheated at 400 ºC was fed into the fixed bed in order to obtain a uniform temperature profile in the reactor at around this value. A first oxidation step was carried out by feeding in 8 Nl/min of air also preheated to 400 ºC. The axial temperature profiles and the composition of the product gas obtained experimentally are depicted in Fig. 10. As the oxidation of Cu is a highly exothermic reaction, there is a dramatic increase in the temperature profile from the very beginning. As the operation continues, the temperature of the oxidation front gradually rises until it reaches a maximum value of about 900 ºC. The inlet gas exchanges heat with the oxidized solids to form a heat exchange front that develops at a lower velocity than the oxidation front. Under adiabatic conditions, a heat plateau should form at temperatures above 900 ºC, but in actual fact the temperature profile is significantly lower because of heat losses (see Fig. 10a). As regards the composition of the outlet gas (represented in Fig. 10b), the O_2 reacts fully in spite of the low starting temperature profile, and only N_2 is observed during the prebreakthrough period. When the oxidation front approaches the reactor exit (t>13 min), the O_2 content in the gas rapidly increases until it reaches 21 vol.% in a relatively short breakthrough period (i. e. around 5 minutes).

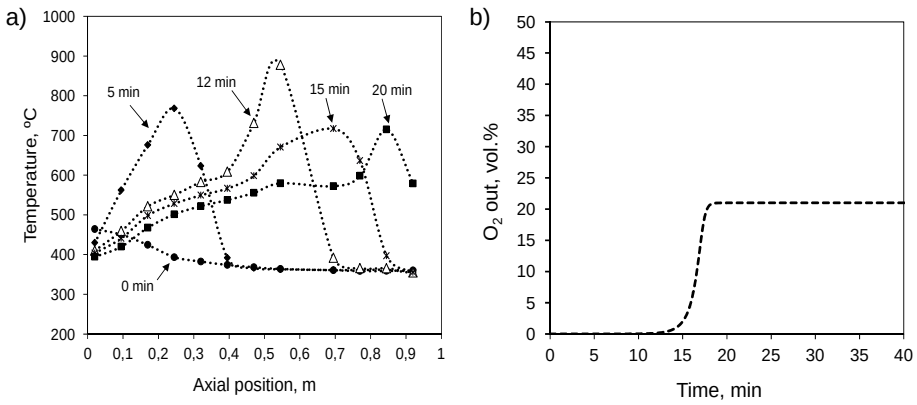

Fig. 10. a) Experimental temperature profiles along the bed during the Cu oxidation stage. b) O_2 breakthrough curve at the reactor exit. Operation carried out with a flow rate 8 Nl/min of air preheated to 400 ºC.

As can be seen in Fig 10, Cu loadings of around 20 wt.% will cause a temperature rise of about 500 ºC in the oxidation front. In the Ca-Cu looping process, a maximum temperature during the Cu oxidation stage of around 830 ºC is recommended in order to minimize the partial calcination of the $CaCO_3$ formed in the previous SER stage [19, 28]. For this reason, the oxidation step should be carried out with very low starting

temperatures in the reactor (which is not suitable for performing the Cu oxidation stage) or with a lower Cu content (i. e. with a higher proportion of inerts in the bed) that will lead to a less compact system with a higher energy penalty in the subsequent $CaCO_3$ calcination stage (since the increasing amount of inerts will act as a thermal ballast during the calcination).

As explained above, another alternative for the management of heat is to recirculate a large fraction of the N_2 obtained at the reactor exit in order to greatly reduce the concentration of O_2 in the feed. In these conditions, the Cu oxidation stage can be carried out with moderate temperature profiles even though a high amount of Cu (>20 wt.%) is present in the fixed bed [19, 28]. To study the effect of feeding a large flow of gas with a very low content of O_2 on the oxidation stage, a flow of 30 Nl/min (3 vol.% of O_2 in nitrogen) was introduced into the reactor preheated to 400 ºC. The initial temperature profile in the bed was around 400 ºC, as in the previous case.

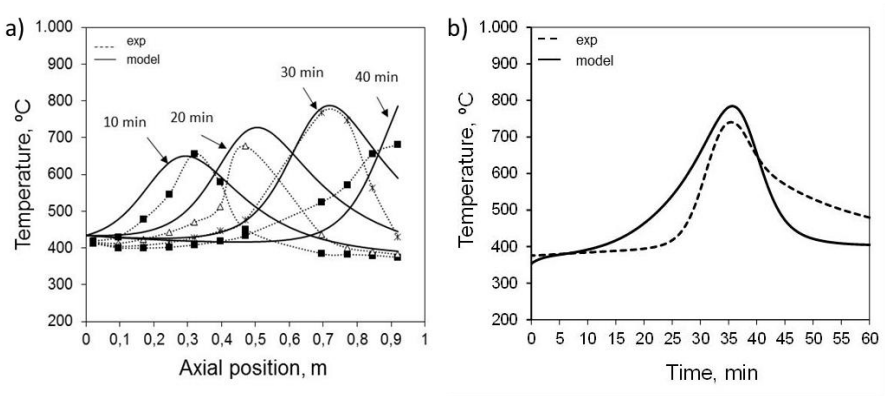

Fig. 11. Temperature profiles obtained during the Cu oxidation step carried out with a flow rate of 30 Nl/min (3 vol.% O_2) at 400 ºC.

Fig. 11 shows the dynamic temperature profiles observed during the Cu oxidation stage. As the gas flows through the reactor, the temperature increases rapidly, which demonstrates that the Cu oxidation rate is fast despite the low content of O_2 in the feed and the low initial temperature of the solids. The oxidation front gradually raises the temperature of the solids as it advances along the bed. In contrast to the previous case, the high dilution of the O_2 in the feed makes the heat exchange front advance ahead of the oxidation front. The inlet gas approaches the oxidation front at the inlet temperature (400 ºC) and it is rapidly heated up due to the energy released from the oxidation of Cu. The large flow of gas passing through the bed transports the heat downstream of the oxidation front, which moderates the temperature profile to a maximum value of about 800 ºC, which is reached after 30 min of operation (see Fig. 11a). Once the oxidation front reaches the reactor exit (t=40 min), the solids bed is left at the temperature of the feed (i. e. 400 ºC), contrary to what occurs in the Cu oxidation test carried out with air, in which the oxidized particles remain at a relatively high temperature after the breakthrough point (see Fig. 10a). These results are in agreement with the previous

modelling of the Ca-Cu looping process [30]. As can be seen in Fig. 11b, the evolution of the exit temperature is in line with the predictions of the model (the maximum temperature is reached after 35 min), although the temperature profile obtained experimentally is lower than the theoretical value because the measuring point is subjected to large heat losses, as explained above.

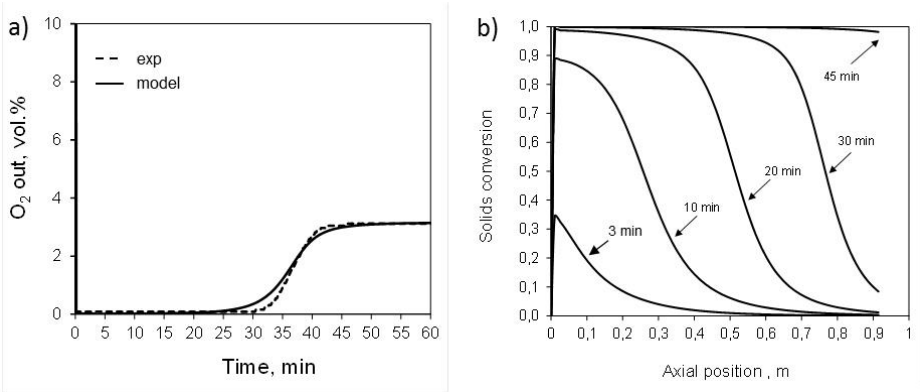

Fig. 12. Dynamic profiles of O_2 and theoretical solids conversion during the Cu oxidation carried out with a flow rate of 30 Nl/min (3 vol.% O_2) at 400 ºC.

The concentration profile of O_2 at the reactor exit is represented in Fig. 12a. In the course of the prebreakthrough period (t<25 min), the O_2 reacts completely and the product gas is virtually pure N_2. The model predicts the shape of the breakthrough curve reasonably well. Fig. 12b shows the theoretical evolution of the oxidation front during the operation. The Cu oxidation takes place in a relatively sharp reaction front even though the feed has a low O_2 content. The low starting temperatures (400 ºC) do not impede the oxidation front moves forward leaving behind the Cu-based particles completely oxidized. By the time the product gas reaches 3 vol.% of O_2, the fixed bed is completely oxidized.

Conclusions

In this work, the feasibility of $CaCO_3$ calcination by means of the simultaneous reduction of CuO with CO and H_2 in a lab-scale packed-bed reactor has been experimentally confirmed. The composition of the reducing gas determines the CuO/$CaCO_3$ molar ratio required in the bed to ensure a suitable reduction/calcination operation. CO and H_2 present a high reactivity with the CuO-based material tested in this work, allowing the complete reduction of CuO to Cu in a sharp reaction front and the total oxidation of the gaseous fuel to CO_2 and H_2O during the pre-breakthrough period, even at temperatures lower than 500 ºC. Due to the high reduction enthalpy of CuO with CO, lower CuO/$CaCO_3$ molar ratios in bed composition are required to counterbalance the increasing amounts of CO in the gas feed in order to maintain

neutral conditions in the reduction/calcination front. Starting temperatures in the solids bed lower than 650 ºC impede a suitable reduction/calcination operation and as a result a fraction of the Ca-based solids is left uncalcined. The Cu-based material catalyzes the reverse water-gas-shift reaction, which is favoured by the high temperature and the high CO_2 content in the atmosphere achieved during the pre-breakthrough period in the reduction/calcination stage. The multicycle operation at high temperature modifies the chemical composition of the functional materials tested in this work and mixed Ca-Cu oxides are formed. These oxides are carbonated in the presence of CO_2 and this affects the CO_2 sorption capacity. The Cu oxidation stage under conditions relevant to the Ca-Cu looping process was also evaluated. The dilution of the O_2 in the feed during the Cu oxidation stage by recirculating a large part of the product gas (virtually pure N_2) allows the maximum temperature to be regulated at around 800 ºC, which would minimize the partial calcination of the Ca-based sorbent during the operation. Low starting temperatures in the bed of around 400 ºC allows the rapid oxidation of Cu in a narrow reaction front and the complete conversion of O_2 is achieved in spite of the very low O_2 content in the feed (i. e., 3 vol.% O_2). A dynamic reactor model has been validated using the experimental results obtained in this work. The model predicts the evolution of the temperature profiles and the composition of the product gas during both the reduction/calcination and Cu oxidation stages reasonably well.

Nomenclature

C_{CO_2}	concentration of CO_2 in the gas phase, kmol m^{-3}
$C_{CO_{2eq}}$	equilibrium concentration of CO_2, kmol m^{-3}
C_i	concentration of component i in the reactor, kmol m^{-3}
C_{in}	concentration of component i in the feed, kmol m^{-3}
C_g	concentration of the gas, kmol m^{-3}
C_{pg}	specific heat capacity of the gas, kJ kg^{-1} K^{-1}
C_{ps}	specific heat capacity of the solid, kJ kg^{-1} K^{-1}
D_{eff}	axial mass dispersion coefficient, m^2 s^{-1}
D_i	inner diameter of the reactor, m
d_p	particle diameter, m
$E_{a,Calc}$	activation energy calcination reaction, kJ mol^{-1}
$E_{a,CO}$	activation energy reduction reaction with CO, kJ mol^{-1}
E_{a,H_2}	activation energy reduction reaction with H_2, kJ mol^{-1}
H_{ri}	Entalphy reaction of gas component i, kJ mol^{-1}

h_w	heat transfer coefficient, W m^{-2} K^{-1}
$k_{0,Calc}$	pre-exponential factor of $CaCO_3$ calcination reaction, mol^{1-n} m^{3n-3} s^{-1}
$k_{0,CO}$	pre-exponential factor of CuO reduction reaction with CO, mol^{1-n} m^{3n-3} s^{-1}
k_{0,H_2}	pre-exponential factor of CuO reduction reaction with H_2, mol^{1-n} m^{3n-3} s^{-1}
k_{cal}	reaction rate constant of the $CaCO_3$ calcination, mol^{1-n} m^{3n-3} s^{-1}
k_{red}	reaction rate constant of the CuO reduction, mol^{1-n} m^{3n-3} s^{-1}
K_g	thermal conductivity of the gas, W K^{-1} m^{-1}
K_s	thermal conductivity of the solids, W K^{-1} m^{-1}
K_3	equilibrium constant of the water gas shift, dimensionless
k_3	reaction rate water gas shift, mol m^{-3} s^{-1}
K_i	equilibrium constants, bar^{-1}
L	reactor length, m
L_{CuO}	layer thickness of CuO, m
L_{Cu}	layer thickness of Cu, m
M_{CaCO_3}	molar mass of $CaCO_3$, kg $kmol^{-1}$
M_{CuO}	molar mass of CuO, kg $kmol^{-1}$
M_{Cu}	molar mass of Cu, kg $kmol^{-1}$
N_u	nusselt number, dimensionless
P	pressure, bar
Pe_{az}	Peclet number, dimensionless
P_r	Prandt number, dimensionless
R_e	Reynolds number, dimensionless
r_i	reaction rate of component i,
r_{cal}	reaction rate of calcination, mol m^{-3} s^{-1}
r_{CO_2}	reaction rate of CO_2 formation, mol m^{-3} s^{-1}
r_{red}	reaction rate of CuO reduction, mol m^{-3} s^{-1}
r_{ox}	reaction rate of Cu oxidation, mol m^{-3} s^{-1}
r_{RWGS}	reaction rate of reverse water shift, mol m^{-3} s^{-1}
S_c	Schmidt number, dimensionless

T	Temperature, K
T_{in}	Temperature at the reactor entrance, K
T_{s0}	initial temperature of the solids in the fixed bed, K
T_w	reference temperature, K
X_{ox}	fractional oxidation conversion of Cu, dimensionless
X_{red}	fractional reduction conversion of CuO, dimensionless
X_{cal}	fractional calcination conversion of $CaCO_3$, dimensionless

Greek letters

ε	bed void fraction, dimensionless
ρ_{CuO}	apparent density of Cu-based material, kg m^{-3}
ρ_g	gas phase density, kg m^{-3}
$\rho_{m,CuO}$	molar density of Cu, mol m^{-3}
ρ_s	apparent density of the mixed solids in reactor, kg m^{-3}
λ_{eff}	effective axial heat dispersion coefficient, W m^{-2} K^{-1}
λ_{0bed}	effective axial heat dispersion with no flow conditions, W m^{-2} K^{-1}
η	effectiveness factor, dimensionless
τ	time for complete solid conversion, dimensionless
μ_g	gas viscosity, kg s^{-1} m^{-1}

Acknowledgments

The authors acknowledge the financial support provided by the EU FP7 under the ASCENT Project (Grant no. 608512), and a PhD fellowship awarded to J. M. Alarcón BES-2013-063835 by the Spanish MINECO. The authors also acknowledge the assistance of M. Rodríguez, M. Alonso and G. Grasa in the TGA tests and XRD measurements.

References

[1] IPCC, 2014- Climate Change 2014: Mitigation of Climate Change. Contribution of Working Group III to the Fifth Assessment Report of the Intergovernmental Panel on Climate Change. Cambridge University Press, Cambridge, United Kingdom and New York, NY, USA.

[2] M.E. Boot-Handford, J.C. Abanades, E.J. Anthony, M.J. Blunt, S. Brandani, N. Mac Dowell, J.R. Fernandez, M.C. Ferrari, R. Gross, J.P. Hallett, R.S. Haszeldine, P. Heptonstall, A.

Lyngfelt, Z. Makuch, E. Mangano, R.T.J. Porter, M. Pourkashanian, G.T. Rochelle, N. Shah, J.G. Yao, P.S. Fennell, Carbon capture and storage update. Energ. Environ. Sci. 7 (2014) 130-189.

[3] IEA, Technology Roadmap. Hydrogen and Fuel Cells. IEA Publications, Paris, France, 2015.

[4] J.R. Rostrup-Nielsen, Steam reforming and chemical recuperation, Catal. Today 145 (2009) 72–75.

[5] D.P. Harrison, Sorption-enhanced hydrogen production: a review. Ind. Eng. Chem. Res. 47 (2008) 6486–501.

[6] Y.J. Wu, P. Li, J.G. Yu, A.F. Cunha, A.E. Rodrigues, Progress on sorption-enhanced reaction process for hydrogen production. Rev. Chem. Eng. 32 (2016) 271-303.

[7] Z. Li, N. Cai, Modeling of Multiple Cycles for Sorption-Enhanced Steam Methane Reforming and Sorbent Regeneration in Fixed Bed Reactor. Energy Fuels 21 (2007) 2909-2918.

[8] H.T.J. Reijers, J. Boon, G.D. Elzinga, P.D. Cobden, W.G. Haije, R.W., Van den Brink, Modeling study of the sorption-enhanced reaction process for CO_2 capture. I. Model development and validation. Ind. Eng. Chem. Res. 48 (2009) 6966–6974.

[9] A.L. Garcia-Lario AL, M. Aznar M, G. Grasa, R. Murillo, Evaluation of process variables on the performance of Sorption Enhanced Methane Reforming. J. Power Sources 285 (2015) 90-99.

[10] I. Aloisi, N. Jand, S. Stendardo, P.U. Foscolo, Hydrogen by sorption enhanced methane reforming: A grain model to study the behavior of bi-functional sorbent-catalyst particles. Chem. Eng. Sci. 149 (2016) 22-34.

[11] A. Antzara, E. Heracleous, A.A. Lemonidou, Energy efficient sorption enhanced-chemical looping methane reforming process for high-purity H_2 production: Experimental proof-of-concept. Appl. Energ. 180 (2016) 457-471.

[12] J. Blamey, E.J. Anthony, J. Wang, P.S. Fennell, The calcium looping cycle for large-scale CO_2 capture. Prog. Energ. Comb. Sci. 36 (2010) 260–279.

[13] A.M. Kierzkowska, R. Pacciani, C.R. Müller, CaO-Based CO_2 Sorbents: From Fundamentals to the Development of New, Highly Effective Materials. Chem. Sus. Chem. 6(7) (2013) 1130-1148.

[14] M. Erans, V. Manovic, E.J. Anthony, Calcium looping sorbents for CO_2 capture. Appl. Energ. 180 (2016) 722‑742.

[15] N. Rodríguez, M. Alonso, G. Grasa, J.C. Abanades, Process for capturing CO_2 arising from the calcination of the CaCO3 used in cement manufacture. Environ. Sci. Technol. 42 (2008) 6980-6984.

[16] I. Martinez, R. Murillo, G. Grasa, N. Rodriguez, J.C. Abanades, Conceptual design of a three fluidised beds combustion system capturing CO_2 with CaO. Int. J.Greenh. Gas Con. 5 (2011) 498–504.

[17] T. Weimer, R. Berger, C. Hawthorne, J.C. Abanades, Lime enhanced gasification of solid fuels: Examination of a process for simultaneous hydrogen production and CO_2 capture. Fuel 87(8–9) (2008) 1678–86.

[18] Z. Chen, J.R. Grace, C.J. Lim, CO_2 capture and hydrogen production in an integrated fluidized bed reformer regenerator system. Ind. Eng. Chem. Res. 50 (2011) 4716-4721.

[19] I. Martínez, M.C. Romano, P. Chiesa, G. Grasa, R. Murillo, Hydrogen production through sorption enhanced steam reforming of natural gas: thermodynamic plant assessment. Int. J. Hydrog. Energ. 38 (2013) 15180–15199.

[20] J.C. Abanades, E.J. Anthony, J. Wang, J.E. Oakey, Fluidized bed combustion systems integrating CO_2 capture with CaO. Environ. Sci. Technol. 39 (2005) 2861-2866.

[21] G. Grasa, J.C. Abanades, Narrow fluidised beds arranged to exchange heat between a combustion chamber and a CO_2 sorbent regenerator. Chem. Eng. Sci. 62 (2007) 619 – 626.

[22] M. Junk, M. Reitz, J. Strohle, B. Epple, Thermodynamic evaluation and cold flow model testing of an indirectly heated carbonate looping process. Chem. Eng. Technol. 36 (2013) 1479-1487.

[23] J. Adanez, A. Abad, F. Garcia-Labiano, P. Gayan, L.F. de Diego, Progress in chemical-looping combustion and reforming technologies. Prog. Energy Combust. Sci. 38 (2012) 215-282.

[24] R. V. Kumar, R.K. Lyon, J.A. Cole, Unmixed reforming: a novel autothermal cyclic steam reforming process. In: Gregoire Padro CEaL, F., editor. Adv Hydrogen Energy. New York, Boston, Dordrecht, London, Moscow: Kluwer Academic Publishers; 2002: p. 31–46.

[25] J. Wolf, J. Yan, Parametric study of chemical looping combustion for tri-generation of hydrogen, heat, and electrical power with CO_2 capture. Int. J. Energy Res. 29 (2005) 739-753.

[26] J.R. Fernández, J.C. Abanades, CO_2 capture from the calcination of $CaCO_3$ using iron oxide as heat carrier. J. Clean Prod. 112 (2016) 1211-1217.

[27] J.C. Abanades, R. Murillo, J. R. Fernandez, G. Grasa, I. Martinez, New CO_2 capture Process for Hydrogen production Combining Ca and Cu Chemical Loops. Environ. Sci. Technol. 44 (2010) 6901-6904.

[28] J.R. Fernández, J.C. Abanades, R. Murillo, G. Grasa, Conceptual design of a hydrogen production process from natural gas with CO_2 capture using a Ca–Cu chemical loop. Int. J. Greenh. Gas Con. 6 (2012) 126–141.

[29] J.R. Fernandez, J.C. Abanades, G. Grasa, Modeling of sorption enhanced steam methane reforming—Part II: Simulation within a novel Ca/Cu chemical loop process for hydrogen production. Chem. Eng. Sci. 84 (2012) 12-20.

[30] J.R. Fernández, J.C. Abanades, R. Murillo, Modeling of Cu oxidation in adiabatic fixed-bed reactor with N_2 recycling in a Ca/Cu chemical loop. Chem. Eng. J. 232 (2013) 442–452.

[31] J.M. Alarcón, J.R. Fernández, $CaCO_3$ calcination by the simultaneous reduction of CuO in a Ca/Cu chemical looping process. Chem. Eng. Sci., 137 (2015) 254−267.

[32] C. Qin, B. Feng, J. Yin, J. Ran, L. Zhang, V. Manovic, Matching of kinetics of $CaCO_3$ decomposition and CuO reduction with CH_4 in Ca-Cu chemical looping, Chem. Eng. Sci. 262 (2015) 665–675.

[33] F.N. Ridha, D. Lu, A. Macchi, R.W. Hughes, Combined calcium looping and chemical looping combustion cycles with CaO-CuO pellets in a fixed bed reactor. Fuel 153 (2015) 202-209.

[34] V. Manovic, EJ Anthony, Integration of Calcium and Chemical Looping Combustion using Composite CaO/CuO-Based Materials. Environ. Sci. Technol. 2011, 45, 10750–10756.

[35] D.C. Ozcan, A. Macchi, D. Lu, A.M. Kierzkowska, H. Ahn, C.R. Müller, S. Brandani, Ca-Cu looping process for CO_2 capture from a power plant and its comparison with Ca-looping, oxy-combustion and amine-based CO_2 capture processes. Int. J. Greenh. Gas Con. 43 (2015) 198-212.

[36] I. Martinez, M.C. Romano, J.R. Fernandez, P. Chiesa, R. Murillo, J.C. Abanades, Process design of a hydrogen production plant from natural gas with CO_2 capture based on a novel Ca/Cu chemical loop. Appl. Energ. 114 (2014) 192−208.

[37] M. Martini, A. van den Berg, F. Gallucci, M. van Sint Annaland, Investigation of the process operability windows for Ca-Cu looping for hydrogen production with CO_2 capture. Chem. Eng. J. 303 (2016) 73–88.

[38] S. Noorman, M. van Sint Annaland, H. Kuipers, Packed bed reactor technology for chemical-looping combustion. Ind. Eng. Chem. Res. 46 (2007), 4212-20.

[39] H.P. Hamers, F. Gallucci, P.D. Cobden, E. Kimball, M. van Sint Annaland, A novel reactor configuration for packed bed chemical-looping combustion of syngas, Int. J. Greenh. Gas Con. 16 (2013), 1–12.

[40] H.P. Hamers, F. Gallucci, P.D. Cobden, E. Kimball, M. van Sint Annaland, CLC in packed beds using syngas and CuO/Al_2O_3 : a model description and experimental validation. Appl. Energ. 119 (2014), 163-172.

[41] V. Spallina, F. Gallucci, M.C. Romano, P. Chiesa, G. Lozza, M. van Sint Annaland, Investigation of heat management for CLC of syngas in packed bed reactors, Chem. Eng. J. 225 (2013) 174–191.

[42] V. Spallina, P. Chiesa, E. Martelli, F. Gallucci, M.C. Romano, G. Lozza, M. van Sint Annaland, Reactor design and operation strategies for a large-scale packed-bed CLC power plant with coal syngas. Int. J. Greenh. Gas Con. 36 (2015) 34-50.

[43] J.R. Fernandez, J.M. Alarcón, Chemical looping combustion process in fixed-bed reactors using ilmenite as oxygen carrier: Conceptual design and operation strategy. Chem. Eng. J. 264 (2015) 797‑806.

[44] L. Han, G.M. Bollas, Dynamic optimization of fixed bed chemical-looping combustion processes. Energy 112 (2016) 1107-1119.

[45] I. Martínez, R. Murillo, G. Grasa, J.R. Fernández, J.C. Abanades, Integrated combined cycle from natural gas with CO_2 capture using a Ca–Cu chemical loop. AIChE J. 59 (2013) 2780–2794.

[46] B. Duhoux, P. Mehrani, D. Lu, R.T. Symonds, E.J. Anthony, A. Macchi, Combined Calcium Looping and Chemical Looping Combustion for Post-Combustion Carbon Dioxide Capture: Process Simulation and Sensitivity Analysis. Energy Technol. 4 (2016) 1-14.

[47] S.Y. Chuang, J.S. Dennis, A.N. Hayhurst, S.A. Scott, Development and performance of Cu-based oxygen carriers for chemical-looping combustion. Combust. Flame. 154 (2008) 109-121.

[48] Q. Imtiaz, A.M. Kierzkowska, M. Broda, C.R. Müller, Synthesis of Cu-Rich, Al_2O_3-Stabilized Oxygen Carriers Using a Coprecipitation Technique: Redox and Carbon Formation Characteristics. Environ. Sci. Technol. 46 (2012) 3561−3566.

[49] A.L. Garcia-Lario, I. Martinez, R. Murillo, G. Grasa, J.R. Fernandez, J.C. Abanades, Reduction Kinetics of a High Load Cu-based Pellet Suitable for Ca/Cu Chemical Loops. Ind. Eng. Chem. Res. 52 (2013) 1481−1490.

[50] V. Manovic, Y. Wu, I. He, E.J. Anthony, Core-in-Shell CaO/CuO-Based Composite for CO_2 Capture. Ind. Eng. Chem. Res. 50 (2011) 12384–12391

[51] Manovic V, Anthony EJ. Integration of calcium and chemical looping combustion using composite CaO/CuO-based materials. Environ Sci Technol 2011; 45: 10750–10756.

[52] C. Qin, J. Yin, W. Liu, H. An, B. Feng, Behavior of CaO/CuO Based Composite in a Combined Calcium and Copper Chemical Looping Process. Ind. Eng. Chem. Res. 51 (2012) 12274−12281.

[53] Qin C, Yin J. Luo C, An H, Liu W, Feng B. Enhancing the performance of CaO/CuO based composite for CO_2 capture in a combined Ca–Cu chemical looping process. Chem. Eng. J. 228 (2013) 75–86.

[54] C.S. Martavaltzi, A.A. Lemonidou, Hydrogen production via sorption enhanced reforming of methane: Development of a novel hybrid material-reforming catalyst and CO_2 sorbent. Chem. Eng. Sci. 65 (2010) 4134-4140.

[55] N. Chanburanasiri, A.M. Ribeiro, A.E. Rodrigues, A. Arpornwichanop, N. Laosiripojana, P. Praserthdam, S. Assabumrungrat, Hydrogen production via sorption enhanced steam methane reforming process using Ni/CaO multifunctional catalyst, Ind. Eng. Chem. Res. 50 (2011) 13662‑13671.

[56] A.L. Garcia-Lario, G. Grasa, R. Murillo, Performance of a combined CaO-based sorbent and catalyst on H_2 production, via sorption enhanced methane steam reforming. Chem. Eng. J. 264 (2015) 697-705.

[57] J.R. Fernández, J.M. Alarcón, J.C. Abanades, Investigation of a Fixed-Bed Reactor for the Calcination of $CaCO_3$ by the Simultaneous Reduction of CuO with a Fuel Gas. Ind. Eng. Chem. Res. 55 (2016) 5128−5132.

[58] G.S. Grasa, J.C. Abanades, CO_2 capture capacity of CaO in long series of carbonation/calcination cycles. Ind. Eng. Chem.Res. 45 (2006) 8846‑51.

[59] B. Gonzalez, G.S. Grasa, M. Alonso, J.C. Abanades, Modeling of the deactivation of CaO in a carbonate loop at high temperatures of calcination. Ind. Eng. Chem. Res. 47(2008) 9256‑9262.

[60] A. Abad, J. Adánez, F. García-Labiano, L.F. de Diego, P. Gayán, Modeling of the chemical-looping combustion of methane using a Cu-based oxygen-carrier. Combus. Flame 157 (2010) 602-615.

[61] V.R. Choudhary, A.M. Rajput, A.S. Mamman, NiO-alkaline earth oxide catalysts for oxidative methane-to-syngas conversion: Influence of alkaline earth oxide on the surface properties and temperature-programmed reduction/reaction by H_2 and methane. J. Catal. 178 (1998) 576-85.

[62] J.D.A. Bellido, J.E. De Souza, J.C. M'Peko, E.M. Assaf, Effect of adding CaO to ZrO_2 support on nickel catalyst activity in dry reforming of methane. Appl. Catal. A: General. 358 (2009) 215-223.

[63] M.F. Edwards, J.F. Richardson, Gas dispersion in packed beds. Chem. Eng. Sci. 23 (1968) 109-123.

[64] D. Vortmeyer, R. Berninger R, Comments on the paper, theoretical prediction of effective heat transfer parameters in packed beds by Anthony Dixon and D. L. Cresswell [AIChE J., 25, 663 (1979)]. AIChE J. 28 (1982) 508-510.

[65] R. Krupiczka, Analysis of thermal conductivity in granular materials. Int. Chem. Eng. 7 (1967) 122-144.

[66] D.J. Gunn, M.M.A. Misbah, Bayesian estimation of heat transport parameters in fixed beds. Int. J. Heat Mass Transf. 36 (1993) 2209-2221.

[67] D. J. Gunn, Axial and radial dispersion in fixed beds. Chem. Eng. Sci. 42 (1987) 363-373.

[68] F. García-Labiano, L.F. de Diego, J. Adánez, A. Abad, P. Gayán, Reduction and oxidation Kinetics of a copper-based oxygen carrier prepared by impregnation for chemical-looping combustion. Ind. Eng. Chem. Res. 43 (2004) 8168-8177.

[69] I. Martínez, G. Grasa, R. Murillo, B. Arias, J.C. Abanades, Kinetics of calcination of partially carbonated particles in a Ca-looping system for CO_2 capture. Energy Fuel 26 (2012) 1432-1440.

[70] J. Xu, G.F. Froment, Methane steam reforming: II. Diffusional limitations and reactor simulation. AIChE J. 35 (1989) 97-103.

[71] J.C. Abanades, D. Alvarez, Conversion Limits in the Reaction of CO_2 with Lime. Energy Fuel 17(2) (2003) 308-315.

[72] M. Ginés, A. Marchi, C. Apesteguia, Kinetic study of the reverse water-gas shift reaction over $CuO/ZnO/Al_2O_3$ catalysts. Appl. Catal. A: General 154 (1997) 155-171.

[73] F. Bustamante, R. Enick, A. Cugini, R. Killmeyer, B. Howard, K. Rothenberger K, et al., High temperature kinetics of the homogeneous reverse water–gas shift reaction. AIChE J. 50 (2004) 1028-41.

[74] A. Kierzkowska, C.R. Müller, Development of calcium-based, copper-functionalised CO_2 sorbents to integrate chemical looping combustion into calcium looping. Energ. Env. Sci. 5 (2012) 6061-6065.

CAPÍTULO VI

CONCLUSIONES

6. CONCLUSIONES

Esta memoria, y las publicaciones presentadas en ella, ha permitido avanzar en la investigación de dos novedosos sistemas de captura de CO_2, que se encuentran en un estado preliminar de desarrollo pero que han confirmado su potencial para un desarrollo futuro hacia sistemas más eficaces y económicos de combustión de gases con transportadores de oxígeno y de producción de H_2 con captura integrada de CO_2.

Las conclusiones específicas extraídas de este trabajo, se resumen a continuación, separadas en secciones similares a los capítulos/publicaciones descritas anteriormente:

Diseño conceptual de un proceso de CLC en reactores de lecho fijo adiabáticos a alta presión con metano empleando ilmenita como trasportador de oxígeno:

- El empleo de lechos fijos a alta presión en procesos de CLC permite una integración eficiente en un ciclo combinado de gas natural, debido a que como producto se obtiene una corriente gaseosa continua a alta temperatura y presión, que directamente se podría alimentar a una turbina de gas para producir electricidad. Sin embargo, este tipo de sistemas requieren estrategias complejas para gestionar el calor, así como el empleo de válvulas que sean capaces de operar a temperatura elevada (aún en desarrollo).

- Los sistemas de CLC en reactores de lecho fijo a presión se presentan como una alternativa competitiva a medio plazo con respecto a otras configuraciones propuestas para CLC. Sin embargo, este tipo de sistemas requieren estrategias complejas para gestionar el calor, así como el empleo de válvulas que sean capaces de operar a temperatura elevada (aún en desarrollo).

- El modelo de reactores desarrollado para la reducción/oxidación de ilmenita indica que, recirculaciones adecuadas de gas permiten controlar el avance de los frentes de reacción y de intercambio de calor en los lechos, mejorando la gestión del calor en este tipo de configuraciones.

- La inclusión de una etapa de reformado de gas natural en la configuración del sistema, permite tener una fuente de gas de síntesis que favorecerá la reacción de reducción de la ilmenita, asegurando la conversión total del gas a CO_2 y $H_2O(v)$, y por tanto mejorando la eficiencia de la combustión en este proceso.

- El estudio preliminar de este proceso, para un flujo de entrada de 10 kg/s de CH_4 (500 MWt), muestra que se requiere un número mínimo de 5 reactores de 10 m de longitud por 6.7 m de diámetro operando en paralelo.

Modelado de reactor de la calcinación del $CaCO_3$ mediante la reducción simultánea de CuO en un reactor de lecho fijo adiabático en el proceso Ca-Cu:

- El modelo dinámico desarrollado demuestra que el calor generado en la reducción de CuO con un gas combustible permite calcinar $CaCO_3$ de forma simultánea sin necesidad de un aporte de energía externo, obteniendo una corriente de CO_2 concentrada para almacenamiento.

- Proporciones adecuadas de $CuO/CaCO_3$ permiten que la operación tenga lugar en condiciones neutras y se regule la temperatura máxima en torno a 900ºC. Un exceso de CuO en el lecho hace que la calcinación del $CaCO_3$ presente no pueda absorber todo el calor generado durante la reacción de reducción, pudiendo dar lugar a la formación de puntos calientes por encima de 900ºC. Si por el contrario hay un exceso de $CaCO_3$, no se produce el calor necesario para la calcinación y parte del $CaCO_3$ queda sin calcinar. Sin embargo, bajo condiciones adecuadas de operación identificadas con el modelo, usando cinéticas disponibles en la literatura, las reacciones tienen lugar en frentes nítidos en los reactores de lecho fijo, que avanzan juntos y dejan atrás sólidos totalmente convertidos.

- La composición del gas de alimentación determina la proporción de CuO y $CaCO_3$ en el lecho. El uso de CO y H_2, con mayores entalpías de reducción de CuO que el metano, hace que la cantidad requerida de CuO para calcinar sea menor, lo que aumenta la eficiencia energética del proceso.

Prueba de concepto de las etapas de reducción del CuO/calcinación del $CaCO_3$ y oxidación en un reactor de lecho fijo en el proceso Ca-Cu.

- La viabilidad del proceso de calcinación del $CaCO_3$ mediante la reducción simultánea del CuO con un combustible gaseoso (H_2 y CO) se ha validado a escala de laboratorio en un reactor de lecho fijo de 1 m de diámetro y 38 mm de diámetro interior, diseñado para operar en condiciones quasi-adiabaticas.

- Los estudios de transmisión de calor realizados en el reactor de lecho fijo han servido para estimar un coeficiente global de transmisión de calor de 5 W/m^2K, que ajusta bien los perfiles experimentales en ensayos de calentamiento y enfriamiento realizados a modo de blanco.

- El material de cobre empleado en este trabajo, un catalizador comercial suministrado por Jhonson Mathey, presenta una alta reactividad a CO y H_2, permitiendo la reducción completa del sólido en un relativamente estrecho frente de reacción y la oxidación total de los gases a CO_2 y H_2O, incluso a temperaturas relativamente bajas (menores de 500ºC).

- El material de cobre cataliza la reacción reversa WGS, favorecida por la alta temperatura alcanzada en el frente de reducción y la presencia de una elevada concentración de CO_2 como consecuencia de la calcinación. Esto explica que parte del H_2 y del CO_2 reaccionen generando pequeñas cantidades de CO en el frente de reducción, que son detectadas experimentalmente.

- Tras varios ciclos de oxidación/reducción y de carbonatación/calcinación se observan mediante XRD algunos cambios en la composición química de los materiales (formándose óxidos mixtos de cobre y calcio) que tienen capacidad de carbonatarse, lo que afecta a la capacidad de absorción de CO_2.

- La oxidación del Cu llevada a cabo con un alto caudal de O_2 diluido permite regular la temperatura máxima en el frente de oxidación a valores cercanos a 800ºC. Esto permite llevar a cabo la oxidación de un lecho con alto contenido en cobre sin calcinar de forma apreciable el $CaCO_3$ (siempre que la operación se realice a alta presión).

- El material de cobre empleado es lo suficientemente reactivo como para llevar a cabo la oxidación del lecho en un frente nítido y lograr de paso la conversión completa de O_2 incluso con concentraciones bajas del mismo (3% vol.) en el gas de entrada.

- El modelo dinámico desarrollado en este trabajo ha sido validado con los resultados experimentales obtenidos. Dicho modelo predice razonablemente la evolución de los perfiles de temperatura y de composición del gas producto durante las etapas de reducción/calcinación y la de oxidación de Cu.

REFERENCIAS

Abanades, J.C., Alonso, M., Rodríguez, N., González, B., Grasa, G., Murillo, R., 2009. Capturing CO_2 from combustion flue gases with a carbonation calcination loop. Experimental results and process development. Energy Procedia 1, 1147-1154.

Abanades, J.C., Anthony, E.J., Lu, D.Y., Salvador, C., Alvarez, D., 2004. Capture of CO_2 from combustion gases in a fluidized bed of CaO. AIChE Journal 50, 1614-1622.

Abanades, J.C., Anthony, E.J., Wang, J., Oakey, J.E., 2005. Fluidized Bed Combustion Systems Integrating CO_2 Capture with CaO. Environmental Science & Technology 39, 2861-2866.

Abanades, J.C., Arias, B., Lyngfelt, A., Mattisson, T., Wiley, D.E., Li, H., Ho, M.T., Mangano, E., Brandani, S., 2015. Emerging CO_2 capture systems. International Journal of Greenhouse Gas Control 40, 126-166.

Abanades, J.C., Murillo, R., Fernandez, J.R., Grasa, G., Martínez, I., 2010. New CO_2 capture process for hydrogen production combining Ca and Cu chemical loops. Environmental Science & Technology 44, 6901-6904.

Abanades, J.C., Murillo, V.R., 2009. Method for recovering CO_2 by means of CaO and the exothermic reduction of a solid. U.S. Patent 20120230897 A1.

Abdulally, I., Beal, C., Andrus, H., Epple, B., Lyngfelt, A., Lani, B., 2012. Alstom's Chemical Looping Prototypes Program Update. 37th International Technical Conference on Clean Coal & Fuel Systems. 3-7 June, Florida, USA

Adanez, J., Abad, A., Garcia-Labiano, F., Gayan, P., de Diego, L.F., 2012. Progress in chemical-looping combustion and reforming technologies. Progress in Energy and Combustion Science 38, 215-282.

Adánez, J., Abad, A., Perez-Vega, R., de Diego, L.F., García-Labiano, F., Gayán, P., 2014. Design and Operation of a Coal-fired 50 kWth Chemical Looping Combustor. Energy Procedia 63, 63-72.

Adánez, J., de Diego, L.F., García-Labiano, F., Gayán, P., Abad, A., Palacios, J.M., 2004. Selection of Oxygen Carriers for Chemical-Looping Combustion. Energy & Fuels 18, 371-377.

Adánez, J., Gayán, P., Celaya, J., de Diego, L.F., García-Labiano, F., Abad, A., 2006. Chemical looping combustion in a 10 kWth prototype using a CuO/Al_2O_3 oxygen carrier: effect of operating conditions on methane combustion. Industrial & Engineering Chemistry Research 45, 6075-6080.

Alarcón, J.M., Fernández, J.R., 2015. $CaCO_3$ calcination by the simultaneous reduction of CuO in a Ca/Cu chemical looping process. Chemical Engineering Science 137, 254-267.

Aloisi, I., Di Giuliano, A., Di Carlo, A., Foscolo, P.U., Courson, C., Gallucci, K., 2017. Sorption enhanced catalytic Steam Methane Reforming: Experimental data and simulations describing the behaviour of bi-functional particles. Chemical Engineering Journal 314, 570-582.

Alonso, M., Rodríguez, N., González, B., Grasa, G., Murillo, R., Abanades, J.C., 2010. Carbon dioxide capture from combustion flue gases with a calcium oxide chemical loop. Experimental results and process development. International Journal of Greenhouse Gas Control 4, 167-173.

Alvarez, D., Abanades, J.C., 2005a. Determination of the Critical Product Layer Thickness in the Reaction of CaO with CO_2. Industrial & Engineering Chemistry Research 44, 5608-5615.

Alvarez, D., Abanades, J.C., 2005b. Pore-Size and Shape Effects on the Recarbonation Performance of Calcium Oxide Submitted to Repeated Calcination/Recarbonation Cycles. Energy & Fuels 19, 270-278.

Andresen, B., Norheim, A., Strand, J., Ulleberg, Ø., Vik, A., Wærnhus, I., 2014. BioZEG – Pilot Plant Demonstration of High Efficiency Carbon Negative Energy Production. Energy Procedia 63, 279-285.

Arias, B., Diego, M.E., Méndez, A., Abanades, J.C., Díaz, L., Lorenzo, M., Sánchez-Biezma, A., 2016. Operating experience in la Pereda 1.7 MWth Calcium Looping pilot. 13th International Conference on Greenhouse Gas Control Technologies, GHGT-13. 14-18 November, Laussane, Switzerland

Arias, B., Grasa, G.S., Abanades, J.C., 2010. Effect of sorbent hydration on the average activity of CaO in a Ca-looping system. Chemical Engineering Journal 163, 324-330.

Arias, B., Grasa, G.S., Alonso, M., Abanades, J.C., 2012. Post-combustion calcium looping process with a highly stable sorbent activity by recarbonation. Energy & Environmental Science 5, 7353-7359.

Bachu, S., 2015. Review of CO_2 storage efficiency in deep saline aquifers. International Journal of Greenhouse Gas Control 40, 188-202.

Baker, E., 1962. The calcium oxide–carbon dioxide system in the pressure range 1—300 atmospheres. Journal of the Chemical Society (Resumed), 464-470.

Berdugo, T., Lind, F., Rydén, M., Thunman, H., 2017. Experience of more than 1000 h of operation with oxygen carriers and solid biomass at large scale. Applied Energy 190, 1174-1183.

Bischi, A., Langørgen, Ø., Saanum, I., Bakken, J., Seljeskog, M., Bysveen, M., Morin, J.X., Bolland, O., 2011. Design study of a 150 kWth double loop circulating fluidized bed reactor system for chemical looping combustion with focus on industrial applicability and pressurization. International Journal of Greenhouse Gas Control 5, 467-474.

Blamey, J., Paterson, N.P.M., Dugwell, D.R., Stevenson, P., Fennell, P.S., 2011. Reactivation of a CaO-based sorbent for CO_2 capture from stationary sources. Proceedings of the Combustion Institute 33, 2673-2681.

Boon, J., Cobden, P.D., van Dijk, H.A.J., van Sint Annaland, M., 2015. High-temperature pressure swing adsorption cycle design for sorption-enhanced water–gas shift. Chemical Engineering Science 122, 219-231.

Boot-Handford, M.E., Abanades, J.C., Anthony, E.J., Blunt, M.J., Brandani, S., Mac Dowell, N., Fernandez, J.R., Ferrari, M.C., Gross, R., Hallett, J.P., Haszeldine, R.S., Heptonstall, P., Lyngfelt, A., Makuch, Z., Mangano, E., Porter, R.T.J., Pourkashanian, M., Rochelle, G.T., Shah, N., Yao, J.G., Fennell, P.S., 2014. Carbon capture and storage update. Energy & Environmental Science 7, 130-189.

Brandvoll, O., Bolland, O., 2004. Inherent CO_2 capture using chemical looping combustion in a natural gas fired power cycle. Journal of Engineering for Gas Turbines and Power 126, 316-321.

Curran, G.P., Fink, C.E., Gorin, E., 1967. CO_2 Acceptor Gasification Process, Fuel Gasification. American Chemical Society, pp. 141-165.

Charitos, A., Hawthorne, C., Bidwe, A., Sivalingam, S., Schuster, A., Spliethoff, H., Scheffknecht, G., 2010. Parametric investigation of the calcium looping process for CO_2 capture in a 10kWth dual fluidized bed. International Journal of Greenhouse Gas Control 4, 776-784.

Chen, Z., Grace, J.R., Lim, C.J., 2011. CO_2 Capture and Hydrogen Production in an Integrated Fluidized Bed Reformer-Regenerator System. Industrial & Engineering Chemistry Research 50, 4716-4721.

Cho, P., Mattisson, T., Lyngfelt, A., 2004. Comparison of iron-, nickel-, copper- and manganese-based oxygen carriers for chemical-looping combustion. Fuel 83, 1215-1225.

Chuang, S.Y., Dennis, J.S., Hayhurst, A.N., Scott, S.A., 2008. Development and performance of Cu-based oxygen carriers for chemical-looping combustion. Combustion and Flame 154, 109-121.

de Diego, L.F., García-Labiano, F., Adánez, J., Gayán, P., Abad, A., Corbella, B.M., Palacios, M.J., 2004. Development of Cu-based oxygen carriers for chemical-looping combustion. Fuel 83, 1749-1757.

de Diego, L.F., García-Labiano, F., Gayán, P., Celaya, J., Palacios, M.J., Adánez, J., 2007. Operation of a 10 kWth chemical-looping combustor during 200 h with a $CuO-Al_2O_3$ oxygen carrier. Fuel 86, 1036–1045

Duhoux, B., Mehrani, P., Lu, D.Y., Symonds, R.T., Anthony, E.J., Macchi, A., 2016. Combined Calcium Looping and Chemical Looping Combustion for Post-Combustion Carbon Dioxide Capture: Process Simulation and Sensitivity Analysis. Energy Technology 4, 1158-1170.

Fan, L.-S., 2010. Chemical Looping Systems for Fossil Energy Conversions. John Wiley & Sons, Inc.

Fernández, J.R., Abanades, J.C., 2016. CO_2 capture from the calcination of $CaCO_3$ using iron oxide as heat carrier. Journal of Cleaner Production 112, Part 1, 1211-1217.

Fernández, J.R., Abanades, J.C., 2017. Optimized design and operation strategy of a Ca-Cu chemical looping process for hydrogen production. Chemical engineering science 166, 144-160.

Fernandez, J.R., Abanades, J.C., Grasa, G., 2012a. Modeling of sorption enhanced steam methane reforming—Part II: Simulation within a novel Ca/Cu chemical loop process for hydrogen production. Chemical Engineering Science 84, 12-20.

Fernandez, J.R., Abanades, J.C., Murillo, R., 2012b. Modeling of sorption enhanced steam methane reforming in an adiabatic fixed bed reactor. Chemical Engineering Science 84, 1-11.

Fernandez, J.R., Abanades, J.C., Murillo, R., 2014. Modeling of Cu oxidation in an adiabatic fixed-bed reactor with N_2 recycling. Applied Energy 113, 1945–1951.

Fernández, J.R., Abanades, J.C., Murillo, R., 2013. Modeling of Cu oxidation in adiabatic fixed-bed reactor with N_2 recycling in a Ca/Cu chemical loop. Chemical Engineering Journal 232, 442–452.

Fernández, J.R., Abanades, J.C., Murillo, R., Grasa, G., 2012. Conceptual design of a hydrogen production process from natural gas with CO_2 capture using a Ca–Cu chemical loop. International Journal of Greenhouse Gas Control 6, 126-141.

Fernández, J.R., Alarcón, J.M., 2015. Chemical looping combustion process in fixed-bed reactors using ilmenite as oxygen carrier: Conceptual design and operation strategy. Chemical Engineering Journal 264, 797-806.

Fernández, J.R., Alarcón, J.M., Abanades, J.C., 2016. Investigation of a Fixed-Bed Reactor for the Calcination of $CaCO_3$ by the Simultaneous Reduction of CuO with a Fuel Gas. Industrial & Engineering Chemistry Research 55, 5128-5132.

Fernández, J.R., Martínez, I., Abanades, J.C., Romano, M.C., 2017. Conceptual design of a Ca–Cu chemical looping process for hydrogen production in integrated steelworks. International Journal of Hydrogen Energy http://dx.doi.org/10.1016/j.ijhydene.2017.02.141.

Gale, J., Abanades, J.C., Bachu, S., Jenkins, C., 2015. Special Issue commemorating the 10th year anniversary of the publication of the Intergovernmental Panel on Climate Change Special Report on CO_2 Capture and Storage. International Journal of Greenhouse Gas Control 40, 1-5.

Galloy, A., Ströhle, J., Epple, B., 2011. Design and operation of a 1 MWth carbonate and chemical looping CCS test rig. VGB PowerTech 91, 64-68.

García-Lario, A.L., Aznar, M., Grasa, G.S., Murillo, R., 2015a. Evaluation of process variables on the performance of Sorption Enhanced Methane Reforming. Journal of Power Sources 285, 90-99.

García-Lario, A.L., Grasa, G.S., Murillo, R., 2015b. Performance of a combined CaO-based sorbent and catalyst on H_2 production, via sorption enhanced methane steam reforming. Chemical Engineering Journal 264, 697-705.

Global CCS, 2016a. Global CCS projects. Global CCS Institute, Melbourne, Australia. https://www.globalccsinstitute.com/projects/large-scale-ccs-projects

Global CCS, 2016b. The global status of CCS. Global CCS Institute, Melbourne, Australia.

González, B., Grasa, G.S., Alonso, M., Abanades, J.C., 2008. Modeling of the deactivation of CaO in a carbonate loop at high temperatures of calcination. Industrial & Engineering Chemistry Research 47, 9256-9262.

Grasa, G., Martínez, I., Diego, M.E., Abanades, J.C., 2014. Determination of CaO Carbonation Kinetics under Recarbonation Conditions. Energy & Fuels 28, 4033-4042.

Grasa, G.S., Abanades, J.C., 2006. CO_2 Capture Capacity of CaO in Long Series of Carbonation/Calcination Cycles. Industrial & Engineering Chemistry Research 45, 8846-8851.

Hamers, H.P., Gallucci, F., Cobden, P.D., Kimball, E., van Sint Annaland, M., 2014. CLC in packed beds using syngas and CuO/Al_2O_3: Model description and experimental validation. Applied Energy 119, 163-172.

Hamers, H.P., Gallucci, F., Williams, G., van Sint Annaland, M., 2015. Experimental demonstration of CLC and the pressure effect in packed bed reactors using $NiO/CaAl_2O_4$ as oxygen carrier. Fuel 159, 828-836.

Harrison, D.P., 2008. Sorption-enhanced hydrogen production: a review. Industrial & Engineering Chemistry Research 47, 6486–6501.

Hofbauer, H., Rauch, R., Bosch, K., Koch, R., Aicherning, C., 2003. Biomass CHP plant Güssing-a sucess history. Bridwater (Ed.), Pyrolisis and Gasification of Biomass and Waste. CPL Press, Newbury, pp. 371-383.

Hossain, M.M., de Lasa, H.I., 2008. Chemical-looping combustion (CLC) for inherent separations—a review. Chemical Engineering Science 63, 4433-4451.

IEA, 2015. Technology roadmap. Hydrogen and fuel cells. International Energy Agency, Paris, France

IEA, 2016. World energy outlook. International Energy Agency, Paris, France

IEA, 2016a. Energy technology perspectives. International Energy Agency, Paris, France

IEA, 2016d. 20 Years of Carbon Capture and Storage. Acelerate future deployment. International Energy Agency, Paris, France

Imtiaz, Q., Kierzkowska, A.M., Broda, M., Müller, C.R., 2012. Synthesis of Cu-Rich, Al_2O_3-Stabilized Oxygen Carriers Using a Coprecipitation Technique: Redox and Carbon Formation Characteristics. Environmental Science & Technology 46, 3561-3566.

IPCC, 2005. Special report on carbon dioxide capture and storage. Intergovernmental Panel on Climate change, IPCC, New York, USA

IPCC, 2014. Climate change 2014: synthesis report. Contribution of working groups I, II and III to the fifth assessment report of the intergovernmental panel on climate change. Intergovernmental Panel on Climate change, IPCC, Ginebra, Suiza

Ishida, M., Jin, H., 1994. A new advanced power-generation system using chemical-looping combustion. Energy 19, 415-422.

Ishida, M., Zheng, D., Akehata, T., 1987. Evaluation of a chemical-looping-combustion power-generation system by graphic exergy analysis. Energy 12, 147-154.

Jansen, D., Gazzani, M., Manzolini, G., Dijk, E.v., Carbo, M., 2015. Pre-combustion CO_2 capture. International Journal of Greenhouse Gas Control 40, 167-187.

Junk, M., Reitz, M., Ströhle, J., Epple, B., 2013. Thermodynamic evaluation and cold flow model testing of an indirectly heated carbonate looping process. Chemical Engineering & Technology 36, 1479-1487.

Kelly, S.M., 2014. Praxair's Oxygen Transport Membranes for Oxycombustion and Syngas Applications.https://www.netl.doe.gov/File%20Library/Events/2014/2014%20NETL%20CO2%20Capture/S-Kelly-PRAXAIR-Praxair-s-Oxygen-Transport-Membranes.pdf

Kierzkowska, A.M., Pacciani, R., Müller, C.R., 2013. CaO-Based CO_2 Sorbents: From Fundamentals to the Development of New, Highly Effective Materials. ChemSusChem 6, 1130-1148.

Kremer, J., Galloy, A., Ströhle, J., Epple, B., 2013. Continuous CO_2 Capture in a 1-MWth Carbonate Looping Pilot Plant. Chemical Engineering & Technology 36, 1518-1524.

Kumar, R., Lyon, R., Cole, J., 2002. Unmixed reforming: A novel autothermal cyclic steam reforming process, Grégoire, P., Catherine, E.L., Francis, L. (Ed.), Advances in Hydrogen Energy. Springer US pp. 31-45.

Lee, D.K., Baek, I.H., Yoon, W.L., 2004. Modeling and simulation for the methane steam reforming enhanced by in situ CO_2 removal utilizing the CaO carbonation for H_2 production. Chemical Engineering Science 59, 931-942.

Lee, S.-Y., Park, S.-J., 2015. A review on solid adsorbents for carbon dioxide capture. Journal of Industrial and Engineering Chemistry 23, 1-11.

Lewis, W., Guilliland, E., Sweeney, M., 1951. Gasification of carbon. Chemical Engineering Progress 47, 251-256.

Li, Z.-s., Cai, N.-s., Yang, J.-b., 2006. Continuous Production of Hydrogen from Sorption-Enhanced Steam Methane Reforming in Two Parallel Fixed-Bed Reactors Operated in a Cyclic Manner. Industrial & Engineering Chemistry Research 45, 8788-8793.

Lin, S.-Y., Suzuki, Y., Hatano, H., Harada, M., 2002. Developing an innovative method, HyPr-RING, to produce hydrogen from hydrocarbons. Energy Conversion and Management 43, 1283-1290.

Luo, C., Zheng, Y., Zheng, C., Yin, J., Qin, C., Feng, B., 2013. Manufacture of calcium-based sorbents for high temperature cyclic CO_2 capture via a sol–gel process. International Journal of Greenhouse Gas Control 12, 193-199.

Lyngfelt, A., 2011. Oxygen carriers for chemical looping combustion 4000 h of operational experience. Oil & Gas Science and Technology 66, 161-172.

Lyngfelt, A., 2013. Chemical looping combustion (CLC) Scala, F. (Ed.), Fluidized Bed Technologies for Near-Zero Emission Combustion and Gasification. Woodhead Publishing, pp. 895-930.

Lyngfelt, A., 2015. Oxygen carriers for chemical-looping combustion, Fennel, P., Anthony, B. (Ed.), Calcium and Chemical Looping Technology for Power Generation and Carbon Dioxide (CO_2) Capture. Woodhead Publishing, pp. 221-254.

Lyngfelt, A., Leckner, B., Mattisson, T., 2001. A fluidized-bed combustion process with inherent CO_2 separation; application of chemical-looping combustion. Chemical Engineering Science 56, 3101-3113.

Lyngfelt, A., Thunman, H., 2005. Construction and 100 h of operational experience of a 10-kW chemical-looping combustor, Thomas, D.C. (Ed.), Carbon Dioxide Capture for Storage in Deep Geologic Formations. Elsevier Science, Amsterdam, pp. 625-645.

Manovic, V., Anthony, E.J., 2009. Long-Term Behavior of CaO-Based Pellets Supported by Calcium Aluminate Cements in a Long Series of CO_2 Capture Cycles. Industrial & Engineering Chemistry Research 48, 8906-8912.

Manovic, V., Lu, D., Anthony, E.J., 2008. Steam hydration of sorbents from a dual fluidized bed CO_2 looping cycle reactor. Fuel 87, 3344-3352.

Manovic, V., Wu, Y., He, I., Anthony, E.J., 2011. Core-in-shell CaO/CuO-based composite for CO_2 capture. Industrial & Engineering Chemistry Research 50, 12384-12391.

Martavaltzi, C.S., Lemonidou, A.A., 2010. Hydrogen production via sorption enhanced reforming of methane: Development of a novel hybrid material—reforming catalyst and CO_2 sorbent. Chemical Engineering Science 65, 4134-4140.

Martínez, I., Armaroli, D., Gazzani, M., Romano, M.C., 2017. Integration of the Ca-Cu process in ammonia production plants. Industrial & Engineering Chemistry Research 56, 5526-5539.

Martínez, I., Murillo, R., Grasa, G., Fernández, J.R., Abanades, J.C., 2013a. Design of a hydrogen production process for power generation based on a Ca-Cu chemical loop. Energy Procedia 37, 626-634.

Martínez, I., Murillo, R., Grasa, G., Fernández, J.R., Abanades, J.C., 2013b. Integrated combined cycle from natural gas with CO_2 capture using a Ca–Cu chemical loop. AIChE Journal 59, 2780-2794.

Martínez, I., Romano, M.C., Chiesa, P., Grasa, G., Murillo, R., 2013c. Hydrogen production through sorption enhanced steam reforming of natural gas: Thermodynamic plant assessment. International Journal of Hydrogen Energy 38, 15180-15199.

Martínez, I., Romano, M.C., Fernández, J.R., Chiesa, P., Murillo, R., Abanades, J.C., 2014. Process design of a hydrogen production plant from natural gas with CO_2 capture based on a novel Ca/Cu chemical loop. Applied Energy 114, 192-208.

Martini, M., Martínez, I., Gallucci, F., Romano, M.C., 2016a. Increasing the carbon capture efficiency of the Ca/Cu looping process with advanced process squemes. 4th Chemical Looping Conference. 26-28th September, Nanjing, China

Martini, M., van den Berg, A., Gallucci, F., van Sint Annaland, M., 2016b. Investigation of the process operability windows for Ca-Cu looping for hydrogen production with CO_2 capture. Chemical Engineering Journal 303, 73-88.

Mattisson, T., Lyngfelt, A., Leion, H., 2009. Chemical-looping with oxygen uncoupling for combustion of solid fuels. International Journal of Greenhouse Gas Control 3, 11-19.

Meyer, J., Mastin, J., Bjørnebøle, T.K., Ryberg, T., Eldrup, N., 2011. Techno-economical study of the zero emission gas power concept. Energy Procedia 4, 1949-1956.

Meyer, J., Mastin, J., Pinilla, C.S., 2014. Sustainable Hydrogen Production from Biogas Using Sorption-Enhanced Reforming. Energy Procedia 63, 6800-6814.

Naqvi, R., Bolland, O., 2007. Multi-stage chemical looping combustion (CLC) for combined cycles with CO_2 capture. International Journal of Greenhouse Gas Control 1, 19-30.

Navarro, M.V., López, J.M., Díez, L., Fernández, J.R., Grasa, G., Murillo, R., 2017. Validation of the SER H_2 production stage under relevant conditions for the Ca/Cu process. Chemical Engineering Journal. https://doi.org/10.1016/j.cej.2017.04.134.

Noorman, S., Gallucci, F., van Sint Annaland, M., Kuipers, H.J.A.M., 2010a. Experimental investigation of a CuO/Al_2O_3 oxygen carrier for chemical-looping combustion. Industrial & Engineering Chemistry Research 49, 9720-9728.

Noorman, S., Gallucci, F., van Sint Annaland, M., Kuipers, J.A.M., 2011a. Experimental investigation of chemical-looping combustion in packed beds: A parametric study. Industrial & Engineering Chemistry Research 50, 1968-1980.

Noorman, S., Gallucci, F., van Sint Annaland, M., Kuipers, J.A.M., 2011b. A theoretical investigation of CLC in packed beds. Part 2: Reactor model. Chemical Engineering Journal 167, 369-376.

Noorman, S., Van Sint Annaland, M., Kuipers, J.A.M., 2007. Packed bed reactor technology for chemical-looping combustion. Industrial & Engineering Chemistry Research 46, 4212-4220.

Noorman, S., van SintAnnaland, M., Kuipers, J.A.M., 2010b. Experimental validation of packed bed chemical-looping combustion. Chemical Engineering Science 65, 92-97.

Numaguchi, T., Kikuchi, K., 1988. Intrinsic kinetics and design simulation in a complex reaction network; steam-methane reforming. Chemical engineering science 43, 2295-2301.

Ochoa-Fernández, E., Rusten, H.K., Jakobsen, H.A., Rønning, M., Holmen, A., Chen, D., 2005. Sorption enhanced hydrogen production by steam methane reforming using Li_2ZrO_3 as sorbent: Sorption kinetics and reactor simulation. Catalysis Today 106, 41-46.

Pera-Titus, M., 2014. Porous Inorganic Membranes for CO_2 Capture: Present and Prospects. Chemical Reviews 114, 1413-1492.

Plötz, S., Bayrak, A., Galloy, A., Kremer, J., Orth, M., Wieczorek, M., Ströhle, J., Epple, B., 2012. First Carbonate Looping Experiments with a 1 MWth Test Facility Consisting of Two Interconnected CFBs 21st International Conference on Fluidized Bed Combustion 3-6 June, Naples, Italy

Qin, C., Feng, B., Yin, J., Ran, J., Zhang, L., Manovic, V., 2015. Matching of kinetics of $CaCO_3$ decomposition and CuO reduction with CH_4 in Ca–Cu chemical looping. Chemical Engineering Journal 262, 665-675.

Qin, C., Yin, J., Liu, W., An, H., Feng, B., 2012. Behavior of CaO/CuO Based Composite in a Combined Calcium and Copper Chemical Looping Process. Industrial & Engineering Chemistry Research 51, 12274-12281.

Ramkumar, S., Iyer, M.V., Fan, L.-S., 2011. Calcium Looping Process for Enhanced Catalytic Hydrogen Production with Integrated Carbon Dioxide and Sulfur Capture. Industrial & Engineering Chemistry Research 50, 1716-1729.

Richter, H.J., Knoche, K.F., 1983. Reversibility of Combustion Processes, Efficiency and Costing. American Chemical Society, pp. 71-85.

Ridha, F.N., Lu, D., Macchi, A., Hughes, R.W., 2015. Combined calcium looping and chemical looping combustion cycles with CaO–CuO pellets in a fixed bed reactor. Fuel 153, 202-209.

Rochelle, G.T., 2016. Conventional amine scrubbing for CO_2 capture, Feron, P. (Ed.), Absorption-Based Post-combustion Capture of Carbon Dioxide. Woodhead Publishing, pp. 35-67.

Rodríguez, N., Alonso, M., Abanades, J.C., 2011. Experimental investigation of a circulating fluidized-bed reactor to capture CO_2 with CaO. AIChE Journal 57, 1356-1366.

Rubin, E.S., Davison, J.E., Herzog, H.J., 2015. The cost of CO_2 capture and storage. International Journal of Greenhouse Gas Control 40, 378-400.

Rydén, M., Lyngfelt, A., 2006. Using steam reforming to produce hydrogen with carbon dioxide capture by chemical-looping combustion. International Journal of Hydrogen Energy 31, 1271-1283.

Ryu, H.-J., Jin, G.-T., Yi, C.-K., 2004. Demonstration of inherent CO_2 separation and no NO_x emission in a 50 kW chemical-looping combustor: continuous reduction and oxidation experiment. Proceedings of the 7th international conference on greenhouse gas control technologies. 5th September, Vancouver, Canada

Sanchez- Bienzma, A.D., L; Lopez, J; Arias, B; Paniagua, J., 2012. La Pereda CO_2: A 1.7 MW Pilot to test Post-combustion CO_2 Capture with CaO 21st International Conference on Fluidized Bed Combustion. 3-6 June, Naples, Italy

Sánchez-Biezma, A., Paniagua, J., Diaz, L., Lorenzo, M., Alvarez, J., Martínez, D., Arias, B., Diego, M.E., Abanades, J.C., 2013. Testing postcombustion CO_2 capture with CaO in a 1.7 MWt pilot facility. Energy Procedia 37, 1-8.

Shimizu, T., Hirama, T., Hosoda, H., Kitano, K., Inagaki, M., Tejima, K., 1999. A Twin Fluid-Bed Reactor for Removal of CO_2 from Combustion Processes. Chemical Engineering Research and Design 77, 62-68.

Silaban, A., Harrison, D., 1995. High temperature capture of carbon dioxide: characteristics of the reversible reaction between CaO(s) and CO_2(g). Chemical Engineering Communications 137, 177-190.

Smit, J., van Sint Annaland, M., Kuipers, J.A.M., 2005. Grid adaptation with WENO schemes for non-uniform grids to solve convection-dominated partial differential equations. Chemical Engineering Science 60, 2609-2619.

Spallina, V., Gallucci, F., Romano, M.C., Chiesa, P., Lozza, G., van Sint Annaland, M., 2013. Investigation of heat management for CLC of syngas in packed bed reactors. Chemical Engineering Journal 225, 174-191.

Sreedhar, I., Vaidhiswaran, R., Kamani, B.M., Venugopal, A., 2017. Process and engineering trends in membrane based carbon capture. Renewable and Sustainable Energy Reviews 68, Part 1, 659-684.

Stanger, R., Wall, T., Spörl, R., Paneru, M., Grathwohl, S., Weidmann, M., Scheffknecht, G., McDonald, D., Myöhänen, K., Ritvanen, J., Rahiala, S., Hyppänen, T., Mletzko, J., Kather, A., Santos, S., 2015. Oxyfuel combustion for CO_2 capture in power plants. International Journal of Greenhouse Gas Control 40, 55-125.

Stevens, J., Rovner, J., 2005. Reactor with carbon dioxide fixing material. U.S. Patent 20050232855 A1

Stevens, J.F., Cao, J.M., Vu, T.M., 2008. Reforming with hydration of carbon dioxide fixing material. U.S. Patent 7384621 B2

Ströhle, J., Junk, M., Kremer, J., Galloy, A., Epple, B., 2014. Carbonate looping experiments in a 1 MWth pilot plant and model validation. Fuel 127, 13-22.

Sun, P., Lim, C.J., Grace, J.R., 2008. Cyclic CO_2 capture by limestone-derived sorbent during prolonged calcination/carbonation cycling. AIChE Journal 54, 1668-1677.

Twigg, M., 1989. Catalyst Handbook. Wolfe Publishing Ltd., UK.

Valverde, J., Sanchez-Jimenez, P., Perez-Maqueda, L.A., 2014. Role of precalcination and regeneration conditions on postcombustion CO_2 capture in the Ca-looping technology. Applied Energy 136, 347-356.

Weimer, T., Berger, R., Hawthorne, C., Abanades, J.C., 2008. Lime enhanced gasification of solid fuels: Examination of a process for simultaneous hydrogen production and CO_2 capture. Fuel 87, 1678-1686.

Wolf, J., Yan, J., 2005. Parametric study of chemical looping combustion for tri-generation of hydrogen, heat, and electrical power with CO_2 capture. International Journal of Energy Research 29, 739-753.

Xiao, R., Song, Q., Song, M., Lu, Z., Zhang, S., Shen, L., 2010. Pressurized chemical-looping combustion of coal with an iron ore-based oxygen carrier. Combustion and Flame 157, 1140-1153.

Xu, J., Froment, G.F., 1989. Methane steam reforming, methanation and water-gas shift: I. Intrinsic kinetics. AIChE Journal 35, 88-96.

Zhao, M., Shi, J., Zhong, X., Tian, S., Blamey, J., Jiang, J., Fennell, P.S., 2014. A novel calcium looping absorbent incorporated with polymorphic spacers for hydrogen production and CO_2 capture. Energy & Environmental Science 7, 3291-3295.

Zhen-shan, L., Ning-sheng, C., Croiset, E., 2008. Process analysis of CO_2 capture from flue gas using carbonation/calcination cycles. AIChE Journal 54, 1912-1925.

Ziock, H.J., Lackner, K.S., Harrison, D.P., 2001. Zero Emission Coal Power, a New Concept First National Conference on Carbon Sequestration. First National Conference on Carbon Sequestration. 14-17 May, Washington DC, USA

ANEXOS

ANEXO I: TAREAS REALIZADAS EN LA UNIVERSIDAD TÉCNICA DE EINDHOVEN (TUe).

Dentro del marco del proyecto ASCENT, entre los meses de febrero y junio de 2016, se ha realizado una estancia de investigación en la universidad técnica de Eindhoven (TUe) (Holanda), en el grupo de intensificación de procesos químicos. Este grupo de investigación y el de captura de CO_2 del INCAR-CSIC, son dos de los socios del proyecto. Entre los objetivos del mismo se encuentra la modelización y prueba de concepto de las etapas que conforman el proceso Ca-Cu.

El objetivo de la estancia fue colaborar en tareas de modelado para realizar una comparación de los modelos desarrollados por ambos grupos de investigación, y la prueba de concepto de la etapa SER del proceso Ca-Cu. Inicialmente se planteó determinar la ventana operativa en un reactor de lecho fijo a presión atmosférica para su posterior escalado y puesta a punto en un reactor de mayores dimensiones capaz de trabajar a presión. Sin embargo, debido a limitaciones en el equipo experimental sólo se realizaron ensayos en el reactor de menor tamaño sin la obtención de resultados satisfactorios.

AI.1 Comparación entre modelos

El INCAR-CSIC y la TUe emplean un modelo pseudo-homogéneo en una dimensión implementado en Matlab y Delphi, respectivamente. Para describir el proceso, ambos grupos asumen las consideraciones y ecuaciones de diseño que se describen en la Publicación II.

Para llevar a cabo la comparación, se procedió a evaluar las cinéticas empleadas, propiedades físicas y otros parámetros para partir de condiciones similares. En cuanto a las cinéticas empleadas, las reacciones SMR y WGS, catalizadas heterogéneamente por un catalizador de níquel, como se ha explicado en la sección 1.3.3, han sido estudiadas en varios trabajos, tales como las propuestas por Xu y Froment (1989) (empleada por el INCAR-CSIC) y Numaguchi y Kikuchi (1988) (empleada por la TUe), las cuales se han considerado en este estudio. Para la carbonatación, las cinéticas de Rodríguez et al., (2011) (empleada por el INCAR-CSIC) y Lee (2004) (empleada por la TUe) que consideran un modelo de núcleo decreciente, han sido seleccionadas.

Las expresiones correspondientes a estas cinéticas y sus parámetros se muestran en las tablas AI.1, AI.2 y AI.3.

Tabla AI.1: cinéticas consideradas en la etapa SER

SMR y WGS Xu y Froment (1989) (Xu y Froment, 1989)
$R_1 = \frac{1}{(DEN)^2}\frac{k_1}{p_{H_2}^{2.5}}\left(p_{CH_4}p_{H_2O} - \frac{p_{CO}p_{H_2}^3}{K_1}\right)$ $R_2 = \frac{1}{(DEN)^2}\frac{k_2}{p_{H_2}^{3.5}}\left(p_{CH_4}p_{H_2O}^2 - \frac{p_{CO_2}p_{H_2}^4}{K_2}\right)$ $R_3 = \frac{1}{(DEN)^2}\frac{k_3}{p_{H_2}}\left(p_{CO}p_{H_2O} - \frac{p_{CO_2}p_{H_2}}{K_3}\right)$ $DEN = 1 + K_{CO}p_{CO} + K_{H_2}p_{H_2} + K_{CH_4}p_{CH_4} + K_{H_2O}\frac{p_{H_2O}}{p_{H_2}}$
SMR y WGS Numaguchi y Kikuchi (1988) (Numaguchi y Kikuchi, 1988)
$r_1 = A_1 e^{\frac{-E_{act,1}}{RT}}\left(\frac{p_{CH_4}p_{H_2O} - \frac{p_{CO}p_{H_2}^3}{K_1}}{p_{H_2O}^{1.596}}\right)$; $r_2 = A_2 e^{\frac{-E_{act,2}}{RT}}\left(\frac{p_{CO}p_{H_2O} - \frac{p_{CO_2}p_{H_2}^3}{K_2}}{p_{H_2O}}\right)$
Carbonatación
$\frac{dX}{dt} = k_{carb}(X_{\max} - X)(\upsilon_{CO_2} - \upsilon_{CO_2,eq})$ (Rodríguez et al., 2011) $r_i = \frac{\rho_i}{M_w^i}A_i e^{\frac{-E_{act,i}}{RT}}(1-X)^{2/3}\left(c_{CO_2} - \frac{p_{CO_2}^{eq}}{RT}\right)\left(\frac{p}{p_0}\right)^{-q_p}$ (Lee et al., 2004)

CO_2 de equilibrio en Rodríguez et al., (2011) en fracción molar y en Lee (2004) en bar, calculadas según (Baker, 1962). q_p, término de corrección de la presión.

Tabla AI.2: parámetros cinéticos de las reacciones SMR y WGS

SMR y WGS Xu y Froment (1989)
$K_1 = \frac{1}{\exp(0.2516Z^4 - 0.3665Z^3 - 0.58101Z^2 + 27.1337Z - 3.2770}$
$K_3 = \exp(-0.29353Z^3 + 0.63508Z^2 + 4.1778Z - 0.31688)^a$
$Z = \frac{1000}{T} - 1,\ K_2 = K_1 \times K_3$
$k_1 = 1.842 \times 10^{-4} \exp\left[\frac{240100}{R}\left(\frac{1}{T} - \frac{1}{648}\right)\right] \quad \frac{bar^{0.5} kmol}{kg_{catalyst} h}$
$k_2 = 2.193 \times 10^{-5} \exp\left[\frac{243900}{R}\left(\frac{1}{T} - \frac{1}{648}\right)\right] \quad \frac{bar^{0.5} kmol}{kg_{catalyst} h}$
$k_1 = 7.558 \exp\left[\frac{63130}{R}\left(\frac{1}{T} - \frac{1}{648}\right)\right] \quad \frac{kmol}{kg_{catalyst} h\ bar}$
$K_{CH_4} = 0.179 \exp\left[\frac{38280}{R}\left(\frac{1}{T} - \frac{1}{823}\right)\right] \quad bar^{-1},$
$K_{H_2O} = 0.4152 \exp\left[\frac{88680}{R}\left(\frac{1}{T} - \frac{1}{823}\right)\right] \quad bar^{-1}$
$K_{H_2} = 0.0296 \exp\left[\frac{82900}{R}\left(\frac{1}{T} - \frac{1}{648}\right)\right] \quad bar^{-1},$
$K_{H_2} = 40.91 \exp\left[\frac{70650}{R}\left(\frac{1}{T} - \frac{1}{648}\right)\right] \quad bar^{-1}$
SMR y WGS Numaguchi y Kikuchi (1988)
$A_1 = 9.28 \text{ x } 10^8\ kmol\ m^{-3}\ h^{-1}\ bar^{-1}$ para SMR
$E_{act1} = 104.7 \text{ x } 10^3 J\ mol^{-1}$ para SMR
$A_2 = 8.69 \text{ x } 10^5\ kmol\ m^{-3}\ h^{-1}\ bar^{-1}$ para WGS
$E_{act2} = 54.5 \text{ x } 10^3 J\ mol^{-1}$ para la WGS

a cogido de (Twigg, 1989)

Tabla AI.3: parámetros cinéticos de la carbonatación

Lee (2004)	Rodríguez et al., (2011)
$A = 1.73 \text{ x } 10^2 \ \frac{m^3}{mol\ s}$ $E_{act} = 72.3 \text{ x } 10^3 J\ mol^{-1}$	$K_{carb} = 0.35\ s^{-1}$

La principal diferencia entre ambos modelos es el modo de resolución. En el caso del modelo en Delphi de la TUe, se emplea un algoritmo donde el tiempo de paso y la malla de resolución en la posición a lo largo del reactor se calculan de forma automática mediante un esquema de resolución WENO (de sus siglas en inglés Weighted Essentially Non-Oscillatory) de tercer orden (Smit et al., 2005). Este modelo permite simular el proceso por etapas o en su conjunto. Por el contrario, en el modelo en Matlab del INCAR-CSIC, se emplea la función ode15s, donde se asume un número fijo de nodos en la malla de resolución en la posición, mediante una discretización del espacio (en la dirección axial) hasta derivadas de 2º orden (descrito en la Publicación II) y un tiempo de paso fijo. Este modelo se implementa de forma separada etapa por etapa.

Aplicando las cinéticas descritas, se llevaron a cabo diferentes simulaciones bajo distintas condiciones de operación. En la simulación que se muestra en esta memoria, para el reformado se usó la cinética de Xu y Froment (1989) y para la carbonatación la de Rodríguez et al., (2011).

Se consideró un reactor de lecho fijo adiabático de 8 m de longitud y 5,3 m de diámetro (L/D de 1.5), y una velocidad del gas de 0.5 m/s para asegurar un tiempo de residencia suficiente que permita alcanzar la composición dada por el equilibrio SER, con una caída de presión inferior al 6% (Fernández et. al, 2012a). El ratio vapor/metano considerado en esta simulación es de 4, siendo los valores usuales en la etapa SER entre 3 y 5 para asegurar purezas elevadas de H_2 (a partir del 90% vol. en base seca) (Fernández y Abanades, 2017; Martínez et al., 2014). En la Tabla AI.4 se muestran las condiciones de operación.

Tabla AI.4: Condiciones de operación empleadas en la simulación

Ratio vapor/metano	4
w_{CaO}, %	35
w_{CaOact}, %	12.25
u (m/s)	0.5
w_{Ni}, %	10.50
w_{Al2O3}, %	54.50
L, m	8
D, m	5.3
Dp, m	0.01
T_{s0}, °C	650
T_{gin}, °C	650
η	0.3
p_s, kg/m^3	1940
ε	0.5
P, bar	20

En la figura AI.1 se muestran los resultados correspondientes a la composición y la temperatura a la salida, y el perfil axial de temperatura para ambos modelos. Las líneas discontinuas corresponden al modelo Matlab y las continuas al Delphi. Se observa que la forma de las curvas de ambos modelos es similar, aunque con algunas diferencias, por lo que se puede decir que la predicción de los datos es correcta. Se observó que a medida que se incrementaba el número de nodos en la malla y se reducía el tiempo de paso en el modelo de Matlab, la solución se acercaba más a la del modelo en Delphi, esta simulación corresponde a un número de nodos de 100 y un tiempo de paso de 0.36 s. Por tanto, la explicación principal a estas pequeñas diferencias se atribuye a que el modelo en Matlab no dispone de una malla adaptable de resolución.

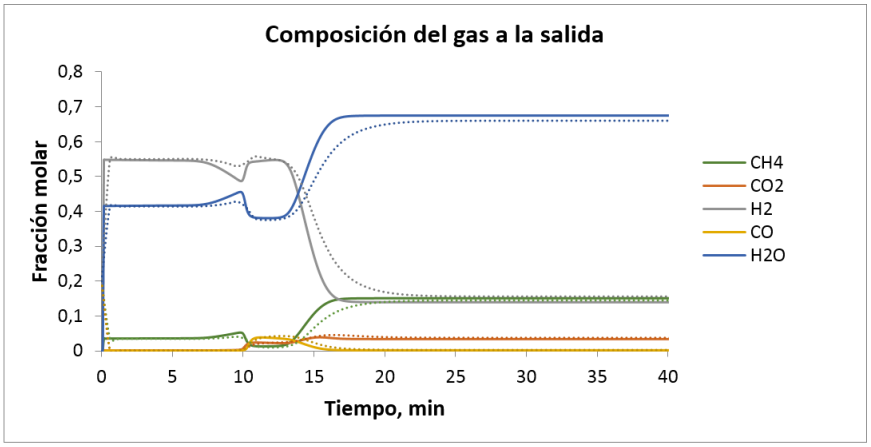

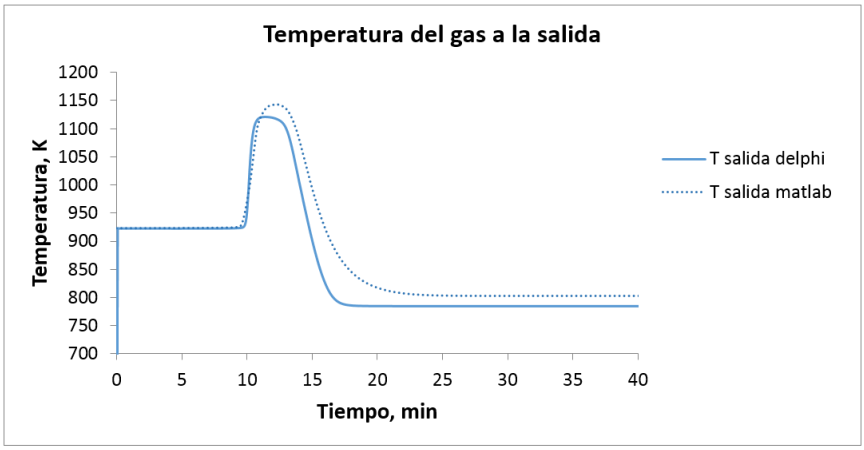

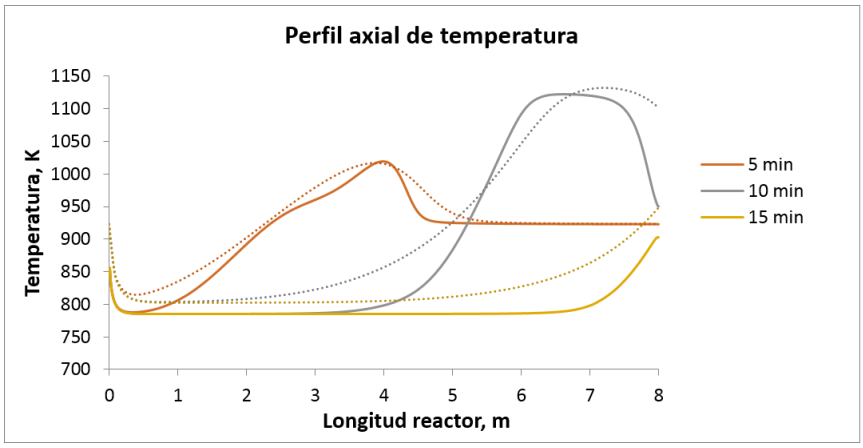

Figura AI.1: comparación entre los modelos desarrollados por el INCAR y la TUe. Perfiles de composición y temperatura a la salida, y perfil axial de temperatura.

AII.1 Prueba de concepto etapa SER

Ensayos preliminares de la etapa SER se han llevado a cabo en un reactor de lecho fijo de 1.5 m de longitud a presión atmosférica. Como se ha mencionado al inicio del anexo, limitaciones en el montaje experimental relacionadas con el límite de detección del analizador de gases y la producción de vapor en el sistema, no dieron lugar a resultados satisfactorios, y por consiguiente no se pudo realizar el escalado al reactor de mayor tamaño a presión, capaz de trabajar a 10 bar. A continuación, en la figura AI.2 se muestran los montajes de la TUe para la prueba de concepto del proceso Ca-Cu dentro del marco del proyecto ASCENT.

Figura AI.2: Dispositivos experimentales de la TUe. Izquierda: reactor de mayor tamaño a presión (DI x L, 0.063 x 1.58 m); derecha: reactor de menor tamaño a presión atmosférica (DI x L, 0.03 x 1.50 m).

- ***Procedimiento experimental***

Los ensayos realizados se llevaron a cabo en el reactor de la derecha mostrado en la figura AI.2. Consiste principalmente en un reactor de acero inoxidable de 0.03 m de diámetro interno y 1,5 m de longitud que contiene la mezcla de sólidos. El reactor se calienta mediante tres hornos cerámicos de 200 W de potencia los cuales están

instalados alrededor del reactor. Para limitar las pérdidas de calor con el ambiente, el reactor y los hornos se encuentran en una caja aislados con lana de cuarzo. La temperatura en el lecho se controla mediante 48 termopares tipo K que se encuentran dentro del reactor en contacto con los sólidos. En la figura AI.3 se muestra una fotografía más detallada de la instalación.

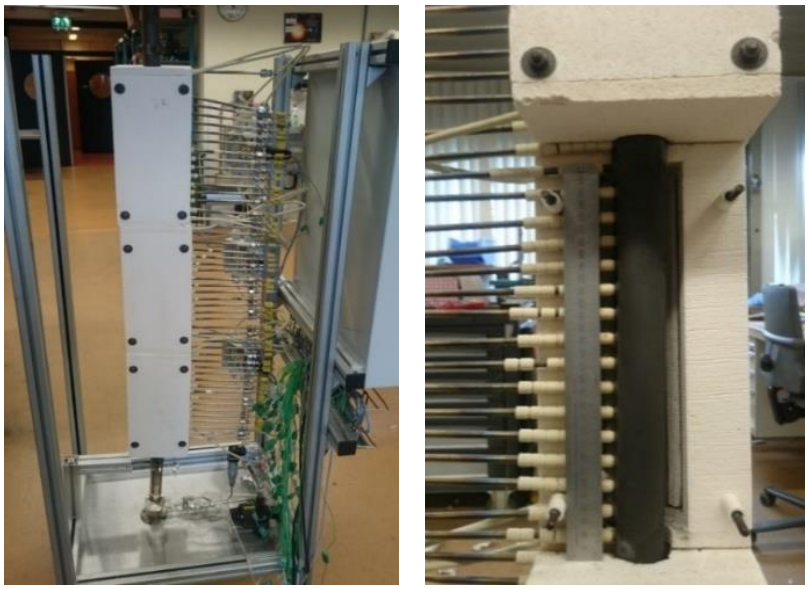

Figura AI.3: Imágenes del reactor de lecho fijo de menor tamaño más detalladas

La alimentación de los gases y su composición se controla mediante medidores/controladores de flujo másico Bronkhorst entre 0-40 lN/min. El sistema también dispone de controladores de presión a contrapresión Bronkhorst a la entrada y a la salida del reactor. Para la generación de vapor se dispone de una bomba HITACHI que capta el agua líquida que se hace pasar por un calderín (justo antes del reactor) encargado de producir el vapor. Para eliminar el mismo de los gases producto se dispone de un condensador a la salida del reactor. La composición en base seca del gas de salida se mide en continuo mediante un espectrómetro de masas (Cirrus 2, MKS Instruments) acoplado con un analizador de CO de infrarrojo (ULTRAMAT 23, Siemens) para distinguir entre las fracciones molares de CO y N_2. Para operar dentro de un rango preciso de medidas, ha de trabajarse con una dilución en N_2 en las mezclas de gases del 60%, diluciones hasta el 50% es lo máximo que admite el equipo, aunque con mayor incertidumbre en las medidas. Desde el ordenador se puede controlar todo el proceso y se registran los datos mediante un sistema SCADA (de sus

siglas inglés Supervisory Control And Data Acquisition). El esquema de la instalación se muestra en la figura AI.4.

En cuanto a los sólidos empleados, JM (Johnson Matthey) suministró el material de Ni con una composición activa del 17% de NiO en peso soportado sobre $CaAl_2O_4$ (partículas entre 1.8-2.8 mm), y el material de calcio usado en este ensayo es el mismo que el empleado en los experimentos de reducción/calcinación proporcionado por Carmeuse con un tamaño de partícula de 3 mm. El reactor se cargó con una mezcla de sólidos de en torno a 0.5 kg, compuesta por el 68% en peso de CaO (una masa activa del 6.6%) y el 32% de material de níquel (masa activa de NiO de 5.8%), correspondiente con un ratio en masa catalizador/sorbente de 0.6, dentro de los rangos de operación para el proceso SER (García-Lario et al., 2015a).

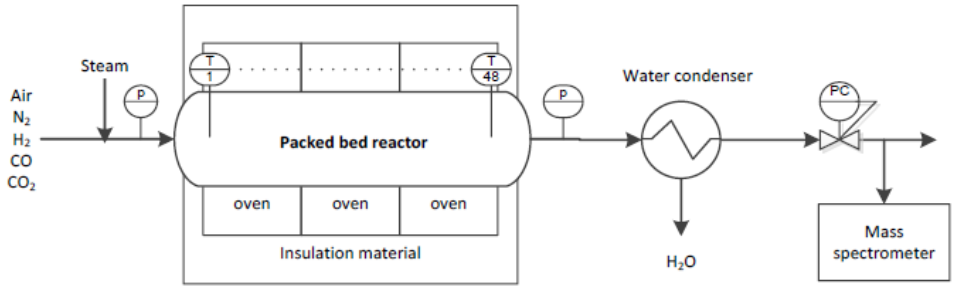

Figura AI.4: Esquema simplificado del reactor de lecho fijo

Los sólidos en el reactor ocuparon una longitud de 0.61 m en la parte central del mismo para trabajar en condiciones isotermas. La parte inferior se rellenó con pellets de 1 cm de longitud de arcilla blanca para precalentar el gas y la parte superior también se rellenó con este mismo material.

Antes de la realización de los experimentos se procedió a la activación del catalizador mediante su reducción, alimentando un caudal de 10 lN/min de H_2 al 30% vol. en N_2 a 900ºC durante 1 h. Se llevaron a cabo ensayos de SER bajo diferentes condiciones de operación, aunque sin la obtención de resultados satisfactorios. En esta memoria se ha seleccionado uno de los ensayos en el que mejor se aprecia el proceso SER. Se empleó un caudal de 10 lN/min alimentando el 10% vol. de CH_4 y 40% vol. vapor en un 50% vol. de N_2. Las condiciones de operación se muestran en la tabla AI.5.

Tabla AI.5: Condiciones de operación etapa SER, reactor de lecho fijo

$w_{NiO/CaAl2O4}$ %	32
w_{CaO} %	68
Masa de sólidos, kg	0.45
L, m	0.61
D, m	0.03
Dp, m	0.003
Caudal, lN/min	10
$H_2O(v)/CH_4$	4
T_{s0}, ºC	650
T_{gin}, ºC	650
P, bar	1

En la figura AI.5 se muestra la composición del gas a la salida. Se observó un período de tiempo inicial de en torno a 8 min en el que la composición del gas mostró inestabilidad hasta empezar a apreciarse el proceso SER. Este comportamiento fue observado en todos los ensayos realizados en el sistema operando con diferentes caudales y ratios vapor/metano. De acuerdo a estos resultados, dicho tiempo de transición, se atribuyó a una producción inestable de vapor. Esto puede ser debido a que la inyección del mismo se localiza muy próxima a la entrada del reactor, y no tiene salida al bypass como el resto de gases, por lo que no hay mucho recorrido para favorecer la mezcla entre ellos, pudiendo ocasionar estas fluctuaciones.

Descartando el tiempo de transición, la forma de las curvas muestra baja reactividad del material de calcio, incrementándose la concentración de CO_2 desde el inicio, y decreciendo la de H_2, por lo que el tiempo previo a la ruptura mientras se están produciendo la carbonatación, SMR y WGS es muy breve, en torno a 3 min (cuando debería estar en torno a 10 min de acuerdo a la cantidad de CaO en el lecho), y no se llega alcanzar la composición dada por el equilibrio SER para un ratio vapor/metano de 4 (para la dilución aplicada correspondería a un 47% vol.). La curva de ruptura es poco nítida y se prolonga en el tiempo, como se observa en la Figura AI.5, y el sorbente no llega a agotarse del todo, dado que en el tiempo posterior a la ruptura no se llega a alcanzar la composición dada por el equilibrio de reformado (correspondiente en este caso a un 37% vol. en base seca de H_2). Este comportamiento puede ser debido a los siguientes motivos: (1) la baja concentración de CO_2 generada en el sistema por la alta dilución en N_2 a la que se opera; (2) la baja capacidad de absorción de CO_2 del material del calcio (0.1 g CO_2/g CaO calcinado); (3) la relativamente elevada velocidad

espacial, 0.8 m/s. Estos factores dan lugar a que la carbonatación no se produzca de forma efectiva.

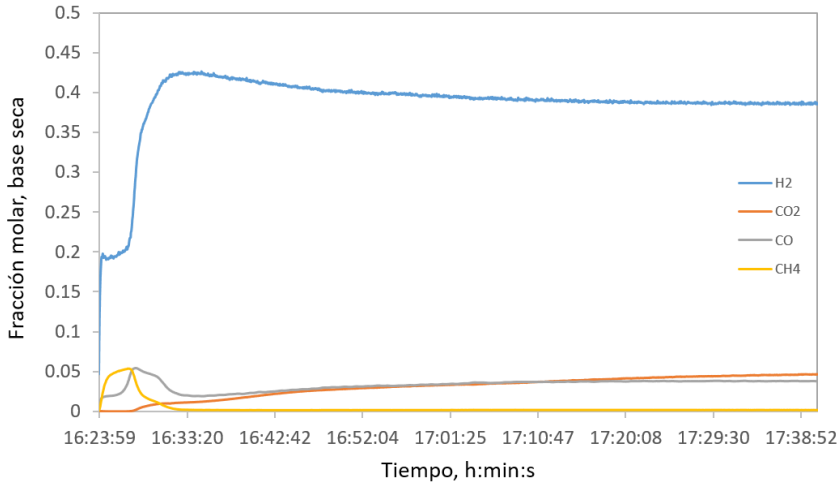

Figura AI.5: composición del gas a la salida etapa SER, ratio vapor/metano 4.

Velocidades superficiales bajas son necesarias para que la carbonatación tenga lugar de forma efectiva, ya que es una reacción más lenta que las reacciones de SMR y WGS. El estudio teórico realizado por Fernández et al., (2012) donde se estudia la influencia de este parámetro, determina que a escala industrial, velocidades del gas de 0.5 m/s permiten que se alcance la máxima pureza del H_2 dada por el equilibrio SER. Estudios experimentales más recientes a escala de micro-reactor realizados por Aloisi et al., (2017), establecen que velocidades inferiores a 8 lN CH_4 h^{-1} g_{Ni}^{-1}, alcanzan la composición dada por el equilibrio SER, mientras que en el presente caso equivale a 13 lN CH_4 h^{-1} g_{Ni}^{-1}. Por lo que el siguiente paso fue probar velocidades más bajas para estudiar el comportamiento del sistema.

A la vista de los ensayos realizados, la TUe trabaja actualmente en la modificación de la instalación para introducir la generación de vapor antes del bypass y de esta forma favorecer la mezcla de los gases antes de pasar a través del lecho. En cuanto a la posibilidad de trabajar a mayores concentraciones de CO_2 (introduciendo mayor proporción de CH_4 en la alimentación) y velocidades de gas más bajas para favorecer la carbonatación, se estudia hacer una recalibración del analizador si fuera posible, para disminuir la dilución necesaria en N_2, o bien introducir una modificación en la

instalación, para llevar a cabo la dilución de la muestra a la salida del reactor, antes de pasar por el analizador.

Nomenclatura

A_i factor preesponencial, m^3 mol^{-1} s^{-1}

D Diámetro reactor, m

D_p Diámetro de partícula, m

E_{acti} Energía de activación, J mol^{-1}

k_i Constantes cinéticas (i=1, 2, 3) bar $^{0.5}$ kmol kg $catalizador^{-1}$ h^{-1}

k_{carb} Constante cinética de carbonatación, s^{-1}

K_i Constantes de absorción (i=CH_4, H_2O, H_2, CO, CO_2), bar^{-1}

K_i Constantes de equilibrio de las reacciones (i=1, 2, 3), bar^2

L Longitud reactor, m

M_w Peso molecular CaO, kg $kmol^{-1}$

P Presión total, bar

p_i Presión parcial del gas (i=CH_4, H_2O, H_2, CO, CO_2), bar

$p_{eq}^{CO_2}$ Presión de equilibrio CO_2, bar

R_i velocidad de reacción, kmol kg $catalizador^{-1}$ h^{-1}

r_i velocidad de reacción, kmol kg $catalizador^{-1}$ h^{-1}

T_{gin} Temperatura de entrada al reactor, ºC

T_{s0} Temperatura inicial del lecho, ºC

u Velocidad del gas, m s^{-1}

w_i porcentaje en masa (i=CaO, $CaO_{act\ (activo)}$, $NiAl_2O_4$), adimensional

X_{max} Conversión molar máxima del CaO, adimensional

X Conversión molar del CaO, adimensional

ε fracción libre de sólidos, adimensional

ϑ_{CO_2} fracción molar de CO_2, adimensional

$\vartheta_{CO_2 eq}$ fracción molar de CO_2 de equilibrio, adimensional

ρ_i densidad aparente de CaO en el reactor, kg m^{-3}

ρ_s densidad aparente de sólidos en el reactor, kg m^{-3}

η factor de eficacia, adimensional

ANEXO II: FACTOR DE IMPACTO DE LAS REVISTAS Y CONTRIBUCIONES A CONGRESOS.

AII.1 Factor de impacto

Tal y como se establece en el reglamento de Doctorado RD 1393/2007, en la tabla AII.1 se exponen los índices de impacto de las revistas en las que se han publicado los trabajos que forman parte de esta tesis doctoral. Éstos corresponden al último año disponible que es 2015, y la fuente es el Journal of Citation Report.

Tabla AII.1: Factor de impacto de las revistas.

Publicación	Año	Revista	Factor de impacto
Chemical looping combustion in fixed-bed reactors using ilmenite as oxygen carrier: conceptual design and operation strategy	2015	Chemical Engineering Journal	5,310
$CaCO_3$ calcination by the simultaneous reduction of CuO in a Ca/Cu chemical looping process	2015	Chemical Engineering Science	2,750
Investigation of a fixed-reactor for the calcination of $CaCO_3$ by the simultaneous reduction of CuO with a fuel gas	2016	Industrial & Engineering Chemistry Research	2,567
Study of a chemical loop for the calcination of $CaCO_3$ in a fixed bed reactor. Enviado	2017	Chemical Engineering Journal	5,310

AII.2 Comunicaciones a congresos a partir del trabajo de esta tesis doctoral.

Alarcón, J.M, Fernández, J.R, Abanades, J.C. Investigation of the calcination of $CaCO_3$ by the simultaneous reduction of CuO with a fuel gas in a fixed-bed reactor. 6th High Temperature Solid Looping Cycles Network Meeting, 1-2 de septiembre, 2015, Milán, Italia.

Fernández, J.R., Alarcón, J.M, Abanades, J.C. Investigation of a fixed-bed reactor for the calcination of $CaCO_3$ by the simultaneous reduction of CuO with a fuel gas. 20-22 de Julio de 2015, Paris, Francia.